

1-17-2012

# The Effect of Elevated Temperature on the Inelastic Deformation Behavior of PMR-15 Solid Polymer

Chad E. C. Ryther

Follow this and additional works at: <https://scholar.afit.edu/etd>

Part of the [Structures and Materials Commons](#)

---

## Recommended Citation

Ryther, Chad E. C., "The Effect of Elevated Temperature on the Inelastic Deformation Behavior of PMR-15 Solid Polymer" (2012). *Theses and Dissertations*. 1064.  
<https://scholar.afit.edu/etd/1064>

This Dissertation is brought to you for free and open access by the Student Graduate Works at AFIT Scholar. It has been accepted for inclusion in Theses and Dissertations by an authorized administrator of AFIT Scholar. For more information, please contact [richard.mansfield@afit.edu](mailto:richard.mansfield@afit.edu).



**THE EFFECT OF ELEVATED TEMPERATURE ON  
THE INELASTIC DEFORMATION BEHAVIOR OF  
PMR-15 SOLID POLYMER**

DISSERTATION

Chad E. C. Ryther, Major, USAF  
AFIT/DS/ENY/12-12

**DEPARTMENT OF THE AIR FORCE  
AIR UNIVERSITY**

***AIR FORCE INSTITUTE OF TECHNOLOGY***

**Wright-Patterson Air Force Base, Ohio**

APPROVED FOR PUBLIC RELEASE; DISTRIBUTION UNLIMITED

The views expressed in this thesis are those of the author and do not reflect the official policy or position of the United States Air Force, Department of Defense, or the United States Government. This material is declared a work of the U.S. Government and is not subject to copyright protection in the United States.

AFIT/DS/ENY/12-12

THE EFFECT OF ELEVATED TEMPERATURE ON THE INELASTIC  
DEFORMATION BEHAVIOR OF PMR-15 SOLID POLYMER

DISSERTATION

Presented to the Faculty  
Department of Aeronautics and Astronautics  
Graduate School of Engineering and Management  
Air Force Institute of Technology  
Air University  
Air Education and Training Command  
In Partial Fulfillment of the Requirements for the  
Degree of Doctor of Philosophy in Aeronautical Engineering

Chad E. C. Ryther, B.S.A.E., M.S.M.E

Major, USAF

January 2012

APPROVED FOR PUBLIC RELEASE; DISTRIBUTION UNLIMITED.

AFIT/DS/ENY/12-12

THE EFFECT OF ELEVATED TEMPERATURE ON THE INELASTIC  
DEFORMATION BEHAVIOR OF PMR-15 SOLID POLYMER

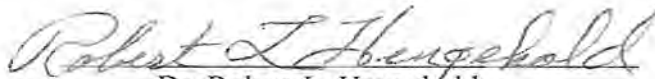
Chad E. C. Ryther, B.S.A.E., M.S.M.E  
Major, USAF

Approved:



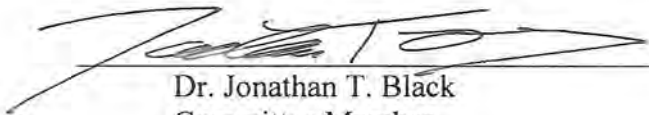
Dr. Marina B. Ruggles-Wren  
Committee Chair

12 Jan 12  
date



Dr. Robert L. Hengehold  
Committee Member

13 Jan '12  
date



Dr. Jonathan T. Black  
Committee Member

14 JAN 2012  
date

Accepted:



Dr. M. U. Thomas  
Dean, Graduate School of Engineering  
and Management

10 Feb 2012  
date

### **Abstract**

The inelastic deformation behavior of PMR-15 neat resin, a high-temperature thermoset polymer, was investigated at temperatures in the 274-316 °C range. The experimental program was developed to explore the influence of temperature on strain-controlled tensile loading, relaxation and creep behaviors. The experimental results clearly demonstrate that the mechanical behavior of PMR-15 polymer exhibits a strong dependence on temperature. During strain-controlled tensile loading, the slope of the stress-strain curve in the quasi-elastic region decreases and the slope of the stress-strain curve in the flow stress region increases with increasing temperature. At a given strain rate, the flow stress level decreases with increasing temperature. Furthermore, the transition from quasi-elastic behavior to inelastic flow becomes less pronounced with increasing temperature. During relaxation, the amount of the stress drop for a given prior strain rate decreases with increasing temperature. At a given prior strain rate and creep stress level, increasing temperature results in increased creep strain accumulation. Based on the experimental results the Viscoplasticity Based on Overstress for Polymers (VBOP) theory was augmented to account for the effects of elevated temperature. Several model parameters were determined to depend on temperature. Those parameters were developed into functions of temperature. The augmented VBOP was then employed to predict the response of the PMR-15 polymer under various test histories at temperatures in the 274-316 °C range. An enhanced procedure for determining VBOP model parameters that utilizes a McLean type dip test to assess the equilibrium stress was developed. Model predictions were considerably improved by employing an enhanced model

characterization procedure. Additionally, the effects of prior isothermal aging at various temperatures in the 260-316 °C range on the inelastic deformation behavior of PMR-15 at 288 °C were evaluated. For PMR-15 aged at 260-302 °C, the initial slope of the stress-strain curve and the flow stress increase with prior aging duration. The shape of the knee of the stress-strain curve becomes more pronounced and the departure from quasi-linear behavior is delayed with increasing prior aging time. Experimental results reveal that there is no relationship between prior aging temperature and elastic modulus, tangent modulus, the shape of the knee of the stress-strain curve or departure from quasi-linear behavior. This implies that for aging temperatures in the 260-302 °C range, mechanical behavior depends only on prior aging duration and not on prior aging temperature. However, testing of PMR-15 aged at 316 °C revealed a decrease in flow stress with increasing prior aging duration. This suggests that a degradation mechanism, not present at lower aging temperatures, is in effect during aging at 316 °C.

## **Acknowledgements**

I would like to thank Dr. Ruggles-Wrenn for her fervent support throughout this endeavor. Her consistent mentoring and advice have been truly exceptional. I would like to thank Dr. Robert Hengehold and Dr. Jonathan Black for serving as members of my committee. I would also like to thank John Hixenbaugh, Barry Page, Chris Zickefoose and Jay Anderson for their guidance and assistance in the laboratory. Of course, none of this would have been possible without the unending love and support of my wife Elena and our two beautiful girls Daniella and Julianna. Thank you for your love and understanding during this undertaking.

Chad E. C. Ryther



## Table of Contents

Abstract.....	iv
Acknowledgements.....	vi
Table of Contents.....	vii
List of Figures.....	xi
List of Tables.....	xxi
List of Symbols.....	xxiii
List of Abbreviations.....	xxv
List of Abbreviations (Continued).....	xxvi
1 Introduction.....	1
1.1 Motivation.....	1
1.2 Material Description.....	3
1.2.1 <i>Micromechanical Mechanisms of Polymer Deformation</i> .....	4
1.2.2 <i>Polymer Degradation</i> .....	5
1.3 Problem Statement.....	6
1.4 Dissertation Outline.....	7
2 Background: Experimental Investigations and Constitutive Modeling.....	9
2.1 Experimental Investigations.....	9
2.1.1 <i>Deformation Behavior of Polymers</i> .....	9
2.1.2 <i>Prior Aging – Effects on Mechanical Behavior</i> .....	14
2.2 Constitutive Modeling.....	19
2.2.1 <i>Viscoelastic Constitutive Models</i> .....	19
2.2.2 <i>Viscoplastic Constitutive Models</i> .....	32
2.3 Objective of Current Work.....	42
3 Theoretical Formulation of Viscoplasticity Based on Overstress for Polymers.....	43
3.1 Basis of Viscoplasticity Based on Overstress – Standard Linear Solid.....	43
3.2 Viscoplasticity Based on Overstress.....	46
3.3 Viscoplasticity Based on Overstress for Polymers.....	49
3.4 Extension of Viscoplasticity Based on Overstress for Polymers to Capture Effects of Prior Aging Time.....	52

4	Experimental Methods .....	53
4.1	Material and Test Specimen.....	53
4.1.1	<i>PMR-15 Solid Polymer</i> .....	53
4.1.2	<i>Material Processing</i> .....	54
4.1.3	<i>Specimen Geometry</i> .....	54
4.1.4	<i>Specimen Preparation</i> .....	55
4.2	Experimental Setup and Testing Procedures .....	56
4.2.1	<i>Mechanical Testing Equipment</i> .....	56
4.2.2	<i>Aging Chamber</i> .....	57
4.2.3	<i>Weight Measurement</i> .....	58
4.2.4	<i>Mechanical Test Procedures</i> .....	58
5	VBOP Model Characterization .....	66
5.1	Experimentally Based Characterization of VBOP .....	66
5.1.1	<i>Elastic Modulus and Tangent Modulus</i> .....	66
5.1.2	<i>Equilibrium Stress and Isotropic Stress</i> .....	67
5.1.3	<i>Viscosity Function and Shape Function</i> .....	68
5.2	Experimental Characterization of the Effects of Test Temperature on Deformation Behaviors .....	69
5.3	Experimental Characterization of the Effects of Prior Aging Time and Prior Aging Temperature on Deformation Behaviors .....	70
5.3.1	<i>Effects of Prior Aging Duration</i> .....	70
5.3.2	<i>Effects of Prior Aging Temperature</i> .....	71
6	Unaged PMR-15 Neat Resin Tested at 274-302 °C: Experimental Observations .....	72
6.1	Assessment of Specimen-to-Specimen Variability.....	72
6.2	Strain Rate Sensitivity.....	74
6.3	Strain Rate History Effect.....	77
6.4	Relaxation Behavior.....	78
6.5	Creep Behavior .....	82
6.6	Summary of the Key Effects of Test Temperature on Deformation Behavior .....	83
7	Implications for Modeling the Effects of Increasing Test Temperature .....	86
7.1	Decrease in Initial Slope of the Stress-Strain Curve.....	86
7.2	Increase in Final Slope of the Stress-Strain Curve .....	86
7.3	Accelerated Departure from Quasi-linear Behavior .....	86
7.4	Decreased Influence of Strain Rate on the Shape of the Knee of the Stress-Strain Curve.....	87
7.5	Decrease in Flow Stress in the Region of Plastic Flow .....	87
7.6	Decrease in Stress Drop during Relaxation .....	88

7.7	Proposed Changes to the VBOP to Account for the Effects of Increasing Test Temperature .....	88
8	Constitutive Modeling of the Inelastic Behavior of Unaged PMR-15 Neat Resin at 274-316 °C .....	90
8.1	Characterization of VBOP Model Parameters for PMR-15 at Various Temperatures .....	90
8.1.1	<i>Characterization of VBOP Model Parameters at 274 °C</i> .....	90
8.1.2	<i>Characterization of VBOP Model Parameters at 288 °C</i> .....	93
8.1.3	<i>Characterization of VBOP Model Parameters at 302 °C</i> .....	97
8.2	VBOP Model Parameters as Functions of Temperature.....	100
8.2.1	<i>Elastic Modulus – Effect of Test Temperature</i> .....	101
8.2.2	<i>Tangent Modulus – Effect of Test Temperature</i> .....	102
8.2.3	<i>Shape Function – Effect of Test Temperature</i> .....	103
8.2.4	<i>Isotropic Stress – Effect of Test Temperature</i> .....	104
8.2.5	<i>Viscosity Function– Effect of Test Temperature</i> .....	105
8.2.6	<i>Calculation of Model Parameters Utilizing the Augmented VBOP</i> .....	106
8.3	Validation of VBOP Model Parameters as Functions of Test Temperature.....	113
8.3.1	<i>Prediction of the Strain Rate Jump Test at 274 °C</i> .....	114
8.3.2	<i>Prediction of the Strain Rate Jump Test at 302 °C</i> .....	114
8.3.3	<i>Prediction of Creep Tests at 274 °C</i> .....	115
8.3.4	<i>Prediction of Creep Tests at 288 °C</i> .....	116
8.3.5	<i>Prediction of Creep Tests at 302 °C</i> .....	117
8.4	Predictions of Deformation Behavior of the PMR-15 Neat Resin at 316 °C.....	119
8.4.1	<i>Strain Controlled Monotonic Loading</i> .....	121
8.4.2	<i>Relaxation Behavior</i> .....	121
8.4.3	<i>Creep Tests</i> .....	123
8.5	Summary of the Constitutive Modeling of the Inelastic Behavior of Unaged PMR-15 at 274-316 °C .....	126
9	PMR-15 Neat Resin Aged at 260-316 °C: Experimental Observations.....	128
9.1	Assessment of Specimen-to-Specimen Variability.....	128
9.2	Test Temperature versus Prior Aging Temperature.....	128
9.3	Strain Rate Sensitivity – Influence of Prior Aging Temperature.....	129
9.4	Relaxation Behavior – Influence of Prior Aging Temperature.....	153
9.5	Thermal Degradation of PMR-15 .....	161
9.6	Summary of the Key Effects of Prior Aging at Various Elevated Temperatures on the Deformation Behavior of PMR-15 .....	164

10	Enhanced Procedure for the Characterization of the VBOP Model.....	166
	10.1 Brief Review of the VBOP Formulation and Existing Characterization Procedure.....	166
	10.1.1 <i>VBOP Formulation</i> .....	166
	10.1.2 <i>Characterization Procedure</i> .....	168
	10.2 Under-Prediction of the Flow Stress and the Equilibrium Stress in the Region of Fully Developed Plastic Flow.....	171
	10.2.1 <i>VBOP Model Behavior during Change of Rate</i> .....	173
	10.3 Alternate Method to Assess the Equilibrium Stress .....	179
	10.3.1 <i>Utilization of the McLean Type Dip Test to Measure the Equilibrium Stress</i> .....	180
	10.3.2 <i>Creep Rate Reversal</i> .....	181
	10.4 Experimental Observations.....	184
	10.4.1 <i>MTDT Results at 274 °C</i> .....	185
	10.4.2 <i>MTDT Results at 302 °C</i> .....	188
	10.5 Comparison of Different Techniques to Determine Equilibrium Stress.....	191
11	Conclusions and Recommendations.....	195
	11.1 Conclusions.....	195
	11.2 Recommendation for Future Research.....	195
12	Appendix .....	198
13	Bibliography.....	203

## List of Figures

Figure 1.1 Molecular structure of PMR-15. Figure from [24].	3
Figure 2.1 Stress-strain curves for PMR-15 neat resin obtained at three different stress rates at 23 °C. Nonlinear rate sensitivity is apparent. Reproduced from [4].	13
Figure 2.2 The influence of loading rate on the loading and unloading behavior of PMR-15 at 288 °C. The nonlinear rate sensitivity and curved unloading are apparent. Reproduced from [1].	15
Figure 2.3 Creep strain versus time at 20 MPa and 288 °C. Effect of prior stress rate on creep strain is apparent. Creep strain increases nonlinearly with prior loading rate. Reproduced from [1].	15
Figure 2.4 Stress controlled test with intermittent creep periods of 1 h duration at 288 °C. A reversal in the creep strain rate is observed during unloading. Reproduced from [1].	16
Figure 2.5 (a) Linear elastic and (b) viscoelastic stress-strain behaviors. Viscoelastic material exhibits a nonzero strain upon unloading to zero stress and recovers this strain if given time to do so.	20
Figure 2.6 Schematic of (a) viscoelastic and (b) viscoplastic creep and recovery.	22
Figure 2.7 Comparison between experimental and predicted stress-strain curves for PMR-15 neat resin at 288 °C at constant stress rates of (a) 1.0 MPa/s and (b) 0.01 MPa/s. Reproduced from [1].	24
Figure 2.8 Comparison between experimental and predicted strain versus time curves for PMR-15 neat resin at 288 °C for various prior loading rates for (a) creep at 20 MPa and (b) recovery at zero stress. Reproduced from [1].	25
Figure 2.9 Comparison between experimental and predicted stress-strain behavior of stepwise creep test of PMR-15 at 288 °C. Reproduced from [2].	26
Figure 2.10 (a) Stepwise creep behavior and (b) recovery following stepwise creep of PMR-15 at 288 °C: Experiment, Schapery's Model and Schapery's Model with Viscoplastic Strain. Reproduced from [19].	277
Figure 2.11 Xia and Ellyin's viscoelastic model.	29
Figure 2.12 (a) viscoelastic and (b) viscoplastic stress-strain behavior.	33
Figure 2.13 Schematic showing uniaxial stress-strain curve, equilibrium stress $g$ and kinematic stress $f$ curves, overstress $\sigma - g$ , and isotropic stress $A$ .	34
Figure 2.14 Schematic showing equidistance of stress-strain curves produced in response to loading at different strain rates in the region of fully established plastic flow.	36

Figure 3.1 Schematic of the Standard Linear Solid. ....	44
Figure 3.2 Schematic showing the responses of a SLS in monotonic loading. ....	46
Figure 3.3 Schematic showing uniaxial stress-strain curve, equilibrium stress $\mathbf{g}$ and kinematic stress $\mathbf{f}$ curves, overstress $\boldsymbol{\sigma} - \mathbf{g}$ , and isotropic stress $\mathbf{A}$ . ....	48
Figure 4.1 Test specimen. ....	55
Figure 4.2 Schematic of monotonic tensile tests performed at several strain rates. ....	60
Figure 4.3 Stress-strain curves obtained for PMR-15 in tensile tests to failure conducted at constant strain rates of $10^{-6}$ , $10^{-5}$ , $10^{-4}$ , and $10^{-3} \text{ s}^{-1}$ at 288 °C. The dependence of the stress-strain behavior on the strain rate is evident. Reproduced from McClung [19] Figure 5.1. ....	60
Figure 4.4 Schematic of a constant strain rate test with intermittent periods of relaxation. ....	62
Figure 4.5 Stress-strain curves obtained for PMR-15 in constant strain rate tests with intermittent periods of relaxation at 288 °C. Reproduced from [19]. ....	62
Figure 4.6 Schematic of stress-strain curves obtained during a strain rate jump test. ....	64
Figure 4.7 Schematic of stress-strain curve obtained during a McLean type dip test. ....	65
Figure 6.1 Stress-strain curves obtained for the PMR-15 polymer in tensile tests to failure conducted at constant strain rates of $10^{-6}$ , $10^{-5}$ , $10^{-4}$ , and $10^{-3} \text{ s}^{-1}$ at 274 °C. The dependence of the stress-strain behavior on the strain rate is evident. ....	75
Figure 6.2 Stress-strain curves obtained for the PMR-15 polymer in tensile tests to failure conducted at constant strain rates of $10^{-6}$ , $10^{-4}$ , and $10^{-3} \text{ s}^{-1}$ at 288 °C. The dependence of the stress-strain behavior on the strain rate is evident. Data from [81] are included. ....	75
Figure 6.3 Stress-strain curves obtained for the PMR-15 polymer in tensile tests to failure conducted at constant strain rates of $10^{-6}$ , $10^{-4}$ , and $10^{-3} \text{ s}^{-1}$ at 302 °C. The dependence of the stress-strain behavior on the strain rate is evident. ....	76
Figure 6.4 Stress-strain curves obtained for the PMR-15 polymer in strain rate jump tests and in constant strain rate tests at: (a) 274 °C and (b) 302 °C. Upon a change in the strain rate, the material returns to the stress-strain curve characteristic for that particular strain rate. ....	79
Figure 6.5 Stress decrease versus relaxation time for the PMR-15 polymer at 274 °C. The influence of prior strain rate on the stress drop during relaxation is evident. ....	81

Figure 6.6 Stress decrease versus relaxation time for the PMR-15 polymer at 288 °C. The influence of prior strain rate on the stress drop during relaxation is evident. Data from [81].	81
Figure 6.7 Stress decrease versus relaxation time for the PMR-15 polymer at 302 °C. The influence of prior strain rate on the stress drop during relaxation is evident.	82
Figure 6.8 Creep strain versus time at 21 MPa and 274 °C. Effect of prior strain rate on creep is apparent. Creep strain increases nonlinearly with prior strain rate.	84
Figure 6.9 Creep strain versus time at 21 MPa and 288 °C. Effect of prior strain rate on creep is apparent. Creep strain increases nonlinearly with prior strain rate. Data from [81].	84
Figure 6.10 Creep strain versus time at 21 MPa and 302 °C. Effect of prior strain rate on creep is apparent. Creep strain increases nonlinearly with prior strain rate.	85
Figure 8.1 A comparison between experimental results and simulated stress-strain curves obtained for PMR-15 polymer in tensile tests to failure conducted at constant strain rates of $10^{-6}$ , $10^{-5}$ , $10^{-4}$ and $10^{-3}$ s <sup>-1</sup> at 274 °C. The model successfully represents the strain rate dependence of the material at elevated temperature.	92
Figure 8.2 A comparison between experimental results and simulated stress drop during relaxation obtained for PMR-15 polymer at 274 °C. Loading prior to relaxation is conducted at constant strain rates of $10^{-6}$ , $10^{-5}$ , $10^{-4}$ and $10^{-3}$ s <sup>-1</sup> . The model successfully represents the stress drop throughout the entire relaxation period.	93
Figure 8.3 A comparison between experimental results and simulated stress-strain curves obtained for PMR-15 polymer in tensile tests to failure conducted at constant strain rates of $10^{-6}$ , $10^{-4}$ and $10^{-3}$ s <sup>-1</sup> at 288 °C. The model successfully represents the strain rate dependence of the material at elevated temperature. Data from [19] are also included.	96
Figure 8.4 A comparison between experimental results and simulated stress drop during relaxation obtained for PMR-15 polymer at 288 °C. Loading prior to relaxation is conducted at constant strain rates of $10^{-6}$ , $10^{-5}$ and $10^{-4}$ s <sup>-1</sup> . The model successfully represents the stress drop throughout the entire relaxation period. Data from [19] are also included.	97
Figure 8.5 A comparison between experimental results and simulated stress-strain curves obtained for PMR-15 polymer in tensile tests to failure conducted at constant strain rates of $10^{-6}$ , $10^{-4}$ and $10^{-3}$ s <sup>-1</sup> at 302 °C. The model successfully represents the strain rate dependence of the material at elevated temperature.	99

Figure 8.6 A comparison between experimental results and simulated stress drop during relaxation obtained for PMR-15 polymer at 302 °C. Loading prior to relaxation is conducted at constant strain rates of $10^{-6}$ , $10^{-5}$ , $10^{-4}$ and $10^{-3} \text{ s}^{-1}$ . The model successfully represents the stress drop throughout the entire relaxation period.....	100
Figure 8.7 Elastic modulus versus temperature for PMR-15 neat resin. ....	102
Figure 8.8 Tangent modulus versus temperature for PMR-15 neat resin. ....	103
Figure 8.9 Shape function parameter <b>C2</b> versus temperature for PMR-15 neat resin. ....	104
Figure 8.10 Isotropic stress <b>A</b> versus temperature for PMR-15 neat resin. ....	105
Figure 8.11 Viscosity function parameter <b>k2</b> versus temperature for PMR-15 resin. ....	106
Figure 8.12 A comparison between experimental results and simulated stress-strain curves obtained for PMR-15 polymer in tensile tests to failure conducted at constant strain rates of $10^{-6}$ , $10^{-5}$ , $10^{-4}$ and $10^{-3} \text{ s}^{-1}$ at 274 °C. Model parameters for simulations were calculated utilizing the augmented VBOP. The augmented VBOP successfully represents the strain rate dependence of the material at elevated temperature. ....	108
Figure 8.13 A comparison between experimental results and simulated stress drop during relaxation obtained for PMR-15 polymer at 274 °C. Loading prior to relaxation is conducted at constant strain rates of $10^{-6}$ , $10^{-5}$ , $10^{-4}$ and $10^{-3} \text{ s}^{-1}$ . Model parameters for simulations were calculated utilizing the augmented VBOP. The augmented VBOP successfully represents the stress drop throughout the entire relaxation period.....	109
Figure 8.14 A comparison between experimental results and simulated stress-strain curves obtained for PMR-15 polymer in tensile tests to failure conducted at constant strain rates of $10^{-6}$ , $10^{-4}$ and $10^{-3} \text{ s}^{-1}$ at 288 °C. Model parameters for simulations were calculated utilizing the augmented VBOP. The augmented VBOP successfully represents the strain rate dependence of the material at elevated temperature. ....	110
Figure 8.15 A comparison between experimental results and simulated stress drop during relaxation obtained for PMR-15 polymer at 288 °C. Loading prior to relaxation is conducted at constant strain rates of $10^{-6}$ , $10^{-5}$ and $10^{-4} \text{ s}^{-1}$ . Model parameters for simulations were calculated utilizing the augmented VBOP. The augmented VBOP successfully represents the stress drop throughout the entire relaxation period.....	111



Figure 8.16 A comparison between experimental results and simulated stress-strain curves obtained for PMR-15 polymer in tensile tests to failure conducted at constant strain rates of $10^{-6}$ , $10^{-4}$ and $10^{-3} \text{ s}^{-1}$ at 302 °C. Model parameters for simulations were calculated utilizing the augmented VBOP. The augmented VBOP successfully represents the strain rate dependence of the material at elevated temperature. ....	112
Figure 8.17 A comparison between experimental results and simulated stress drop during relaxation obtained for PMR-15 polymer at 302 °C. Loading prior to relaxation is conducted at constant strain rates of $10^{-6}$ , $10^{-5}$ , $10^{-4}$ and $10^{-3} \text{ s}^{-1}$ . Model parameters for simulations were calculated utilizing the augmented VBOP. The augmented VBOP successfully represents the stress drop throughout the entire relaxation period.....	113
Figure 8.18 A comparison between experimental and predicted stress-strain curves obtained for PMR-15 polymer in a strain rate jump test conducted at 274 °C. The augmented VBOP model successfully represents the strain rate dependence and the absence of a strain rate history effect. ....	114
Figure 8.19 A comparison between experimental and predicted stress-strain curves obtained for PMR-15 polymer in a strain rate jump test conducted at 302 °C. The augmented VBOP model successfully represents the strain rate dependence and the absence of a strain rate history effect. ....	115
Figure 8.20 Creep strain versus time at 21 MPa and 274 °C. The effect of prior strain rate on creep is apparent. Creep strain increases nonlinearly with prior strain rate. The model accurately predicts the effects of prior loading rate within 0.5% of the experimental results.....	116
Figure 8.21 Creep strain versus time at 21 MPa and 288 °C. The effect of prior strain rate on creep is apparent. Creep strain increases nonlinearly with prior strain rate. The extended model accurately predicts the effects of prior loading rate at 288 °C within 1.0% of the experimental results.....	118
Figure 8.22 Creep strain versus time at 21 MPa and 302 °C. The effect of prior strain rate on creep is apparent. Creep strain increases nonlinearly with prior strain rate. The extended model accurately predicts the effects of prior loading rate at 302 °C within 1.0% of the experimental results.....	120
Figure 8.23 A comparison between experimental results and predicted stress-strain curves obtained for PMR-15 polymer in tensile tests to failure conducted at constant strain rates of $10^{-6}$ , $10^{-4}$ and $10^{-3} \text{ s}^{-1}$ at 316 °C. The model successfully represents the strain rate dependence of the material at elevated temperature. ....	122
Figure 8.24 A comparison between experimental results and predicted stress drop during relaxation obtained for PMR-15 polymer at 316 °C. Loading prior to relaxation is conducted at constant strain rates of $10^{-6}$ , $10^{-5}$ , $10^{-4}$ and $10^{-3} \text{ s}^{-1}$ . The model successfully represents the stress drop throughout the entire relaxation period.....	123

Figure 8.25 Creep strain versus time at 21 MPa and 316 °C. The effect of prior strain rate on creep is apparent. Creep strain increases nonlinearly with prior strain rate. The extended model accurately predicts the effects of prior loading rate at 316 °C within 1.0% of the experimental results.....	125
Figure 8.26 Creep strain versus time at 12 MPa and 316 °C. The effect of prior strain rate on creep is apparent. Creep strain increases nonlinearly with prior strain rate. The extended model accurately predicts the effects of prior loading rate at 316 °C within 1.0% of the experimental results. Data from [27, 82]. .....	126
Figure 9.1 Stress-Strain curves for PMR-15 specimens aged for 250 h at 260 °C in argon obtained in tensile tests to failure conducted at constant strain rates of $10^{-6}$ , $10^{-5}$ , $10^{-4}$ and $10^{-3} \text{ s}^{-1}$ at 288 °C. The dependence of the stress-strain behavior on the strain rate is evident.....	130
Figure 9.2 Stress-Strain curves for PMR-15 specimens aged for 250 h at 274 °C in argon obtained in tensile tests to failure conducted at constant strain rates of $10^{-6}$ , $10^{-5}$ , $10^{-4}$ and $10^{-3} \text{ s}^{-1}$ at 288 °C. The dependence of the stress-strain behavior on the strain rate is evident. Data from [21].....	131
Figure 9.3 Stress-Strain curves for PMR-15 specimens aged for 250 h at 288 °C in argon obtained in tensile tests to failure conducted at constant strain rates of $10^{-6}$ , $10^{-5}$ , $10^{-4}$ and $10^{-3} \text{ s}^{-1}$ at 288 °C. The dependence of the stress-strain behavior on the strain rate is evident. Data from [19].....	131
Figure 9.4 Stress-Strain curves for PMR-15 specimens aged for 250 h at 302 °C in argon obtained in tensile tests to failure conducted at constant strain rates of $10^{-6}$ , $10^{-5}$ , $10^{-4}$ and $10^{-3} \text{ s}^{-1}$ at 288 °C. The dependence of the stress-strain behavior on the strain rate is evident.....	132
Figure 9.5 Stress-Strain curves for PMR-15 specimens aged for 250 h at 316 °C in argon obtained in tensile tests to failure conducted at constant strain rates of $10^{-6}$ , $10^{-5}$ , $10^{-4}$ and $10^{-3} \text{ s}^{-1}$ at 288 °C. The dependence of the stress-strain behavior on the strain rate is evident.....	132
Figure 9.6 Stress-strain curves for PMR-15 aged at 260 °C in argon obtained in tensile tests to failure conducted at 288 °C at constant strain rates of (a) $10^{-6} \text{ s}^{-1}$ and (b) $10^{-4} \text{ s}^{-1}$ . .....	134
Figure 9.7 Stress-strain curves for PMR-15 aged at 302 °C in argon obtained in tensile tests to failure conducted at 288 °C at constant strain rates of (a) $10^{-6} \text{ s}^{-1}$ and (b) $10^{-4} \text{ s}^{-1}$ . .....	135
Figure 9.8 Stress-strain curves for PMR-15 specimens aged for various durations in argon at 316 °C obtained in tensile tests to failure conducted at 288 °C and constant strain rate of $10^{-6} \text{ s}^{-1}$ . .....	137
Figure 9.9 Stress-strain curves for PMR-15 specimens aged for various durations in argon at 316 °C obtained in tensile tests to failure conducted at 288 °C and constant strain rate of $10^{-5} \text{ s}^{-1}$ . .....	137

Figure 9.10 Stress-strain curves for PMR-15 specimens aged for various durations in argon at 316 °C obtained in tensile tests to failure conducted at 288 °C and constant strain rate of $10^{-4} \text{ s}^{-1}$ .	138
Figure 9.11 Stress-strain curves for PMR-15 specimens aged for various durations in argon at 316 °C obtained in tensile tests to failure conducted at 288 °C and constant strain rate of $10^{-3} \text{ s}^{-1}$ .	138
Figure 9.12 Stress-strain curves for PMR-15 specimens aged for 250 h in argon at 260 °C obtained in tensile tests to failure conducted at 260 and 288 °C and constant strain rates of $10^{-4}$ and $10^{-6} \text{ s}^{-1}$ . The influence of test temperature on the deformation behavior is evident. Data at 260 °C from [20].	140
Figure 9.13 Stress-strain curves for PMR-15 specimens aged for 250 h in argon at 316 °C obtained in tensile tests to failure conducted at 288 and 316 °C and constant strain rates of $10^{-4}$ and $10^{-6} \text{ s}^{-1}$ . The influence of test temperature on the deformation behavior is evident. Data at 316 °C from [27].	141
Figure 9.14 Stress-strain curves for PMR-15 specimens aged for 50 h at 260, 274, 288, 302 and 316 °C Obtained in tensile tests to failure at constant strain rate $10^{-6} \text{ s}^{-1}$ . Data from [21] and [19] included.	143
Figure 9.15 Stress-strain curves for PMR-15 specimens aged for 50 h at 260, 274, 288, 302 and 316 °C Obtained in tensile tests to failure at constant strain rate $10^{-5} \text{ s}^{-1}$ . Data from [21] and [19] included.	143
Figure 9.16 Stress-strain curves for PMR-15 specimens aged for 50 h at 260, 274, 288, 302 and 316 °C Obtained in tensile tests to failure at constant strain rate $10^{-4} \text{ s}^{-1}$ . Data from [21] and [19] included.	144
Figure 9.17 Stress-strain curves for PMR-15 specimens aged for 50 h at 260, 274, 288, 302 and 316 °C Obtained in tensile tests to failure at constant strain rate $10^{-3} \text{ s}^{-1}$ . Data from [21] and [19] included.	144
Figure 9.18 Stress-strain curves for PMR-15 specimens aged for 100 h at 260, 274, 288, 302 and 316 °C Obtained in tensile tests to failure at constant strain rate $10^{-6} \text{ s}^{-1}$ . Data from [21] and [19] included.	145
Figure 9.19 Stress-strain curves for PMR-15 specimens aged for 100 h at 260, 274, 288, 302 and 316 °C Obtained in tensile tests to failure at constant strain rate $10^{-5} \text{ s}^{-1}$ . Data from [21] and [19] included.	145
Figure 9.20 Stress-strain curves for PMR-15 specimens aged for 100 h at 260, 274, 288, 302 and 316 °C Obtained in tensile tests to failure at constant strain rate $10^{-4} \text{ s}^{-1}$ . Data from [21] and [19] included.	146
Figure 9.21 Stress-strain curves for PMR-15 specimens aged for 100 h at 260, 274, 288, 302 and 316 °C Obtained in tensile tests to failure at constant strain rate $10^{-3} \text{ s}^{-1}$ . Data from [21] and [19] included.	146

Figure 9.22 Stress-strain curves for PMR-15 specimens aged for 250 h at 260, 274, 288, 302 and 316 °C Obtained in tensile tests to failure at constant strain rate $10^{-6} \text{ s}^{-1}$ . Data from [21] and [19] included.....	147
Figure 9.23 Stress-strain curves for PMR-15 specimens aged for 250 h at 260, 274, 288, 302 and 316 °C Obtained in tensile tests to failure at constant strain rate $10^{-5} \text{ s}^{-1}$ . Data from [21] and [19] included.....	147
Figure 9.24 Stress-strain curves for PMR-15 specimens aged for 250 h at 260, 274, 288, 302 and 316 °C Obtained in tensile tests to failure at constant strain rate $10^{-4} \text{ s}^{-1}$ . Data from [21] and [19] included.....	148
Figure 9.25 Stress-strain curves for PMR-15 specimens aged for 250 h at 260, 274, 288, 302 and 316 °C Obtained in tensile tests to failure at constant strain rate $10^{-3} \text{ s}^{-1}$ . Data from [21] and [19] included.....	148
Figure 9.26 Stress-strain curves for PMR-15 specimens aged for 500 h at 260, 274, 288, 302 and 316 °C Obtained in tensile tests to failure at constant strain rate $10^{-6} \text{ s}^{-1}$ . Data from [21] and [19] included.....	149
Figure 9.27 Stress-strain curves for PMR-15 specimens aged for 500 h at 260, 274, 288, 302 and 316 °C Obtained in tensile tests to failure at constant strain rate $10^{-5} \text{ s}^{-1}$ . Data from [21] and [19] included.....	149
Figure 9.28 Stress-strain curves for PMR-15 specimens aged for 500 h at 260, 274, 288, 302 and 316 °C Obtained in tensile tests to failure at constant strain rate $10^{-4} \text{ s}^{-1}$ . Data from [21] and [19] included.....	150
Figure 9.29 Stress-strain curves for PMR-15 specimens aged for 500 h at 260, 274, 288, 302 and 316 °C Obtained in tensile tests to failure at constant strain rate $10^{-3} \text{ s}^{-1}$ . Data from [21] and [19] included.....	150
Figure 9.30 Stress-strain curves for PMR-15 specimens aged for 1000 h at 274, 288, and 302 °C Obtained in tensile tests to failure at constant strain rate $10^{-6} \text{ s}^{-1}$ . Data from [21] and [19] included.....	151
Figure 9.31 Stress-strain curves for PMR-15 specimens aged for 1000 h at 274, 288, and 302 °C Obtained in tensile tests to failure at constant strain rate $10^{-5} \text{ s}^{-1}$ . Data from [21] and [19] included.....	151
Figure 9.32 Stress-strain curves for PMR-15 specimens aged for 1000 h at 274, 288, and 302 °C Obtained in tensile tests to failure at constant strain rate $10^{-4} \text{ s}^{-1}$ . Data from [21] and [19] included.....	152
Figure 9.33 Stress-strain curves for PMR-15 specimens aged for 1000 h at 274, 288, and 302 °C Obtained in tensile tests to failure at constant strain rate $10^{-3} \text{ s}^{-1}$ . Data from [21] and [19] included.....	152
Figure 9.34 Stress decrease vs. relaxation time for PMR-15 specimens aged for 50 h at various temperatures in the 260-316 °C range. Stress drop during relaxation of a fixed duration is independent of prior aging temperature. Data from [21] and [19] are included. ....	154

Figure 9.35 Stress decrease vs. relaxation time for PMR-15 specimens aged for 100 h at various temperatures in the 274-302 °C range. Stress drop during relaxation of a fixed duration is independent of prior aging temperature. Data from [21] and [19] are included. ....	155
Figure 9.36 Stress decrease vs. relaxation time for PMR-15 specimens aged for 250 h at various temperatures in the 260-302 °C range. Stress drop during relaxation of a fixed duration is independent of prior aging temperature. Data from [21] and [19] are included. ....	156
Figure 9.37 Stress decrease vs. relaxation time for PMR-15 specimens aged for 500 h at various temperatures in the 274-302 °C range. Stress drop during relaxation of a fixed duration is independent of prior aging temperature. Data from [21] and [19] are included. ....	157
Figure 9.38 Stress decrease vs. relaxation time for PMR-15 specimens aged for 1000 h at various temperatures in the 274-302 °C range. Stress drop during relaxation of a fixed duration is independent of prior aging temperature. Data from [21] and [19] are included. ....	158
Figure 9.39 Stress decrease vs. relaxation time for PMR-15 specimens aged for various durations at 260 °C. Stress drop during relaxation of a fixed duration is independent of prior aging time. ....	159
Figure 9.40 Stress decrease vs. relaxation time for PMR-15 specimens aged for various durations at 274 °C. Stress drop during relaxation of a fixed duration is independent of prior aging time. Data from [21] are included. ....	160
Figure 9.41 Stress decrease vs. relaxation time for PMR-15 specimens aged for various durations at 302 °C. Stress drop during relaxation of a fixed duration is independent of prior aging time. ....	161
Figure 9.42 Comparison of percent weight loss for PMR-15 neat resin aged in argon at 260, 274, 288, 302 and 316 °C. Data at 260 °C from [20]. Data at 274 °C from [21]. Data at 288 °C from [22]. Data at 316 °C from [27]. ....	163
Figure 10.1 Flowchart showing the systematic characterization procedure for VBOP model parameters. ....	170
Figure 10.2 Flowchart showing detail of the enhanced systematic characterization procedure for VBOP model parameters. Validation steps omitted for clarity. ....	172
Figure 10.3 Evolution of applied and equilibrium stresses during (a) prior loading and (b) relaxation. VBOP predicts the applied stress will eventually catch up with the equilibrium stress and the relaxation will terminate. ....	177
Figure 10.4 Evolution of applied and equilibrium stresses during creep. VBOP predicts that during positive creep, the equilibrium stress will increase until the equilibrium stress equals the flow stress and the overstress becomes zero at which time creep will cease. ....	179

Figure 10.5 Schematic showing typical creep strain versus time curve obtained during McLean type dip tests conducted during this effort. Creep strain rate reversal is apparent. Note the initial negative and then positive creep strain rates are very small and can be approximated with $\dot{\epsilon} = 0$ .	184
Figure 10.6 Experimental results obtained for PMR-15 polymer during three McLean type dip tests consisting of monotonic loading at $10^{-6} \text{ s}^{-1}$ to 4.5 % strain followed by stress dip at 150 MPa/s and creep at 23.6, 28.1 and 32.1 MPa at 274 °C. Creep strain rate reversal was observed at 28.1 MPa and at 32.1 MPa. The creep test at 32.1 MPa produced only a small amount of negative creep prior to creep strain rate reversal suggesting that the applied stress and the equilibrium stress were equal.	187
Figure 10.7 Creep curve pertaining to the MTDT with the creep stress of 32.1 MPa shown in Figure 10.6. Very slight negative creep is followed by creep strain rate reversal. Creep strain rate during first 200 seconds can be approximated with $\dot{\epsilon} = 0$ indicating the applied stress and the equilibrium stress are equal.	188
Figure 10.8 Experimental results obtained for PMR-15 polymer during two McLean type dip tests consisting of monotonic loading at $10^{-6} \text{ s}^{-1}$ to 5 % strain followed by stress dip at 150 MPa/s and creep at 9.1 and 11.7 MPa at 302 °C. Creep strain rate reversal was observed at 9.1 MPa and at 11.7 MPa. The creep test at 11.7 MPa produced only a small amount of negative creep prior to creep strain rate reversal suggesting that the applied stress and the equilibrium stress were equal.	190
Figure 10.9 Creep curve pertaining to the MTDT with the creep stress of 11.7 MPa shown in Figure 10.8. Very slight negative creep is followed by creep strain rate reversal. Creep strain rate during first 200 seconds can be approximated with $\dot{\epsilon} = 0$ indicating the applied stress and the equilibrium stress are equal.	191
Figure 10.10 Experimental results obtained for PMR-15 polymer during monotonic loading at $10^{-6} \text{ s}^{-1}$ to 4.5 % strain followed by relaxation for 15 h at 274 °C. Relaxation terminated at the stress of 25.6 MPa.	193
Figure 10.11 Experimental results obtained for PMR-15 polymer during monotonic loading at $10^{-6} \text{ s}^{-1}$ to 5 % strain followed by relaxation for 15 h at 302 °C. Relaxation terminated at the stress of 8 MPa.	194

## List of Tables

Table 1.1 Air Force Research Laboratory Free Standing Post Cure Cycle for PMR-15 Neat Resin. ....	4
Table 6.1 Comparison of the Average Room Temperature Elastic Moduli of PMR-15 Neat Resin Measured by Various Researchers [19-21, 27].....	73
Table 8.1 VBOP Parameters for PMR-15 Neat Resin Subjected to Mechanical Loading at 274 °C .....	90
Table 8.2 VBOP Parameters for PMR-15 Neat Resin Subjected to Mechanical Loading at 288 °C .....	93
Table 8.3 VBOP Parameters for PMR-15 Neat Resin Subjected to Mechanical Loading at 302 °C .....	98
Table 8.4 Summary of the VBOP Parameters Dependent on Test Temperature for PMR-15 Neat Resin at Various Temperatures.....	101
Table 8.5 Summary of VBOP Parameters Calculated Utilizing the Augmented VBOP .....	107
Table 8.6 Calculated VBOP Parameters for PMR-15 Neat Resin Subjected to Mechanical Loading at 316 °C.....	121
Table 10.1 Comparison of the Isotropic Stress Calculated from the Equilibrium Stress Obtained during Relaxation and McLean Type Dip Tests at 274 and 302 °C.....	194
Table 12.1 Cross-Reference of Experimental Data Obtained During Monotonic Tensile Tests to Failure of Unaged PMR-15 at Various Elevated Temperatures and Strain Rates.....	198
Table 12.2 Cross-Reference of Experimental Data Obtained During Relaxation Following Monotonic Loading of Unaged PMR-15 at Various Elevated Temperatures and Strain Rates.....	199
Table 12.3 Cross-Reference of Experimental Data Obtained During Creep Following Monotonic Loading of Unaged PMR-15 at Various Elevated Temperatures and Strain Rates.....	199
Table 12.4 Cross-Reference of Experimental Data Obtained During Monotonic Tensile Tests to Failure of PMR-15 Aged for 50-250 h at Elevated Temperature .....	200
Table 12.5 Cross-Reference of Experimental Data Obtained During Monotonic Tensile Tests to Failure of PMR-15 Aged for 500-1000 h at Elevated Temperature .....	201
Table 12.6 Cross-Reference of Experimental Data Obtained During Relaxation Following Monotonic Loading of PMR-15 Aged for Various Durations at Elevated Temperature .....	202





## List of Symbols

<b>Symbol</b>	<b>Definition</b>
$\Gamma$	overstress invariant
$\varepsilon$	strain
$\dot{\varepsilon}^{el}$	elastic strain rate
$\dot{\varepsilon}^{in}$	inelastic strain rate
$\eta$	viscosity constant
$\sigma$	stress
$\Psi$	shape function
$A$	isotropic stress
$A_f$	saturated value of isotropic stress
$C_1, C_2, C_3$	shape function parameters
$E$	modulus of elasticity
$E_t$	tangent modulus
$f$	kinematic stress
$g$	equilibrium stress
$h$	hours
$k$	viscosity function
$k_1, k_2, k_3$	viscosity function parameters
$T_g$	glass transition temperature
$t$	time
$t_a$	prior aging time
$s$	seconds
$a$	modulus ratio

Superscript dot means it is a time derivative (i.e.  $\dot{\varepsilon}$  is strain rate)



## List of Abbreviations

### Abbreviation

AFIT	Air Force Institute of Technology
DMA	dynamic mechanical analysis
FEM	finite element method
h	hours
HDPE	high-density polyethylene
HTPMCs	high-temperature polymer matrix composites
MTDT	McLean type dip test
PC	polycarbonate
PEEK	polyetheretherketone
PEI	polyetherimide
PES	polyethersulfone
PET	polyethylene-terephthalate
PMR-15	Polymerization of Monomeric Reactants-15
PMMA	poly(methyl methacrylate)
POM	polyoxymethylene
PP	polypropylene
PPO	polyphenylene oxide
s	seconds
SCFH	standard cubic feet per hour
SLS	standard linear solid

## **List of Abbreviations (Continued)**

### **Abbreviation**

SRJT	strain rate jump test
VBO	Viscoplasticity Based on Overstress
VBOP	Viscoplasticity Based on Overstress for Polymers

# **THE EFFECT OF ELEVATED TEMPERATURE ON THE INELASTIC DEFORMATION BEHAVIOR OF PMR-15 SOLID POLYMER**

## **1 Introduction**

### **1.1 Motivation**

High-temperature polymer matrix composites (HTPMCs) are increasingly being used in a variety of load bearing applications. Before HTPMCs can be widely used in high-temperature aerospace applications, their long-term durability and structural integrity must be assured. To provide that assurance, experimentally-based, durability-driven design and life prediction methodologies must be developed. To analyze or predict the service life of the composite structure subjected to mechanical loading, high temperature and varying environmental factors such as moisture, it is necessary to account for complex thermo-mechanical behaviors taking place in the composite constituents. The damage evolution, aging and thermo-oxidative processes occurring in the fibers, matrix, and at the fiber-matrix interface must be addressed. Whereas carbon fibers may be more resistant to oxidation, the time-dependent processes in the composite matrices and at the fiber-matrix interface are critical to the evolution of damage and failure of the composite. Thorough understanding of polymer aging and thermal mechanisms and their effects on the mechanical properties and deformation behavior of the polymer matrix is essential. Constitutive models that account for the effects of thermal aging and degradation on the behavior of the matrix material are vital to accurate prediction of service life and performance of HTPMC structural components.

Research at the Air Force Institute of Technology (AFIT) demonstrated that various polymer matrix materials exhibit rate-dependent behavior at elevated temperatures that is not well represented by the nonlinear viscoelastic constitutive model of Schapery [1-4]. The substantial effects of loading rate on material behavior are better represented by rate-dependent viscoplasticity.

A variety of viscoplastic models which account for some of this deformation behavior exist. Although originally developed to describe the behavior of metals, Viscoplasticity Based on Overstress (VBO) has been demonstrated to account for some aspects of the deformation behavior of polymers [5-16, 16, 17]. VBO was further specialized to better represent the mechanical behavior of polymers. This specialization of VBO is called Viscoplasticity Based on Overstress for Polymers (VBOP) [9, 12-14, 18].

Recent efforts at AFIT have produced a consistent, experimentally based model characterization procedure for VBOP [19]. Additionally, experiments with Polymerization of Monomeric Reactants-15 (PMR-15) neat resin revealed the need for a predictive model that was capable of representing the rate-dependent deformation response of this material at various elevated temperatures as well as of accounting for the effects of prior thermal aging at various temperatures on the inelastic material behavior of PMR-15 [20, 21]. Researchers at AFIT extended VBOP to represent the effects of prior isothermal aging at 288 °C in argon on inelastic deformation behavior of the PMR-15 polyimide [19]. Several VBOP model parameters were made dependent on prior aging time and the resulting model was used to predict the high-temperature behavior of PMR-15 polymer subjected to prior aging of various durations. However, this extension

of VBOP does not represent the effects of test temperature or prior aging temperature on the inelastic behavior. The present research aims to develop these capabilities in order to extend the constitutive model such that it could be employed by designers to predict the high temperature behavior of PMR-15 at temperatures throughout its operationally relevant range. Additionally, a better understanding of how elevated temperature affects aging would only serve to enhance service life prediction methodologies.

## 1.2 Material Description

This research will focus on the elevated temperature behavior of PMR-15, a high-temperature polymer matrix material developed by NASA in the 1970's and commonly used as a matrix material in HTPMCs. This highly cross-linked polyimide resin was specifically designed for use at temperatures that approach its glass transition temperature ( $T_g$ ) for long periods of time. The PMR-15 solid polymer is a thermosetting polyimide with a  $T_g$  of  $\sim 347$  °C (the exact  $T_g$  depends on processing) [22] and a long-term use temperature of 288 °C [23]. A schematic of the molecular structure of PMR-15 is shown in Figure 1.1. The post-cured PMR-15 neat resin material was supplied by HyComp, Inc. (Cleveland, Ohio). The material was cured in accordance with the Air Force Research Laboratory freestanding post-cure cycle shown in Table 1.1.

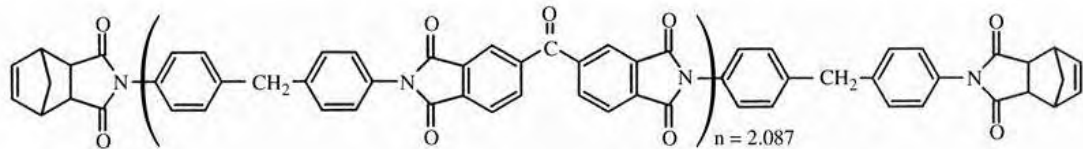


**Figure 1.1 Molecular structure of PMR-15. Figure from [24].**

**Table 1.1 Air Force Research Laboratory Free Standing Post Cure Cycle for PMR-15 Neat Resin.**

Step	Description
1	Heat to 204 °C in 2 h and hold for 1-h
2	Heat to 260 °C in 1 h and hold for 1-h
3	Heat to 316 °C in 2 h and hold for 16-h
4	Cool to room temperature at a rate of 1 °C/min

### 1.2.1 Micromechanical Mechanisms of Polymer Deformation

According to Sperling [25], the study of polymeric mechanical behavior involves the interrelationship of elasticity, flow and molecular motion. While the exact molecular nature of the deformation behavior of PMR-15 is unknown, it is instructive to review some of the known causes of time-dependent deformation in polymers. These can be grouped into four general categories:

1. *Chain scission.* A reduction in macroscopic stiffness can be observed when bonds making up the polymeric backbone are broken.
2. *Bond interchange.* Bonds between neighboring chains are interchanged or rearranged such that stress is reduced or elongation is experienced
3. *Viscous flow.* Polymeric chains in close proximity slip past one another
4. *Theron relaxation.* Entangled crosslinks slither past or around one another in a snake like motion

While the current research will focus on a phenomenological approach to the modeling of the high-temperature deformation behavior of PMR-15, cognizance of the typical micromechanical mechanisms of polymer deformation serves to provide additional confidence in the resulting model.



### *1.2.2 Polymer Degradation*

In addition to understanding the rate-dependent deformation behavior of polymers at elevated temperatures, one must also understand the mechanical stability of the material as it ages. In a high-temperature environment, the chemical bonds that make up a polymer begin to break down in a process called pyrolysis. This process is independent of environment and generally occurs rapidly when a polymer is exposed to temperatures in excess of the glass transition temperature. Pyrolysis also occurs at lower temperatures albeit at a slower rate. Chain scission and additional crosslinking typically occur in conjunction with the pyrolysis of thermoset polymers. A combination of these processes causes changes in the mechanical behavior of the polymer over time. These changes in behavior are known as pyrolytic aging. In PMR-15, C-N and then C-C bonds break during pyrolysis. As molecules cleave and vaporize, and as new crosslinks are formed, the material loses weight, and becomes stiffer and more brittle.

Pyrolysis is not the only mechanism that can change the mechanical properties of polymers over a period of time. Varieties of oxidative degradation mechanisms are known. Thermo-oxidative degradation of a polymer involves the exposure of the polymer to high temperatures in the presence of oxygen. Thermo-oxidative stability of polymers has been an area of intense research and in many cases, thermo-oxidative degradation has been found to have significant influence on mechanical properties of polymers. In the case of PMR-15, an oxidized damaged layer forms on the outer surface of the specimen after a relatively short exposure to high temperature. The mechanical properties of this layer are dramatically different from those of the bulk material. Bowles [26] concluded that the rate of diffusion of O<sub>2</sub> into the polymer controlled the rate

of oxidative degradation of PMR-15. Additionally, the oxidized layer itself served as a diffusion barrier, limiting the thickness of the oxidized layer to 0.17 mm regardless of the aging temperature for aging durations up to 4000 h.

### **1.3 Problem Statement**

Previous experimental investigations suggest that the deformation behavior of PMR-15 is dependent on test temperature [19, 20, 27]. The VBOP was shown to qualitatively represent the rate dependent behaviors of polymers observed in experiments at elevated temperature but does not explicitly consider test temperature [28]. The VBOP model in its present form must be characterized at each temperature of interest to provide quantitatively accurate predictions at that temperature. Additionally, while the effect of prior aging duration is well known, the effect of prior aging temperature is not well understood. The VBOP extended to represent the effects of prior isothermal aging does not represent the effects of prior aging temperature on the inelastic behavior of PMR-15.

The objective of this effort is two-fold. First, the effects of elevated test temperature on the deformation behavior of PMR-15 neat resin will be investigated experimentally. Based on the results of this experimental study, the VBOP constitutive model is augmented to account for the effects of test temperature on the time-dependent deformation response of PMR-15. Second, the effects of prior aging temperature on the deformation behavior of PMR-15 solid polymer are investigated experimentally. Based on the experimental findings additional modifications to the VBOP may be implemented. The resulting viscoplastic constitutive model will enable designers and analysts to

accurately predict service life and assure structural integrity and environmental durability of HTPMCs in high-temperature aerospace applications.

The following problem statement summarizes the objectives of this research:

*Experimentally determine the temperature range where PMR-15 exhibits viscoplastic deformation behavior and identify the effects of test temperature on that deformation behavior. Develop an analytical capability within the VBOP to account for the effects of test temperature on the inelastic behavior of PMR-15. Demonstrate that the developed constitutive model is capable of representing the observed behaviors. Elucidate the key features of the deformation behavior of the PMR-15 polymer subjected to prior aging in argon at various temperatures. Identify the phenomenological indicators of aging from experimental results. Assess the implications for constitutive modeling.*

#### **1.4 Dissertation Outline**

Chapter 2 gives a detailed review of prior work focusing on experimental investigation of the deformation behavior of polymers at elevated temperatures and the effects of prior aging. Additionally, the viscoelastic and viscoplastic models that led to the current research are discussed. In Chapter 3 the theoretical development of the proposed constitutive framework is traced from the governing equations of the Standard Linear Solid (SLS), through the development of VBO, VBOP and ultimately the extension of VBOP to account for the effect of prior aging time. Chapter 4 discusses additional details regarding the test material. In addition, specific details of the experimental equipment and the experimental methods that were employed to characterize the constitutive model and explore the effects of (1) constant test temperature and (2) prior aging temperature on deformation behavior are considered.

Chapter 5 presents the existing model characterization procedure and details the strategy utilized for determining the effects of test temperature and prior aging temperature on the deformation behavior of polymers. Chapter 6 is devoted to the experimental observations of unaged PMR-15 tested at various elevated temperatures. Chapter 7 discusses the implications for modeling the test temperature dependence of the material behavior. Chapter 8 is devoted to the modeling of the effects of test temperature on the inelastic behavior of PMR-15. This chapter also includes a detailed validation of the augmented model. Chapter 9 focuses on the experimental observations of the effects of prior aging temperature and the implications for modeling. Chapter 10 discusses an enhanced procedure to assist in the characterization of the VBOP model. Suggestions for future research as well as concluding remarks are offered in Chapter 11.

## 2 Background: Experimental Investigations and Constitutive Modeling

The purpose of this chapter is to describe the experimental investigations and constitutive modeling efforts that preceded the current research. The following provides the foundation upon which this effort is built.

### 2.1 Experimental Investigations

According to Krempl, “*our understanding of the mechanical behavior of materials is intimately connected with the capabilities of the equipment which we use to test the material. Our knowledge of material behavior in turn contributed to the theory which in turn stimulates ideas about new experiments, at which point, the cycle starts over again*” [29]. Any attempt to produce a phenomenological constitutive model rightfully begins with experimental investigation aimed at precisely determining the behavior that is to be modeled. This section describes some experiments with polymers, the conditions under which they were performed and the observed material response. The following section will describe the evolution of several constitutive models based (at least partially) on these observations.

#### 2.1.1 Deformation Behavior of Polymers

This section discusses some of the unique deformation behaviors of polymers. Both room temperature and elevated temperature effects are examined.

##### 2.1.1.1 Various Polymers

Kitagawa and Matsutani [30] conducted uniaxial compression experiments on Polypropylene (PP) rods at 15, 25 and 40 °C. In these tests, they observed that the initial

slope of the stress-strain curve does not depend on strain rate but at higher strains, the stress-strain curves are sensitive to strain rate and stress-strain curves produced at different strain rates are parallel to each other. It is important to note that engineering alloys exhibit similar mechanical behavior. Kitagawa and Matsutani also examined more complex strain histories and found that an instantaneous change in strain rate caused the change in stress such that the stress-strain curve characteristic for the given strain rate was reached. Additionally, Kitagawa and Matsutani performed relaxation tests of fixed duration starting at various points along the monotonic stress-strain curve. Results demonstrated that the stress values reached at the end of the relaxation tests were independent of the stress and strain at the beginning of the relaxation test. Furthermore, the points at the end of the relaxation tests appeared to form a curve that had a shape of a stress-strain diagram. The authors suggested that this was evidence that an equilibrium stress-strain curve existed, which corresponded to the stress-strain curve produced at a very slow strain rate. In tests with Poly(methyl methacrylate) (PMMA), amorphous Polycarbonate (PC) and Polyoxymethylene (POM) at 25 °C, Kitagawa and coworkers [31] reported an interesting rate reversal behavior during unloading. Kitagawa et al found that the stress (strain) rate might change signs during relaxation (creep) when performed on the unloading path.

Bordonaro [5] examined the mechanical behaviors of Nylon-66, polyetheretherketone (PEEK) and polyetherimide (PEI). Tests were conducted in both stress and strain control. Bordonaro confirmed that the rate reversal behavior on the unloading path that Kitagawa observed with PMMA and POM was also seen for Nylon-66, PEEK and PEI. Additionally, Bordonaro's results revealed several differences

between the mechanical response of engineering alloys and solid polymers. In the case of Nylon-66 tested at various strain rates, the stress-strain curves appeared to merge as the strain increased. In addition, Nylon-66, PEEK and PEI demonstrated higher relaxation rates than commonly found for engineering alloys. Finally, each of the polymers tested exhibited nonlinear (curved) unloading behavior. The slope of the unloading curve was found to be independent of strain rate while the initial stress level upon unloading affected the amount of strain recovered by shifting the unloading curves left or right. The significant amount of strain recovered after unloading to zero stress was affected by the prior unloading rate and the strain at the start of the recovery period.

Khan [11] built on Bordonaro's work and examined the deformation behavior of a variety of polymers: PC, Nylon-66, high-density polyethylene (HDPE), polyethylene-terephthalate (PET), polyethersulfone (PES) and polyphenylene oxide (PPO). Khan discovered that there was no difference in the qualitative nature of the deformation behavior of amorphous polymers (PC, PPO and PES) and crystalline polymers (Nylon-66, HDPE and PET). Additionally, Khan reported that for each of the materials:

- Positive nonlinear rate sensitivity was observed during loading
- Creep, relaxation and recovery responses were profoundly influenced by prior loading rate
- The stress drop in a relaxation test was independent of the stress and strain at the beginning of the relaxation test
- Reversal of stress (strain) rate was observed in relaxation (creep) test performed during unloading. This phenomenon is referred to as "rate reversal."

Together, the work of Kitagawa and Matsutani, Bordonaro and Khan provides strong evidence that a consistent, phenomenologically based constitutive model could be used to represent the deformation behavior of polymers. Each of these researchers examined the capability of the existing Viscoplasticity Theory Based on Overstress (VBO) [5, 6, 11, 30, 31] to represent the deformation behavior of polymers. They concluded that VBO, which was created to model the behavior of engineering alloys, could also represent some of the features of the inelastic behavior of solid polymers. Khan [11] noted that the curved unloading and rate reversal were beyond the capabilities of VBO. Specific details of the VBO model are developed in Section 2.2.2.1.

#### *2.1.1.2 PMR-15 – Stress-Controlled Experiments and Modeling at AFIT*

A considerable amount of research on the time-dependent behavior of PMR-15 has been conducted at AFIT. Westberry [4] investigated the behavior of PMR-15 at 23 and 288 °C. The effects of loading rate on monotonic stress-strain, creep and recovery behaviors were examined in stress-controlled experiments. Falcone and Ruggles-Wrenn [1, 2] investigated the mechanical response at 288 °C in stress control and characterized Schapery's nonlinear viscoelastic model using creep and recovery tests at 288 °C.

##### *2.1.1.2.1 Stress-Controlled Experiments at Room Temperature*

Westberry [4] conducted experiments at three different loading rates (0.75, 0.075 and 0.0075 MPa/s) at 23 °C and concluded that PMR-15 exhibits nonlinear rate sensitivity during monotonic loading. Westberry's monotonic loading results are reproduced in Figure 2.1. Clearly, the stress-strain curve has almost no dependence on rate in the quasi-elastic region, but has significant nonlinear rate dependence in the



inelastic region. Westberry also conducted creep tests with various prior stress rates and found that creep behavior showed little if any effect of prior stress rate at 23 °C. In stepwise creep tests, creep was observed in the quasi-elastic region for all prior stress rates. Increased stress generally resulted in increased creep strain accumulation except in certain cases in the inelastic region that Westberry attributed to the effect of overstress (discussed in more detail in Section 3.2).

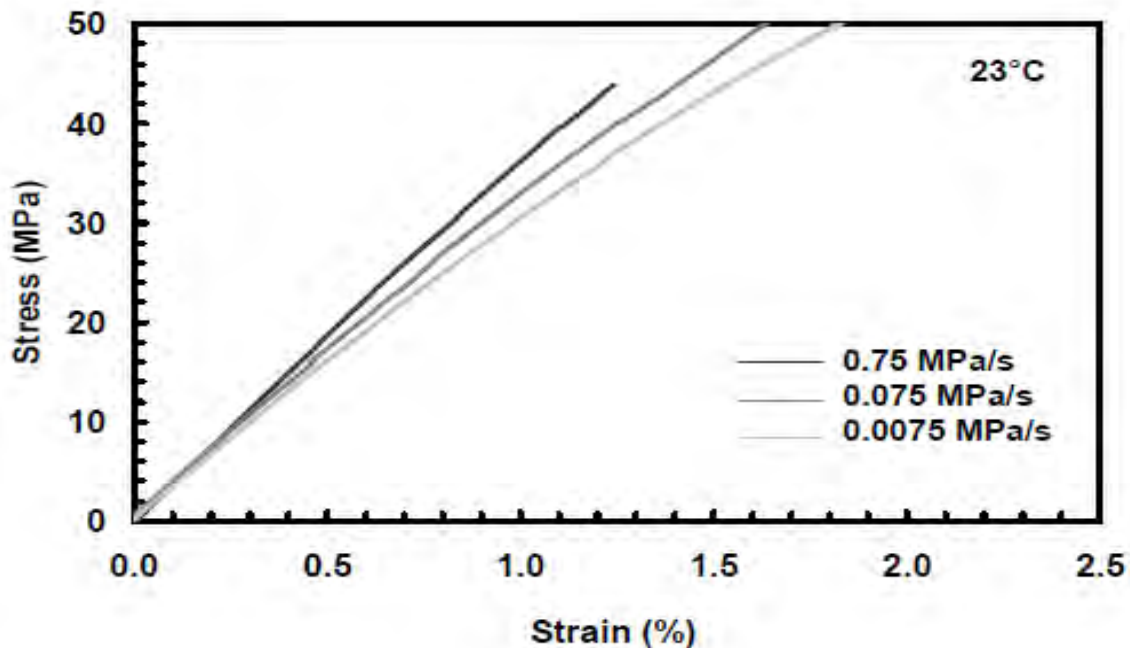


**Figure 2.1 Stress-strain curves for PMR-15 neat resin obtained at three different stress rates at 23 °C. Nonlinear rate sensitivity is apparent. Reproduced from [4].**

#### *2.1.1.2.2 Stress-Controlled Experiments at Elevated Temperature*

Falcone and Ruggles-Wrenn [1] conducted additional stress-controlled experiments on PMR-15 at 288 °C. The effect of stress rate on the stress-strain behavior during both loading and unloading at elevated temperature is clearly seen in Figure 2.2 reproduced from Falcone and Ruggles-Wrenn [1]. In contrast to Westberry's results

obtained at 23 °C, Falcone and Ruggles-Wrenn found that creep behavior at 288 °C was strongly influenced by prior stress rate. The creep response of PMR-15 at 288 °C is reproduced in Figure 2.3 from [1]. Also of note, both Westberry, and Falcone and Ruggles-Wrenn observed negative creep and strain rate reversal during creep on the unloading path at 288 °C as previously described for other polymers in Section 2.1.1.1. An example of this phenomenon is shown in Figure 2.4 reproduced from [1]. Based on a series of creep and recovery tests conducted at 288 °C, Falcone [2] characterized Schapery's nonlinear viscoelastic model and employed the model to predict the response of PMR-15 under monotonic loading/unloading and multistep load histories. The model was generally capable of qualitatively predicting the nonlinear behavior of the PMR-15 polymer at 288 °C, but predictions were not quantitatively accurate. Most importantly, the model was unable to account for rate effects.

### *2.1.2 Prior Aging – Effects on Mechanical Behavior*

Lemaitre [32] identifies aging as a process that occurs when the characteristic properties of a material change with time. The effects of aging are determined by comparing responses to characteristic tests on identical specimens before and after waiting a prescribed period of time. Krempl [33] noted that the microstructural changes that affect the phenomenological response of a material under test could have two separate causes. Diffusion induced changes occur with time and are caused by chemical reactions. These reactions can be within the material itself or may involve an interaction with an aggressive environment. Deformation can also be a cause of microstructural changes such as changes in dislocation density, which can alter the mechanical response

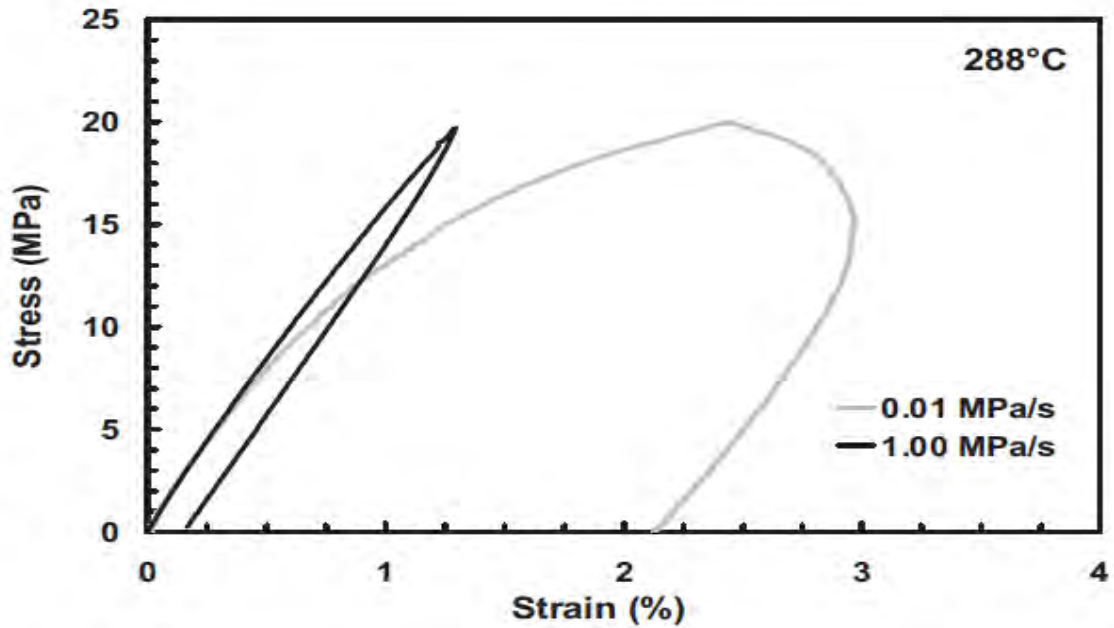


Figure 2.2 The influence of loading rate on the loading and unloading behavior of PMR-15 at 288 °C. The nonlinear rate sensitivity and curved unloading are apparent. Reproduced from [1].

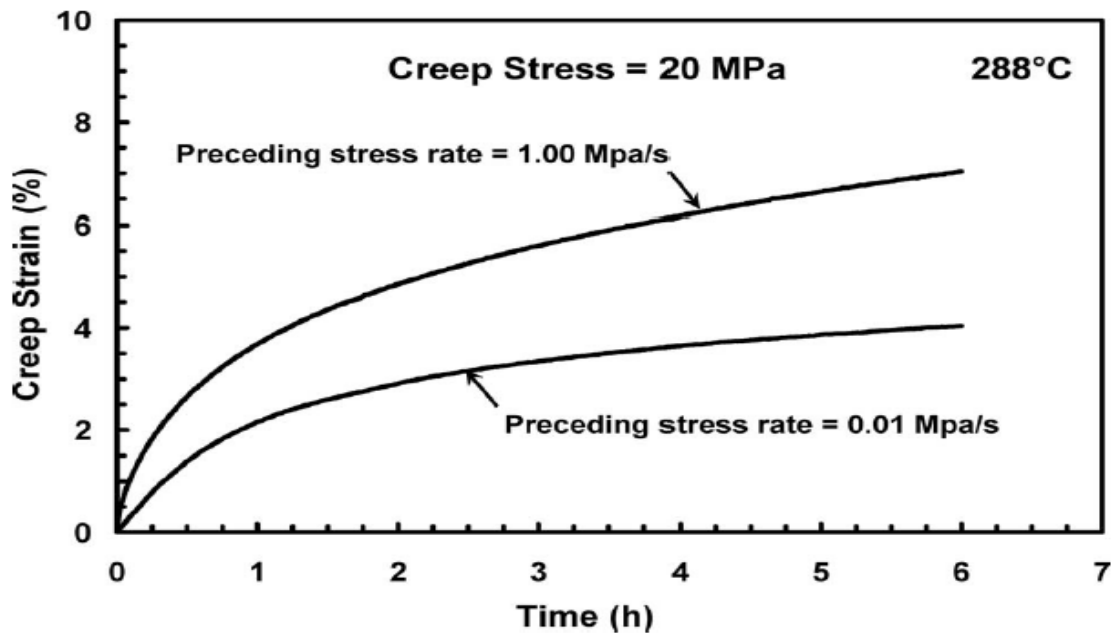
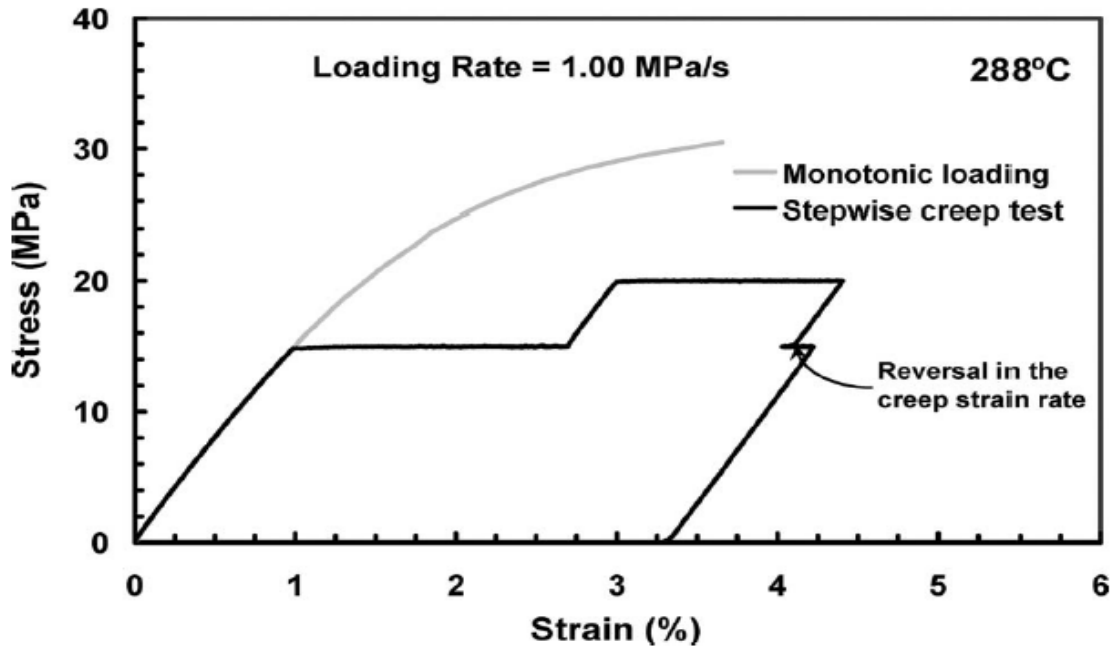


Figure 2.3 Creep strain versus time at 20 MPa and 288 °C. Effect of prior stress rate on creep strain is apparent. Creep strain increases nonlinearly with prior loading rate. Reproduced from [1].



**Figure 2.4 Stress controlled test with intermittent creep periods of 1 h duration at 288 °C. A reversal in the creep strain rate is observed during unloading. Reproduced from [1].**

of the material. Thus, aging can be the result of simply time passing or the result of a certain deformation history occurring over a period of time. Both of these phenomena appear to meet Lemaitre’s definition of aging. To minimize confusion we must be more specific when we utilize the word “aging.” For the purposes of this research, the term “prior aging” will be defined to mean mechanical property/behavior changes induced by exposure to elevated temperature prior to deformation.

While there may be other mechanisms that cause aging in a given material prior to loading, we are most interested in the pyrolytic aging of PMR-15. This is not an arbitrary choice of subject matter. PMR-15 was specifically developed to be employed at elevated temperatures and pyrolytic aging is known to occur at those temperatures [26]. Note that this definition specifically excludes strain aging (property changes induced by

deformation) or oxidative aging (property changes induced by exposure to oxygen at elevated temperature). An inert environment (argon) was used during the aging process to virtually eliminate the occurrence of thermo-oxidative aging. Additionally, we note that pyrolytic aging is necessarily a broad term. We do not attempt to discern the specific micromechanical mechanism(s) that cause the pyrolytic aging phenomenon. Whether those mechanisms are the formation, deformation or breaking of crosslink bonds, chain scission or some other interaction at the molecular level, the goal of this research is to develop a phenomenological approach that is independent of the specific polymer chemistry. What is important is the general class of behavior that is observed and how that can be modeled within the chosen constitutive framework.

Ruggles and Krempl [34] investigated the effect of prior aging on AISI Type 304 stainless steel. No qualitative effect of prior aging was observed. Quantitatively though, increased prior aging time resulted in increased flow stress values. The material was aged by submitting it to a precipitation treatment at 650° C for 0, 200 and 2000 h, which served to increase the degree of precipitation over time. Although the prior aging of AISI Type 304 stainless steel was accomplished via a different mechanism than prior aging of PMR-15, this work serves to establish the method for observing the effects of prior aging.

Ruggles-Wrenn and Broeckert [35] examined the effects of prior aging on PMR-15 in air and in argon at 288 °C. Ruggles-Wrenn and Broeckert found that prior isothermal aging increased the elastic modulus and decreased the material's capacity to accumulate creep strain. The difference between aging in air and in argon environments had little effect on creep and recovery behavior. Conversely, aging in air dramatically decreased tensile strength. The glass transition temperature reportedly increased from ~330 °C to

~336 °C after 1000 h in either environment. A visibly damaged surface layer was observed for PMR-15 aged in air. The authors attributed the increase in glass transition temperature to increased crosslink density, which was caused by pyrolytic aging that occurred due to exposure in both the air and argon environments. The decreased tensile strength found in specimens aged in air was attributed to the oxidized surface layer, which provided a crack initiation site and promoted early failure.

McClung and Ruggles-Wrenn [36] continued to investigate the effects of prior aging in argon on mechanical behavior of PMR-15. McClung and Ruggles-Wrenn concluded that the time-dependent mechanical behavior of PMR-15 is strongly influenced by prior aging at 288 °C. McClung and Ruggles-Wrenn noted that not only did the elastic modulus increase with prior aging time, but the departure from quasi-linear behavior was also delayed. Inelastic flow stresses and the tangent modulus increased with prior aging time as well. Additionally, prior aging decreased the material's capacity for inelastic straining. Notably, relaxation response was not affected by prior aging. Finally, for specimens aged for 2000 h tensile strength was significantly diminished.

More recently, Ozmen [27] evaluated the effects of prior aging at 316 °C on the inelastic behavior of PMR-15 at 316 °C. Specimens aged for more than 50 h in argon typically exhibited only quasi-linear behavior until failure. PMR-15 specimens aged for more than 50 h showed a decreased ultimate tensile strength, little or no capacity for inelastic straining and failed prematurely. Diedrick [20] conducted tests to assess the effects of prior aging at 260 °C on the inelastic behavior of PMR-15 at 260 °C. Diedrick noted that as was the case with aging at 288 and 316 °C the modulus of elasticity increased with prior aging duration at 260 °C. Diedrick also reported that PMR-15

becomes more brittle with increasing prior aging time. Wahlquist [21] assessed the effects of prior aging at 274 °C on the inelastic behavior of PMR-15 at 288 °C. Wahlquist found the effects of prior aging at 274 °C to be qualitatively and quantitatively similar to those of prior aging at 288 °C.

## **2.2 Constitutive Modeling**

With the material response to a given forcing function duly recorded during a series of experiments, the relationships between the forcing functions and the response functions are obtained. From these relationships, the constitutive equations are synthesized. First, material properties and behaviors are simplified and idealized. Then, the forms of the constitutive equations are chosen. Finally, the constitutive equations are used to predict the response to an untested forcing function and the constitutive equations are critically evaluated and possibly modified. This section will review several constitutive models that have been applied to high-temperature polymers, and will demonstrate the evolution of the current formulation of VBOP.

### *2.2.1 Viscoelastic Constitutive Models*

Although plasticity is usually considered separate from viscoelasticity, it can be shown that the viscoplastic constitutive equations that will be used in this research originate with the standard linear solid (SLS) of viscoelasticity [37]. For this reason, it is useful to examine some of the related viscoelastic constitutive models.

Viscoelasticity is best understood when compared to simple linear elastic behavior. Examples of linear elastic behavior and viscoelastic behavior are shown in Figure 2.5. Linear elastic materials load and unload along the same path and return to

zero strain when unloaded to zero stress. Viscoelastic materials do not necessarily unload along the loading path and do not immediately return to zero strain when unloaded to zero stress. Viscoelastic materials though, do return to zero strain if they are given enough time at zero stress [38].

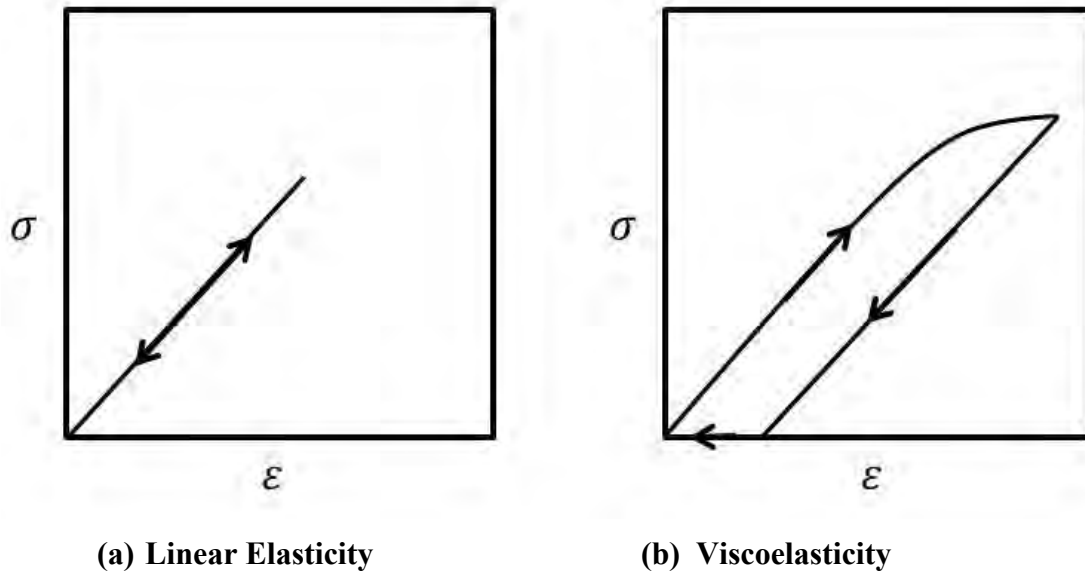


**Figure 2.5 (a) Linear elastic and (b) viscoelastic stress-strain behaviors. Viscoelastic material exhibits a nonzero strain upon unloading to zero stress and recovers this strain if given time to do so.**

Various formulations of viscoelastic models are possible and they are generally categorized as integral or differential models. In the following sections, several viscoelastic models will be briefly discussed before we move on to viscoplastic models in Section 2.2.2.

#### 2.2.1.1 An Integral Model (Nonlinear Viscoelastic Model of Schapery)

Schapery's nonlinear viscoelastic model [39] is an example of a widely used integral model. It was developed in an attempt to model the behavior of polymeric



materials beyond the linear response range. This is critical for polymeric materials, because the linear range is often quite small compared to the total range available prior to fracture. This model's popularity likely stems from the straightforward, systematic approach prescribed by the author to characterize the model. Although Schapery's model was developed from empirical relations, it was later shown to be consistent with thermodynamics [40].

For the uniaxial case, the nonlinear governing equation of Schapery's model is

$$\epsilon(t) = g_0 D_0 \sigma + g_1 \int_{0-}^t \Delta D(\psi - \psi') \frac{dg_2 \sigma}{d\tau} d\tau \quad (2.1)$$

where  $D_0 \stackrel{\text{def}}{=} D(0)$  is the initial value of the creep compliance

$$D(t) = \frac{\epsilon}{\sigma} \quad (2.2)$$

The transient component of compliance is  $\Delta D(\psi)$

$$\Delta D(\psi) = D(t) - D_0 \quad (2.3)$$

$\psi$  is the reduced time

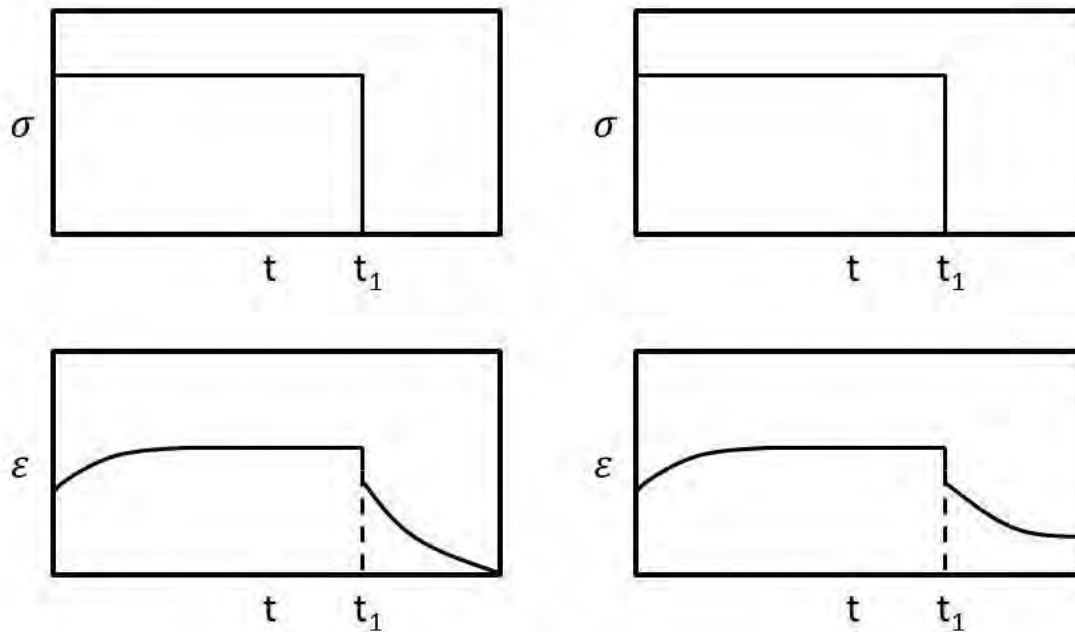
$$\psi \stackrel{\text{def}}{=} \int_0^t \frac{dt'}{a_\sigma[\sigma(t')]} \quad (a_\sigma > 0) \quad (2.4)$$

and

$$\psi' \stackrel{\text{def}}{=} \psi(\tau) \stackrel{\text{def}}{=} \int_0^\tau \frac{dt'}{a_\sigma[\sigma(t')]} \quad (2.5)$$

The model parameters  $g_0$ ,  $g_1$ ,  $g_2$ , and  $a_\sigma$  are functions of stress. These functions are characterized for a particular material by curve fitting experimental creep and

recovery data in both the linear and nonlinear ranges [39]. Creep is defined as the time-dependent strain developed after the specimen has been brought to the desired constant stress. Recovery is defined as the decrease in strain after the removal of stress. The difference between how viscoelastic and viscoplastic models represent creep and recovery is schematically shown in Figure 2.6. In a viscoelastic model, strain eventually returns to zero with time, whereas in a viscoplastic model some finite amount of permanent strain remains.



(a) Viscoelasticity

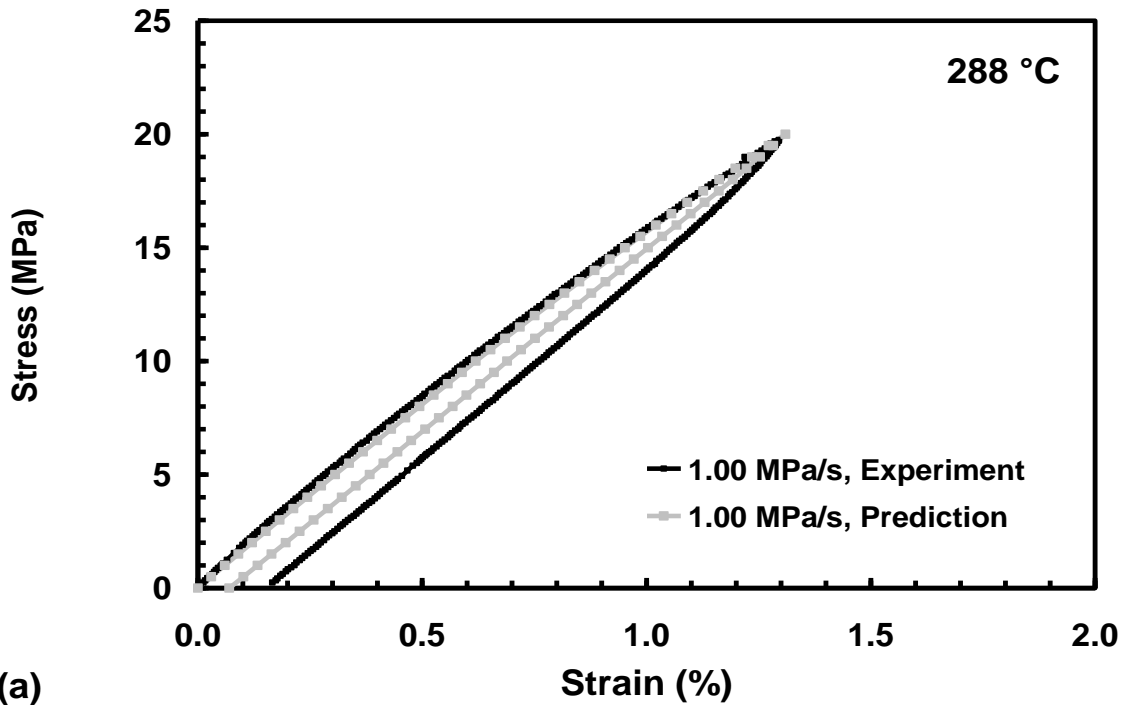
(b) Viscoplasticity

**Figure 2.6 Schematic of (a) viscoelastic and (b) viscoplastic creep and recovery.**

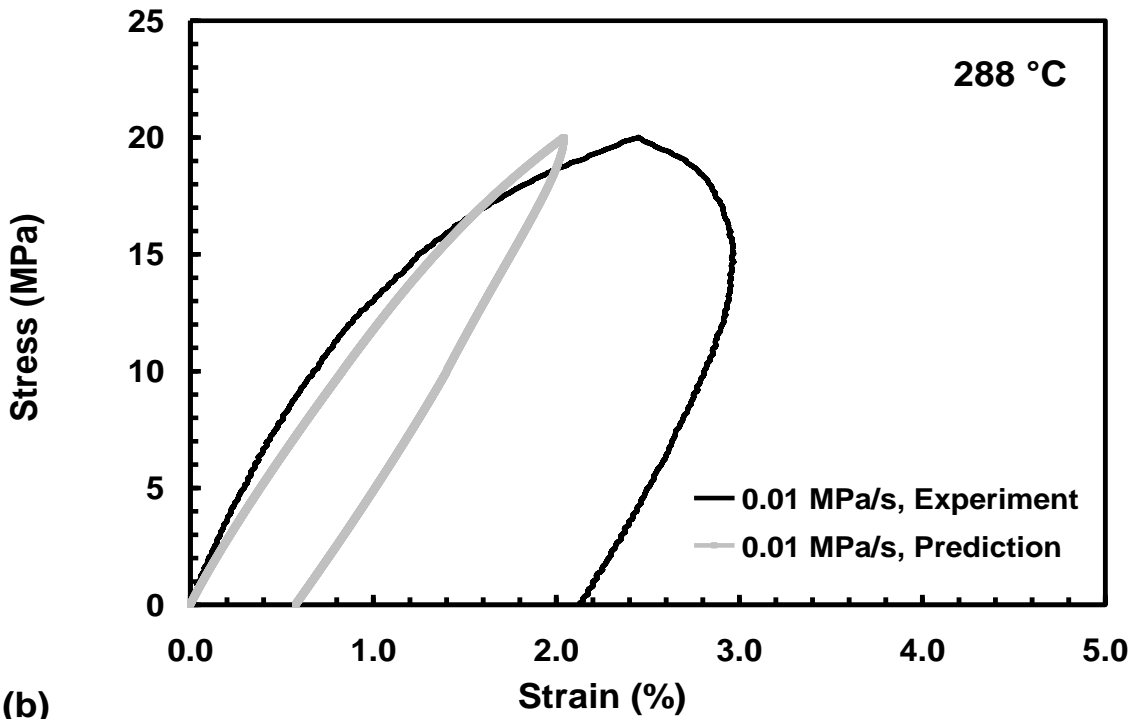
As discussed in Section 2.1.1.2, Falcone and Ruggles-Wrenn [1] conducted experiments on PMR-15 at 288 °C in an effort to characterize Schapery’s model and discover the associated material functions for PMR-15. The authors observed that

Schapery's model was only partially capable of representing the observed behaviors of the material. While the model qualitatively reproduced the loading and nonlinear unloading behavior of the material at constant stress rates, quantitative accuracy depended on the stress rate. Figure 2.7 (reproduced from [1]) demonstrates the inadequacies of Schapery's model in representing the rate-dependent loading/unloading behavior of PMR-15 at 288 °C. In addition, Schapery's model does not account for the effect of prior stress rate on creep or recovery responses as seen in Figure 2.8 reproduced from [1]. Falcone demonstrated that the strain rate-reversal observed in experiments (Figure 2.4) could be represented, at least qualitatively, by Schapery's model as demonstrated in Figure 2.9 (reproduced from [2]).

In an effort to account for permanent deformations not considered in the original formulation of Schapery's model, McClung [19] expanded on Falcone's work and added a viscoplastic term to the creep and recovery equations following the approach of Zaoutsos, Papanicolaou and Cardon [41] and Papanicolaou, Zaoutsos and Cardon [42]. The viscoplastic term was in a power law form suggested by Cardon, Qin and Vossole [43]. Using model parameters obtained by Falcone through her experiments with PMR-15 at 288 °C, McClung produced the predictions for stepwise creep, and recovery following stepwise creep, shown in Figure 2.10 (Reproduced from [19]). McClung's predictions of recovery improved upon Schapery's standard model but the modified model still had no mechanism to account for variation in prior loading rate.



(a)



(b)

Figure 2.7 Comparison between experimental and predicted stress-strain curves for PMR-15 neat resin at 288 °C at constant stress rates of (a) 1.0 MPa/s and (b) 0.01 MPa/s. Reproduced from [1].

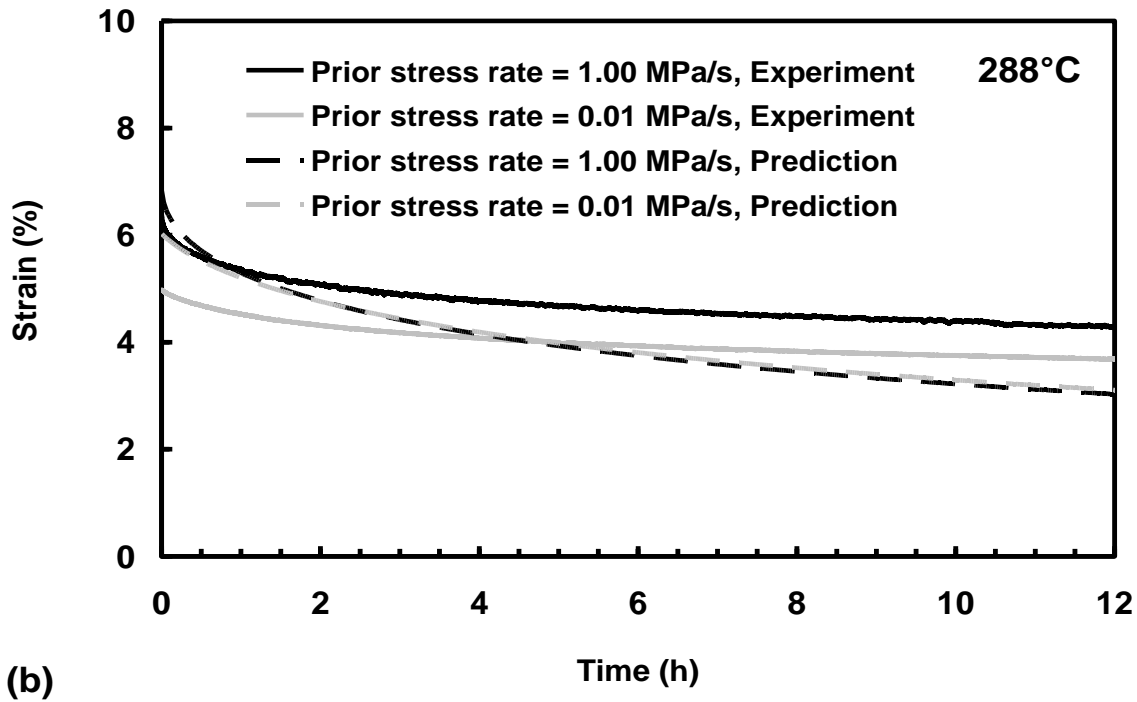
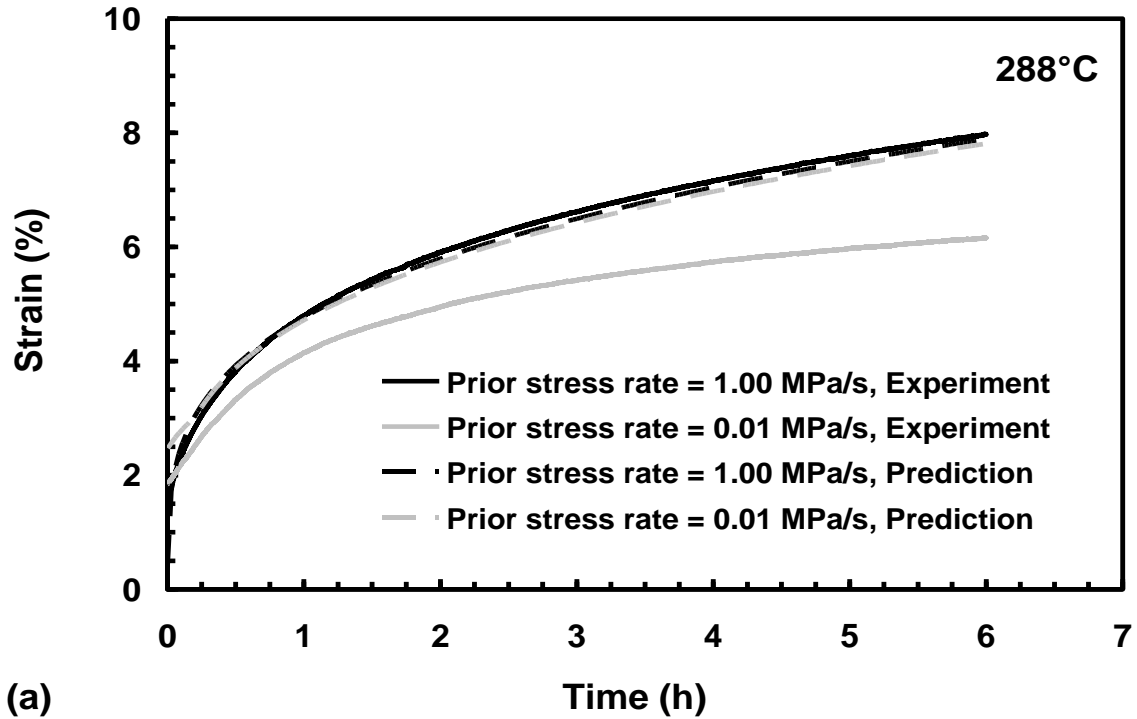


Figure 2.8 Comparison between experimental and predicted strain versus time curves for PMR-15 neat resin at 288 °C for various prior loading rates for (a) creep at 20 MPa and (b) recovery at zero stress. Reproduced from [1].

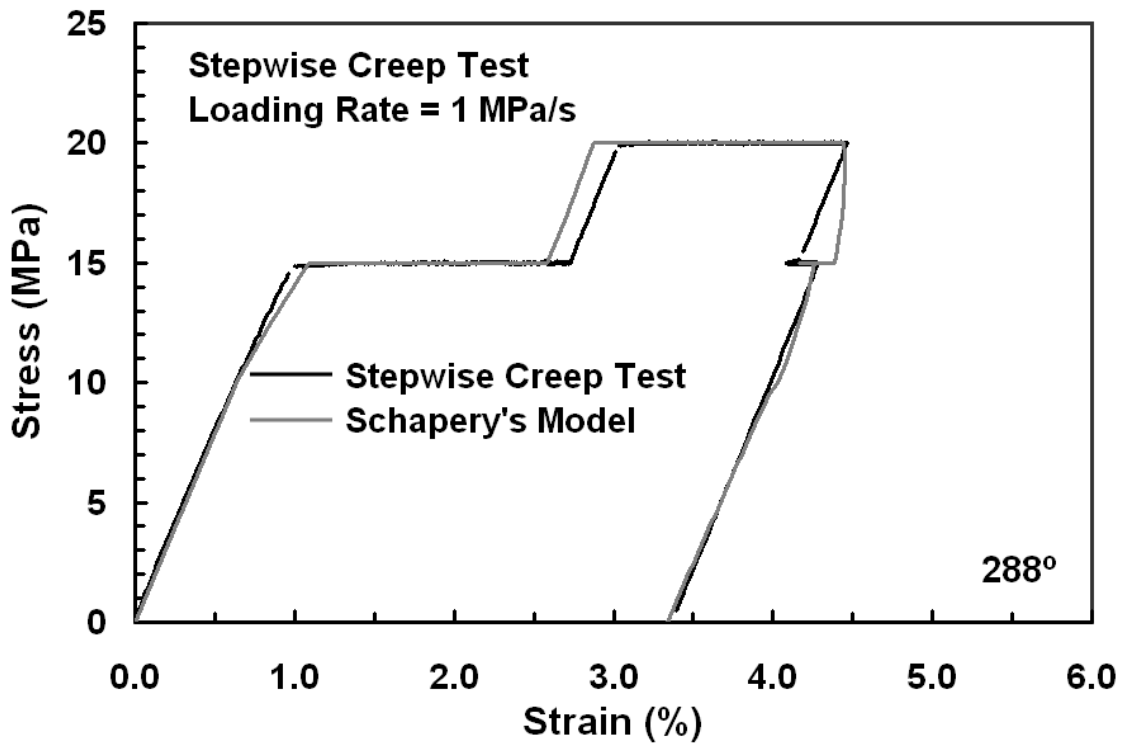
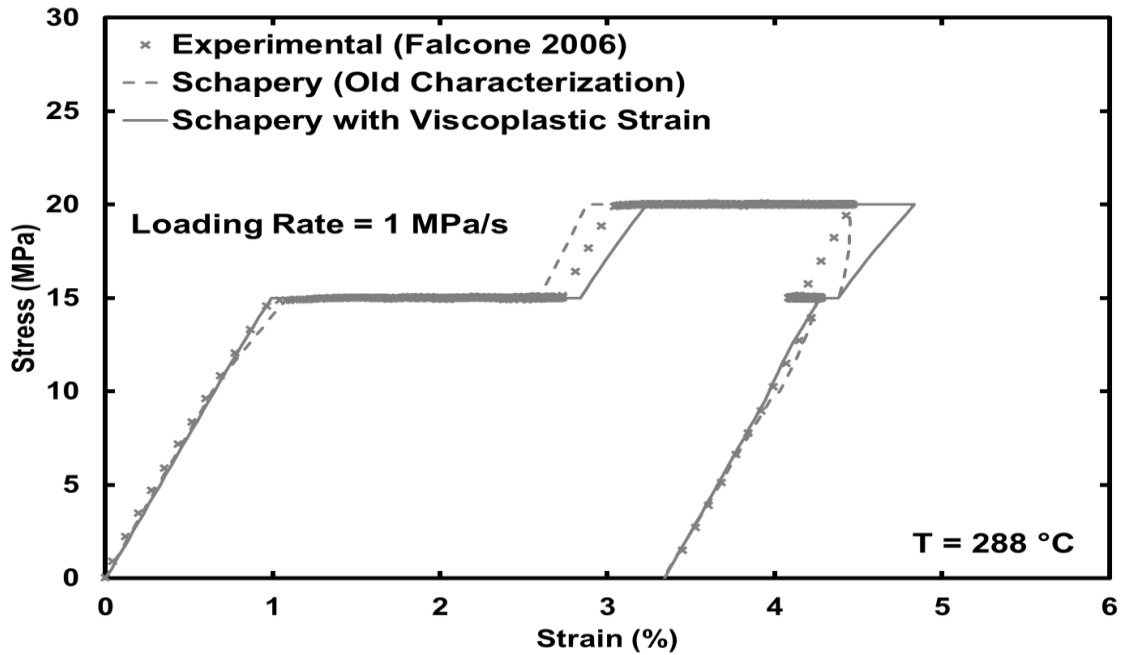
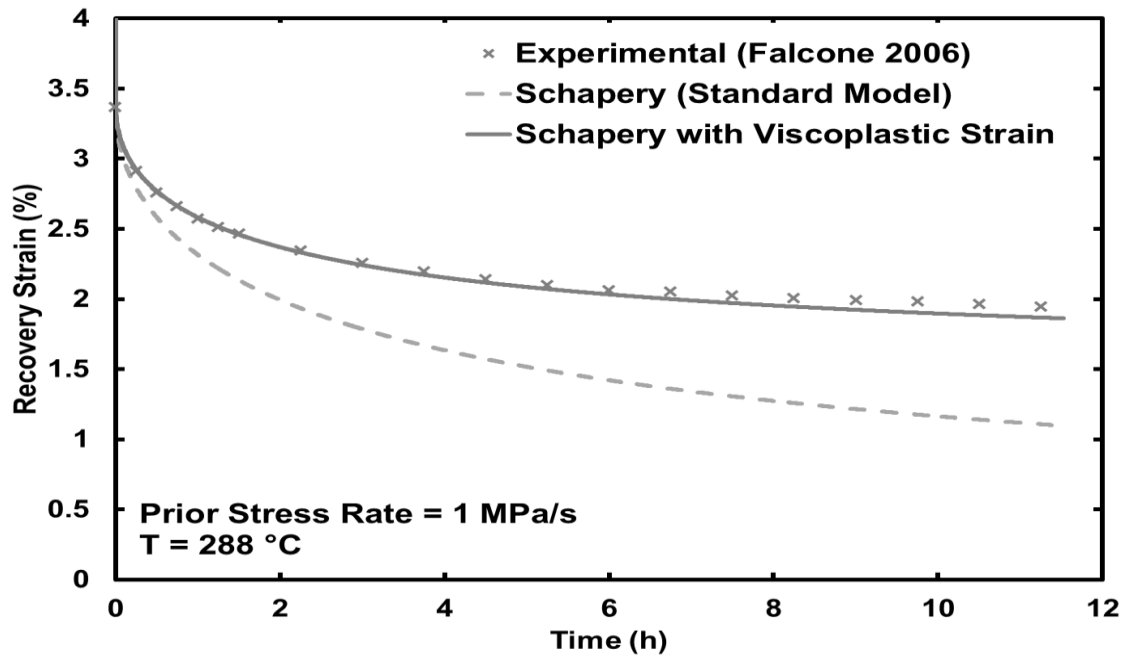


Figure 2.9 Comparison between experimental and predicted stress-strain behavior of stepwise creep test of PMR-15 at 288 °C. Reproduced from [2].



(a)



(b)

Figure 2.10 (a) Stepwise creep behavior and (b) recovery following stepwise creep of PMR-15 at 288 °C: Experiment, Schapery's Model and Schapery's Model with Viscoplastic Strain. Reproduced from [19].

Falcone [2] demonstrated that Schapery's standard model was unable to accurately predict recovery behavior, and could not account for the rate effects for PMR-15 at 288 °C. Based on Falcone's recommendations, McClung introduced a permanent strain function into Schapery's model and had some success improving predictive capability. However, Schapery's model still had no mechanism to account for rate effects. Falcone suggested that a viscoplastic model such as VBO might better describe inelastic behavior of the PMR-15 polymer citing that model's lack of a purely elastic region as particularly useful.

#### *2.2.1.2 Xia and Ellyin's Differential Model*

Integral formulations of viscoelastic models, like Schapery's model discussed in the previous section, may describe time-dependent behavior in a more general manner than differential models, but this can come at the cost of more complicated mathematics. Differential forms of constitutive equations can be easier to implement numerically. Some differential models have been implemented in numerical analyses such as finite element code for this reason. One example of a differential formulation offered by Ellyin and co-workers is discussed below.

Xia and Ellyin [44] extended a linear viscoelastic model to the nonlinear range and used it to simulate a variety of different types of tests on an epoxy polymer. This model, shown in Figure 2.11, consists of two Kelvin elements connected in series, that were made nonlinear and then coupled with a linear spring element. Xia and Ellyin suggested that a convenient way to extend the model into the nonlinear regime was to assume a power law function for stress instead of a linear one.



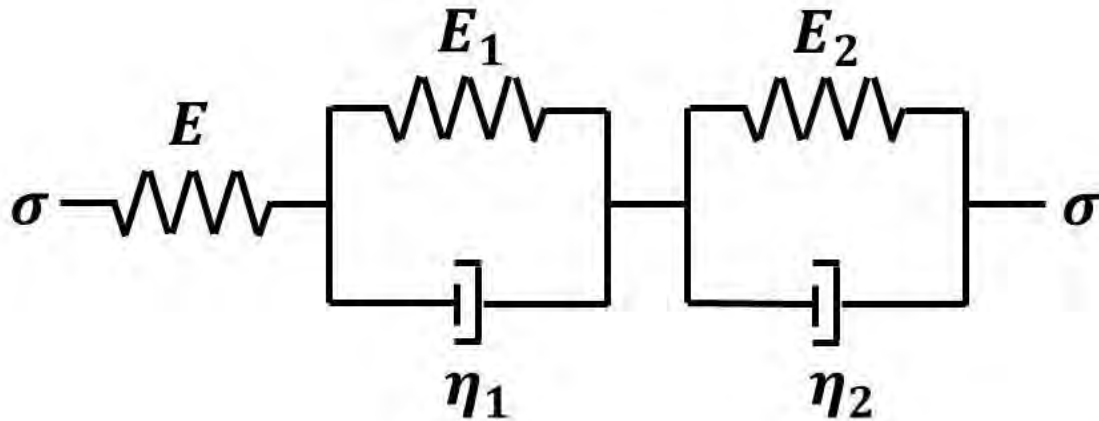


**Figure 2.11 Xia and Ellyin's viscoelastic model.**

To characterize the model, Xia and Ellyin conducted strain recovery and relaxation tests along with uniaxial loading/unloading tests at both slow and fast stress rates. Using the material constants determined from those tests, Xia and Ellyin simulated uniaxial compressive stress-strain, strain recovery after compressive loading/unloading, and compressive stress relaxation with a reasonable degree of qualitative and quantitative success. When the authors attempted to predict creep behavior though, the quantitative results were poor. Xia and Ellyin also characterized the model parameters using the results of the creep tests and were able to improve the accuracy of creep simulation but predictions of recovery and other types of tests became very poor. While Xia and Ellyin's model equations might be useful under certain circumstances, it is incorrect to consider them an effective constitutive model. Professor Krempl wrote, *"Sometimes a response function is erroneously identified with the constitutive equation of the material and used to predict the material response for a different forcing function, e.g., the creep response function is used to predict the relaxation behavior. Although such a procedure*

*may sometimes lead to acceptable results, such a treatment is conceptually incorrect and should not be relied upon in the development of proper material representation. A response function is the answer of the material to a specific forcing function. For another forcing function, another response will in general be obtained”* [29]. While the work of Xia and Ellyin provides several concepts that may prove useful for modeling the deformation behavior of PMR-15, it clearly does not represent the basis for the constitutive equations we seek.

For most polymers, the unloading behavior is significantly different from the response to loading [45]. Xia, Hu and Ellyin [46] introduced a *current loading surface*, which is a stress envelope on which the current stress resides. This allows a criterion to be developed which defines a change from loading to unloading or vice versa. For loading, a stress dependent modulus function was determined from experimental creep data using a nonlinear least squares fit procedure. For unloading behavior, the modulus was assumed to remain constant and have the value of the modulus function at the point of unloading. This not only fit experimental data reasonably well but also served to satisfy the continuity requirement during transition from loading to unloading. A procedure for determining material constants and the material modulus function was prescribed. The authors noted that six Kelvin elements were used in their formulation. Model predictions were compared to a variation of Schapery’s model and the differential model predicted the behavior of the tested epoxy more accurately than the integral model in most cases. Xia, Shen and Ellyin [47], expanded upon this concept and modified the switching rule to accommodate cyclic loading cases. It can generally be seen from cyclic test data, that the first hysteresis loop is different from the remaining loops. Xia and

coworkers noted that the modulus must follow a different rule after the first switch from the loading to the unloading path. Their switching rule was based on a *stress memory surface* in contrast to the earlier described *current loading surface*. While the current research does not include a switching rule, we appreciate that a constitutive model appropriate for polymeric materials would require some mechanism to differentiate between loading and unloading behaviors. The ability to model loading and unloading within the same equation represents a critical advantage of the constitutive framework utilized in the current research.

Zhang, Xia and Ellyin [48], presented a method for discounting the contribution of the matrix material in a representative volume element of a composite consisting of an elastic fiber and a nonlinear viscoelastic matrix material after critical damage occurs. The previously described nonlinear constitutive model is applied to the behavior of the matrix material until an experimentally determined maximum principal strain damage criterion is met. Then a crack in the plane perpendicular to the direction of the strain is deemed to have initiated. Once the crack has formed, it is assumed that shear and normal stresses are not transferred across the crack. It is assumed that the tangent modulus is the value of the modulus of the matrix material under uniaxial tensile loading just prior to the time that damage occurred. The post-damage constitutive model causes the stress components to decay to zero over a very short period of time. This approach can be inserted into a finite element code to model the evolution of damage during strain aging. It would be less useful in modeling the changes in material properties caused by pyrolytic aging or temperature since it is focused on the rapid phase out of the matrix contribution

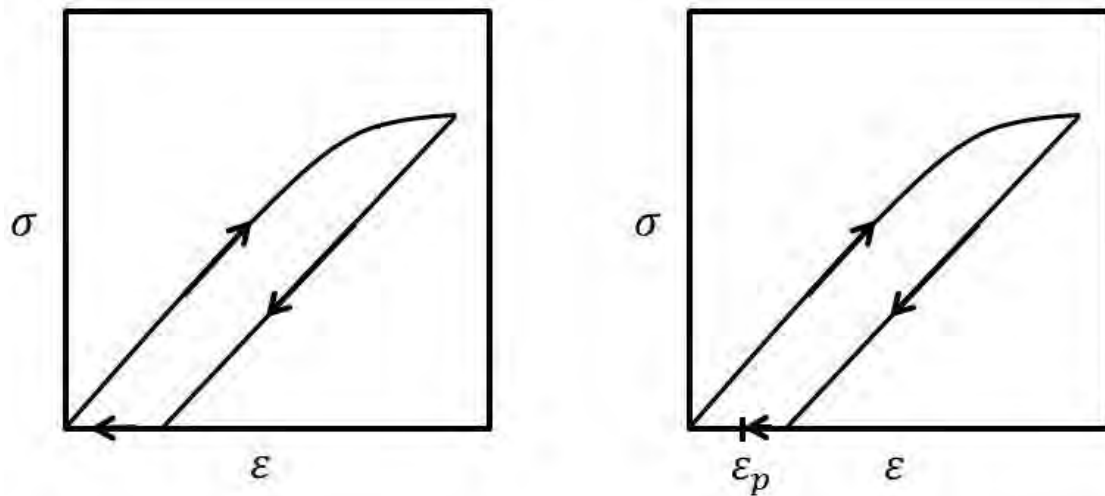
when a critical strain is achieved as opposed to the gradual change in material properties with exposure to elevated temperature.

### *2.2.2 Viscoplastic Constitutive Models*

Various authors have noted that many polymeric materials appear to exhibit viscoplastic rather than viscoelastic behavior [5, 9, 11, 19, 49]. Viscoplasticity can be readily understood by comparing it to viscoelasticity. Figure 2.12 shows a schematic comparison of (a) viscoelastic behavior and (b) viscoplastic behavior. Viscoelastic materials exhibit nonzero strain immediately after unloading to zero stress, but return to zero strain if given enough time. Viscoplastic materials, on the other hand, fail to recover 100% of the accumulated strain and a permanent strain  $\varepsilon_p$  will remain. A variety of viscoplastic models have been proposed in the literature. The viscoplastic models of Perzyna [50], Phillips/Wu [51], Chaboche [52-54], Bodner [55], and Krempl/Yao [56] are a testament to the wide variety of models that fall into this category. For the remainder of this discussion we shall restrict ourselves to a discussion of Viscoplasticity Based on Overstress and its various specializations.

#### *2.2.2.1 Viscoplasticity Based on Overstress*

Beginning in the 1970's, Krempl [29] examined the need for a constitutive model that could accurately represent deformation behavior of structural materials under cyclic loading at high homologous temperatures. He examined the existing literature and concluded that available constitutive equations did not completely reproduce the behavior seen during experiments. Krempl noted the difficulties of including the effects of aging, rate-dependence and history-dependence in a comprehensive constitutive law. He



(a) Viscoelasticity

(b) Viscoplasticity

**Figure 2.12 (a) viscoelastic and (b) viscoplastic stress-strain behavior.**

pointed out that without a set of constitutive equations, which considered such factors, a massive database of material properties at various conditions would be required. Krempl provided extensive guidance on utilizing a phenomenological approach to develop an appropriate constitutive model.

VBO is a unified viscoplastic constitutive model developed by Krempl and co-workers over a period of several years in the late 1970's and 1980's. In a unified model like VBO, inelastic strain is not subdivided into creep and plastic strains. VBO borrows from Phillips [57] the concept of an equilibrium stress  $g[\varepsilon]$ , which is defined as the stress-strain behavior in response to loading at an infinitesimally slow strain rate. Cernocky and Krempl [58] also introduced the concept of overstress as it is applied to a unified viscoplastic model. Overstress is defined as the difference between the applied or flow stress and the equilibrium stress. The flow stress is simply the applied stress in the region of fully developed plastic flow. In Figure 2.13,  $\sigma$  is the applied stress curve and  $g$

is the equilibrium stress curve. The difference between those curves,  $\sigma - g$  is known as the overstress.

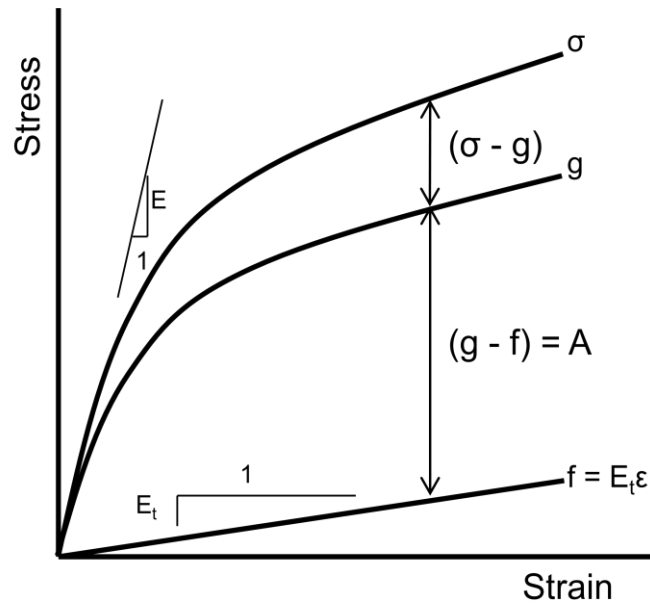


**Figure 2.13 Schematic showing uniaxial stress-strain curve, equilibrium stress  $g$  and kinematic stress  $f$  curves, overstress  $(\sigma - g)$ , and isotropic stress  $A$ .**

To provide a better understanding of VBO we examine its origins. In 1979, Cernocky and Krempl [58, 59] suggested a first order nonlinear differential equation as the core of a constitutive model for viscoplasticity. For the uniaxial case they proposed

$$m[\sigma, \varepsilon]\dot{\varepsilon} + g[\varepsilon] = \sigma + k[\sigma, \varepsilon]\dot{\sigma} \quad (2.6)$$

where  $m$ ,  $k$ , and  $g$  are material functions that must be determined from experiments. The square brackets indicate “function of” and a raised dot, the first time derivative. Stress and strain are represented by  $\sigma$  and  $\varepsilon$  respectively and the term  $g$  is defined to be the equilibrium stress. Cernocky and Krempl derived an integral form of (2.6). They also reported a “*useful specialization*” of equation (2.6) where  $m$  and  $k$  are made to depend

on overstress and  $\frac{d\dot{g}[\varepsilon]}{d\varepsilon} = E$  for extremely fast loading. This specialization has several important characteristics. Stress-strain curves for different strain rates become parallel to  $g[\varepsilon]$  in the region of fully developed plastic flow (Figure 2.14). In addition, the model reproduces the following features:

- Initial elastic region
- Initial elastic response upon a large jump in strain rate
- Nonlinear spacing of stress-strain curves produced at various strain rates
- Elastic response to loading at very fast strain rates
- Creep and relaxation behavior

Cernocky and Krempl note that the behavior of this model is very similar to the actual deformation behavior of typical engineering alloys. This “*useful specialization*” of their proposed constitutive equation forms the basis of Viscoplasticity Based on Overstress (VBO).

Liu and Krempl [60] showed that the constitutive model proposed by Cernocky and Krempl could be characterized for an actual material (AISI type 304 stainless steel) and that the model provided a good representation of the deformation behavior of metals as long as the overstress did not change signs. Liu and Krempl determined the material constants for the model from experimental data collected previously by Yamada and Li [61]. Liu and Krempl noted that constitutive law must be modified at certain intervals to account for deformation induced microstructural changes in the material but did not provide any details of how this would be achieved. Liu and Krempl used the determined

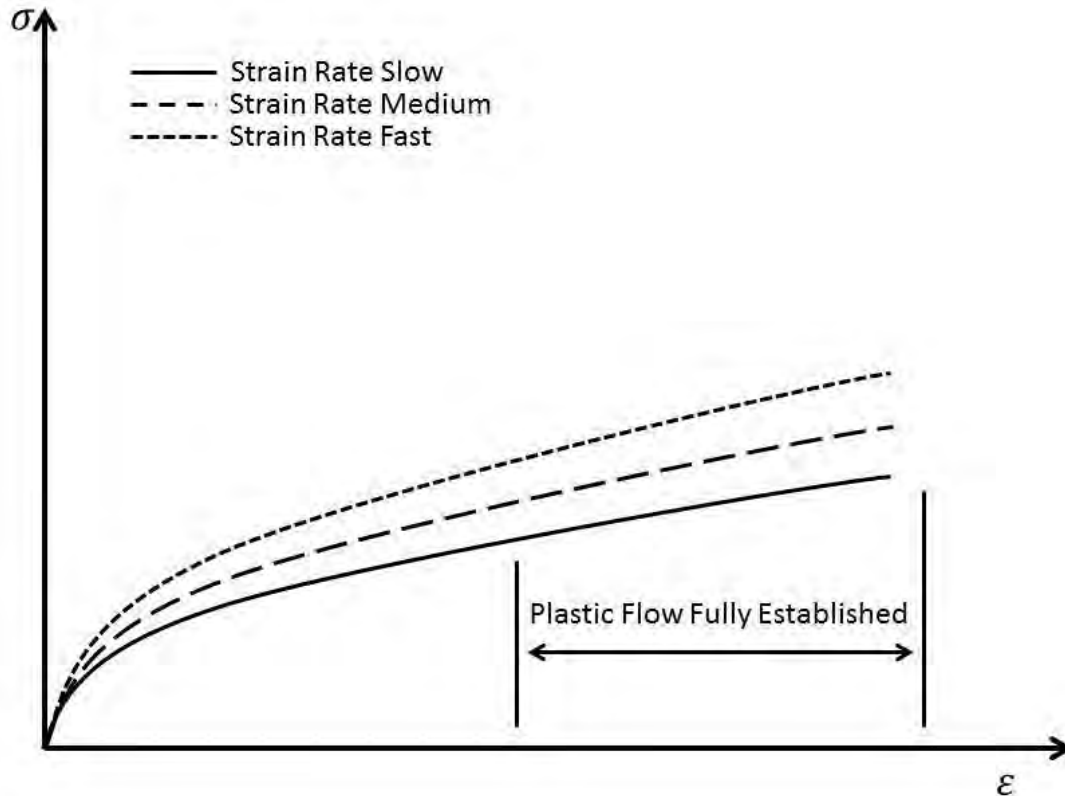


**Figure 2.14 Schematic showing equidistance of stress-strain curves produced in response to loading at different strain rates in the region of fully established plastic flow.**

material constants to simulate deformation behavior and demonstrated that the model could represent the response of the material to complex loadings such as a strain rate jump test or loading with intermittent periods of relaxation. The ability of this model to represent the response of the material to complex loading histories is a critical first step in modeling the behavior of viscoplastic materials that age or otherwise change behavior due to test temperature. However, like the deformation induced microstructural changes referred to by Krempl and Liu, aging processes will require a change to the basic VBO model.



Krempf and Kallianpur [62] described a series of experiments that elucidated the relationship between overstress and the inelastic strain rate. Those experiments showed that inelastic strain rate does not depend on stress alone and that VBO could explain the results of their creep experiments. Krempf [63] provided a definition and a clearly described procedure for characterizing the tangent modulus. Krempf also noted that the viscosity function  $k$  included in the formulation of the VBO could be found with a trial and error curve fit to experimental data. Krempf, McMahon and Yao [64] introduced a shape function  $\psi$ , which controls the shape of the knee of the stress-strain diagram. Krempf et al suggested using an asymptotic value of the equilibrium stress and the tangent modulus to calculate the isotropic stress  $A$  although they still relied on trial and error to establish the viscosity and shape functions. McClung and Ruggles-Wrenn [28] developed a systematic procedure for determining all VBO model parameters from experimental data and employed VBO to predict the response of PMR-15 polymer under various test histories.

As previously discussed, VBO evolved gradually during the early 1980's into its standard form and was effectively applied to model the mechanical behavior of engineering alloys under a wide variety of loading histories. Uniaxial creep, cyclic creep, relaxation, Bauschinger effect and ratcheting behavior of stainless steel were investigated experimentally and modeled using the VBO [62, 63, 65, 66]. The rate-dependent behavior of a Titanium alloy (Ti-7Al-2Cb-1Ta) under monotonic loading, cyclic loading and relaxation tests was also modeled using the VBO [62, 63, 67]. Yao and Krempf [56] characterized VBO for 6061 T6 aluminum alloy and predicted biaxial behavior of this alloy under axial-torsion loading. Based on experimental work by Ruggles, Cheng and

Krempf [68], Majors and Krempf [69] augmented VBO to model the rate-dependent behavior of modified 9wt.%Cr-1wt.%Mo steel at 538 °C. These examples demonstrate the usefulness of VBO in modeling the time-dependent deformation behavior of various engineering alloys at both room and elevated temperatures.

As solid polymers became more widely used in structural applications, the need for an effective predictive constitutive model increased. Since the quasi-elastic regime is limited, and significant part of the load carrying capacity of many polymers lies within the inelastic regime, several researchers turned to viscoplastic models to predict the time-dependent behavior of those polymers. Kitagawa and Matsutani [30] noted that the overstress concept had been applied to the stress-strain relations of metals and postulated that it could also be used to simulate the behavior of polymers. They conducted experiments on PP at 15, 25 and 40 °C and found that stress-strain behaviors under monotonic loading, relaxation and creep could be predicted with a reasonable degree of accuracy. Kitagawa, Zhou and Qui [31] examined additional polymeric materials including both amorphous (PC and PMMA) and crystalline (POM) polymers. They found that Krempf's overstress theory provided a good representation of the mechanical behavior of those materials. They also noticed an anomalous behavior not seen in metals that turned out to be the "rate reversal" phenomenon discussed in Section 2.1.1.1. Kitagawa et al. indicate that this may add to the difficulty in creating an "all-around" set of constitutive equations for polymeric materials.

Bordonaro [5] and Krempf and Bordonaro [15] examined the deformation behavior of Nylon 66, PEI and PEEK. They showed that nonlinear elasticity was not a good model for Nylon 66, PEI and PEEK and demonstrated that VBO did reproduce, at

least qualitatively, the behavior of those polymers. They postulated that while the specific deformation mechanisms for metals and polymers were quite different, the basic structure of the constitutive equations, including the concepts of equilibrium stress and overstress could be the same.

Bordonaro [5] and Krempl and Bordonaro [15] noted that the mechanical behavior of polymers differed from that of metals in several critical ways. This included higher relaxation rates, increased strain recovery after unloading, curved unloading in stress control, reduced rate dependence during unloading and the merging of stress-strain curves produced at different strain rates as strain approaches a large value. Khan [11] reported many of the same features for HDPE and PPO but found that VBO was not able to model “rate reversal” or curved unloading.

#### *2.2.2.2 Viscoplasticity Based on Overstress for Polymers*

Based on the previous research, various authors have suggested improvements to VBO to make it better able to represent the deformation behavior of polymers. Ho [9] and Krempl and Ho [16] created a specialization of VBO that has become known as Viscoplasticity Based on Overstress for Polymers (VBOP). This specialization of VBO with its several optional components, has been shown to model the behavior of Nylon-66 [9, 16], PPO [12], HDPE [13], and PMR-15 [19] more accurately than the original VBO. Again, we note that VBOP is used to model both crystalline and amorphous polymers. A full mathematical development of VBOP is presented in Section 3.3.

Colak [7] and Colak and Dusunceli [8, 70] developed a modification of VBO that better described the curved unloading behavior of polymers. Colak and Dusunceli introduced a function into the elastic strain rate equation that effectively changed the stiffness of the stress-strain curve during loading and unloading. While experiments indicate this modification of VBO represents the unloading behavior of PPO and HDPE better than Krempl and Ho's classical version [16] it does not represent all of the features identified by Bordonaro [5], which differentiate deformation of solid polymers from that of engineering alloys. The modification proposed by Colak cannot account for the higher relaxation rates, the merging of stress-strain curves or cyclic softening/hardening commonly found during deformation of solid polymers. However, Colak's formulation does provide a useful example of how VBO or even VBOP might be further modified to account for other factors like aging.

### *2.2.2.3 Viscoplasticity Based on Overstress with Prior Aging*

As early as the late 1970's, researchers were interested in accounting for prior aging in various constitutive models. Krempl [33] discussed the implications of aging as it applied to an early version of VBO. He assumed that microstructural changes of the material that affect the phenomenological response could be divided into deformation and diffusion controlled responses. This allowed for separation of variables to be employed in the development of the constitutive equations. While this may not always be true, as in the case where deformation increases the rate of diffusion of an aggressive species, it is a good assumption when dealing with the pyrolytic aging of polymers and one we shall retain throughout this research. With this key assumption, aging can be accounted for by

making the appropriate equations of our constitutive model explicitly dependent on time. Krempl states, “*In the absence of aging, constants characteristic of a specific material are present in the functions of our theory.*” With aging, those material constants/functions may vary with time. If the aging environment changes, the time-dependence of those material constants/functions may change. In this research both the duration of the aging and the aging temperature will vary. Discovering the time/temperature dependence of the prior aging of PMR-15 and creating a constitutive model that accounts for the effect of prior aging temperature (in addition to that of prior aging time) on the inelastic behavior is one of our essential tasks.

#### 2.2.2.4 *Viscoplasticity Based on Overstress for Polymers with Prior Aging*

McClung [19] studied the effects of prior aging at 288 °C in argon on the inelastic behavior of PMR-15 at 288 °C. Following the procedure of Krempl [33] where identical specimens are exposed to an elevated temperature for various durations, McClung repeatedly characterized VBOP for specimens aged at 288 °C in argon and found that certain material constants changed with changes in aging duration. Variation in moisture content and oxidative aging were controlled by controlling the storage and aging environments. Krempl [33] suggested that in the case of VBO the equilibrium stress  $g$  and the viscosity function  $k$  would become the slowly changing functions of time. McClung [19] found that in order to characterize VBOP for various prior aging times, elastic modulus  $E$ , tangent modulus  $E_t$ , isotropic stress  $A$  and the shape function parameter  $C_2$  had to be expanded as functions of prior aging time. McClung fit the experimental data for each parameter to a power law formulation with three constant

coefficients. Using these material functions in place of the previous material constants, McClung was able to predict material behavior for prior aging times extrapolated beyond the experimental data. A detailed development of VBO and VBOP describing these material functions is included in Chapter 3.

### **2.3 Objective of Current Work**

The experimental and theoretical work described in this chapter provides the foundation for examining the effect of elevated temperature on the deformation behavior of high-temperature polymers. The current research focuses on both of the major ways temperature affects mechanical behavior. The temperature which the specimen experiences while under load for even short periods clearly affects mechanical behavior. Prior aging at elevated temperature also induces changes in mechanical behavior. These effects are distinct and separable. This research endeavors to determine the individual effects of test temperature and of prior aging temperature. Moreover, once those effects are known, the VBOP is extended to account for them.

### **3 Theoretical Formulation of Viscoplasticity Based on Overstress for Polymers**

The purpose of this chapter is to summarize the mathematical development of the theory of Viscoplasticity Based on Overstress for Polymers (VBOP). The VBOP is selected as a baseline for the current research because it has been effectively used to model the deformation behavior of a variety of polymers including PMR-15 neat resin. Additionally, it has been previously shown [19] that VBOP can be extended to account for prior aging (albeit at only one temperature for one specific material). The goal of this research is to extend the VBOP to accommodate the effect of test temperature and of prior aging at various temperatures and for various durations. To that end, we must thoroughly understand VBOP as it is currently formulated before we seek to extend it.

As discussed in Chapter 2, both VBO and VBOP are unified viscoplastic constitutive models. A “unified model” is one where the creep strain and the plastic strain are not represented by separate terms in the constitutive equations [57]. Following Krempl [37], VBO is developed from the governing equations for the Standard Linear Solid. Then, the VBO is modified to Krempl and Ho’s VBOP formulation to better represent the behavior of solid polymers [16]. Finally, following the approach developed by McClung, VBOP is extended to capture the effects of prior aging of PMR-15 at 288 °C.

#### **3.1 Basis of Viscoplasticity Based on Overstress – Standard Linear Solid**

This section describes the Standard Linear Solid (SLS), which is the simplest linear viscoelastic solid that can model relaxation and creep [37]. The SLS consists of a linear Kelvin element connected in series with a linear spring (Figure 3.1). It is considered a

viscoelastic solid since it can maintain a nonzero stress when the strain rate is zero [37, 71].

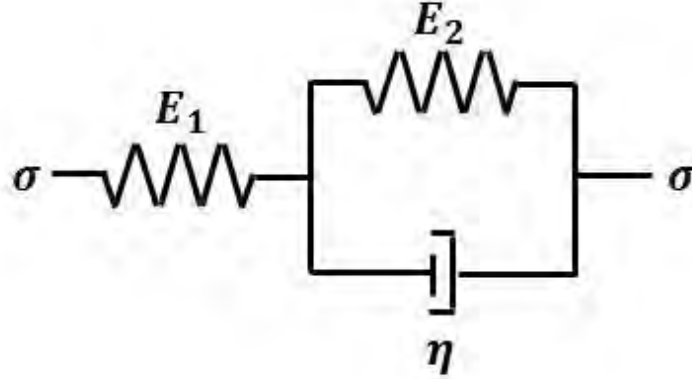


**Figure 3.1 Schematic of the Standard Linear Solid.**

The constitutive equation of the SLS can be written in terms of stress, stress rate, strain and strain rate as:

$$\dot{\varepsilon} + \frac{E_2}{\eta} \varepsilon = \frac{\dot{\sigma}}{E_1} + \left( \frac{E_1 + E_2}{E_1} \right) \frac{\sigma}{\eta} \quad (3.1)$$

where  $E_1$  and  $E_2$  are the elastic spring constants and  $\eta$  is the viscosity constant of the dashpot. Stress and strain are represented by  $\sigma$  and  $\varepsilon$  respectively and a raised dot indicates the time derivative.

The constitutive equation of the SLS can be rearranged in an overstress form

$$\dot{\varepsilon} = \dot{\varepsilon}^{el} + \dot{\varepsilon}^{in} = \frac{\dot{\sigma}}{E_1} + \frac{\sigma - aE_2\varepsilon}{a\eta} \quad (3.2)$$

$$a = \frac{E_1}{E_1 + E_2} \quad (3.3)$$



where the term  $\sigma - aE_2\varepsilon$  represents the overstress and  $a$  is the modulus ratio. If we allow all rates to approach zero we find the numerator of the second term of (3.2) yields the equilibrium stress  $g$ .

$$g = aE_2\varepsilon \quad (3.4)$$

For extremely fast loading ( $\dot{\sigma} \rightarrow \infty$ ), it can be shown that strain rate is governed by  $E_1$  and the output of the constitutive equations of the SLS simplifies to Hooke's law.

The creep response is obtained by setting  $\dot{\sigma} = 0$  in Equation (3.2)

$$\dot{\varepsilon}^{in} = \frac{\sigma_o - aE_2\varepsilon}{a\eta} \quad (3.5)$$

where the subscript “o” indicates that quantity is kept constant.

The SLS constitutive equation for relaxation is obtained in a similar manner by setting  $\dot{\varepsilon} = 0$  in Equation (3.2)

$$\frac{\dot{\sigma}}{E_1} = -\frac{\sigma - aE_2\varepsilon_o}{a\eta} \quad (3.6)$$

A schematic of the SLS stress-strain response at various loading rates is shown in Figure 3.2.

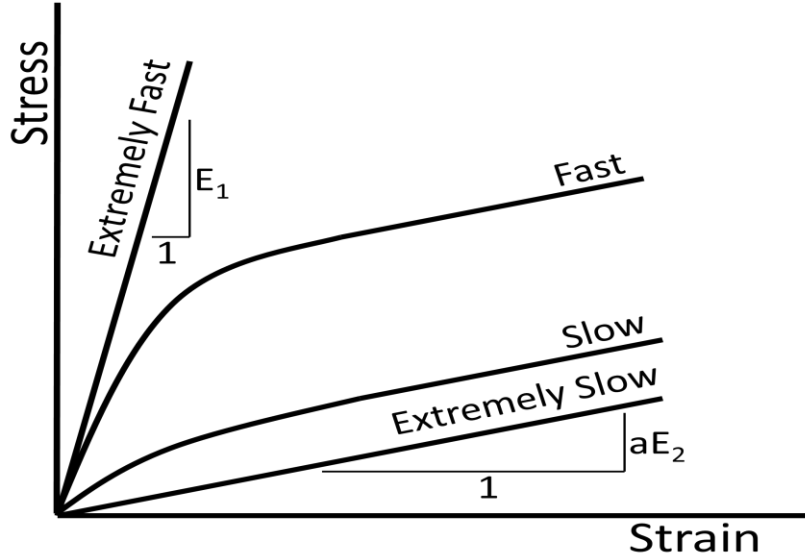


**Figure 3.2 Schematic showing the responses of a SLS in monotonic loading.**

### 3.2 Viscoplasticity Based on Overstress

Starting with the SLS, VBO can be developed by making certain properties of the SLS nonlinear and providing a formulation for the evolution of the equilibrium stress  $g$ . Referring to Equation (3.2) this is accomplished by making the spring of the Kelvin element a nonlinear function of strain and letting the viscosity of the dashpot be a function of overstress  $k[\sigma - g[\varepsilon]]$  [37] where square brackets indicate “a function of.”

The governing equation of VBO is

$$\dot{\varepsilon} = \varepsilon^{el} + \varepsilon^{in} = \frac{\dot{\sigma}}{E} + \frac{\sigma - g}{Ek} \quad (3.7)$$

where  $E$  is the elastic modulus,  $g$  is the equilibrium stress, and  $k$  is the viscosity function.

The growth of the equilibrium stress is

$$\dot{g} = \Psi \frac{\dot{\sigma}}{E} + \frac{\Psi}{E} \left[ \frac{\sigma - g}{k} - \frac{g - f(\sigma - g)}{A} \frac{\sigma - g}{k} \right] + \left( 1 - \frac{\Psi}{E} \right) \dot{f} \quad (3.8)$$

where  $A$  is the isotropic stress,  $\Psi$  is the shape function, and  $f$  is the kinematic stress.

Krempf [63] prescribes several forms of the viscosity function  $k$  but the following has become accepted as the standard for VBO:

$$k = k_1 \left( 1 + \frac{|\sigma - g|}{k_2} \right)^{-k_3} \quad (3.9)$$

The viscosity function is the repository of nonlinear viscous behavior and  $k_1$ ,  $k_2$ , and  $k_3$  are material constants [72].

The kinematic (rate dependent) stress  $f$  controls the tangent modulus  $E_t$ , defined as the slope of the stress-strain curve in the region of fully developed plastic flow. The simplest form of a growth law for kinematic stress associated with VBO is [73]

$$\dot{f} = E_t \frac{(\sigma - g)}{Ek} \quad (3.10)$$

As shown in Figure 3.3, the isotropic stress  $A$  represents the difference between the equilibrium stress  $g$  and the kinematic stress  $f$  [73]. The purpose of the isotropic stress  $A$  is to model work hardening or softening [74]. For a cyclically neutral material, isotropic stress can be selected to be a constant.

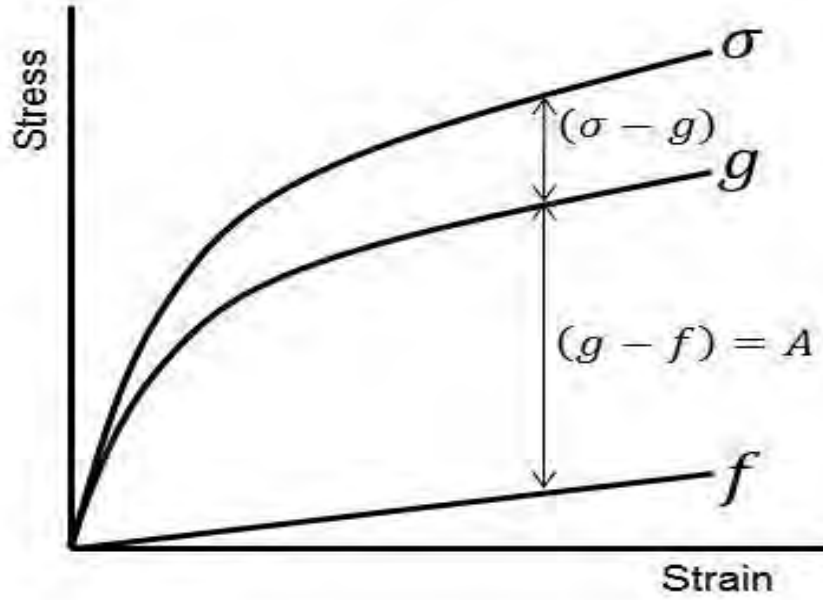


**Figure 3.3 Schematic showing uniaxial stress-strain curve, equilibrium stress  $g$  and kinematic stress  $f$  curves, overstress  $(\sigma - g)$ , and isotropic stress  $A$ .**

The evolution of the isotropic stress is [75]

$$\dot{A} = A_c [A_f - A] \left| \frac{\sigma - g}{Ek} \right| \quad (3.11)$$

where  $A_c$  controls the speed with which saturation of hardening (or softening) is reached and  $A_f$  is the final value of the isotropic stress  $A$  [75].

The shape function  $\Psi$  governs the transition from the initial quasi-elastic behavior to fully developed plastic flow [73]. The shape function can be thought of as controlling the shape of the “knee” in the stress-strain curve. The standard form of the shape function is [56]

$$\Psi = C_1 + (C_2 - C_1)e^{-C_3|\epsilon^{in}|} \quad (3.12)$$

where  $C_1$ ,  $C_2$ , and  $C_3$  are material constants.

Various modifications of the standard version of VBO have been created. They generally share a flow law and the existence of the state variables  $g$ ,  $A$ , and  $f$ . However, each modification varies in the formulation of those state variables. The modification proposed by Ho and Krempl [10] has been used to demonstrate positive and negative rate sensitivity or even the inverse rate insensitivity due to dynamic strain aging. Two simplified versions of VBO (SVBO and ISVBO) seek to reduce the number of model parameters to make the models easier to characterize [77, 78]. VBOP (discussed in more detail below) grew out of VBO in an effort to better represent the deformation behavior of polymers [9].

### 3.3 Viscoplasticity Based on Overstress for Polymers

VBOP was developed by Ho [9] and Krempl and Ho [16] to better model the deformation behavior of polymers. Specifically, Ho and Krempl and Ho augmented the baseline VBO to model the deformation behavior of Nylon-66 reported by Bordonaro and Krempl [6], Bordonaro [5], and Krempl and Bordonaro [15]. Khan [12, 14] subsequently employed VBOP to model the mechanical behavior of PC, PPO, PES, HDPE, PET and Nylon-66. Later McClung [19, 28, 49] demonstrated that VBOP was useful in modeling the behavior of PMR-15 at 288 °C. Following Ho [9, 16], VBOP is recapitulated below concentrating on the differences between VBOP and VBO.

The governing equation of VBOP retains the same form as governing equation of VBO

$$\dot{\varepsilon} = \dot{\varepsilon}^{el} + \dot{\varepsilon}^{in} = \frac{\dot{\sigma}}{E} + \frac{\sigma - g}{Ek} \quad (3.13)$$

The evolution of the equilibrium stress  $g$  is made almost rate-independent at large strain and is modified by adding a term, which is dependent on the overstress rate [9].

$$\dot{g} = \Psi \frac{\dot{\sigma}}{E} + \Psi \left[ \frac{(\sigma - g)}{Ek} - \frac{(g - f)}{A} \left| \frac{(\sigma - g)}{Ek} \right| + \frac{(\dot{\sigma} - \dot{g})}{E} n \right] + \left[ 1 - \frac{\Psi}{E} \right] \dot{f} \quad (3.14)$$

The term representing the difference between the stress rate  $\dot{\sigma}$  and the equilibrium stress rate  $\dot{g}$  influences the equilibrium stress during relaxation. This modification allows VBOP to capture the higher relaxation rates observed in polymers. As deformation becomes large, this term approaches zero. The quantity  $0 \leq n \leq 1$  is a material constant that controls the relaxation rate. In the case of Nylon-66, Ho [9] set  $n = 1$ , while McClung [19] found that  $n = 0$  produced better results for PMR-15.

The viscosity function for VBOP is modified as follows [9]

$$k = k_1 \left[ 1 + \left( 1 + \frac{A_0 - A}{A_0 - A_f} \right) \frac{\Gamma}{k_2} \right]^{-k_3} \quad (3.15)$$

Here  $A_0$  and  $A_f$  are the initial and final values of isotropic stress respectively and  $k_1$ ,  $k_2$ , and  $k_3$  are material constants. The dependence on isotropic stress allows the stress-strain curves at various strain rates to merge.

In the formulation of VBOP, the evolution of the kinematic stress is also modified as follows [9]:

$$\dot{f} = \left[ \frac{|\sigma|}{\Gamma + |g|} \right] E_t \frac{(\sigma - g)}{Ek} \quad (3.16)$$

where  $\Gamma$  is the uniaxial overstress invariant

$$\Gamma = |\sigma - g| \quad (3.17)$$

The inclusion of the term in brackets in the kinematic stress, increases strain recovery after unloading to zero stress [9]. This is achieved by slowing the decrease of equilibrium stress.

The isotropic stress is unchanged from the standard VBO and equation (3.11) is repeated here

$$\dot{A} = A_c [A_f - A] \left| \frac{\sigma - g}{Ek} \right| \quad (3.18)$$

In the case of a cyclically neutral material equation (3.18) may be simplified by setting  $A_c = 0$  and making  $A$  a constant. While this is an acceptable assumption for many polymers like PMR-15 [19], Ho demonstrated that this is not the case for Nylon-66 which exhibits cyclic softening. However, for a cyclically neutral material where  $A$  is a constant, the viscosity function shown in equation (3.15) simplifies to the same form utilized for VBO

$$k = k_1 \left( 1 + \frac{|\sigma - g|}{k_2} \right)^{-k_3} \quad (3.19)$$

Ho [9] also suggested a slight modification to the shape function  $\Psi$  to better manage the transition between quasi-elastic and inelastic deformation and the shape of the unloading curve.

$$\Psi = C_1^* + (C_2 - C_1^*) e^{-C_3 |\varepsilon^{in}|} \quad (3.20)$$

where

$$C_1^* = C_1 \left[ 1 + C_4 \left( \frac{|g|}{A + |f| + \Gamma^2} \right) \right] \quad (3.21)$$

here  $\Gamma$  is the effective overstress  $\Gamma = |\sigma - g|$  and  $C_1$ ,  $C_2$ ,  $C_3$ , and  $C_4$  are material constants. Although Ho found this modification was necessary to accurately model Nylon-66, McClung [19] observed that employing the shape function from the standard VBO (Equation (3.12)) more accurately captured the knee of the stress-strain curve of PMR-15 and simplified the model formulation.

### **3.4 Extension of Viscoplasticity Based on Overstress for Polymers to Capture Effects of Prior Aging Time**

McClung [19] extended VBOP to capture the effects of prior aging at 288 °C by determining which material constants became material functions explicitly dependent on aging time. As previously discussed in Section 2.2.2.4, McClung determined that the elastic modulus  $E$ , tangent modulus  $E_t$ , isotropic stress  $A$  and the shape function parameter  $C_2$  were each functions of prior aging time. McClung described how each material function changed with prior aging time and used the functional relationships to accurately predict deformation behavior for PMR-15 aged for 2000-h. McClung obtained the coefficients for each material function from experimental data. While these material functions were not directly employed during this effort, a similar constitutive modeling strategy did prove fruitful.



## 4 Experimental Methods

This chapter describes the experimental arrangements and procedures needed to examine the strain rate-dependent behavior of PMR-15 at elevated temperature as well as the effects of prior aging temperature on the inelastic deformation behavior of the material. First, a detailed description of the test material is provided including specifics of material processing and specimen preparation. Then, experimental equipment and test procedures are reviewed.

### 4.1 Material and Test Specimen

The objective of the current research is to extend the VBOP to account for the effects of test temperature and prior aging temperature. While this is conceptually independent from any specific material, experiments must be conducted with a material that (1) exhibits test temperature specific behavior (2) is susceptible to aging at elevated temperature and (3) exhibits inelastic behavior that can be modeled with VBOP. To that end, PMR-15 neat resin was selected as the material of interest for this research effort.

#### 4.1.1 *PMR-15 Solid Polymer*

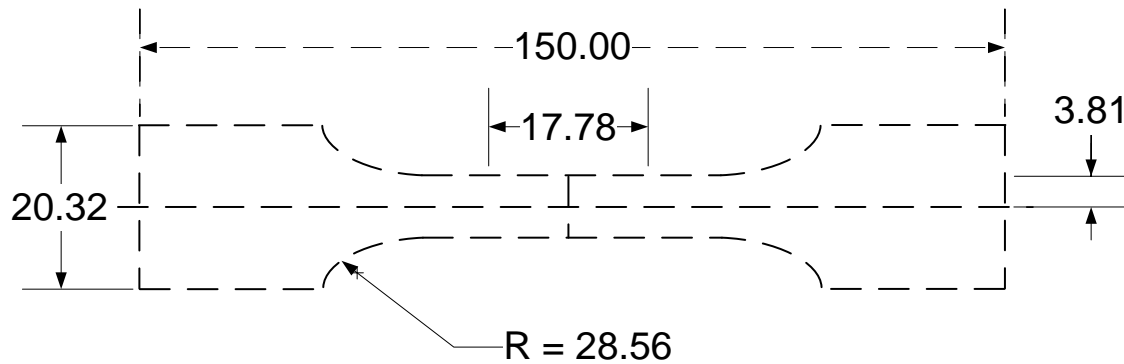
PMR-15 is a highly cross-linked thermosetting polyimide designed by NASA in the 1970's for use as a matrix material for high-temperature polymer matrix composites. It has a long-term use temperature of 288 °C with a  $T_g$  of ~347 °C (the specific  $T_g$  depends on processing and other factors) [22].

#### *4.1.2 Material Processing*

The PMR-15 neat resin that is used in the current research was supplied by HyComp Inc. of Cleveland Ohio in the form of 6 inch by 1 inch rectangular blanks with a nominal thickness of 0.125 inches. The PMR-15 blanks were post-cured by HyComp Inc. using the Air Force Research Laboratory standard post cure cycle shown in Table 1.1. Prior to machining, the blanks were screened for material quality and flatness. Blanks with obvious defects, such as voids or excessive curvature, that could affect mechanical testing were set aside. Slightly less than 10% of blanks were determined to be defective. This was attributed to the difficulty of producing panels of homogenous neat resin and does not reflect the typical defect rate when producing a composite with PMR-15 matrix.

#### *4.1.3 Specimen Geometry*

Standard dogbone-shaped specimens (shown in Figure 4.1) were machined from rectangular blanks by diamond grinding. Specimen thickness varied between 2.5 and 4.2 mm but was consistent along a given specimen. Some rectangular blanks were not machined into tensile specimens, but retained for measurement of weight change during aging.



Dimensions in millimeters  
All tolerances are  $\pm 0.025$  mm

**Figure 4.1 Test specimen.**

#### 4.1.4 Specimen Preparation

After machining, specimens were cleaned with a 2% solution of Micro 90 soap in water and were thoroughly rinsed with distilled water. After cleaning, all specimens were handled with nitrile gloves to prevent any contamination by skin oils. Specimens were then dried in an Isotemp Model 282A vacuum oven at 105 °C at approximately 1.1 inches of mercury for 10 days in order to remove as much moisture as possible. Specimens were determined to be “dry” when the weight measurements of several sample specimens stabilized and ceased decreasing. Weight measurements were conducted on a Mettler Toledo laboratory balance accurate to 0.01 mg. All dogbone-shaped specimens and rectangular blanks were stored at room temperature ( $\sim 23$  °C) in a dry-air-purged desiccator maintained at approximately 10 percent relative humidity until used in order to prevent moisture re-absorption and limit moisture effects on the material behavior. Specimens used for mechanical testing had two small dimples made in the edge of the gauge section to mount the extensometer. The dimples were made with a tool

specifically provided with the MTS extensometer. To prevent the textured surface of the mechanical testing machine grip from damaging the specimen, the gripping portions of each specimen were covered with a small piece of fiberglass composite prior to installation in the machine. Elastic modulus measurements were performed prior to aging. Since modulus tests are conducted at relatively low loads and at room temperature, the fiberglass tabs were held on with scotch tape. The tabs were removed before aging. After aging but prior to any high-temperature testing, the tabs were bonded to the specimens with M-Bond 200 adhesive to protect the specimens from being crushed by the grips.

## **4.2 Experimental Setup and Testing Procedures**

This section describes the material and equipment used to conduct the experimental investigation of the mechanical behavior of the PMR-15 neat resin. Additionally, specific mechanical test procedures are detailed.

### *4.2.1 Mechanical Testing Equipment*

An MTS Systems Corporation servo-hydraulic testing machine with water-cooled hydraulic wedge grips, a compact resistance furnace and a temperature controller were used for all mechanical testing. The MTS 810 Material Testing System was equipped with a 3-KIP load cell and a 318.10 vertically configured load frame. Input signal generation and data acquisition were accomplished with a FlexTest 40 digital controller.

A MTS single zone furnace model 653.01A, with an MTS model 409.83 temperature controller, was used for all elevated temperature tests. For elevated temperature testing, the furnace was calibrated on a periodic basis. For calibration, a

thermocouple was attached to a test specimen using high-temperature gasket material, alumina insulation, Kapton tape and wire. The instrumented specimen was then placed into the furnace. The furnace controller (using a separate non-contacting thermocouple exposed to the ambient environment near the test specimen) was adjusted to determine the oven temperature needed to achieve the desired temperature on the test specimen. The determined oven temperature was then used in actual tests. The temperature controller was tuned to avoid temperature overshoots and oscillation while testing. The MTS model 647.02B wedge grips were water cooled to prevent overheating when used in conjunction with the furnace. A grip pressure of 8 MPa was utilized to prevent slipping and to avoid crushing the specimen. Strain measurements were accomplished with a MTS model 632.53E-14 low contact force, high-temperature uniaxial extensometer of 12.5-mm gauge length. The system permitted testing under strain control, load control and displacement control. In addition, the immediate control mode switch capability of the system allowed for complex load histories such as loading a specimen at a constant strain rate under strain control and then seamlessly switching to load control upon reaching a target value of stress to conduct a creep test.

#### *4.2.2 Aging Chamber*

Specimens were aged at a variety of temperatures for durations up to 1000 h. It is an important assumption that the aging of PMR-15 at room temperature is negligible and that the only significant aging occurs at elevated temperature. The isothermal aging process was accomplished in a Blue M model 7780 air-circulating oven that was modified to continuously replenish the oven atmosphere with an externally provided inert

gas. In this case, ultra-high purity argon gas (99.999% pure) was supplied to the oven to displace the ambient atmosphere and eliminate oxidative degradation of PMR-15 during aging. When specimens were removed from the oven for test or inspection, the interior of the oven was briefly exposed to the ambient atmospheric and thermal conditions. When the oven door was closed, the oven automatically entered an 18-minute purge cycle that flushed out the internal oven chamber with argon. The flow rate of argon to the oven chamber was ~30 standard cubic feet per hour (SCFH) during normal operation and ~150 SCFH during the purge cycle. It is assumed that the thermal and atmospheric cycling that occurred when the oven was opened to retrieve specimens did not degrade or otherwise change the material. However, access to the oven was restricted to the absolute minimum required while aging was in progress to limit any possible effects from thermal cycling.

#### *4.2.3 Weight Measurement*

During aging, the weight of the rectangular blanks was periodically measured on a Mettler Toledo laboratory balance accurate to 0.01 mg and scaled by specimen volume to account for variations in specimen thickness. Note that the rectangular blanks were subjected to the same aging regimen as the dogbone-shaped specimens.

#### *4.2.4 Mechanical Test Procedures*

Various tests were performed to elucidate the rate-dependent behavior of PMR-15 at elevated temperatures. The following tests were conducted on both aged and unaged specimens. These tests reveal aspects of rate (time)-dependent mechanical behavior as

well as provided a means of collecting the data required for VBOP model characterization and subsequent model validation.

#### *4.2.4.1 Room Temperature Elastic Modulus*

Specimen to specimen variability needed to be assessed prior to testing to ensure accurate results. This was accomplished by measuring the room-temperature elastic modulus of every specimen prior to any aging or testing at elevated temperature. Each specimen was identified with a unique identifier and the gauge section width and thickness were measured to determine cross sectional area. Then each specimen was loaded in stress control to 3 MPa at a rate of 1 MPa/s and unloaded to zero stress at the same stress rate. The specific magnitude of load and load rate were after Broeckert's [22] suggestion for PMR-15 and were chosen to ensure that the stresses remain in the quasi-elastic regime for the entire test. Data collected during these tests were fitted to a first order linear polynomial  $p(x) = p_1x + p_2$  with the MATLAB command 'polyfit(x,y,n)' where  $x$  = strain data and  $y$  = stress data and  $n=1$ . MATLAB output best-fit values for  $p_1$  and  $p_2$  where  $p_1$  = elastic modulus. Specimens with exceptionally high or low elastic moduli were then removed from consideration.

#### *4.2.4.2 Monotonic Tensile Test at Constant Strain Rate*

Tensile tests to failure conducted at constant strain rates varying from  $10^{-6}$  to  $10^{-3} \text{ s}^{-1}$  are useful for exploring the effect of strain rate. Results from these tests identify the relationship between strain rate and flow stress, elastic modulus, and tangent modulus. In this effort, a set of tensile tests at constant strain rates were accomplished for each combination of test temperature, prior aging temperature and duration. Tensile tests

to failure conducted at several constant strain rates are shown schematically in Figure 4.2. An example of the effect of strain rate on the stress-strain behavior of PMR-15 is shown in Figure 4.3 (reproduced from McClung [19]).

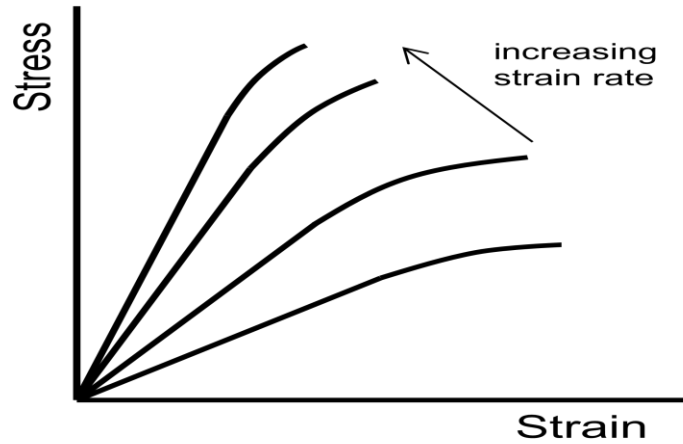


Figure 4.2 Schematic of monotonic tensile tests performed at several strain rates.

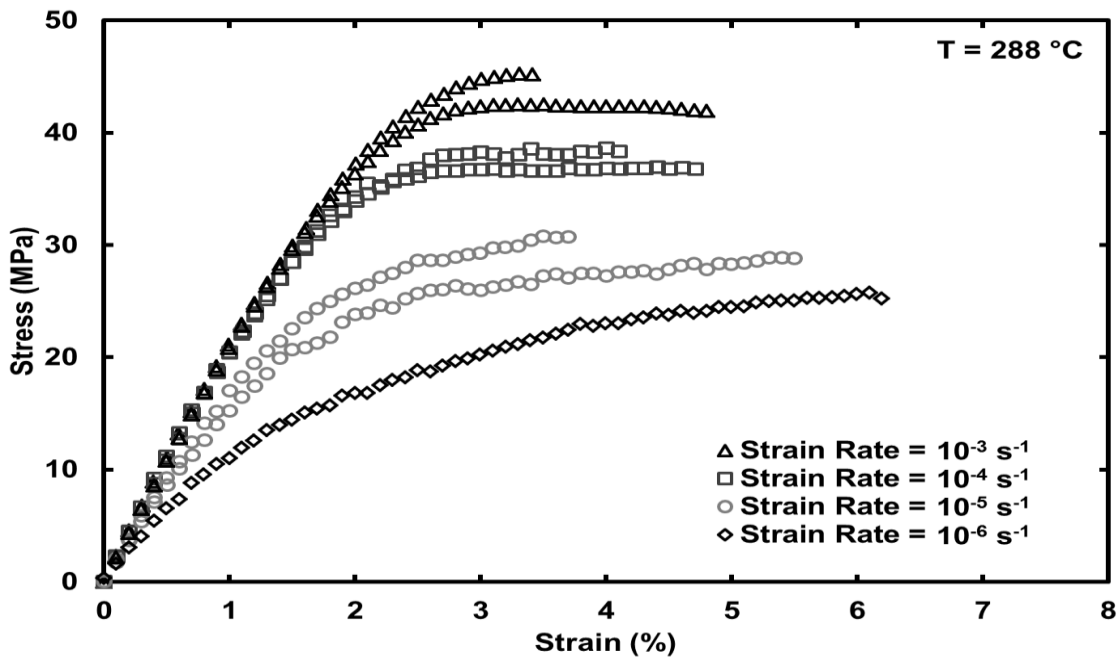


Figure 4.3 Stress-strain curves obtained for PMR-15 in tensile tests to failure conducted at constant strain rates of  $10^{-6}$ ,  $10^{-5}$ ,  $10^{-4}$ , and  $10^{-3} \text{ s}^{-1}$  at 288 °C. The dependence of the stress-strain behavior on the strain rate is evident. Reproduced from McClung [19] Figure 5.1.



#### 4.2.4.3 *Constant Strain Rate Test with Intermittent Period of Relaxation*

Relaxation is defined as a change in stress with time when strain is held constant. A relaxation test is conducted by holding strain constant while measuring time and stress. According to Ruggles and Krempf [66], the stress at the end of a relaxation test that has been allowed to proceed long enough to reach the asymptotic solution is very near the equilibrium stress, which is considered the time-independent contribution to the applied stress. The constant strain rate test with intermittent periods of relaxation consists of loading at a constant strain rate until a specific strain is reached. Then the strain rate is held at zero and the relaxation test starts during which stress and time are carefully recorded. Once stress ceases to change, loading at the original strain rate is resumed as shown schematically in Figure 4.4. If possible, the relaxation test is repeated several times before failure. The strain interval between relaxation periods should be sufficiently large in order to allow the stress to increase until the flow stress level characteristic of the loading strain rate is reached. Additionally, it is important that the next period of relaxation not be started before transients such as the overshoots evident on the  $10^{-5}\text{s}^{-1}$  curves in Figure 4.5 (reproduced from [19]) have disappeared.

Multiple constant strain rate tests with a single period of relaxation introduced at different values of strain can be used to identify the equilibrium stress curve. By carrying out these tests at several strain rates one can explore the dependence of the relaxation behavior on prior strain rate.

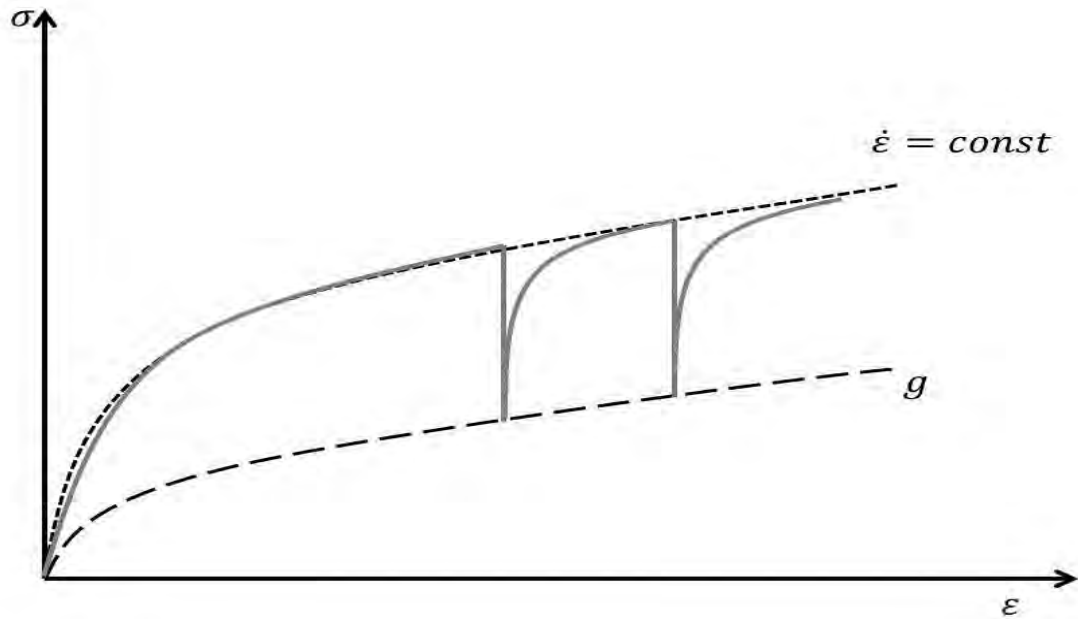


Figure 4.4 Schematic of a constant strain rate test with intermittent periods of relaxation.

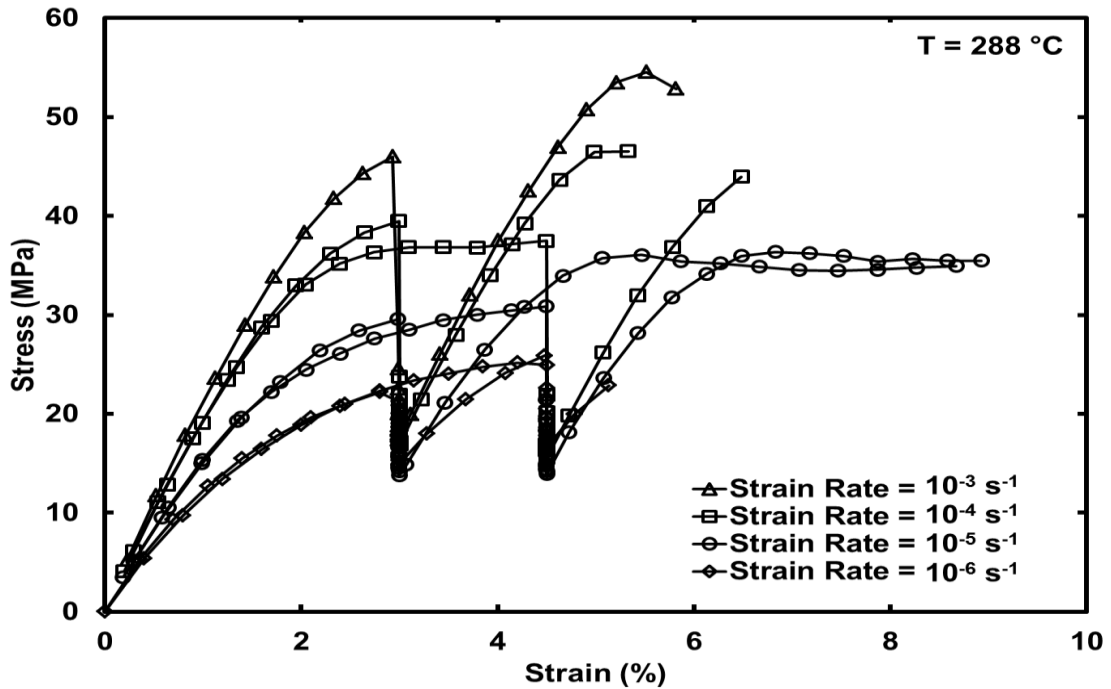


Figure 4.5 Stress-strain curves obtained for PMR-15 in constant strain rate tests with intermittent periods of relaxation at 288 °C. Reproduced from [19].

#### *4.2.4.4 Strain Rate Jump Test*

The Strain Rate Jump Test (SRJT) consists of segments of monotonic loading conducted at two or more different strain rates. The results of this test are compared to the stress-strain curves produced in monotonic tensile tests performed at each strain rate of interest. Upon a change of strain rate, materials that do not exhibit the strain rate history effect (SRHE) (in the sense used by Klepaczko [79], and defined by Ruggles and Krempl [34]) will quickly reach the stress-strain curve characteristic of a given strain rate as shown schematically in Figure 4.6. The SRJT provides an insight into the existence or lack of SRHE. The lack of SRHE implies that once the inelastic flow is fully established, a unique stress-strain curve is established for a given strain rate and during the SRJT the material “forgets” the prior history of straining at different rates and “returns” to the stress-strain curve characteristic of a given strain rate.

#### *4.2.4.5 Creep Test*

The influence of prior strain rate on creep behavior was explored in creep tests of 6 h duration by loading the specimen at a constant strain rate to a target stress of 21 MPa and then instantaneously switching the mode to stress control to perform the creep test. Creep tests were repeated for several prior strain rates to assess the effect of prior strain rate on creep.

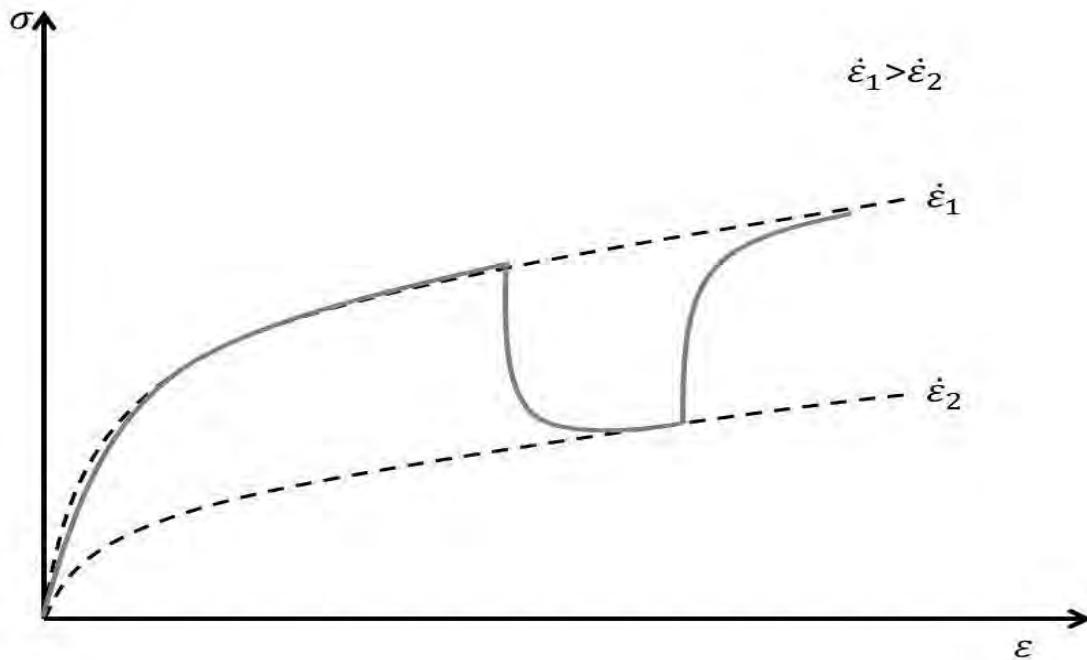


**Figure 4.6 Schematic of stress-strain curves obtained during a strain rate jump test.**

#### 4.2.4.6 McLean-Type Dip Test

The McLean-Type Dip Test (MTDT) consists of monotonic loading (in stress or strain control) to a given stress or strain, followed by an instantaneous reduction in stress (dip) followed by a period of creep as shown in Figure 4.7. Each creep period was continued until strain ceased to change in a measurable way. The MTDT was conducted to determine the current value of the equilibrium stress. Positive (negative) creep strain indicates that the creep stress is currently greater (less) than the equilibrium stress. Zero creep strain indicates that the creep stress and the equilibrium stress are at the same value.

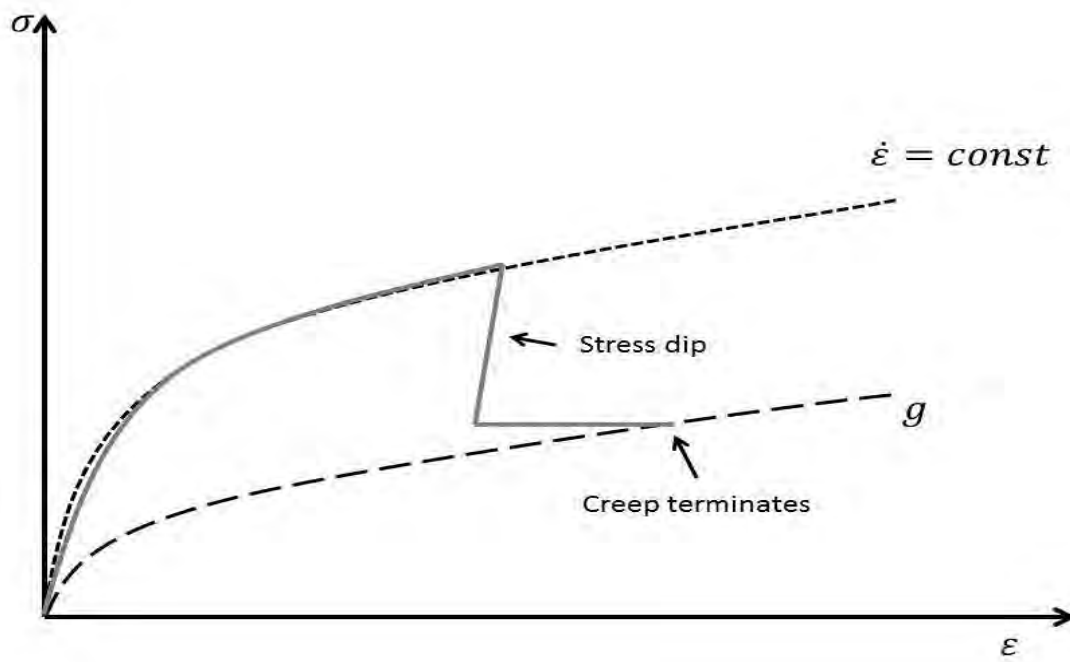


Figure 4.7 Schematic of stress-strain curve obtained during a McLean type dip test.

## 5 VBOP Model Characterization

This chapter provides a conceptual description of the model characterization techniques utilized during this effort. It includes a brief discussion of McClung's model characterization procedure for VBOP. In addition, this chapter discusses the strategy utilized for determining the effects of test temperature and of prior aging temperature on the deformation behavior of polymers.

### 5.1 Experimentally Based Characterization of VBOP

McClung [19] proposed a well-defined procedure for the characterization of the material parameters of VBOP. The model is characterized from experimental data collected during a limited number of tests. The characterization procedure is repeated for specimens exposed to different aging and mechanical test conditions to determine how the material parameters of VBOP vary as these conditions are changed.

#### 5.1.1 *Elastic Modulus and Tangent Modulus*

The elastic modulus is the slope of the stress-strain curve in the quasi-elastic region. Care was taken to avoid calculating this slope from "noisy" data points close to the origin. The tangent modulus is defined as the slope of the stress-strain curve at the largest strain of interest and is taken directly from the experimental data. It is important that the tangent modulus be measured in a region of fully developed plastic flow (past the knee) so that it truly represents a tangent modulus. This can be difficult to achieve when material experiences early failures.

### 5.1.2 Equilibrium Stress and Isotropic Stress

During constant strain rate tests with intermittent periods of relaxation, McClung [19] noted that the stress-strain values at the end of sufficiently long periods of relaxation form a curve that has a shape of a stress-strain diagram. Hence, it may be expedient to postulate that the relaxation comes to rest at nonzero stresses that form the equilibrium boundary. This may be interpreted as the stress-strain curve for a vanishing strain rate. In the context of the VBOP, a point on the equilibrium stress curve is found when the Cauchy (applied) stress becomes stationary. Therefore, the curve formed by the stress-strain points at the end of the relaxation tests is postulated to be, in fact, the equilibrium stress curve itself. Thus, the results of a sufficiently long relaxation test identify a specific point on the equilibrium stress curve. If that point along the equilibrium stress curve is contrived to occur at a sufficiently large strain, such that the asymptotic solution can be assumed, then the following equation [57] for the isotropic stress  $A$  holds

$$A = \{g - E_t \varepsilon\} \quad (5.1)$$

where the brackets  $\{n\}$  designate the asymptotic limit of  $n$ . Equation (5.1) can be illustrated by the schematic in Figure 3.3 and is confirmed by recalling that for the asymptotic solution  $f = E_t \varepsilon$ . Since all values on the right-hand side of equation (5.1) are known from the experimental data, the isotropic stress for that particular value of strain can be readily calculated. If the material is cyclically neutral, then the isotropic stress is constant and known for all values of strain. If the material exhibits cyclic hardening

(softening), then the isotropic stress evolves according to equation (3.18) and must be experimentally evaluated through fully reversed cyclic tests.

### 5.1.3 Viscosity Function and Shape Function

The viscosity function is the repository of the rate-dependent portion of the material response. The material parameters  $k_1$ ,  $k_2$ , and  $k_3$  of the viscosity function  $k$  can be determined from the data collected during relaxation tests conducted with various prior strain rates. Recall that the strain rate during a relaxation test is zero and the governing equation (3.13) of the VBOP simplifies to

$$-k\dot{\sigma} = \sigma - g \quad (5.2)$$

The value of the equilibrium stress is found as discussed in Section 5.1.2 and the stress and stress rate are obtained directly from the experimental data. McClung [19] noted that only relaxation data obtained in the fully established plastic regime should be used to characterize the viscosity function because transients in the material behavior before or near the knee of the stress-strain curve will distort the value of the viscosity function. McClung also noted that the parameter  $k_1$  controls the strain at which the stress-strain curve departs from the quasi-linear regime. Thus, viscosity function parameters  $k_1$ ,  $k_2$ , and  $k_3$  are selected to capture experimental relaxation behavior and the departure from the quasi-linear behavior.

McClung further noted that both the shape function  $\Psi$  and the viscosity function  $k$  affect the model behavior in the region around the knee of the stress-strain curve. Sequentially determining first the viscosity function and then the shape function does not acknowledge this relationship. Failure to account for this interplay caused



unreasonable model behavior. McClung applied an iterative strategy that involved fitting the viscosity function to the stress values during the last two hours of relaxation followed by a least squares fit of the shape function to the experimental data around the knee of the stress-strain curve. If acceptable results were not observed, the viscosity function was re-evaluated with the new shape function parameters and then the shape function was again determined utilizing the new viscosity function parameters. This process was repeated until parameters that produced acceptable results were found.

## **5.2 Experimental Characterization of the Effects of Test Temperature on Deformation Behaviors**

It is clear to anyone who has accidentally left a compact disc made of polycarbonate on the dashboard of an automobile on a hot summer day, that temperature can have a dramatic effect on the deformation behavior of polymers. In the absence of a direct knowledge of the microstructural changes that occur at every temperature, a phenomenological approach has been selected. The essential concept is to repeat a specific test or series of tests on identically prepared specimens at various temperatures of interest. If enough data are collected at a sufficient number of temperatures then any significant temperature-dependent behavior should manifest itself in the results of the tests. The key is to select the test(s) that will reveal the temperature-dependent behavior. While several material properties such as ultimate tensile strength and modulus, are known to be temperature-dependent for polymers [80] more complicated aspects of mechanical behavior of solid polymers like the transition to inelastic flow are less well understood. In the current research, standard VBOP model characterization tests will be

conducted at multiple test temperatures while maintaining other variables constant. The results of these experiments are discussed in Chapter 6.

### **5.3 Experimental Characterization of the Effects of Prior Aging Time and Prior Aging Temperature on Deformation Behaviors**

The effect of prior aging on the deformation behavior of PMR-15 has been clearly demonstrated [19, 20, 27, 36, 49]. In the past, researchers have typically selected a common aging and test temperature. Several specific temperatures (260, 288 and 316 °C) have been studied with dramatic results. While the selection of a common aging/test temperature does accurately represent the typical use scenario, where aging occurs as the material is in service at an elevated temperature, it has a downside in that *two* independent variables are modified for each selected temperature. In this work, it is postulated that the aging temperature and the test temperature are different variables that affect mechanical behavior in different ways and must be separated for a careful study of the effects of test temperature and prior aging temperature on deformation behavior.

#### *5.3.1 Effects of Prior Aging Duration*

For PMR-15, the experimental evidence shows that prior isothermal aging is a long-term phenomenon with a time scale from the tens of hours to many hundreds of hours. Loading histories that have been explored thus far have occurred, at most, over 10-20 hours and aging has been assumed to be negligible during this short-term loading. That prior aging duration affects mechanical behavior is without question. As an example, at 288 °C, increased prior aging time resulted in [19]

- an increase in elastic modulus

- an increase in the tangent modulus
- a delay in the departure from quasi-linear behavior
- an increase in flow stress level
- a decrease in inelastic straining capacity
- a reduction in strength for aging durations greater than 1000 hours

What is unknown is the effect of prior aging *temperature* on mechanical behavior.

### 5.3.2 *Effects of Prior Aging Temperature*

To determine the effect of prior aging temperature on the inelastic deformation behavior of PMR-15, specimens are exposed to various prior aging temperatures for durations up to 1000 h while the test temperature is held constant. Note that the temperature for mechanical testing is not selected arbitrarily. It has been selected such that fully established plastic flow can be reached during testing for specimens subjected to a wide range of the prior aging temperatures and times. Standard VBOP model characterization tests are conducted on specimens aged for various durations at the chosen aging temperatures while maintaining test temperature constant. The results of these experiments are discussed in Chapter 9.

## **6 Unaged PMR-15 Neat Resin Tested at 274-302 °C: Experimental Observations**

This chapter discusses the results of mechanical tests on unaged PMR-15 polymer tested at 274, 288 and 302 °C.

### **6.1 Assessment of Specimen-to-Specimen Variability**

PMR-15 test specimens are known to exhibit a certain amount of specimen-to-specimen variability. To avoid drawing false conclusions from specimens that display uncharacteristic behavior it is necessary to evaluate this variability. To accomplish this, the room temperature elastic modulus of each specimen is measured. Previous testing has shown that at room temperature PMR-15 exhibits nearly linear elastic behavior for stresses below 3 MPa [19-21, 27]. Elastic modulus testing was accomplished by conducting a simple tensile test in stress control. Loading was increased at 1 MPa/s until the stress of 3 MPa was reached, at which point the specimen was unloaded to zero stress. To limit data scatter, only data collected at stresses above 0.5 MPa were utilized to calculate the room temperature elastic modulus. In addition, to eliminate any hysteresis effect only data from the loading portion of the stress-strain curve were considered. Then, a least squares linear fit to the data was used to determine the room temperature elastic modulus for each specimen. The average room temperature elastic modulus for the batch of PMR-15 neat resin specimens used for this research was 3.708 GPa with a standard deviation of 0.20 GPa. This compares favorably with data collected by McClung [19], Ozmen [27], Diedrick [20] and Wahlquist [21] (see Table 6.1). Moduli produced by individual specimens were compared to the average room temperature elastic modulus to determine if they were representative of the current batch of resin. No

specimens were determined to be anomalous due to an exceptionally high or low modulus. It should be noted that the batch of PMR-15 neat resin specimens tested by McClung [19] exhibited a slightly higher average modulus than typically observed by other researchers. This is attributed to a batch-to-batch difference that does not appear to significantly affect the overall mechanical behavior of the material.

**Table 6.1 Comparison of the Average Room Temperature Elastic Moduli of PMR-15 Neat Resin Measured by Various Researchers [19-21, 27]**

Researcher	Average Room Temperature Elastic Modulus (GPa)	Standard Deviation (GPa)
McClung	4.2	0.25
Ozmen	3.77	0.19
Diedrick	3.63	0.22
Wahlquist	3.63	0.20
Ryther	3.708	0.20

Data collected by other researchers were utilized as part of this research. Since these data were produced using several different batches of PMR-15 neat resin specimens over a period of several years, some specimen-to-specimen and batch-to-batch variability existed. In an effort to reduce data scatter, results obtained by other researchers were scaled by the average room temperature elastic modulus obtained in this research effort. This was accomplished by scaling the measured value of stress  $\sigma$  by the ratio of the average room temperature elastic modulus obtained in this research,  $\bar{E}_{RT}$  and the room temperature elastic modulus of the specimen,  $E_{RT}$  as shown below

$$\sigma_{scaled} = \sigma \frac{\bar{E}_{RT}}{E_{RT}} \quad (6.1)$$

In the majority of test histories where multiple specimens were tested, this technique significantly reduced the scatter observed in the experimental data. All strain-controlled tests, including relaxation tests, were scaled in this manner.

## **6.2 Strain Rate Sensitivity**

Previous studies [81, 82] revealed that PMR-15 polymer exhibited positive, nonlinear strain rate sensitivity at 288 and at 316 °C. To further explore the effect of temperature on strain rate sensitivity of PMR-15 neat resin, specimens were subjected to tensile tests at constant strain rates of  $10^{-6}$ ,  $10^{-5}$ ,  $10^{-4}$  and  $10^{-3}$  s<sup>-1</sup> at 274 and at 302 °C. To evaluate possible batch-to-batch differences between specimens tested by previous researchers and specimens produced for the current effort, several additional constant strain rate tests were conducted at 288 °C. The results of these tests indicate that batch-to-batch variability had a negligible effect on the mechanical behavior of the material. Results are typified in Figure 6.1, Figure 6.2 and Figure 6.3 where the stress-strain curves obtained at 274-302 °C are presented. Note that data from McClung and Ruggles-Wrenn [81] are included in Figure 6.2 together with results from the present study. The conditions of each tensile test conducted during this effort are listed in Table 12.1.

The stress-strain curves produced at 274, 288 and 302 °C do not show a distinct linear range. However, the stress-strain curves obtained at different strain rates at each given temperature exhibit the same quasi-elastic slope upon leaving the origin. It is seen that this quasi-elastic slope decreases with increasing temperature. After the transition from the initial quasi-elastic to the inelastic regime, the material exhibits positive, nonlinear strain rate sensitivity. At 274, 288 and 302 °C, the flow stress level increases

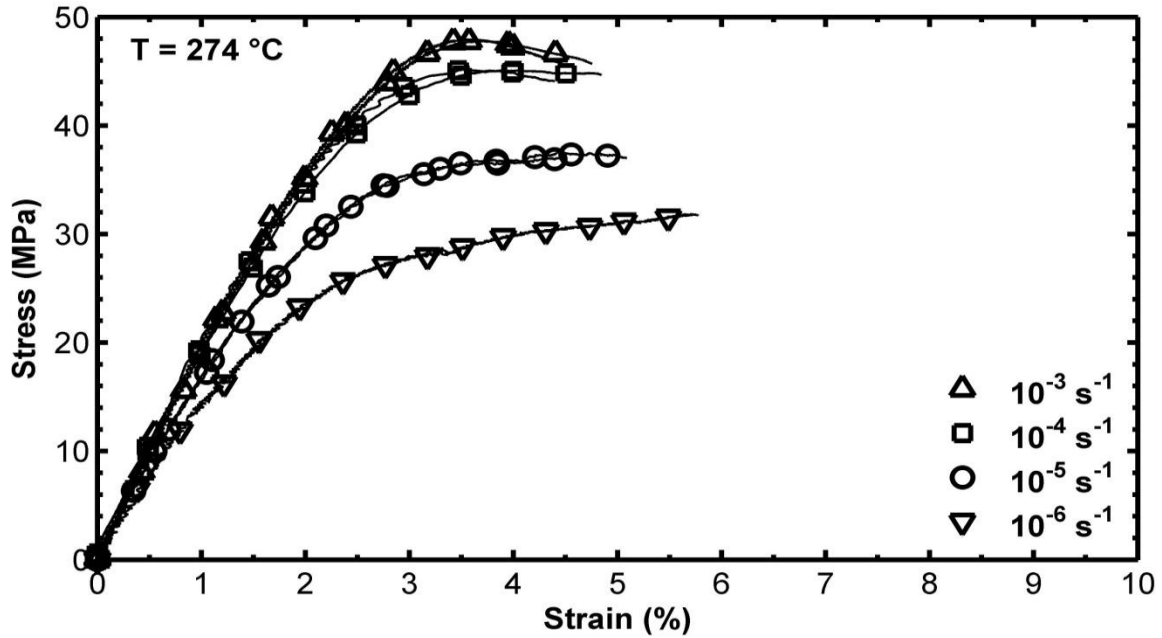


Figure 6.1 Stress-strain curves obtained for the PMR-15 polymer in tensile tests to failure conducted at constant strain rates of  $10^{-6}$ ,  $10^{-5}$ ,  $10^{-4}$ , and  $10^{-3} \text{ s}^{-1}$  at 274 °C. The dependence of the stress-strain behavior on the strain rate is evident.

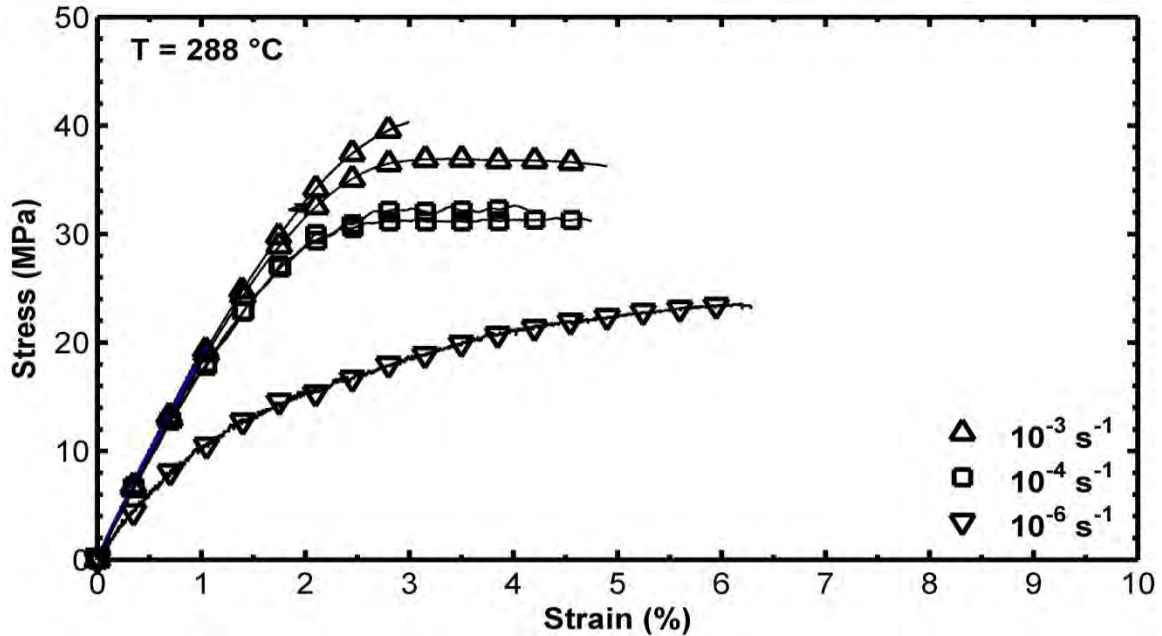
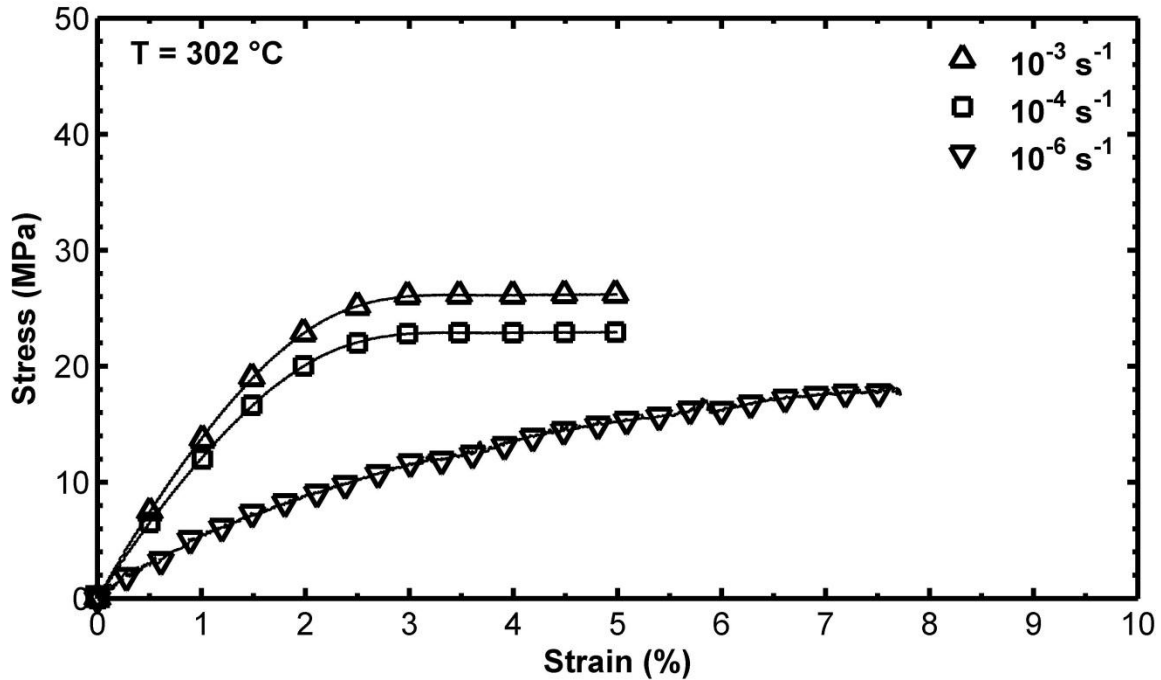


Figure 6.2 Stress-strain curves obtained for the PMR-15 polymer in tensile tests to failure conducted at constant strain rates of  $10^{-6}$ ,  $10^{-4}$ , and  $10^{-3} \text{ s}^{-1}$  at 288 °C. The dependence of the stress-strain behavior on the strain rate is evident. Data from [81] are included.



**Figure 6.3** Stress-strain curves obtained for the PMR-15 polymer in tensile tests to failure conducted at constant strain rates of  $10^{-6}$ ,  $10^{-4}$ , and  $10^{-3} \text{ s}^{-1}$  at  $302 \text{ }^\circ\text{C}$ . The dependence of the stress-strain behavior on the strain rate is evident.

with increasing strain rate. At a given strain rate, the flow stress level decreases with increasing temperature. The tangent modulus (slope of the stress-strain curve obtained at the largest strain) increases with increasing temperature. Additionally, the shape of the stress-strain curve gradually changes as the strain rate increases. Transition from quasi-elastic behavior to inelastic flow becomes more pronounced with increasing strain rate. Moreover, at a given strain rate this transition becomes more prominent with decreasing temperature. The stress-strain curves obtained at slower strain rates depart from near linear behavior at much lower stress levels than those obtained at higher strain rates. As temperature increases, this effect is magnified.

Note, that due to the limited ductility of the PMR-15 polymer, specimens often fail before the stress-strain curves reach the region where plastic flow is fully established.



Experiments on PMR-15 conducted by Diedrick [20] at 23, 230 and 260 °C revealed that in monotonic tensile tests, the quasi-linear behavior frequently persisted until failure. Diedrick reported that although most specimens failed prior to entering the flow stress regime, strain rate dependence was still evident in the quasi-elastic region. Of note is that the quasi-elastic slope of the stress-strain curves decreased as the temperature increased from 23 to 260 °C. In the 230-302 °C temperature range, the failure strain increased with decreasing strain rate. Furthermore, for a given strain rate the failure strain increased with increasing temperature.

### **6.3 Strain Rate History Effect**

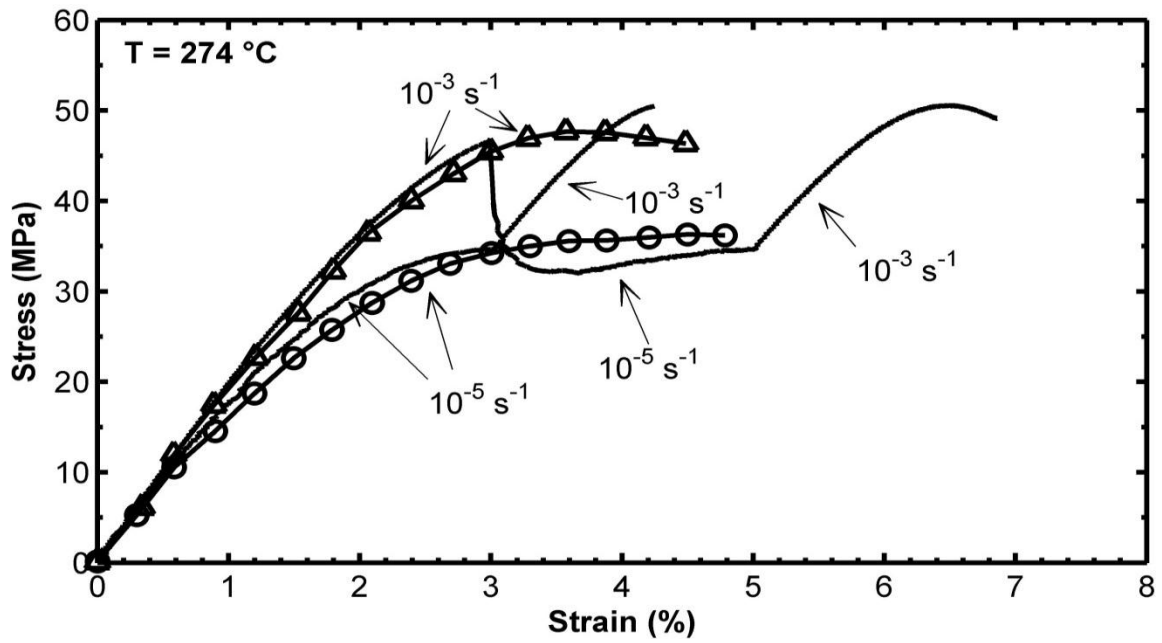
The Strain Rate Jump Test (SRJT) [34, 68] consisting of segments of monotonic loading at two different strain rates, was performed to assess whether the PMR-15 polymer exhibits the strain rate history effect at 274 and 302 °C. The strain rates were  $10^{-3}$  and  $10^{-5} \text{ s}^{-1}$ . The stress-strain curves produced at 274 °C are plotted in Figure 6.4(a) together with the stress-strain curves obtained at constant strain rates of  $10^{-3}$  and  $10^{-5} \text{ s}^{-1}$ . A reduction in strain rate by two orders of magnitude causes a sharp decrease in stress, with the flow stress reaching a level characteristic of the lower strain rate. The portion of the stress-strain curve obtained at  $10^{-5} \text{ s}^{-1}$  quickly becomes coincident with the stress-strain curve produced in the constant strain rate test conducted at the same rate. When the strain rate is later increased from  $10^{-5}$  to  $10^{-3} \text{ s}^{-1}$  the stress increases to the flow stress level associated with the  $10^{-3} \text{ s}^{-1}$  strain rate. Comparable behavior is seen when the SRJT is conducted with the  $10^{-5} \text{ s}^{-1}$  strain rate followed by a jump to the  $10^{-3} \text{ s}^{-1}$  strain rate. In this case, specimen failure occurred prior to returning to the lower strain rate of  $10^{-5} \text{ s}^{-1}$  at

the strain of 5%. Qualitatively similar results for tests conducted at 302 °C are shown in Figure 6.4(b).

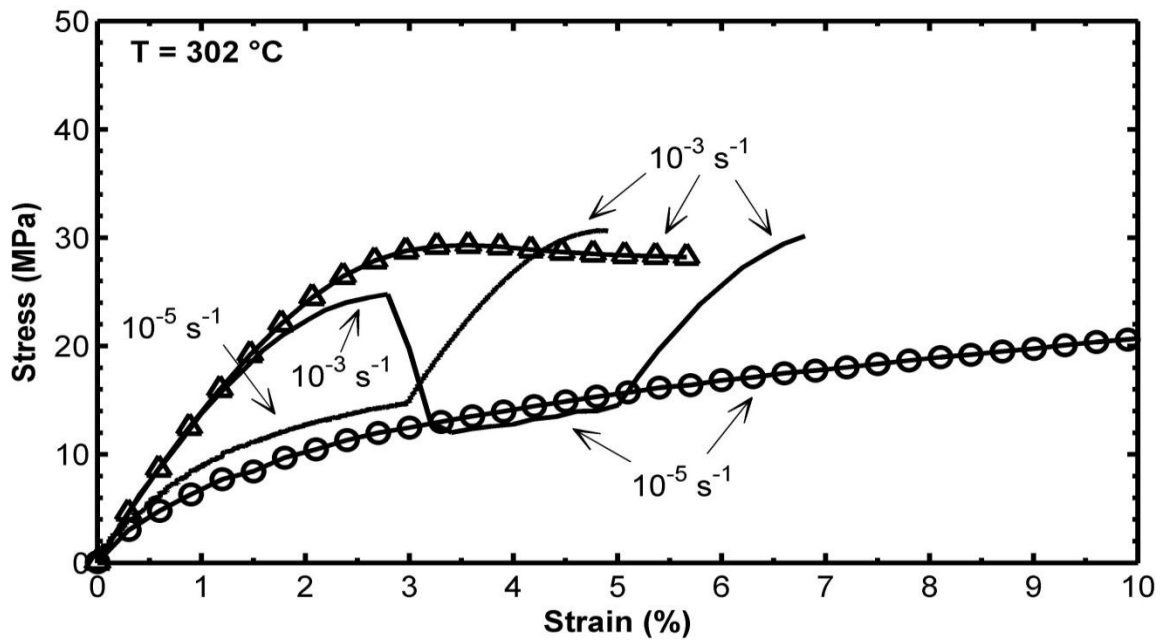
Results in Figure 6.4 suggest that once the inelastic flow is fully established, a unique stress-strain curve is obtained for a given strain rate and temperature. At 274 and 302 °C, the PMR-15 polymer does not exhibit the strain rate history effect, i.e., the material “forgets” prior history of straining at different rates and “returns” to the stress-strain curve characteristic of the given strain rate and temperature. McClung [81] and Ruggles-Wrenn [82] reported similar results for PMR-15 neat resin at 288 and 316 °C, respectively. Combined evidence suggests that PMR-15 neat resin does not exhibit strain rate history effect in the 274-316 °C temperature range. Additionally, it appears that temporarily reducing strain rate and then returning to the original, higher strain rate (as done during this SRJT) may allow the PMR-15 polymer achieve larger strain prior to failure than if the original, higher strain rate had been maintained throughout the test.

#### **6.4 Relaxation Behavior**

Relaxation behavior was studied in monotonic tests with a period of relaxation of fixed duration at 274, 288 and 302 °C. In these tests, the specimen is loaded at a constant strain rate to a target strain in the region of fully established inelastic flow, where a 12-h relaxation period is introduced. At the end of the relaxation period, straining resumes at the given strain rate and continues until specimen failure. The tests were conducted under strain control using strain rates of  $10^{-6}$ ,  $10^{-5}$ ,  $10^{-4}$  and  $10^{-3} \text{ s}^{-1}$  during loading and of course,  $\dot{\epsilon} = 0 \text{ s}^{-1}$  during the relaxation intervals. In tests conducted at 274, 288 and 302 °C a relaxation period was incorporated at  $\epsilon = 4.5$ , 4.5 and 5.0 %, respectively. The



(a)



(b)

Figure 6.4 Stress-strain curves obtained for the PMR-15 polymer in strain rate jump tests and in constant strain rate tests at: (a) 274 °C and (b) 302 °C. Upon a change in the strain rate, the material returns to the stress-strain curve characteristic for that particular strain rate.

target strains for relaxation periods conducted at different temperatures were selected to be the largest strains that could be achieved prior to failure at all strain rates. Results are typified in Figure 6.5, Figure 6.6 and Figure 6.7, where stress drop during relaxation is presented as a function of relaxation time. Note that the results at 288 °C in Figure 6.6 are from [81].

The plots in Figure 6.5 - Figure 6.7 show that the change in stress during relaxation is profoundly influenced by prior strain rate at all temperatures in the 274-302 °C range. At each temperature, a much larger decrease in stress is observed after loading at  $10^{-3} \text{ s}^{-1}$  than in relaxation following loading at  $10^{-6} \text{ s}^{-1}$ . In addition, the magnitude of the stress drop for a given prior strain rate decreases with increasing temperature. This may be a result of the decrease in flow stress levels with increasing temperature. Note that the relaxation rate was not zero when the relaxation tests were stopped. Upon continuation of the relaxation tests, the stress would have dropped further at an ever-decreasing rate, finally coming to rest at a nonzero level. However, because the stress rate at the end of the relaxation test was small, it is reasonable to conjecture that the rest stress levels were nearly reached after 12 h of relaxation. It is noteworthy that the stress rate at the end of the relaxation period, while still small, is measurably larger for tests conducted at lower temperatures than for those conducted at higher temperatures in the 274–302 °C range. As expected, the relaxation rate is clearly influenced by temperature. For a complete accounting of test conditions during each relaxation test conducted during this effort, refer to the test matrix found in Table 12.2.

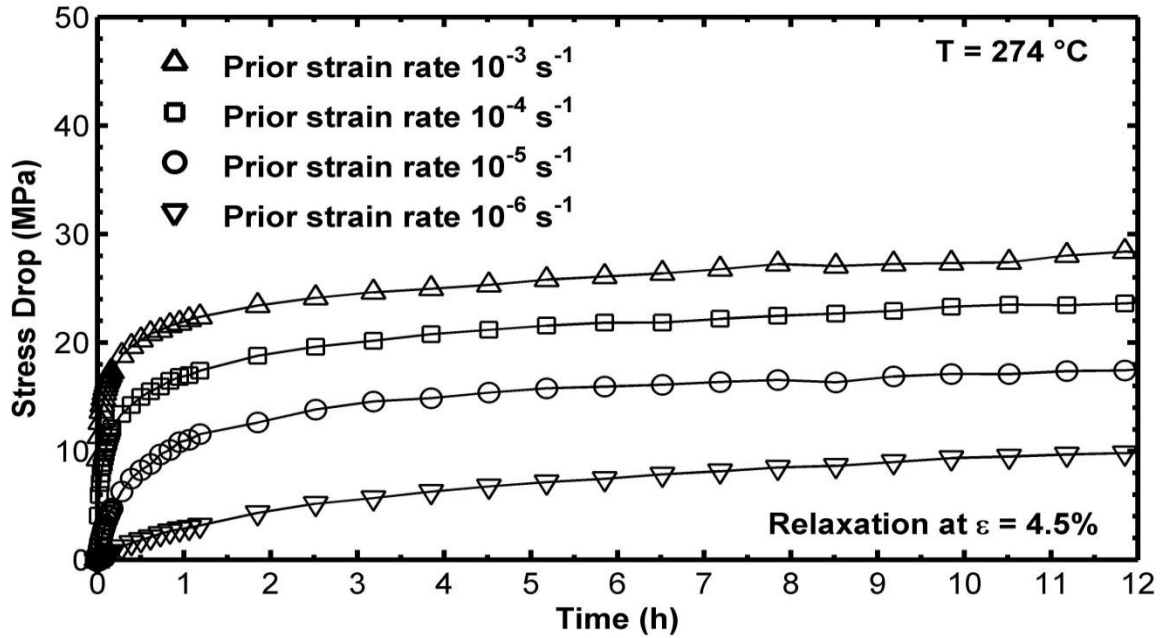


Figure 6.5 Stress decrease versus relaxation time for the PMR-15 polymer at 274 °C. The influence of prior strain rate on the stress drop during relaxation is evident.

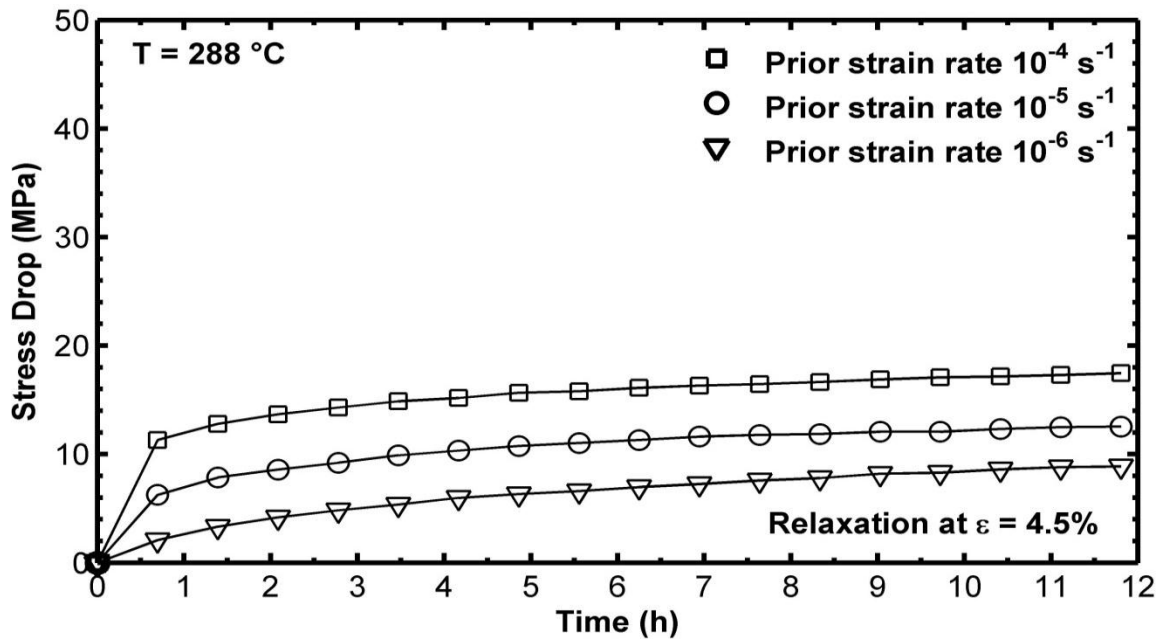
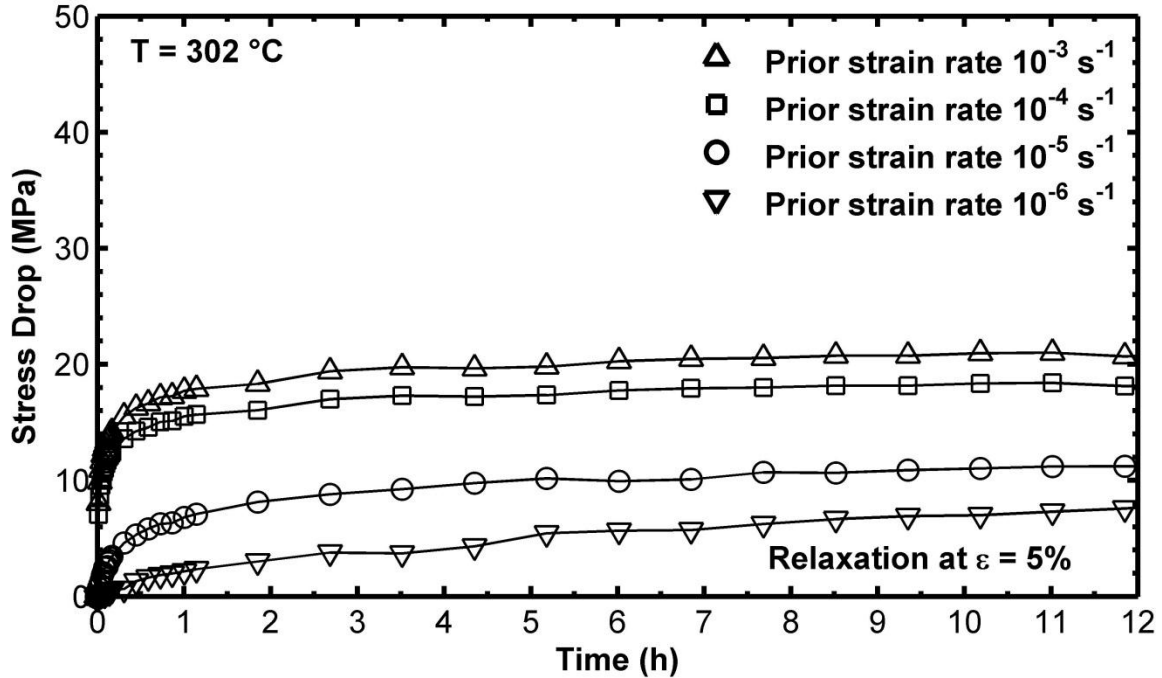


Figure 6.6 Stress decrease versus relaxation time for the PMR-15 polymer at 288 °C. The influence of prior strain rate on the stress drop during relaxation is evident. Data from [81].



**Figure 6.7** Stress decrease versus relaxation time for the PMR-15 polymer at 302 °C. The influence of prior strain rate on the stress drop during relaxation is evident.

## 6.5 Creep Behavior

The influence of prior strain rate on creep behavior was explored in 6-h creep tests conducted at temperatures in the range of interest. The capability of the testing system to instantaneously switch control mode made it possible to load a specimen to the target creep stress at a constant strain rate under strain control, and then switch the mode to load control to perform a creep test. At 274, 288 and 302 °C, the specimens were loaded to the target creep stress of 21 MPa at constant strain rates of  $10^{-6}$  and  $10^{-4} \text{ s}^{-1}$ . Additional tests were conducted at 302 °C where specimens were loaded to 21 MPa at  $10^{-5}$  and  $10^{-3} \text{ s}^{-1}$ . The creep strain vs. time curves are presented in Figure 6.8, Figure 6.9 and Figure 6.10. For a complete listing of the specific conditions of each creep test conducted during this study, please refer to the test matrix found in Table 12.3.

It is evident that prior strain rate strongly influences creep behavior at all temperatures in the 274–302 °C range. For a given temperature and stress level, creep strain accumulation increases nonlinearly with increased prior strain rate. An increase of one order of magnitude in prior strain rate results in much less than a tenfold increase in creep strain. Results produced in creep tests conducted at 274 and 288 °C reveal modest amounts of primary creep for prior strain rates of  $10^{-6}$  and  $10^{-4}$  s<sup>-1</sup>. At 302 °C, large creep strains are accumulated at 21 MPa in tests conducted with prior strain rates of  $10^{-5}$ ,  $10^{-4}$  and  $10^{-3}$  s<sup>-1</sup>. Conversely, repeated tests performed with the loading rate of  $10^{-6}$  s<sup>-1</sup> produced little or no creep strain before failure. This is likely due to the large amount of inelastic strain accumulated prior to reaching 21 MPa at the beginning of the creep period.

## **6.6 Summary of the Key Effects of Test Temperature on Deformation Behavior**

The inelastic deformation behavior of PMR-15 neat resin was investigated at temperatures in the 274-302 °C range. At all temperatures considered in this study, PMR-15 exhibits positive, nonlinear strain rate sensitivity in monotonic loading. A unique stress-strain curve is produced for each strain rate in the inelastic flow region. For a given strain rate, temperature has significant quantitative effects on the stress-strain behavior of the PMR-15 polymer. The elastic modulus decreases with increasing temperature. Departure from the quasi-linear behavior is accelerated with increasing temperature. The tangent modulus (slope of the stress-strain curve obtained at the largest strain) increases with increasing temperature. The stress level in the region of fully established inelastic flow decreases with increasing temperature. The change in flow

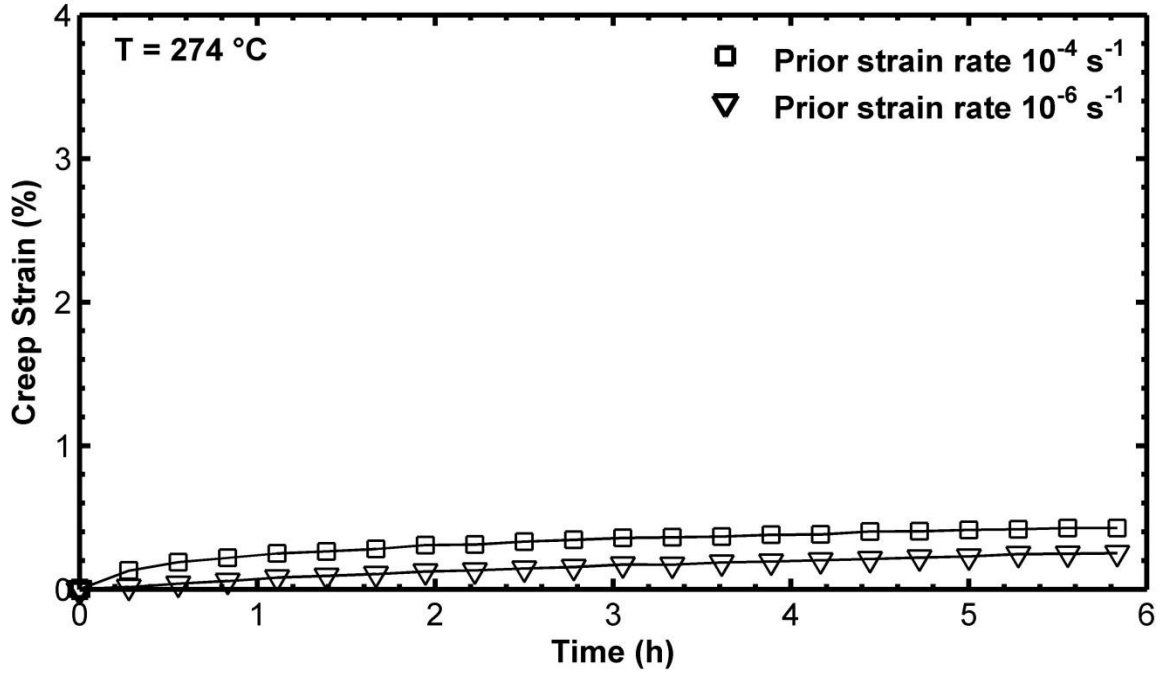


Figure 6.8 Creep strain versus time at 21 MPa and 274 °C. Effect of prior strain rate on creep is apparent. Creep strain increases nonlinearly with prior strain rate.

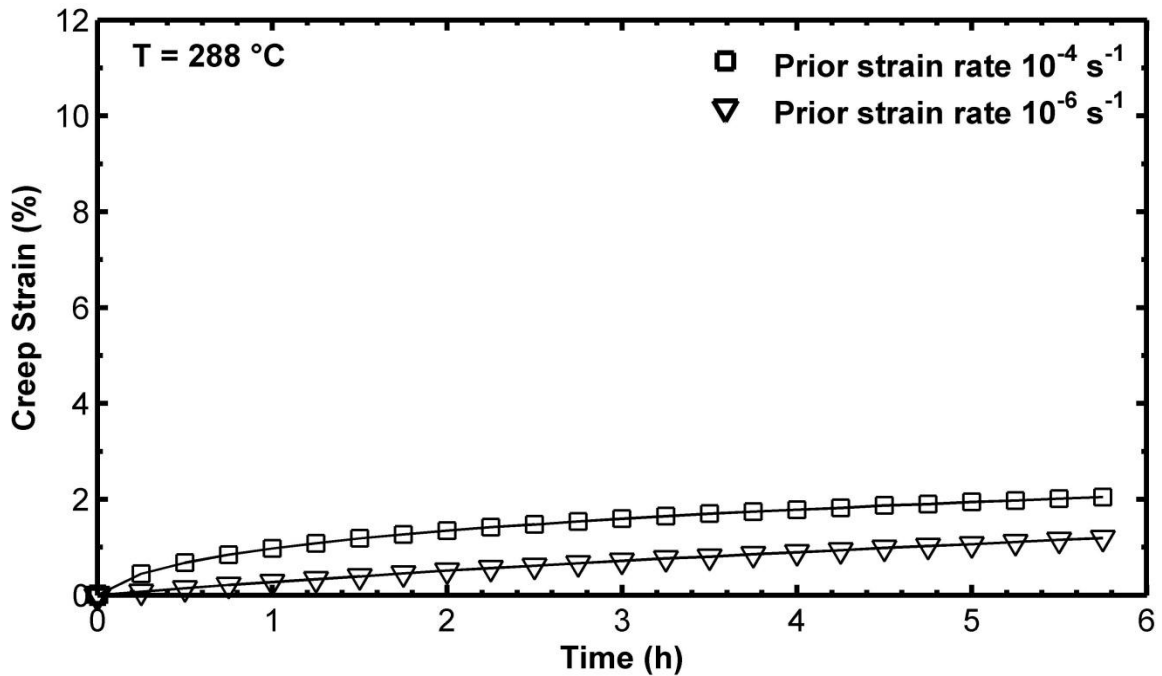
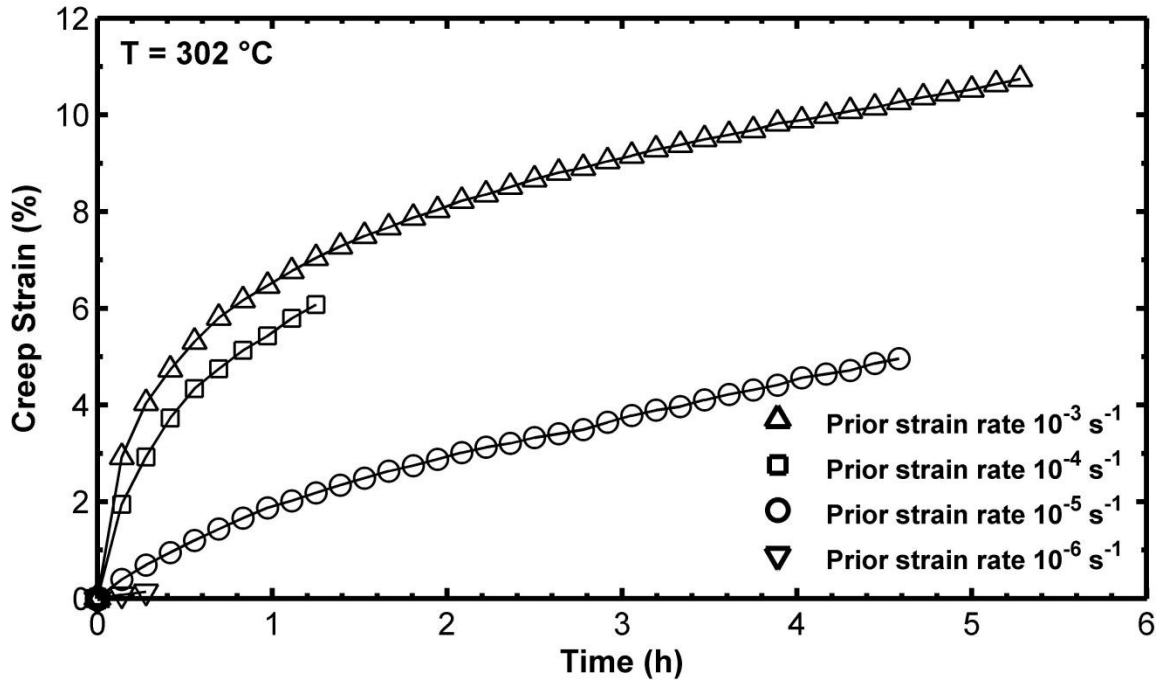


Figure 6.9 Creep strain versus time at 21 MPa and 288 °C. Effect of prior strain rate on creep is apparent. Creep strain increases nonlinearly with prior strain rate. Data from [81].





**Figure 6.10 Creep strain versus time at 21 MPa and 302 °C. Effect of prior strain rate on creep is apparent. Creep strain increases nonlinearly with prior strain rate.**

stress due to temperature is independent of the strain rate. Relaxation behavior is profoundly influenced by prior strain rate at all temperatures investigated. Additionally, relaxation behavior is strongly affected by temperature. For a given prior strain rate, the relaxation stress drop decreases with increasing temperature. Likewise, creep response is strongly affected by prior strain rate at all temperatures of interest. For a given temperature and stress level, creep strain accumulation increases nonlinearly with increasing prior strain rate. Creep behavior is also noticeably affected by temperature. Creep strain accumulation increases with increasing temperature. Noting the key effects of test temperature on the deformation behavior of PMR-15, we now contemplate the implications for modeling those effects.

## **7 Implications for Modeling the Effects of Increasing Test Temperature**

The experimental results reported in Chapter 6 reveal several key features of the deformation behavior of unaged PMR-15 polymer that are influenced by an increase in test temperature. In this chapter, those features are reviewed and the ability of the VBOP to model the effect of increasing test temperature is assessed.

### **7.1 Decrease in Initial Slope of the Stress-Strain Curve**

It is seen from the experimental data in Figure 6.1, Figure 6.2 and Figure 6.3 that the initial slope of the stress-strain curve is strongly affected by temperature. It is seen that an increase in temperature of only a few degrees results in a substantial decrease in slope. In the VBOP, the elastic modulus  $E$  represents the initial slope of the stress-strain curve. Therefore, the decrease in initial slope can be accounted for by formulating the elastic modulus as a decreasing function of temperature.

### **7.2 Increase in Final Slope of the Stress-Strain Curve**

Experimental data also reveal that the final slope of the stress-strain curve in the flow stress region increases with increasing test temperature. In the VBOP, the tangent modulus  $E_t$  is the final slope of the stress-strain curve. To account for the increase in the final slope, the tangent modulus can be made an increasing function of temperature.

### **7.3 Accelerated Departure from Quasi-linear Behavior**

Also observed in the data obtained during monotonic tensile tests is an accelerated departure from quasi-elastic behavior with increasing test temperature. In the VBOP, the shape function  $\Psi$  governs the transition from quasi-elastic to inelastic behavior.

Specifically, the shape function parameter  $C_2$  governs the departure from quasi-linear behavior. Therefore, an accelerated departure from quasi-linear behavior can be achieved in the VBOP by decreasing  $C_2$  as test temperature increases.

#### **7.4 Decreased Influence of Strain Rate on the Shape of the Knee of the Stress-Strain Curve**

The experimental data also shows that the knee of the stress-strain curve becomes less pronounced and is less influenced by the strain rate with increasing test temperature. Again, it is noted that in the VBOP, the shape function  $\Psi$  defines the shape of the knee in the stress-strain diagram. Within the shape function, the parameter  $C_2$  also governs the degree of sharpness of the knee at various strain rates. The less pronounced knee in the stress-strain curve observed at higher temperatures can be modeled in the VBOP by representing  $C_2$  as a decreasing function of temperature.

#### **7.5 Decrease in Flow Stress in the Region of Plastic Flow**

Again, the monotonic data reveal that flow stress levels decrease with increasing temperature. Notably the decrease in flow stress is independent of strain rate. In the VBOP, the equilibrium stress is representative of the stress-strain behavior in response to loading at an infinitesimally slow strain rate. Thus, the equilibrium stress represents the flow stress produced at an infinitesimally slow strain rate. Therefore, to represent the decrease in flow stress with an increase in test temperature, the equilibrium stress must decrease with increasing temperature. Referring to Figure 3.3, the isotropic stress  $A$  establishes the difference between the kinematic stress and the equilibrium stress in the region of inelastic flow. Hence the decrease in the equilibrium stress (and consequently

in the flow stress) with increasing temperature can be accomplished by making the isotropic stress a decreasing function of temperature.

## **7.6 Decrease in Stress Drop during Relaxation**

As shown in Figure 6.5, Figure 6.6 and Figure 6.7, temperature has a profound effect on relaxation behavior. At a given strain rate increased temperature results in a decrease in stress drop during relaxation. This result has important implications for modeling with VBOP because it indicates that temperature must affect the viscosity function  $k$ . Within the viscosity function, the parameter  $k_2$  governs the degree of strain rate sensitivity during monotonic loading and the stress drop during relaxation. By decreasing the degree of strain rate sensitivity of the flow stress, the overstress at a given strain rate is decreased. The resulting decrease in the overstress will result in a decrease in the stress drop during relaxation. Thus, the decrease in the stress drop during relaxation can be accomplished by making the viscosity function parameter  $k_2$  a decreasing function of temperature.

## **7.7 Proposed Changes to the VBOP to Account for the Effects of Increasing Test Temperature**

Based on experimental results obtained at temperatures in the 274-302 °C range and the capabilities of the current formulation of the VBOP model, the following changes in the VBOP model are proposed to account for the effects of increasing test temperature:

- Elastic modulus decreases with increasing temperature
- Tangent modulus increases with increasing temperature
- Shape function parameter  $C_2$  decreases with increasing temperature

- Isotropic stress  $A$  decreases with increasing temperature
- Viscosity function parameter  $k_2$  decreases with increasing temperature

Next the functional dependence of elastic modulus, tangent modulus, shape function parameter  $C_2$ , isotropic stress  $A$  and viscosity function parameter  $k_2$  on temperature must be determined. The aforementioned VBOP parameters are expanded into functions of temperature in Chapter 8.

## 8 Constitutive Modeling of the Inelastic Behavior of Unaged PMR-15 Neat Resin at 274-316 °C

This chapter discusses the constitutive modeling of unaged PMR-15 subjected to mechanical loading at various temperatures. The VBOP model is augmented to account for the effects of test temperature based on experimental observations described in Chapter 6.

### 8.1 Characterization of VBOP Model Parameters for PMR-15 at Various Temperatures

The systematic model characterization procedure described in Chapter 5 was used to determine the VBOP model parameters for the PMR-15 neat resin from experimental data collected at 274, 288 and 302 °C. The VBOP model parameters obtained for PMR-15 at 274, 288 and 302 °C are reported in Table 8.1, Table 8.2 and Table 8.3, respectively. Comparisons of VBOP model simulations with experimental data are shown in Figure 8.1 - Figure 8.6.

#### 8.1.1 Characterization of VBOP Model Parameters at 274 °C

The characterization procedure described in Chapter 5 was employed to determine the VBOP model parameters for PMR-15 at 274 °C, which are summarized in Table 8.1.

**Table 8.1 VBOP Parameters for PMR-15 Neat Resin Subjected to Mechanical Loading at 274 °C**

Moduli	$E = 2089 \text{ MPa}, E_t = 49.9 \text{ MPa}$
Isotropic Stress	$A = 24 \text{ MPa}$
Viscosity Function	$k_1 = 1.0e5 \text{ s}, k_2 = 170 \text{ MPa}, k_3 = 80$
Shape Function	$C_1 = 1000 \text{ MPa}, C_2 = 1200 \text{ MPa}, C_3 = 10$

The VBOP simulation of the monotonic tensile loading (Figure 8.1) is in good agreement with the experimental results. The stress-strain curve for the  $10^{-3} \text{ s}^{-1}$  strain rate shows a small overprediction of the sharpness of the knee of the stress-strain curve while the sharpness of the knee of the  $10^{-4} \text{ s}^{-1}$  curve is slightly underpredicted. The knee of the simulated stress-strain curves is primarily driven by the value of the shape function parameter  $C_2$ . The value of  $C_2$  was selected to best reproduce the knee of the stress-strain curves at each strain rate. Although there are minor differences between the simulated and experimental data, the representation is considered acceptable. Model parameters were selected to best match the totality of experimental data and no one set of parameters could precisely represent the experimental data for each strain rate. Instead, model parameters were selected such that differences at each strain rate were minimized.

Figure 8.2 shows stress drop during relaxation as a function of relaxation time for the prior strain rates of  $10^{-6}$ ,  $10^{-5}$ ,  $10^{-4}$  and  $10^{-3} \text{ s}^{-1}$ . Experimental results are shown together with VBOP simulations. The simulation of the stress drop at 4.5% strain accurately represents the behavior observed throughout the 12-h relaxation period. The stress drop after loading at a constant strain rate of  $10^{-3} \text{ s}^{-1}$  is slightly overpredicted but is within the typical specimen-to-specimen variation and the overall simulation is excellent. Recall that the behavior during relaxation dictates the initial value of the isotropic stress and the viscosity function parameters. In this case, the viscosity function parameters were selected to ensure a good representation of both short and long-term relaxation data.

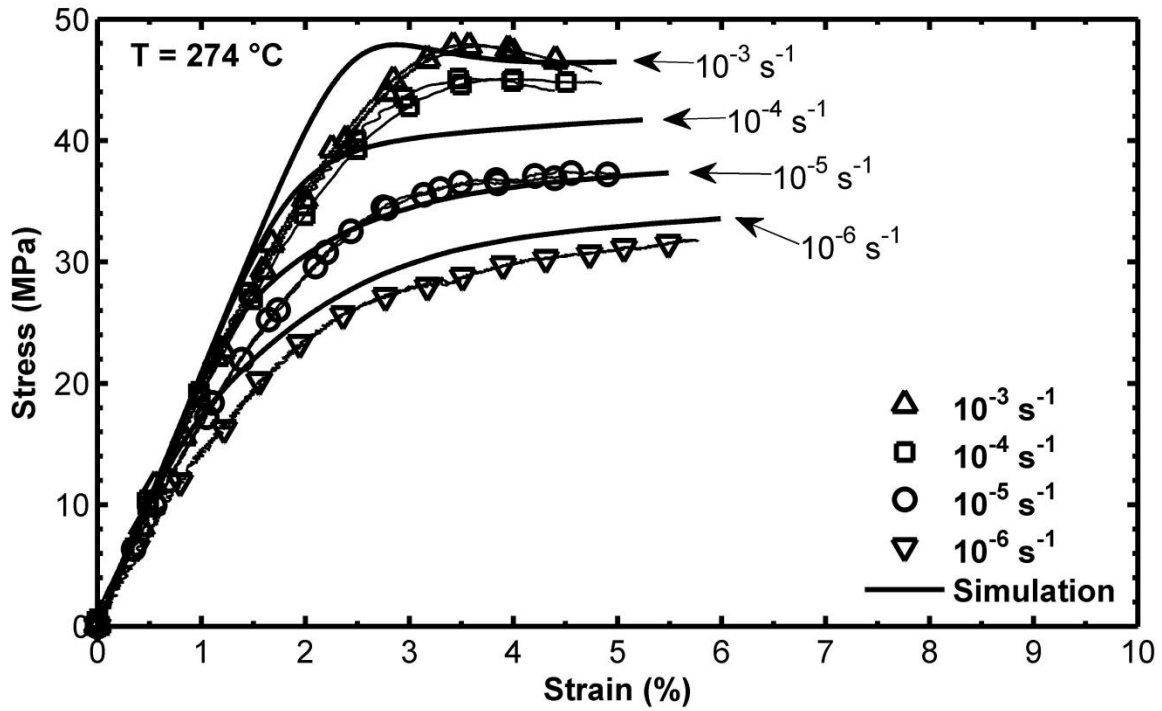
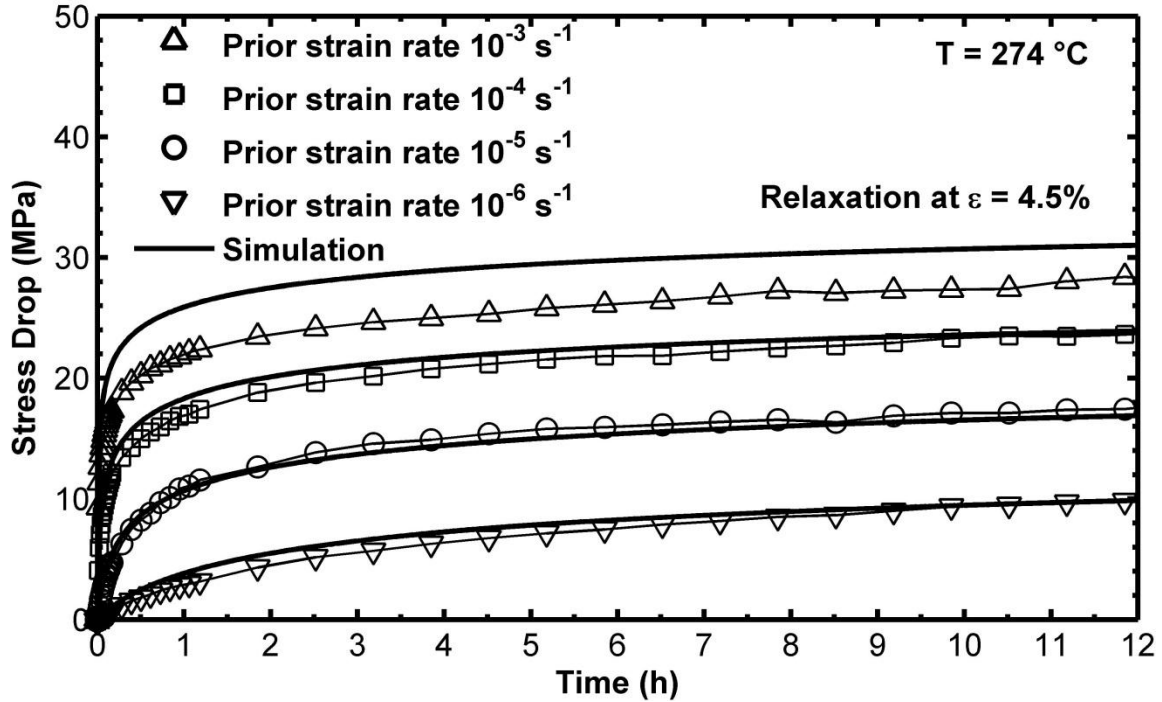


Figure 8.1 A comparison between experimental results and simulated stress-strain curves obtained for PMR-15 polymer in tensile tests to failure conducted at constant strain rates of  $10^{-6}$ ,  $10^{-5}$ ,  $10^{-4}$  and  $10^{-3} \text{ s}^{-1}$  at 274 °C. The model successfully represents the strain rate dependence of the material at elevated temperature.





**Figure 8.2** A comparison between experimental results and simulated stress drop during relaxation obtained for PMR-15 polymer at 274 °C. Loading prior to relaxation is conducted at constant strain rates of  $10^{-6}$ ,  $10^{-5}$ ,  $10^{-4}$  and  $10^{-3}$  s $^{-1}$ . The model successfully represents the stress drop throughout the entire relaxation period.

### 8.1.2 Characterization of VBOP Model Parameters at 288 °C

The model characterization procedure was utilized to obtain the VBOP model parameters for PMR-15 at 288 °C. Both newly collected data and the data from prior work [19] were utilized in model characterization. The resulting model parameters are summarized in Table 8.2.

**Table 8.2** VBOP Parameters for PMR-15 Neat Resin Subjected to Mechanical Loading at 288 °C

Moduli	$E = 1771$ MPa, $E_t = 62.4$ MPa
Isotropic Stress	$A = 15$ MPa
Viscosity Function	$k_1 = 1.0e5$ s, $k_2 = 155$ MPa, $k_3 = 80$
Shape Function	$C_1 = 1000$ MPa, $C_2 = 900$ MPa, $C_3 = 10$

Measurement of the slope of the stress-strain curve in the quasi-elastic region yielded a slightly lower value of elastic modulus than reported by McClung [19]. Recall, that in order to account for specimen-to-specimen and batch-to-batch variation, the measured stress values were scaled by the average room temperature modulus of the specimens used in this study as described in Section 6.1. The elastic modulus reported in Table 8.2 is based on both newly collected data and data from prior work [19] that have been scaled. Since the batch of PMR-15 tested by McClung had a somewhat higher average room temperature elastic modulus than the PMR-15 specimens tested by other researchers (see Table 6.1), the scaling procedure tended to reduce the reported elastic modulus of that particular batch of PMR-15. This is provided as an explanation of the difference in elastic modulus as reported in Table 8.2 and that reported by McClung [49].

Measurement of the tangent modulus is, at best, a challenging endeavor. Due to the limited ductility of the PMR-15 polymer, specimens often failed before the stress-strain curves reached the region where plastic flow was fully established. Generally, the largest failure strains were produced in tests conducted at the slowest strain rate. Therefore, only data from tests conducted at the  $10^{-6} \text{ s}^{-1}$  strain rate were utilized to determine the tangent modulus. The isotropic stress was established utilizing the procedure described in Section 5.1.2.

As described in Section 5.1.3, the viscosity function was determined by a fit to the experimental stress drop during relaxation. In a departure from the procedure suggested by McClung, the viscosity function parameters were selected to fit the VBOP simulations to the experimental stress values throughout the relaxation period instead of just the final two hours. As seen in Figure 8.4, this provides a much better fit to both the short and

long-term relaxation response. Additionally, the much higher value of the viscosity function parameter  $k_1$  allows VBOP to better represent strain rate sensitivity during monotonic loading. It is postulated that the fitting of the full 12-h relaxation response results in a parameter set that more accurately simulates both short and long-term responses such as loading at both fast and slow strain rates.

The shape function parameters were determined by a fit to the knee of the experimental stress-strain curve using the procedure described in Section 5.1.3. The order of magnitude difference in the viscosity function parameter  $k_1$  while enhancing modeling accuracy of relaxation and strain rate sensitivity also required a substantial difference in the shape function parameters. Shape function parameter  $C_1$  was increased by an order of magnitude and  $C_2$  was substantially altered to ensure a reasonable simulation of the experimental data.

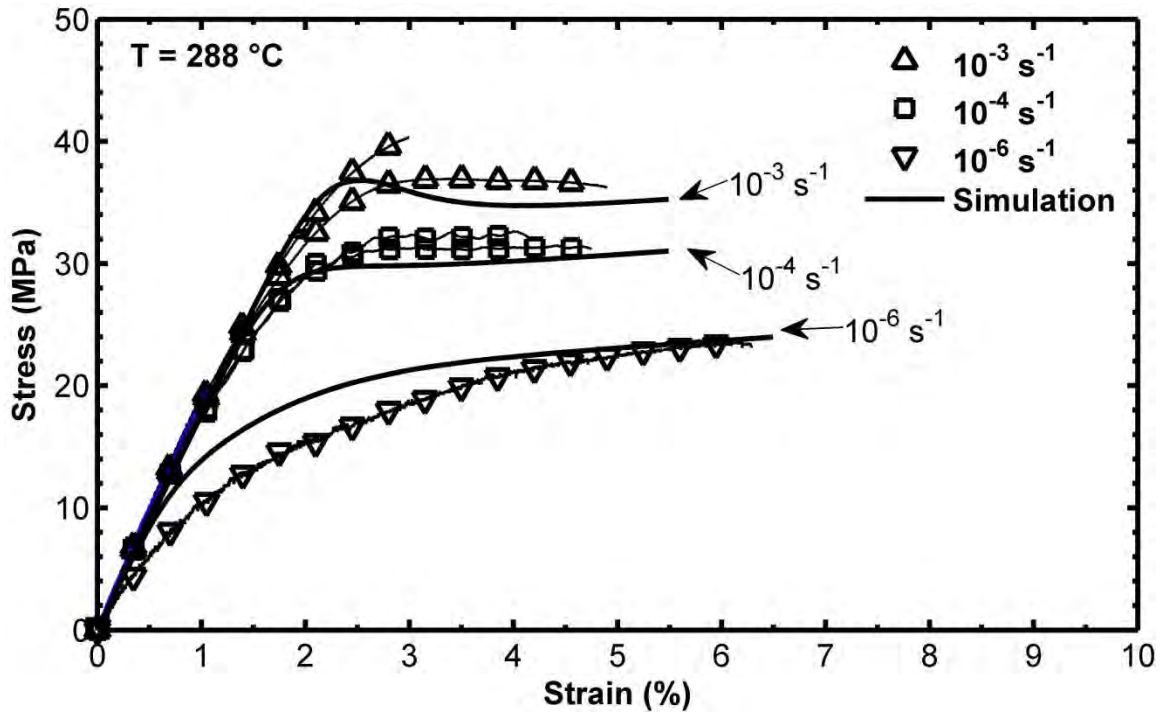
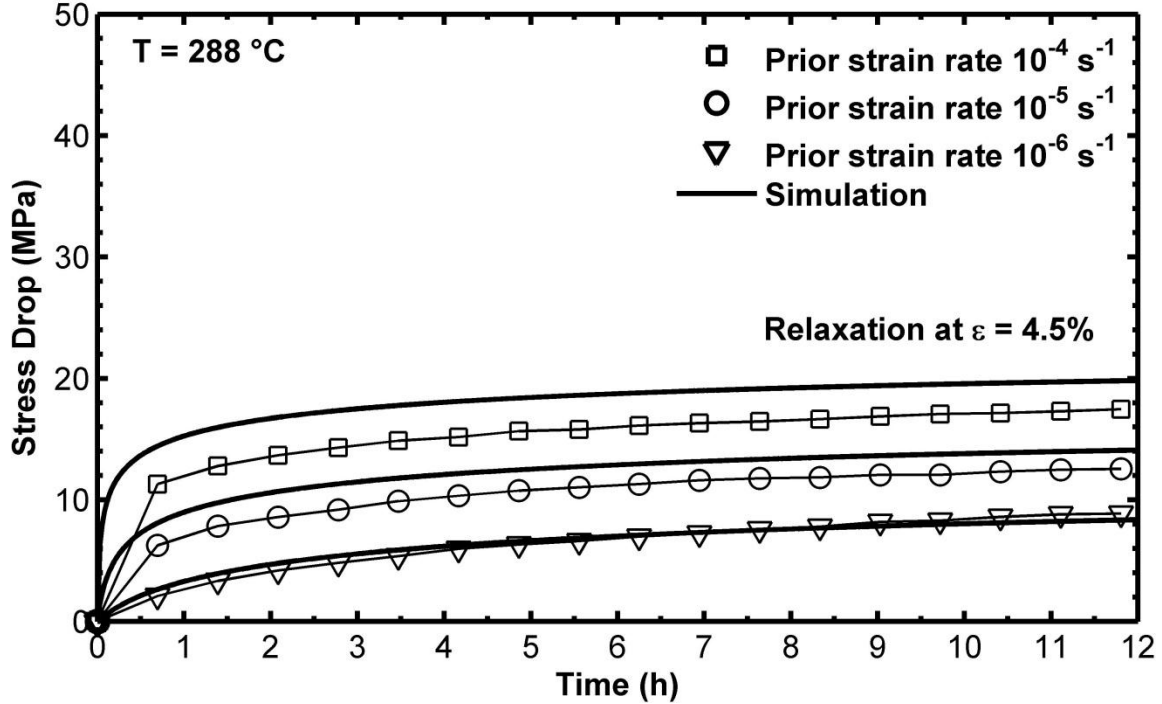


Figure 8.3 A comparison between experimental results and simulated stress-strain curves obtained for PMR-15 polymer in tensile tests to failure conducted at constant strain rates of  $10^{-6}$ ,  $10^{-4}$  and  $10^{-3} \text{ s}^{-1}$  at 288 °C. The model successfully represents the strain rate dependence of the material at elevated temperature. Data from [19] are also included.



**Figure 8.4** A comparison between experimental results and simulated stress drop during relaxation obtained for PMR-15 polymer at 288 °C. Loading prior to relaxation is conducted at constant strain rates of  $10^{-6}$ ,  $10^{-5}$  and  $10^{-4} \text{ s}^{-1}$ . The model successfully represents the stress drop throughout the entire relaxation period. Data from [19] are also included.

### 8.1.3 Characterization of VBOP Model Parameters at 302 °C

A model characterization procedure identical to that utilized for PMR-15 polymer tested at 274 and 288 °C was applied to data collected during tests conducted at 302 °C. The characterization procedure described in Chapter 5, along with the scaling scheme described in 6.1 was employed to determine the VBOP model parameters for PMR-15 at 302 °C. Note that the viscosity function parameters were selected to fit the viscosity data for the entire 12-h test as opposed to the final 2 h of the relaxation period. The resulting model parameters are found in Table 8.3.

**Table 8.3 VBOP Parameters for PMR-15 Neat Resin Subjected to Mechanical Loading at 302 °C**

Moduli	$E = 1453 \text{ MPa}, E_t = 71.6 \text{ MPa}$
Isotropic Stress	$A = 8 \text{ MPa}$
Viscosity Function	$k_1 = 1.0e5 \text{ s}, k_2 = 140 \text{ MPa}, k_3 = 80$
Shape Function	$C_1 = 1000 \text{ MPa}, C_2 = 600 \text{ MPa}, C_3 = 10$

Model simulations based on the parameters shown in Table 8.3 are compared to experimental monotonic data in Figure 8.5. The simulation of the stress-strain curve for the  $10^{-3} \text{ s}^{-1}$  strain rate shows a small overprediction of the sharpness of the knee of the stress-strain curve. However, overall the simulations of the strain-controlled monotonic loading are in good agreement with the experimental data.

Figure 8.6 shows stress drop during relaxation as a function of relaxation time for the prior strain rates of  $10^{-6}$ ,  $10^{-5}$ ,  $10^{-4}$  and  $10^{-3} \text{ s}^{-1}$ . Experimental results are shown together with VBOP simulations. The simulation of the stress drop at 5% strain is an excellent representation of the behavior observed throughout the 12-h relaxation period.

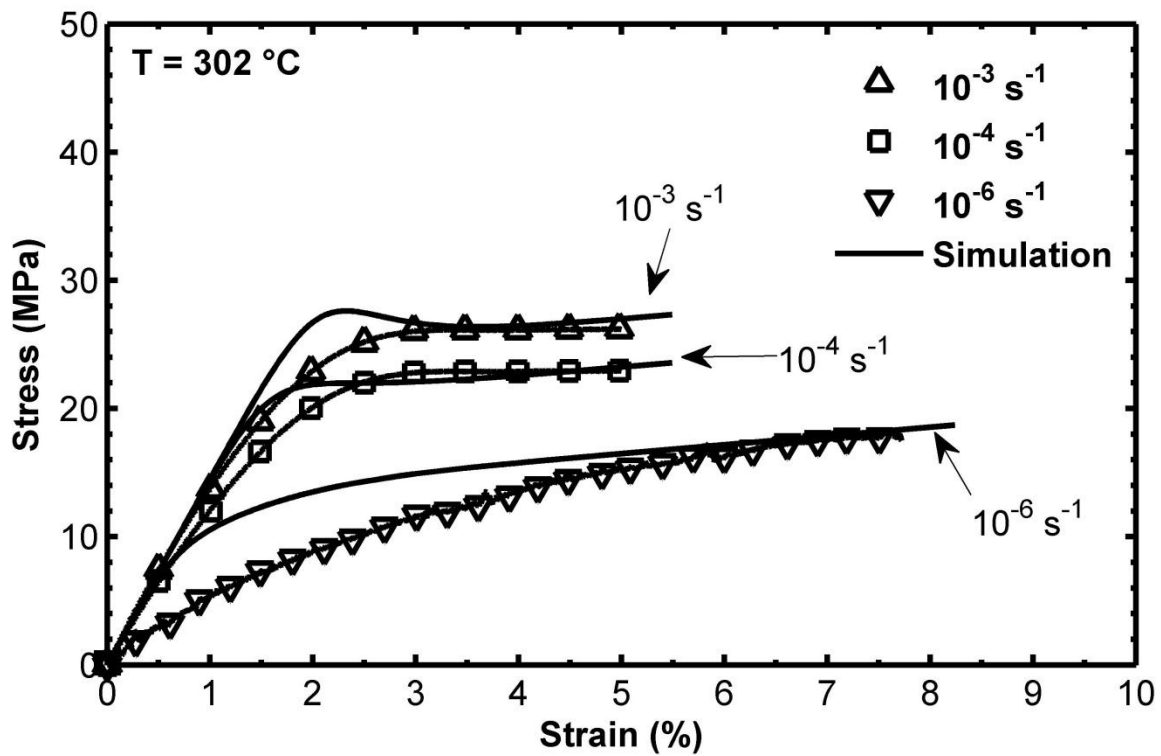
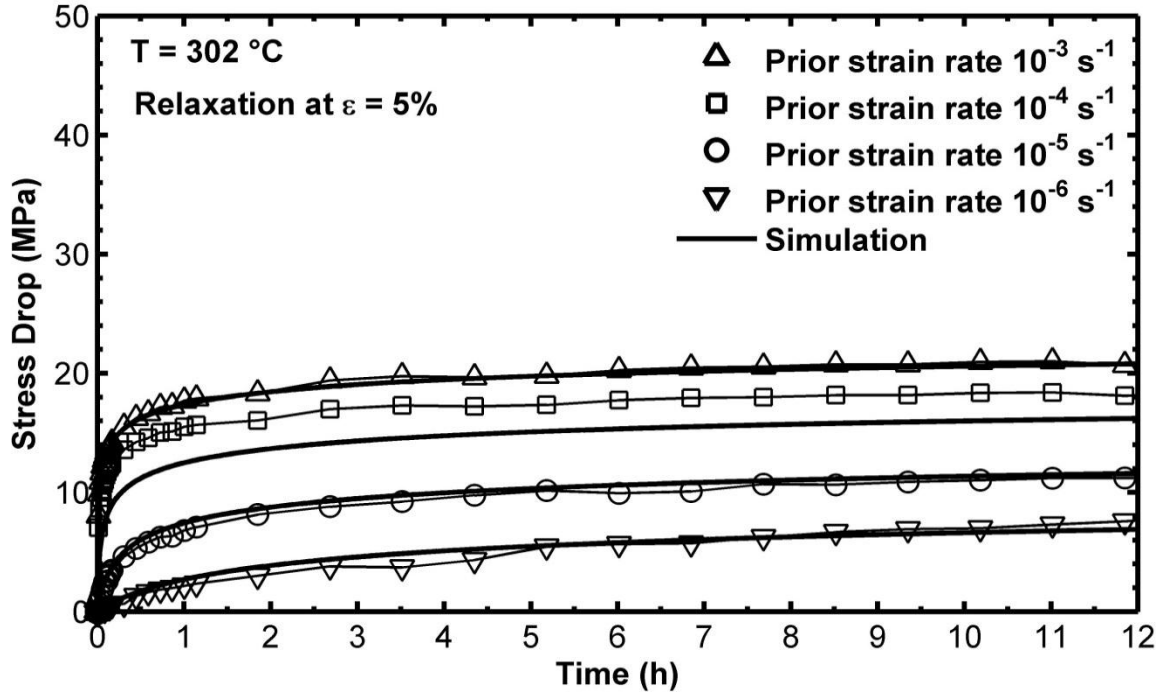


Figure 8.5 A comparison between experimental results and simulated stress-strain curves obtained for PMR-15 polymer in tensile tests to failure conducted at constant strain rates of  $10^{-6}$ ,  $10^{-4}$  and  $10^{-3} \text{ s}^{-1}$  at 302 °C. The model successfully represents the strain rate dependence of the material at elevated temperature.



**Figure 8.6** A comparison between experimental results and simulated stress drop during relaxation obtained for PMR-15 polymer at 302 °C. Loading prior to relaxation is conducted at constant strain rates of  $10^{-6}$ ,  $10^{-5}$ ,  $10^{-4}$  and  $10^{-3} \text{ s}^{-1}$ . The model successfully represents the stress drop throughout the entire relaxation period.

## 8.2 VBOP Model Parameters as Functions of Temperature

In the previous section, the systematic model characterization procedure was employed to determine model parameters at each test temperature. Examination of the experimental data in Figure 8.1 - Figure 8.6 and of the resulting model parameters in Table 8.1, Table 8.2 and Table 8.3 reveals a strong effect of test temperature on the mechanical behavior of and on model parameters for PMR-15 polymer. In the remainder of this section, it will be shown which model parameters depend on test temperature and those parameters will be developed into functions of test temperature. The VBOP model parameters that depend on test temperature are presented in Table 8.4.



**Table 8.4 Summary of the VBOP Parameters Dependent on Test Temperature for PMR-15 Neat Resin at Various Temperatures**

<i>Parameter</i>	<i>274 °C</i>	<i>288 °C</i>	<i>302 °C</i>
<i>Moduli</i>			
<i>E (MPa)</i>	2089	1771	1453
<i>E<sub>t</sub> (MPa)</i>	49.9	62.4	71.6
<i>Isotropic Stress</i>			
<i>A (MPa)</i>	24	15	8
<i>Viscosity Function</i>			
<i>k<sub>2</sub> (MPa)</i>	170	155	140
<i>Shape Function</i>			
<i>C<sub>2</sub> (MPa)</i>	1200	900	600

### 8.2.1 Elastic Modulus – Effect of Test Temperature

The elastic modulus decreases with increasing test temperature as shown in Table 8.4. The elastic modulus is plotted versus test temperature in Figure 8.7. It is seen that an increase in temperature of only a few degrees results in a substantial decrease in the elastic modulus. Based on results in Figure 8.7, the elastic modulus  $E$  is established as a decreasing function of test temperature

$$E = 8308 - 22.7T \quad (8.1)$$

where  $T$  is test temperature in degrees Celsius. For reference, Equation (8.1) is plotted in Figure 8.7. It should be noted that this equation might not be valid for temperatures at which the material does not exhibit viscoplastic behavior. Although the data shown in Figure 8.7 may appear to be better represented by a higher order function, such functions did not improve model predictions and so the simpler formulation was retained.

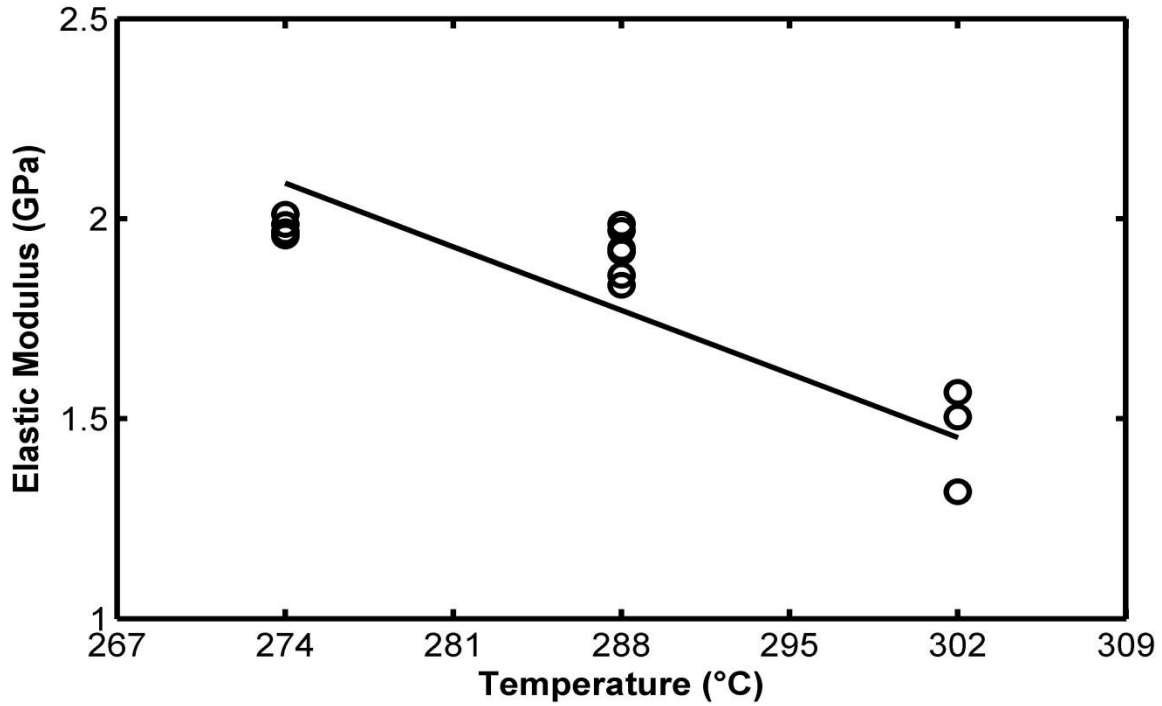


**Figure 8.7 Elastic modulus versus temperature for PMR-15 neat resin.**

### 8.2.2 Tangent Modulus – Effect of Test Temperature

The tangent modulus increases with increasing test temperature as shown in Figure 8.8. The graph in Figure 8.8 reveals that the tangent modulus can be represented by the following increasing function of temperature

$$E_t = 0.775T - 161.9 \quad (8.2)$$

where  $T$  is test temperature in degrees Celsius. Recall, that due to the limited ductility of PMR-15, only data from tests conducted at the  $10^{-6} \text{ s}^{-1}$  strain rate are included in Figure 8.8. For reference, Equation (8.2) is plotted in Figure 8.8.

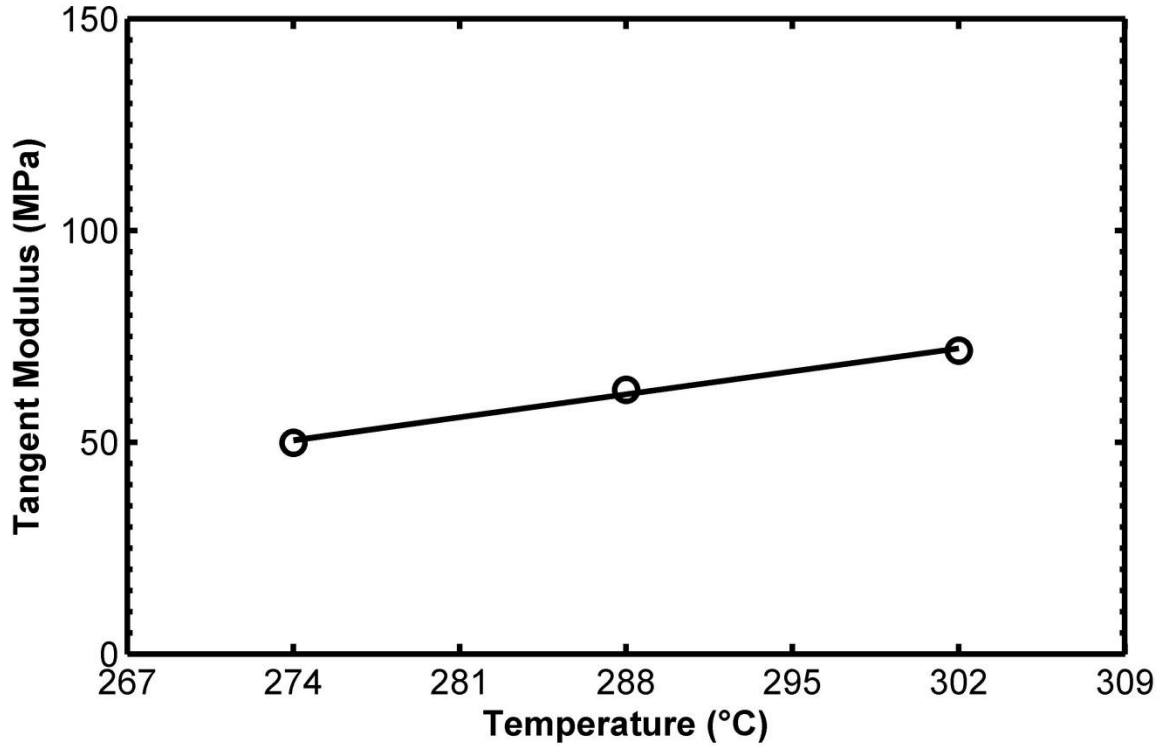


**Figure 8.8 Tangent modulus versus temperature for PMR-15 neat resin.**

### 8.2.3 Shape Function – Effect of Test Temperature

The shape function parameter  $C_2$  decreases with increasing test temperature as shown in Figure 8.9. Results in Figure 8.9 indicate that  $C_2$  can be represented by a decreasing function of temperature

$$C_2 = 7071 - 21.42T \quad (8.3)$$

where  $T$  is test temperature in degrees Celsius.

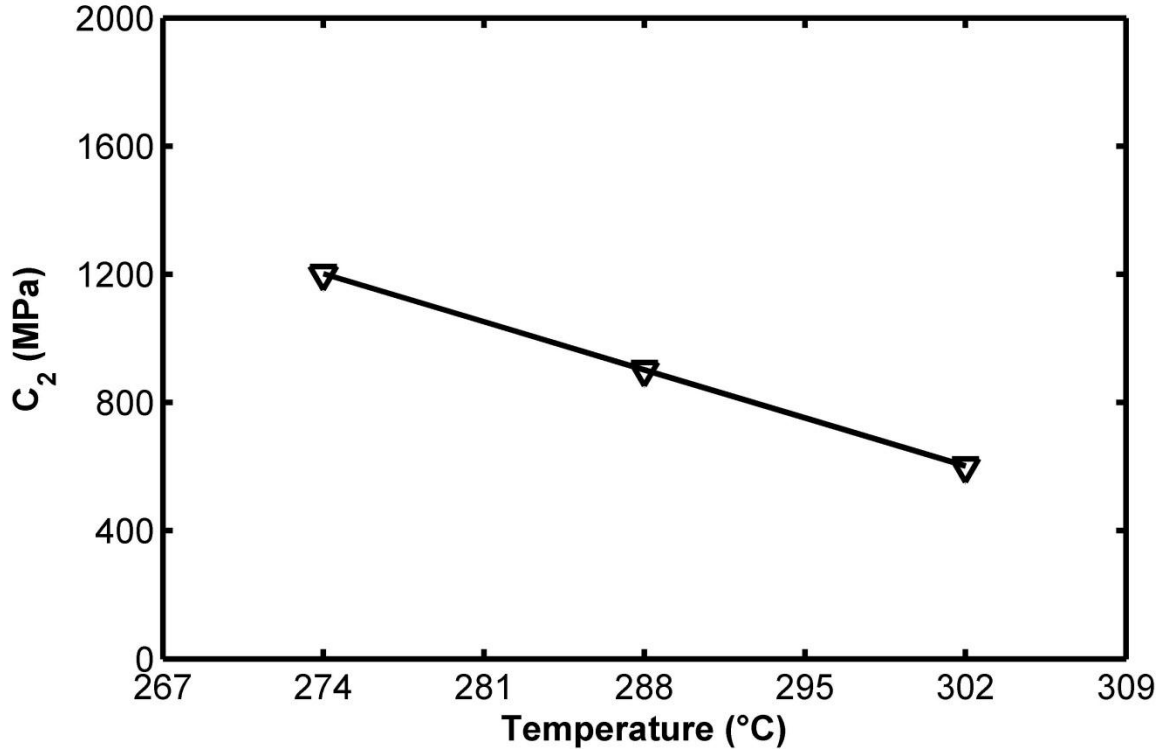


**Figure 8.9** Shape function parameter  $C_2$  versus temperature for PMR-15 neat resin.

#### 8.2.4 Isotropic Stress – Effect of Test Temperature

The isotropic stress  $A$  decreases with increasing test temperature as shown in Figure 8.10. Based on the experimental results shown in Figure 8.10, isotropic stress  $A$  can be established as a decreasing function of temperature

$$A = 648000e^{-0.03721T} \quad (8.4)$$

where  $T$  is test temperature in degrees Celsius.

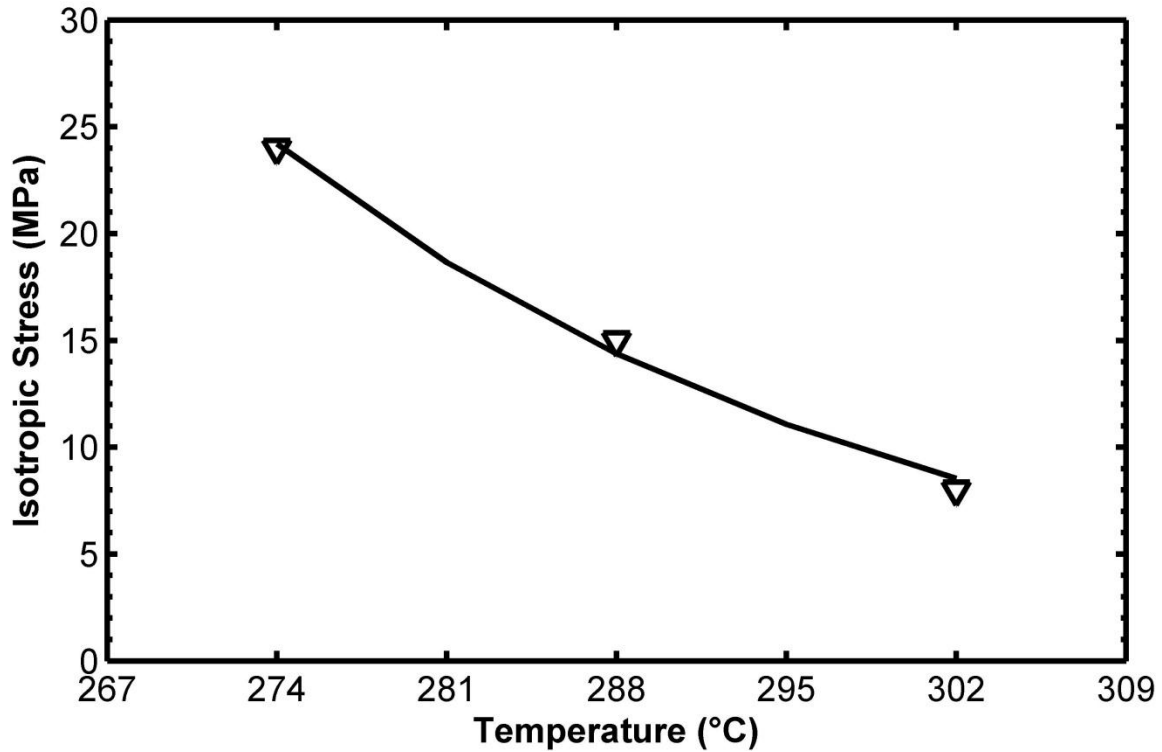


**Figure 8.10** Isotropic stress  $A$  versus temperature for PMR-15 neat resin.

### 8.2.5 Viscosity Function– Effect of Test Temperature

As shown in Chapter 7, test temperature has a profound effect on relaxation behavior of PMR-15 polymer. This is a strong indication that the viscosity function  $k$  should be made dependent on test temperature. Using the experimental results shown in Figure 8.11, the viscosity function parameter  $k_2$  is represented as a decreasing function of temperature

$$k_2 = 463.57 - 1.0714T \quad (8.5)$$

where  $T$  is test temperature in degrees Celsius.

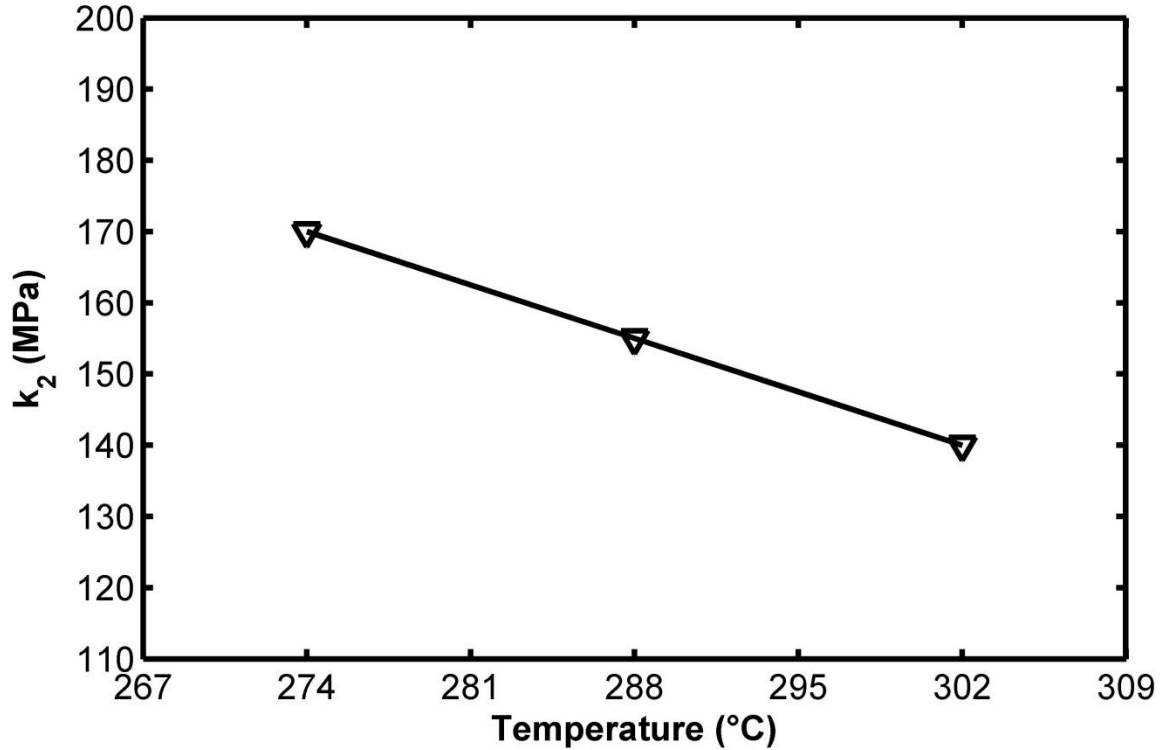


**Figure 8.11** Viscosity function parameter  $k_2$  versus temperature for PMR-15 resin.

The remaining VBOP parameters for the PMR-15 polymer do not vary with test temperature.

#### 8.2.6 Calculation of Model Parameters Utilizing the Augmented VBOP

In the previous five sections, specific model parameters were shown to depend on temperature and were developed into functions of temperature. Those functions are now utilized to calculate model parameters and those parameters are used to produce simulations of tensile tests to failure and stress drop during relaxation at 274, 288 and 302 °C. Model parameters calculated utilizing the augmented VBOP are shown in Table 8.5. Simulations of stress-strain and relaxation behavior at 274 °C utilizing the calculated parameters shown in Table 8.5 are compared to experimental results in

Figure 8.12 and Figure 8.13, respectively. Similar comparisons of PMR-15 tested at 288 and 302 °C are shown in Figure 8.14, Figure 8.15, Figure 8.16 and Figure 8.17. Comparisons of model simulations produced utilizing the augmented VBOP (shown in Figure 8.12 through Figure 8.17) with the corresponding simulations shown in Figure 8.1 through Figure 8.6, demonstrate that the augmented VBOP produces simulations that are essentially identical to those created by manually characterizing the VBOP constitutive model at each temperature of interest. Noting that the augmented VBOP successfully simulates the inelastic behavior of PMR-15 throughout the 274-302 °C temperature range, we turn now to a discussion of model validation.

**Table 8.5 Summary of VBOP Parameters Calculated Utilizing the Augmented VBOP**

<i>Parameter</i>	<i>274 °C</i>	<i>288 °C</i>	<i>302 °C</i>
<i>Moduli</i>			
<i>E (MPa)</i>	2088.2	1770.4	1452.6
<i>E<sub>t</sub> (MPa)</i>	50.45	61.3	72.15
<i>Isotropic Stress</i>			
<i>A (MPa)</i>	24.194	14.37	8.535
<i>Viscosity Function</i>			
<i>k<sub>2</sub> (MPa)</i>	170.006	155.007	140.007
<i>Shape Function</i>			
<i>C<sub>2</sub> (MPa)</i>	1201.92	902.04	602.16

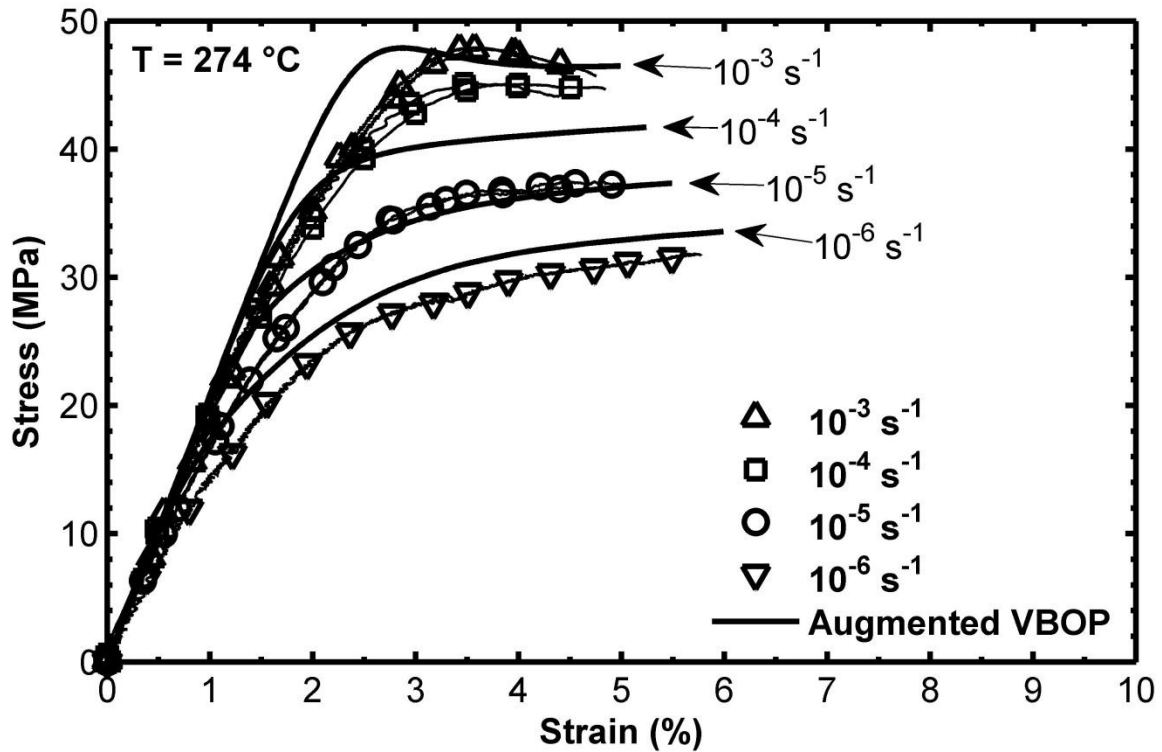


Figure 8.12 A comparison between experimental results and simulated stress-strain curves obtained for PMR-15 polymer in tensile tests to failure conducted at constant strain rates of  $10^{-6}$ ,  $10^{-5}$ ,  $10^{-4}$  and  $10^{-3} \text{ s}^{-1}$  at 274 °C. Model parameters for simulations were calculated utilizing the augmented VBOP. The augmented VBOP successfully represents the strain rate dependence of the material at elevated temperature.



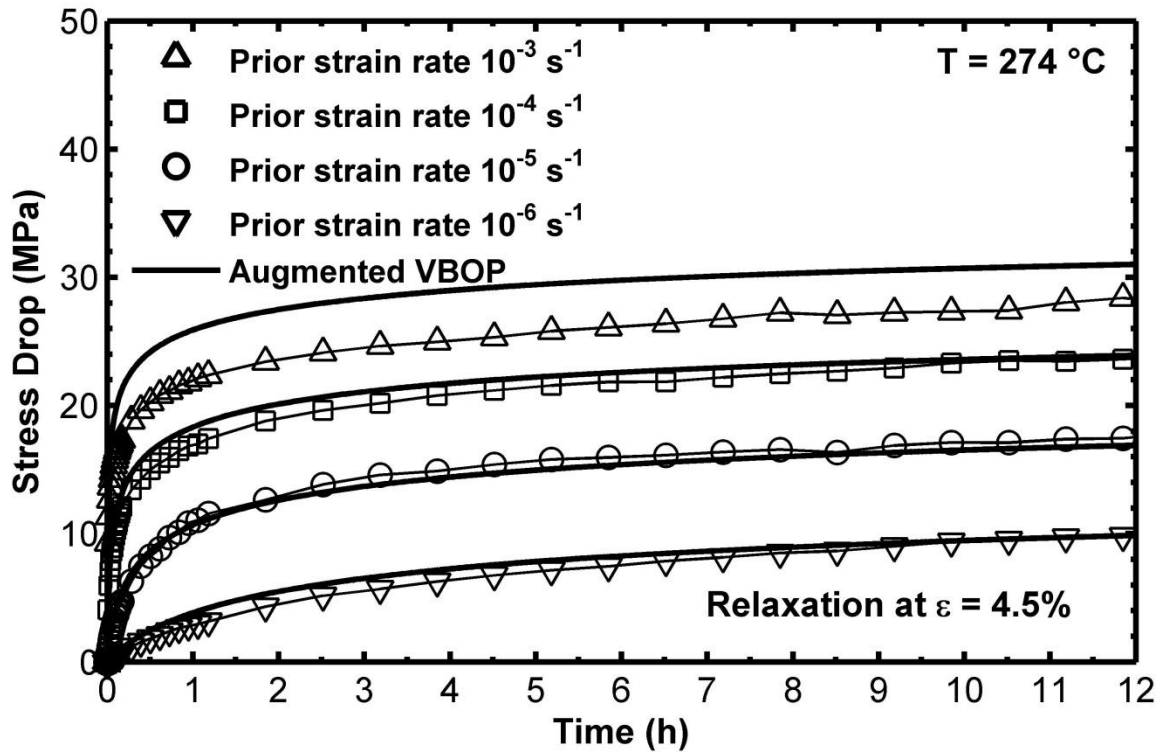


Figure 8.13 A comparison between experimental results and simulated stress drop during relaxation obtained for PMR-15 polymer at 274 °C. Loading prior to relaxation is conducted at constant strain rates of  $10^{-6}$ ,  $10^{-5}$ ,  $10^{-4}$  and  $10^{-3}\text{ s}^{-1}$ . Model parameters for simulations were calculated utilizing the augmented VBOP. The augmented VBOP successfully represents the stress drop throughout the entire relaxation period.

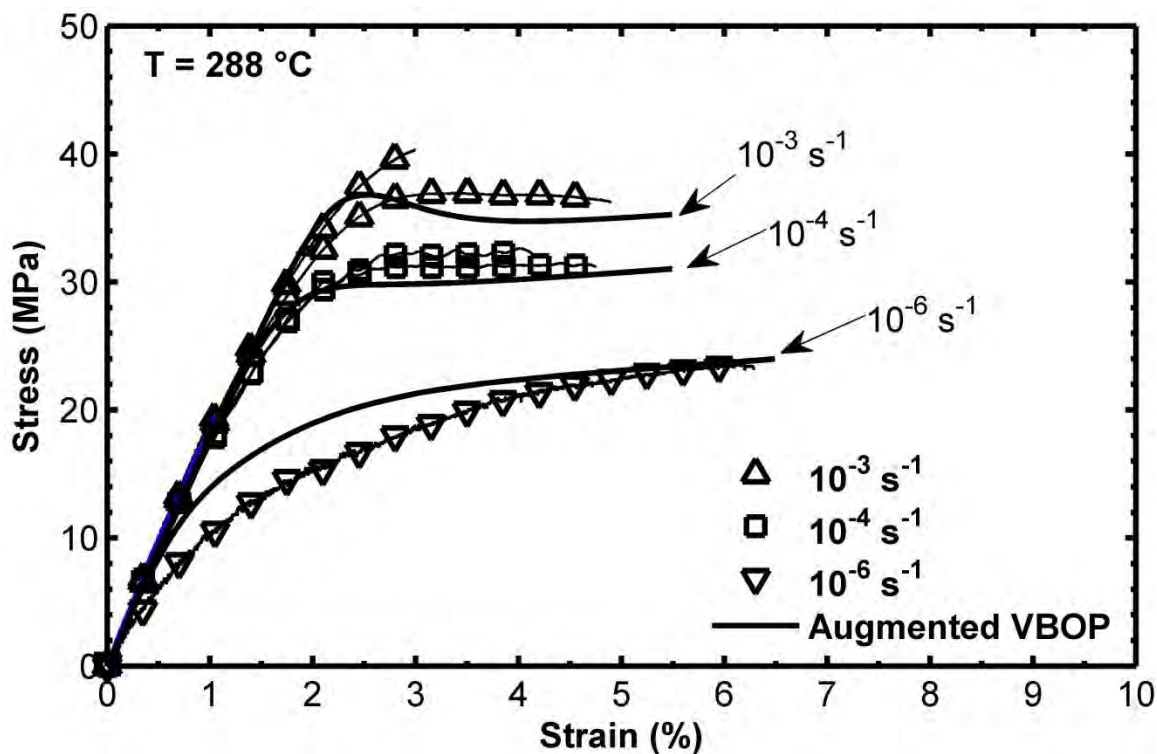


Figure 8.14 A comparison between experimental results and simulated stress-strain curves obtained for PMR-15 polymer in tensile tests to failure conducted at constant strain rates of  $10^{-6}$ ,  $10^{-4}$  and  $10^{-3} \text{ s}^{-1}$  at 288 °C. Model parameters for simulations were calculated utilizing the augmented VBOP. The augmented VBOP successfully represents the strain rate dependence of the material at elevated temperature.

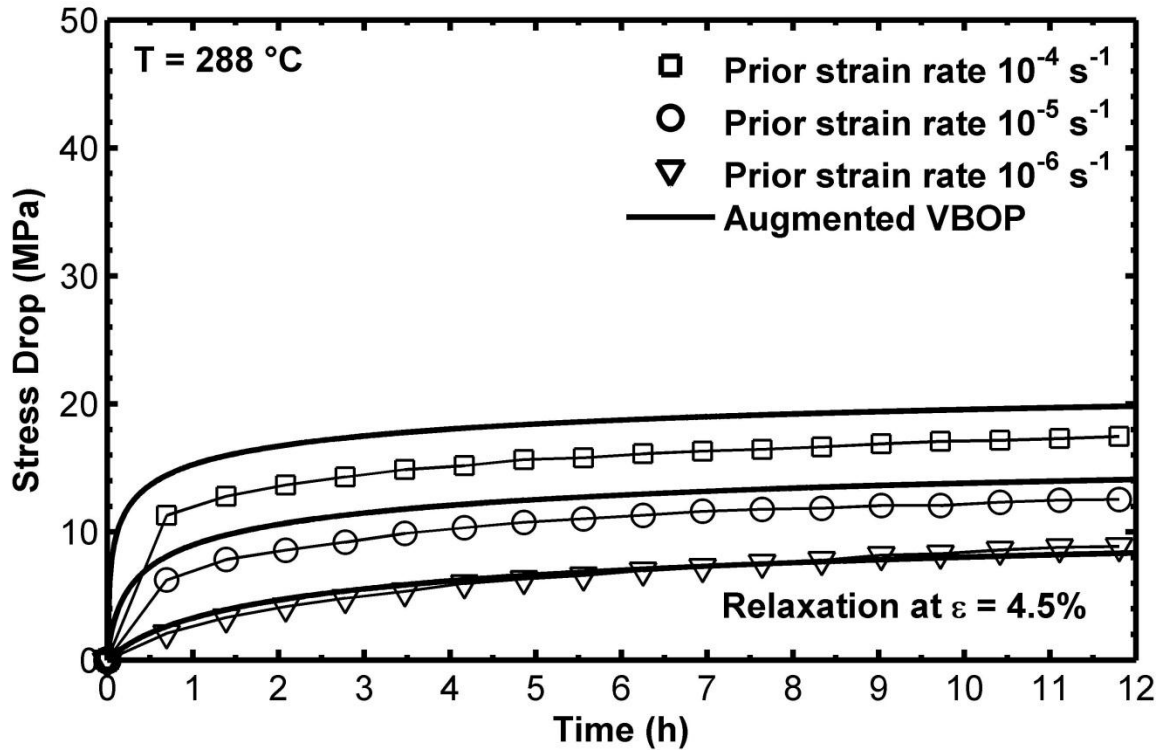


Figure 8.15 A comparison between experimental results and simulated stress drop during relaxation obtained for PMR-15 polymer at 288 °C. Loading prior to relaxation is conducted at constant strain rates of  $10^{-6}$ ,  $10^{-5}$  and  $10^{-4} \text{ s}^{-1}$ . Model parameters for simulations were calculated utilizing the augmented VBOP. The augmented VBOP successfully represents the stress drop throughout the entire relaxation period.

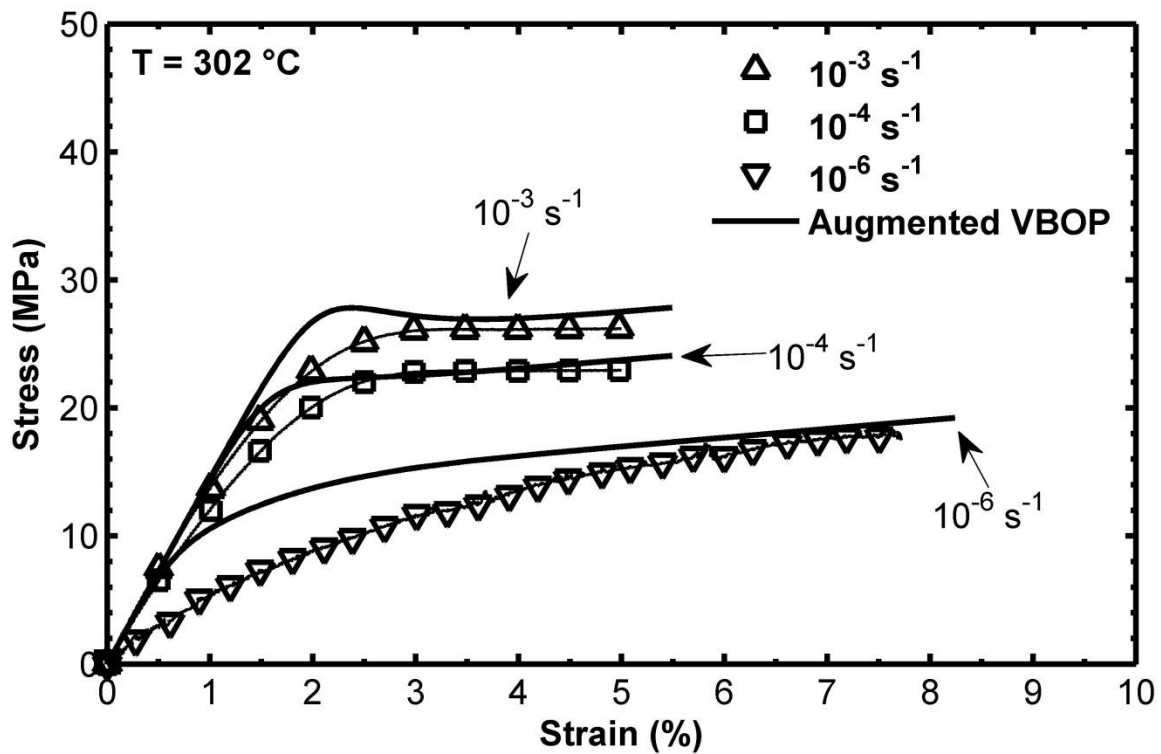


Figure 8.16 A comparison between experimental results and simulated stress-strain curves obtained for PMR-15 polymer in tensile tests to failure conducted at constant strain rates of  $10^{-6}$ ,  $10^{-4}$  and  $10^{-3} \text{ s}^{-1}$  at 302 °C. Model parameters for simulations were calculated utilizing the augmented VBOP. The augmented VBOP successfully represents the strain rate dependence of the material at elevated temperature.

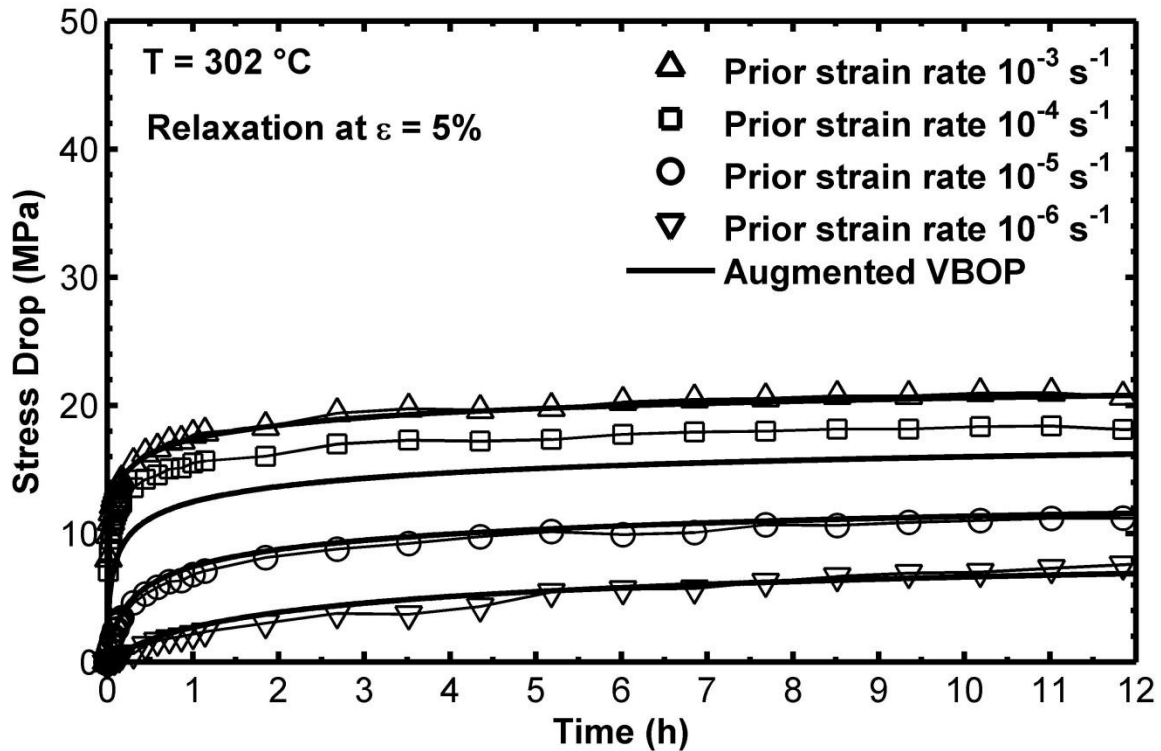


Figure 8.17 A comparison between experimental results and simulated stress drop during relaxation obtained for PMR-15 polymer at 302 °C. Loading prior to relaxation is conducted at constant strain rates of  $10^{-6}$ ,  $10^{-5}$ ,  $10^{-4}$  and  $10^{-3} \text{ s}^{-1}$ . Model parameters for simulations were calculated utilizing the augmented VBOP. The augmented VBOP successfully represents the stress drop throughout the entire relaxation period.

### 8.3 Validation of VBOP Model Parameters as Functions of Test Temperature

The capability of the augmented VBOP to model the effect of test temperature was assessed by comparing the predictions with experimental results obtained in tests that differ in kind from those used for model characterization. Numerical simulations of both stress- and strain-controlled test histories were carried out. Predictions of the strain rate jump test and of creep tests were performed and compared to experimental results.

### 8.3.1 Prediction of the Strain Rate Jump Test at 274 °C

Model prediction of a strain rate jump test (conducted at 274 °C in strain control with strain rates of  $10^{-3}$  and  $10^{-5}$  s $^{-1}$ ) is shown together with the experimental data in Figure 8.18. The augmented VBOP accurately represents the material response during the strain rate jump test: upon a change in strain rate the material “forgets” the prior history of straining at different rates and “returns” to the stress-strain curve characteristic of the given strain rate.

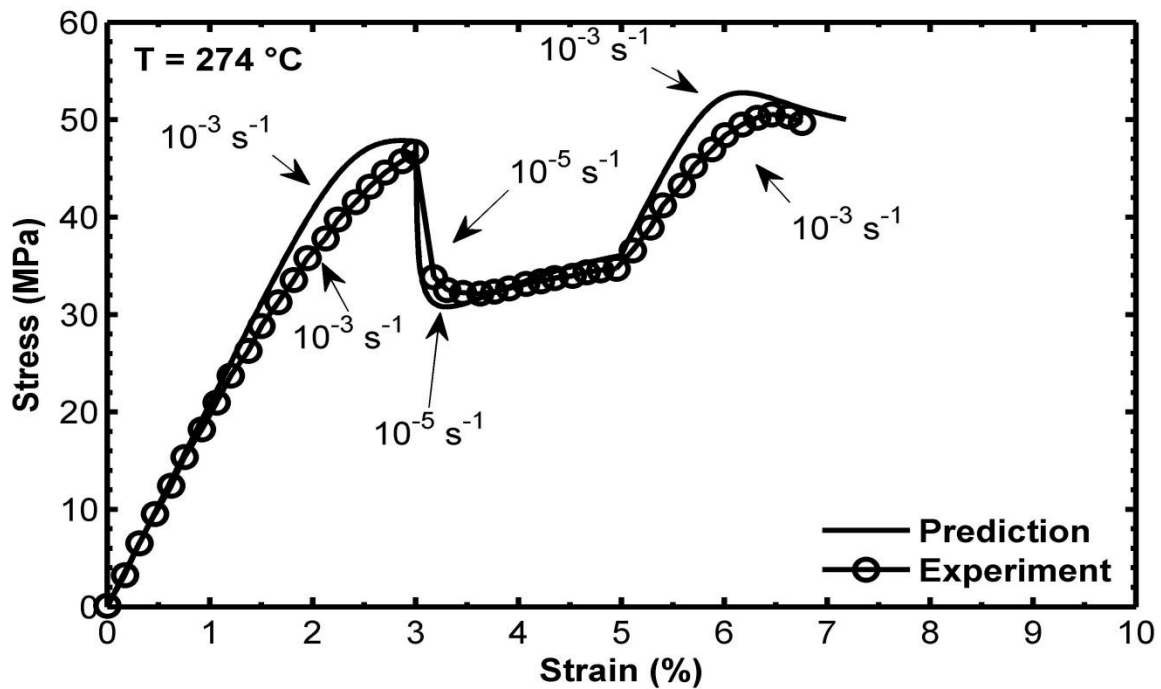


**Figure 8.18** A comparison between experimental and predicted stress-strain curves obtained for PMR-15 polymer in a strain rate jump test conducted at 274 °C. The augmented VBOP model successfully represents the strain rate dependence and the absence of a strain rate history effect.

### 8.3.2 Prediction of the Strain Rate Jump Test at 302 °C

Prediction of the strain rate jump test (conducted at 302 °C in strain control with the strain rates of  $10^{-3}$  and  $10^{-5}$  s $^{-1}$ ) is shown together with the experimental data in

Figure 8.19. While the stress during the initial loading at  $10^{-3} \text{ s}^{-1}$  is slightly overpredicted the overall agreement is good. The extended VBOP predictions are within 4 MPa of the experimental data which is within the typical value of specimen-to-specimen scatter. As with modeling of the strain rate jump tests at 274 °C, the augmented VBOP model successfully represents the strain rate dependence and the absence of a strain rate history effect at 302 °C.

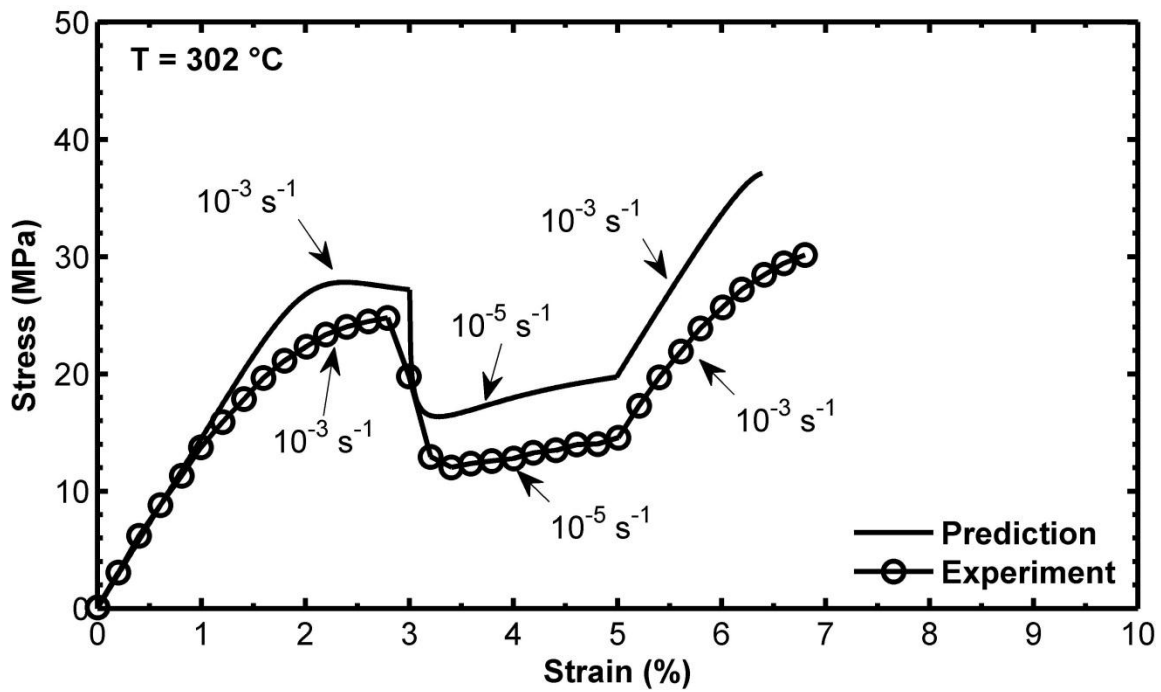


**Figure 8.19** A comparison between experimental and predicted stress-strain curves obtained for PMR-15 polymer in a strain rate jump test conducted at 302 °C. The augmented VBOP model successfully represents the strain rate dependence and the absence of a strain rate history effect.

### 8.3.3 Prediction of Creep Tests at 274 °C

Because model characterization employs tests conducted in strain control, predictions of material response in stress-controlled tests provide a more rigorous examination of the VBOP extended to include the effect of test temperature. The effect

of prior strain rate on creep behavior at 274 °C was explored in creep tests of 6 h duration preceded by monotonic loading to a target creep stress of 21 MPa at  $10^{-6}$  and  $10^{-4}$  s $^{-1}$ . Results in Figure 8.20 demonstrate that at 274 °C the creep strain increases nonlinearly with prior loading rate. Predictions of the stress-controlled creep tests are also shown in Figure 8.20. The extended model predicts the effects of prior loading rate at 274 °C within 0.5% of the experimental results.

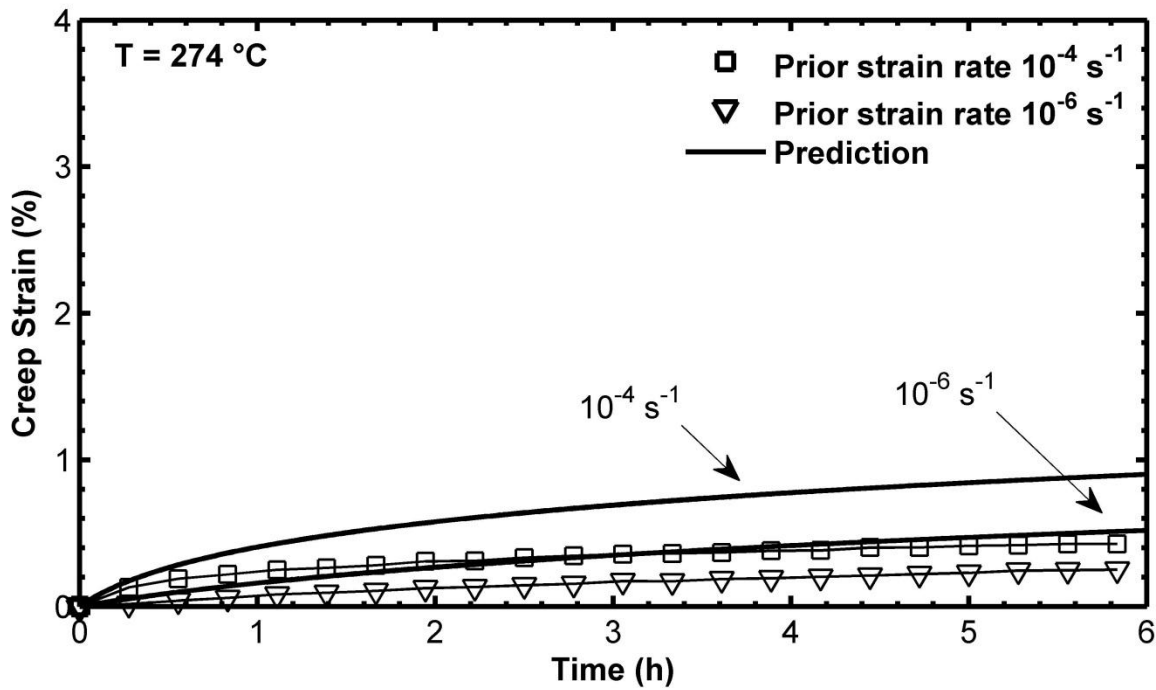


**Figure 8.20** Creep strain versus time at 21 MPa and 274 °C. The effect of prior strain rate on creep is apparent. Creep strain increases nonlinearly with prior strain rate. The model accurately predicts the effects of prior loading rate within 0.5% of the experimental results.

#### 8.3.4 Prediction of Creep Tests at 288 °C

In an effort to explore the capability of the extended model to predict mechanical behavior during stress-controlled tests at other elevated temperatures, additional creep tests were performed at 288 °C. During these tests, the effect of prior strain rate on creep behavior at 288 °C was explored in creep tests of 6 h duration preceded by monotonic



loading to a target creep stress of 21 MPa at  $10^{-6}$  and  $10^{-4}$   $s^{-1}$ . Results in Figure 8.21 demonstrate that at 288 °C the creep strain increases nonlinearly with prior loading rate. Predictions of the stress-controlled creep tests are also shown in Figure 8.21. The extended model accurately predicts the effects of prior loading rate at 288 °C within 1.0% of the experimental results. This reflects a slightly larger absolute discrepancy between predicted and experimental creep strain after prior loading at  $10^{-4}$   $s^{-1}$  than was observed at 274 °C. It should be noted though that the experimental creep strain measured at 288 °C is approximately five times larger than that observed at 274 °C and that a 1% deviation from the model prediction is therefore considered acceptable.

### 8.3.5 *Prediction of Creep Tests at 302 °C*

In order to validate the model over the full temperature range utilized for model characterization, creep tests were also performed at 302 °C. The effect of prior strain rate on creep behavior at 302 °C was explored in creep tests of 6 h duration preceded by monotonic loading to a target creep stress of 21 MPa at  $10^{-6}$ ,  $10^{-5}$ ,  $10^{-4}$  and  $10^{-3}$   $s^{-1}$ . Results in Figure 8.22 demonstrate that at 302 °C the creep strain increases nonlinearly with prior loading rate. Predictions of the stress-controlled creep tests are also shown in Figure 8.22. At 302 °C, when compared to 274 and 288 °C, considerably more creep strain accumulated for all but the slowest prior strain rate. Referring to Figure 8.5, it is noted that during loading to 21 MPa, the specimen loaded at  $10^{-6}$   $s^{-1}$  accumulated far more strain prior to beginning the creep period than specimens loaded at  $10^{-3}$  and  $10^{-4}$   $s^{-1}$ . It is suggested that the large amount of strain accumulated at  $10^{-6}$   $s^{-1}$  prior to the specimen

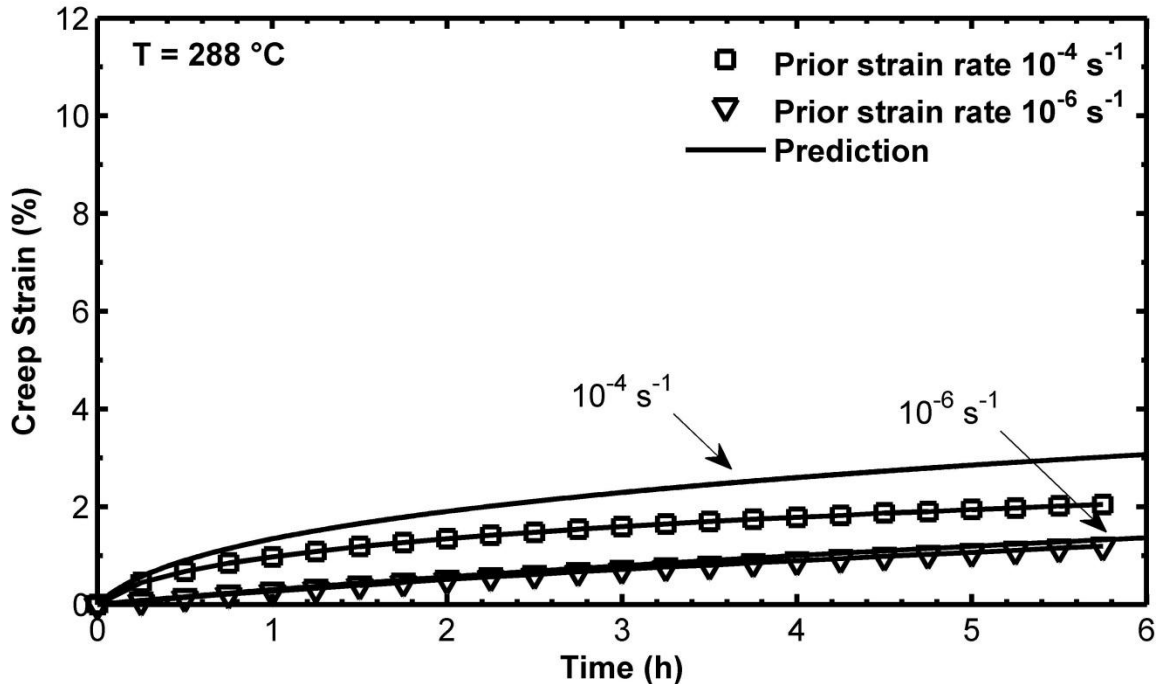


**Figure 8.21** Creep strain versus time at 21 MPa and 288 °C. The effect of prior strain rate on creep is apparent. Creep strain increases nonlinearly with prior strain rate. The extended model accurately predicts the effects of prior loading rate at 288 °C within 1.0% of the experimental results.

entering the creep portion of the loading history is the reason why so little creep strain was accumulated prior to failure. It is also notable that creep strain vs. time curves produced after prior loading at  $10^{-3} \text{ s}^{-1}$  and  $10^{-4} \text{ s}^{-1}$  are very similar. Again, referring to Figure 8.5, the accumulated strains after loading to 21 MPa at  $10^{-3} \text{ s}^{-1}$  and  $10^{-4} \text{ s}^{-1}$  are 1.8 and 2.1 % strain respectively. This suggests that the strain at the beginning of the creep period affects the behavior during the subsequent period of creep. In the VBOP, this behavior is accommodated using the overstress concept. At a given creep stress level (in this case 21 MPa), the specimen loaded at  $10^{-3} \text{ s}^{-1}$  will experience a slightly higher value of overstress when it begins a period of creep at 1.8 % strain as compared to the specimen loaded at  $10^{-4} \text{ s}^{-1}$  when it begins a period of creep at 2.1 % strain. When predicting creep

strain using the VBOP, this slightly greater value of overstress will serve to generate slightly more creep strain as shown in Figure 8.22. As expected, substantially different strains at the start of creep, such as seen when comparing the  $10^{-3} \text{ s}^{-1}$  and  $10^{-4} \text{ s}^{-1}$  with the  $10^{-5} \text{ s}^{-1}$  or  $10^{-6} \text{ s}^{-1}$  prior strain rates, yield substantially different creep strain curves. The ability of the extended model to accurately predict the effects of prior loading rate at 302 °C within 1.0% of the experimental results is significant for two reasons. First, the extended VBOP accurately predicts the general increase in creep strain with the increase in test temperature at each strain rate. Additionally, the extended VBOP accurately predicts that periods of creep that begin with the same creep stress level and nearly the same strain accumulated during prior loading, will produce similar creep curves. As a corollary, the model predicts that the opposite is true when substantially different magnitudes of overstress are perceived at the start of the creep test.

#### **8.4 Predictions of Deformation Behavior of the PMR-15 Neat Resin at 316 °C**

The augmented VBOP model was further validated by comparing the model predictions with experimental results obtained in tests performed at 316 °C, a temperature outside the range used for model characterization.

To provide a yet more thorough verification of the VBOP formulation extended to account for the effects of temperature, equations (8.1) - (8.5) were employed to calculate the model parameters for 316 °C, shown in Table 8.6. Predictions of deformation behavior were then performed using these calculated parameters.

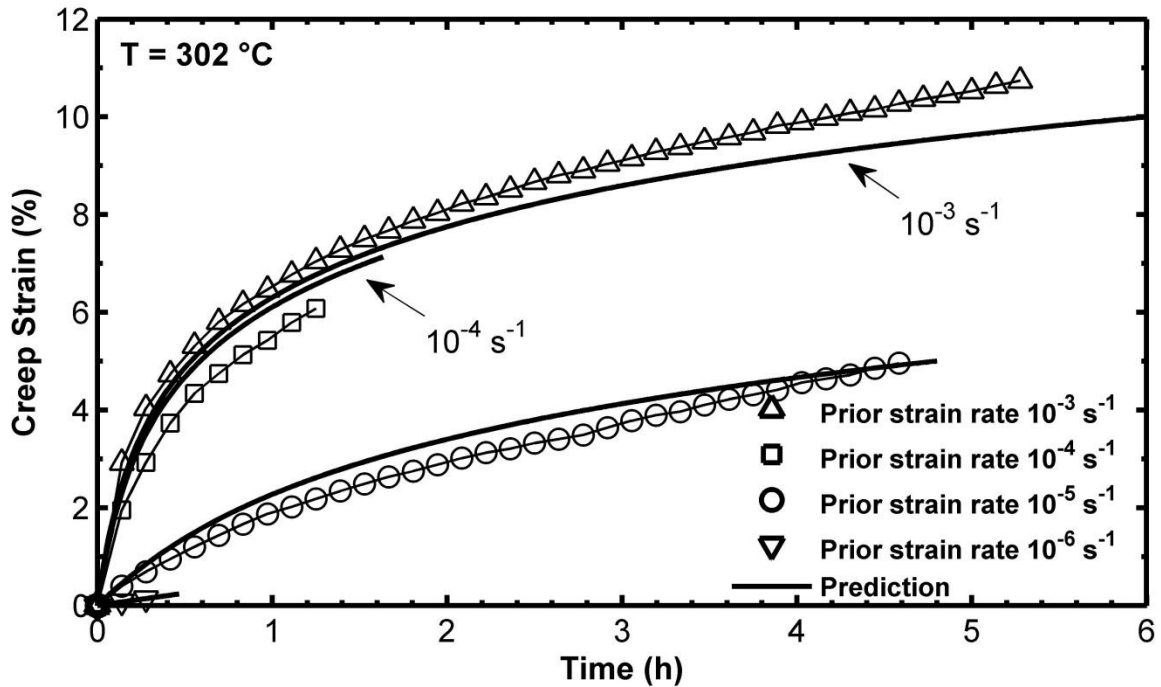


Figure 8.22 Creep strain versus time at 21 MPa and 302 °C. The effect of prior strain rate on creep is apparent. Creep strain increases nonlinearly with prior strain rate. The extended model accurately predicts the effects of prior loading rate at 302 °C within 1.0% of the experimental results.

**Table 8.6 Calculated VBOP Parameters for PMR-15 Neat Resin Subjected to Mechanical Loading at 316 °C**

Moduli	$E = 1135 \text{ MPa}, E_t = 83.0 \text{ MPa}$
Isotropic Stress	$A = 5.07 \text{ MPa}$
Viscosity Function	$k_1 = 1.0e5 \text{ s}, k_2 = 125 \text{ MPa}, k_3 = 80$
Shape Function	$C_1 = 1000 \text{ MPa}, C_2 = 300 \text{ MPa}, C_3 = 10$

#### 8.4.1 Strain Controlled Monotonic Loading

Predictions of strain-controlled monotonic tension tests at 316 °C are compared to experimental data in Figure 8.23. The predictions at each strain rate are in excellent agreement with the experimental data. The model predicts a smaller quasi-elastic region than observed at lower temperatures. Additionally the departure from quasi-elastic behavior occurs earlier, especially at the  $10^{-3} \text{ s}^{-1}$  strain rate. Decreased flow stress levels at this elevated temperature are also modeled well. Finally, the model accurately predicts a much less pronounced knee of the stress-strain curve. Overall, the model is in excellent agreement with the experimental data.

#### 8.4.2 Relaxation Behavior

Data obtained during relaxation tests following strain-controlled loading exhibit the strong influence of increasing test temperature. Decreased stress drop during relaxation is observed for every prior strain rate when compared to lower test temperatures. Additionally, the sensitivity of the stress drop with respect to prior strain rate is further diminished with increased test temperature. As shown in Figure 8.24, the model predictions and the experimental results are in excellent agreement for each prior strain rate throughout the entire relaxation period.

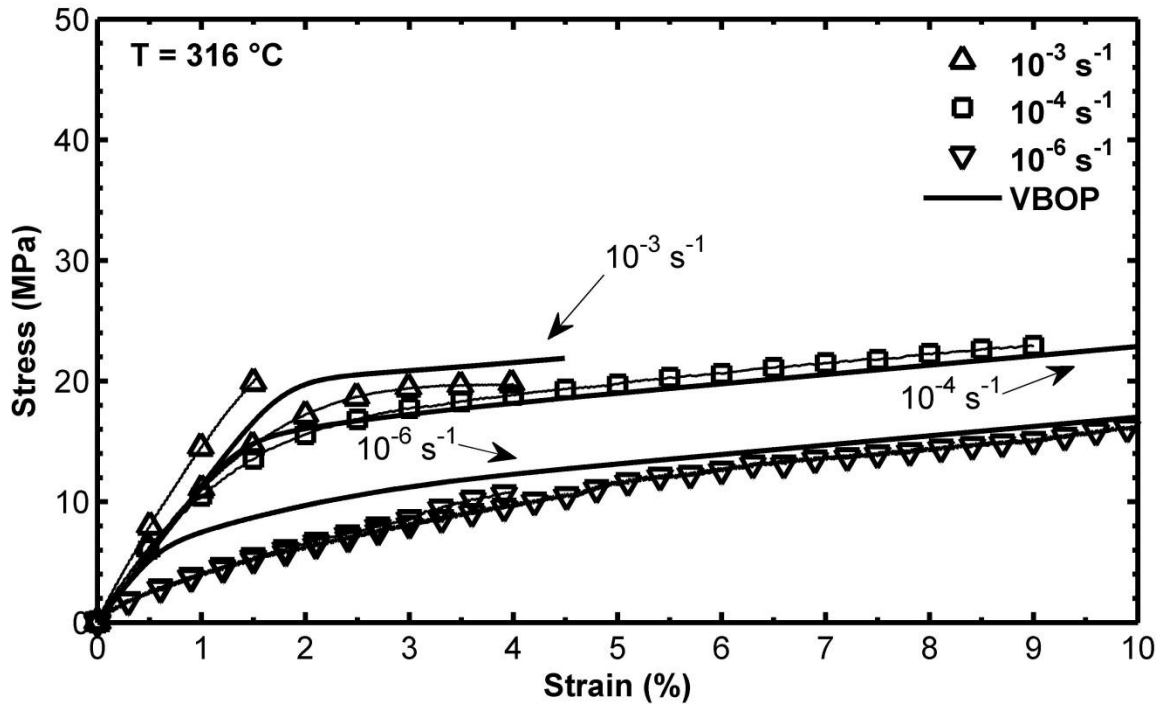
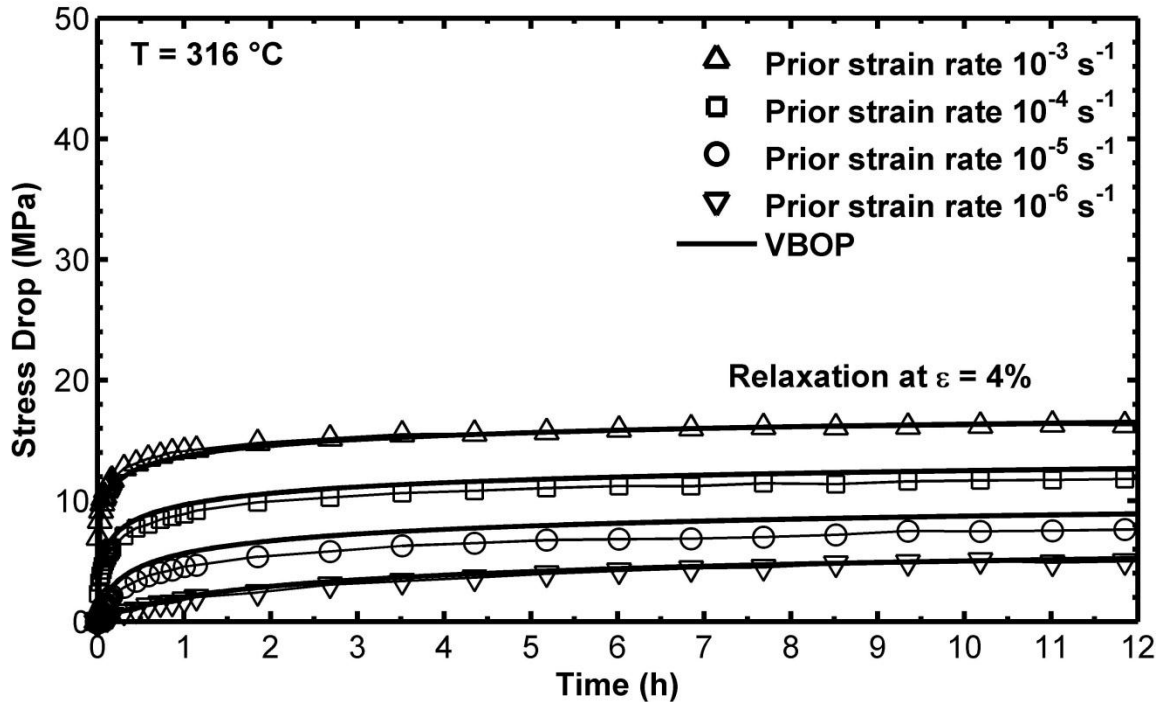


Figure 8.23 A comparison between experimental results and predicted stress-strain curves obtained for PMR-15 polymer in tensile tests to failure conducted at constant strain rates of  $10^{-6}$ ,  $10^{-4}$  and  $10^{-3} \text{ s}^{-1}$  at 316 °C. The model successfully represents the strain rate dependence of the material at elevated temperature.



**Figure 8.24** A comparison between experimental results and predicted stress drop during relaxation obtained for PMR-15 polymer at 316 °C. Loading prior to relaxation is conducted at constant strain rates of  $10^{-6}$ ,  $10^{-5}$ ,  $10^{-4}$  and  $10^{-3} \text{ s}^{-1}$ . The model successfully represents the stress drop throughout the entire relaxation period.

#### 8.4.3 Creep Tests

In the previous two sections, the VBOP formulation extended to account for the effects of temperature was validated by predicting the mechanical behavior of the PMR-15 polymer at a temperature outside the range used for model characterization. In both cases, the model and experimental data were in excellent agreement. A possible criticism of the validation thus far could be that the results predicted at 316 °C, while at a temperature outside the range utilized for model characterization, were of the same *type* as tests utilized for model characterization. In an effort to alleviate this possible criticism, model predictions of stress-controlled rather than strain-controlled tests at 316 °C were performed.

The effect of prior strain rate on creep behavior at 316 °C was examined in creep tests of 6 h duration preceded by uninterrupted loading to a target creep stress of 21 MPa at  $10^{-5}$  and  $10^{-3} \text{ s}^{-1}$ . As previously discussed, prediction of the material response during stress-controlled tests such as creep, provides a more rigorous examination of the modeling capability of the extended VBOP. Coupling tests of a different type with test temperatures outside the range utilized for characterization provides a yet more rigorous validation of the extended VBOP. As demonstrated in Figure 8.25, the extended model predicts the effects of prior loading rate during creep at 316 °C to within 1.0% of the experimental results. Similar to the model performance at 302 °C, the extended VBOP accurately predicts creep strain versus time curves for periods of creep initiated at 21 MPa but with substantially different initial values of strain. It is suggested that the ability of the extended VBOP to accurately model the loading history prior to the start of creep is critical to the accurate prediction of creep strain.

To further explore the capabilities of the extended VBOP, additional predictions of mechanical behavior during creep were conducted. The effect of prior strain rate on creep behavior at 316 °C was explored in creep tests of 6 h duration preceded by uninterrupted loading to a target creep stress of 12 MPa at  $10^{-6}$ ,  $10^{-5}$  and  $10^{-4} \text{ s}^{-1}$ . Unlike the period of creep initiated with a target creep stress of 21 MPa, creep tests conducted at only 12 MPa were initiated after prior loading was conducted entirely within the quasi-elastic region. As shown in Figure 8.26, the extended model fairly accurately predicts the effects of prior loading at 316 °C to within 1.0% of experimental results collected by Ruggles-Wrenn and Ozmen [27, 82].



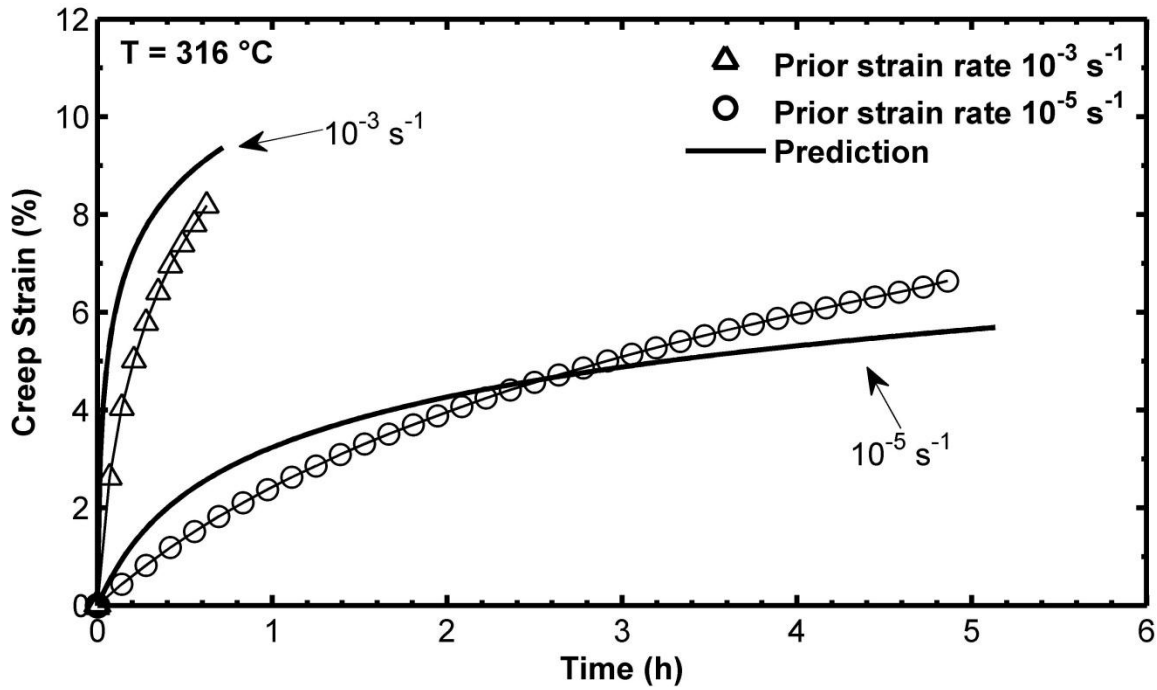


Figure 8.25 Creep strain versus time at 21 MPa and 316 °C. The effect of prior strain rate on creep is apparent. Creep strain increases nonlinearly with prior strain rate. The extended model accurately predicts the effects of prior loading rate at 316 °C within 1.0% of the experimental results.

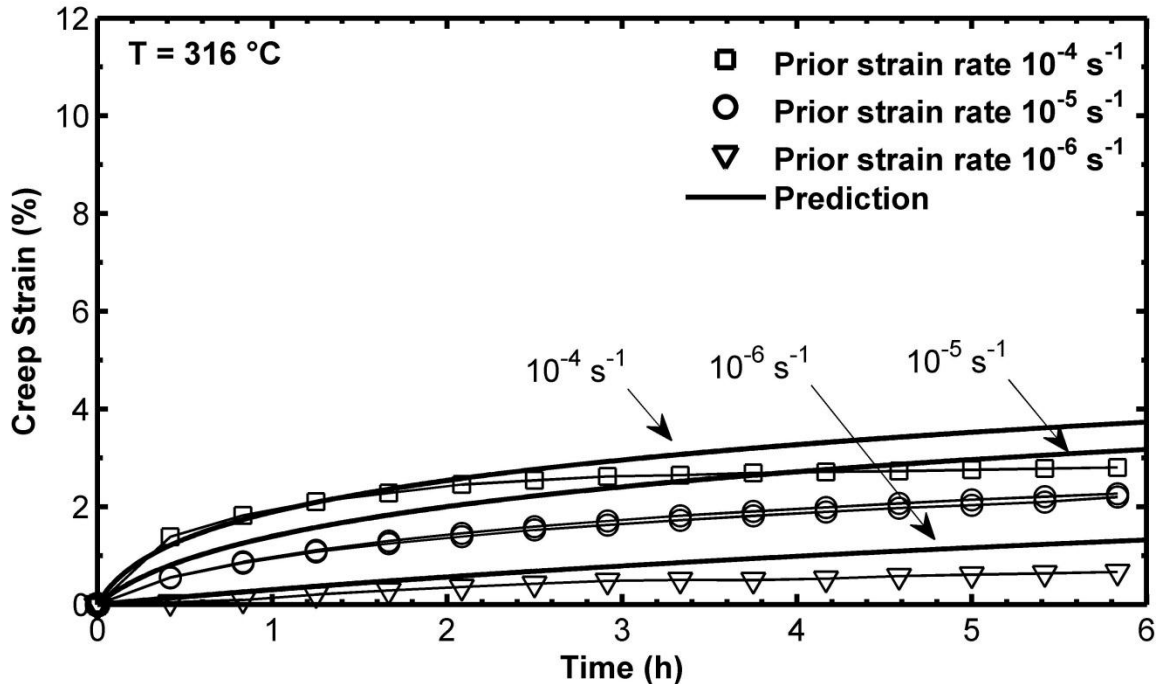


Figure 8.26 Creep strain versus time at 12 MPa and 316 °C. The effect of prior strain rate on creep is apparent. Creep strain increases nonlinearly with prior strain rate. The extended model accurately predicts the effects of prior loading rate at 316 °C within 1.0% of the experimental results. Data from [27, 82].

### 8.5 Summary of the Constitutive Modeling of the Inelastic Behavior of Unaged PMR-15 at 274-316 °C

The experimental results clearly demonstrate that the mechanical behavior of PMR-15 polymer exhibits a strong dependence on test temperature. Of specific interest are the decrease in the slope of the quasi-elastic region and the increase in slope of the flow stress region with increasing test temperature. At a given strain rate, the flow stress level decreases with increasing temperature. Additionally, the transition from quasi-elastic behavior to inelastic flow becomes less pronounced with increasing temperature. During relaxation, the magnitude of the stress drop for a given prior strain rate decreases with increasing test temperature. It is evident that prior strain rate strongly influences

creep behavior at all temperatures in the 274 – 316 °C range. At a given prior strain rate and creep stress level, increasing temperature results in increased creep strain.

The VBOP was augmented to account for the effects of elevated test temperature. The elastic modulus  $E$  was established as a decreasing function of test temperature while the tangent modulus  $E_t$  was represented by an increasing function of temperature. The shape function parameter  $C_2$  was represented by a decreasing function of temperature to reproduce the decreasing prominence of the knee of the stress-strain curve. The isotropic stress  $A$  was made to decrease with increasing test temperature to model the decrease in flow stress levels with increasing temperature. The viscosity function parameter  $k_2$  was represented as a decreasing function of temperature to model the decrease in stress drop during relaxation with increasing test temperature.

The augmented VBOP was then employed to predict the response of the PMR-15 polymer at a temperature outside the range utilized for model characterization. Additionally, predictions for several loading histories of a type different from those used for model characterization were compared to experimental results. The augmented VBOP model predictions were in excellent agreement with the experimental data obtained in a variety of monotonic tension, relaxation and creep tests.

This chapter concludes the portion of this manuscript that addresses the development of an analytical capability to represent the effects of test temperature on the inelastic behavior of PMR-15. The following chapter will reflect on the effect of prior aging temperature and its implications for modeling.

## **9 PMR-15 Neat Resin Aged at 260-316 °C: Experimental Observations**

The objective of this chapter is to discuss the influence of prior isothermal aging temperature on the rate dependent mechanical behavior of PMR-15 polymer. The PMR-15 polymer was aged at various temperatures in the 260-316 °C range then tested at 288 °C.

### **9.1 Assessment of Specimen-to-Specimen Variability**

The room-temperature modulus measurements described in Section 6.1 were also carried out for all PMR-15 specimens subjected to isothermal aging. These measurements were conducted prior to any aging treatment. Note that, the scaling procedures outlined in Section 6.1 were applied to all data obtained during tests of aged specimens.

### **9.2 Test Temperature versus Prior Aging Temperature**

Previous studies [20, 21, 27, 36] revealed that the time-dependent mechanical behavior of the PMR-15 polymer is strongly influenced by prior isothermal aging. Previous researchers examined the effect of prior isothermal aging after conducting tests on specimens aged for various durations at a given temperature. McClung [19, 36] aged and tested PMR-15 polymer at 288 °C while Ozmen [27, 82] aged and tested the same material at 316 °C. Diedrick studied the impact of prior isothermal aging at 260 °C on deformation behavior of PMR-15 at 260 °C. Each researcher noted the effects of increased aging duration at their individual temperatures of interest. In order to discern the effect of *prior aging temperature* though, the test temperature and prior aging temperature variables must be separated. To this end, tests were conducted at a single

test temperature while prior aging temperatures were varied from 260 to 316 °C. The test temperature was selected to be 288 °C since that is the long-term use temperature of the PMR-15 polymer. Concurrent with this research effort, Wahlquist [21] explored the effects of prior aging at 274 °C on the deformation response of PMR-15 polymer at 288 °C. Wahlquist's specimens were aged at 274 °C and tested at 288 °C thus allowing direct comparison of his results with those obtained as part of this study.

### **9.3 Strain Rate Sensitivity – Influence of Prior Aging Temperature**

To explore the effect of prior aging temperature on the strain rate sensitivity of the PMR-15 polymer, specimens that had been previously aged for various durations at 260, 274, 288, 302 and 316 °C were subjected to tensile tests at constant strain rates of  $10^{-6}$ ,  $10^{-5}$ ,  $10^{-4}$ , and  $10^{-3} \text{ s}^{-1}$  at 288 °C. Results are typified in Figure 9.1 through Figure 9.5 where the stress-strain curves obtained for specimens aged for 250 h at the aforementioned temperatures are presented. Results in Figure 9.1 through Figure 9.5 demonstrate that the qualitative influence of strain rate on stress-strain behavior is unaffected by prior aging temperature. Like the stress-strain curves obtained for the unaged PMR-15 polymer shown in Figure 8.3, the stress-strain curves in Figure 9.1 through Figure 9.5 do not exhibit a truly linear range upon leaving the origin. The stress-strain curves obtained at different strain rates for the same prior aging temperature and duration do however exhibit the same quasi-elastic slope upon leaving the origin. After the transition from the initial quasi-elastic behavior to the inelastic regime, the material exhibits positive strain rate sensitivity. The flow stress level increases with increasing strain rate. Additionally, the shape of the stress-strain curve undergoes a gradual change

as the strain rate increases. At higher strain rates, the “knee” of the stress-strain curve is more pronounced than at the slower strain rates. Stress-strain curves obtained at slower strain rates depart from linearity at a much lower stress level than those obtained at faster strain rates. For each prior aging temperature in the 260–316 °C range, the influence of strain rate is qualitatively similar to that observed for the unaged material. The previously described characteristics of the material aged for 250 h were typical of all prior aging durations and temperatures explored in this study. Hence, we conclude that prior aging temperature has little qualitative influence on strain rate sensitivity. A summary of the test conditions for each tensile test conducted during this study on aged PMR-15 can be found in Table 12.4 and Table 12.5.

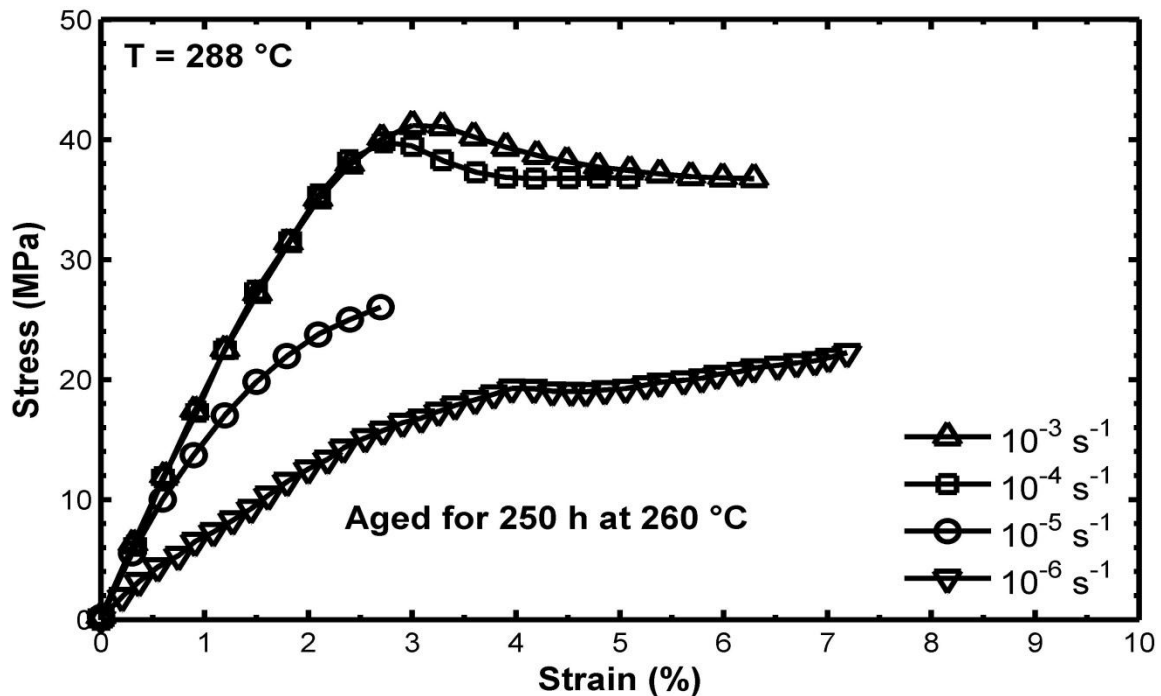


**Figure 9.1** Stress-Strain curves for PMR-15 specimens aged for 250 h at 260 °C in argon obtained in tensile tests to failure conducted at constant strain rates of  $10^{-6}$ ,  $10^{-5}$ ,  $10^{-4}$  and  $10^{-3} \text{ s}^{-1}$  at 288 °C. The dependence of the stress-strain behavior on the strain rate is evident.

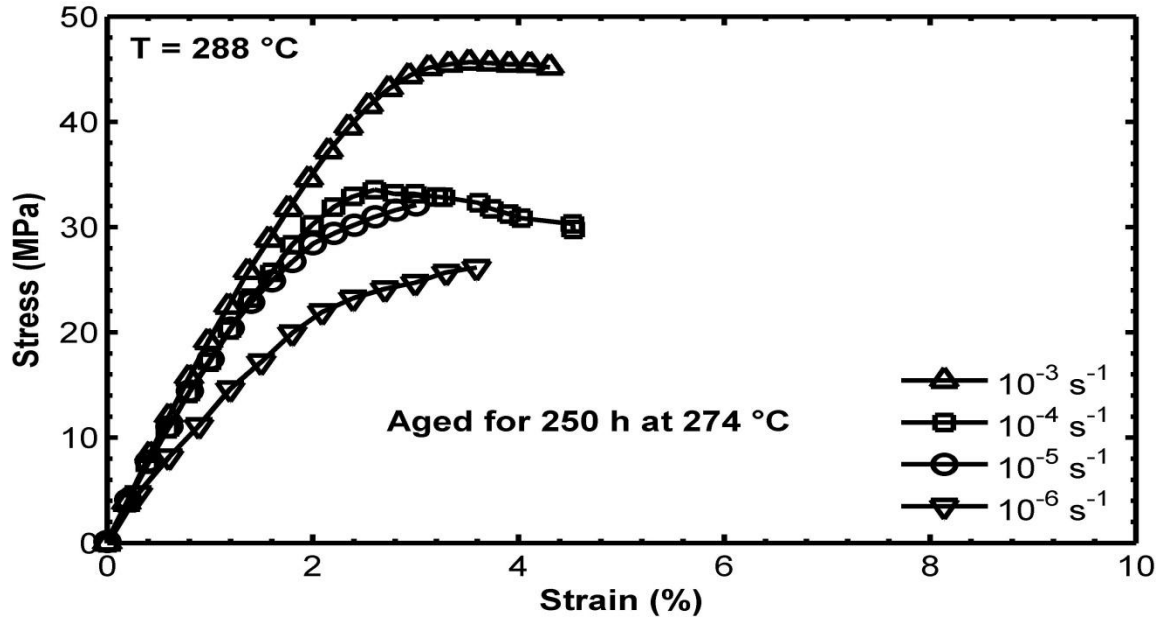


Figure 9.2 Stress-Strain curves for PMR-15 specimens aged for 250 h at 274 °C in argon obtained in tensile tests to failure conducted at constant strain rates of  $10^{-6}$ ,  $10^{-5}$ ,  $10^{-4}$  and  $10^{-3} \text{ s}^{-1}$  at 288 °C. The dependence of the stress-strain behavior on the strain rate is evident. Data from [21].

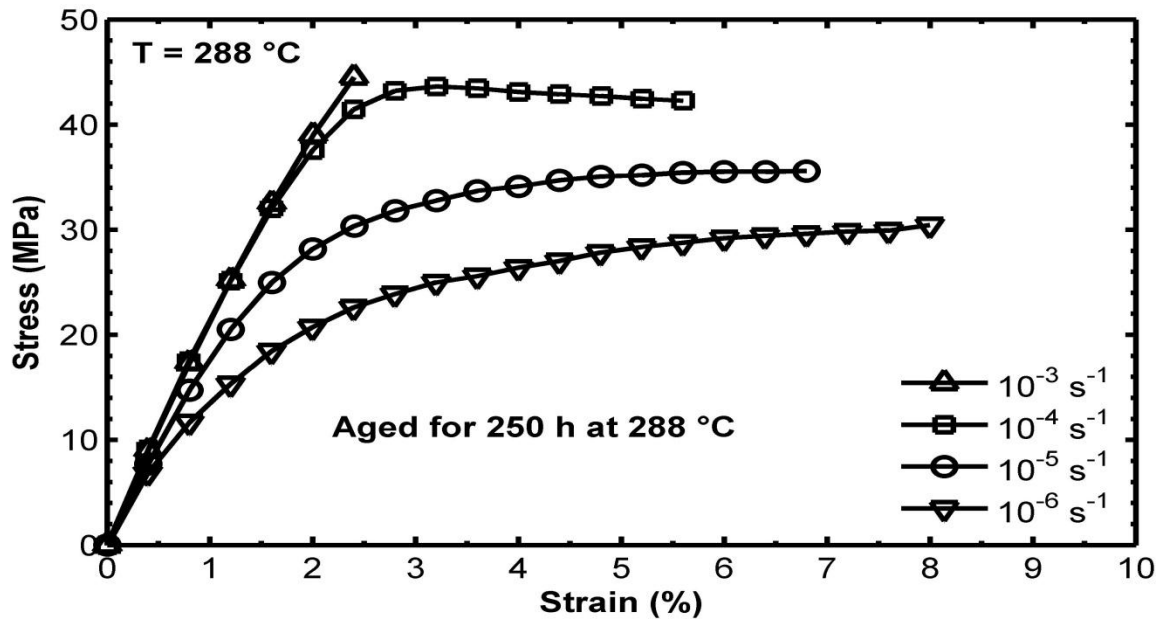


Figure 9.3 Stress-Strain curves for PMR-15 specimens aged for 250 h at 288 °C in argon obtained in tensile tests to failure conducted at constant strain rates of  $10^{-6}$ ,  $10^{-5}$ ,  $10^{-4}$  and  $10^{-3} \text{ s}^{-1}$  at 288 °C. The dependence of the stress-strain behavior on the strain rate is evident. Data from [19].

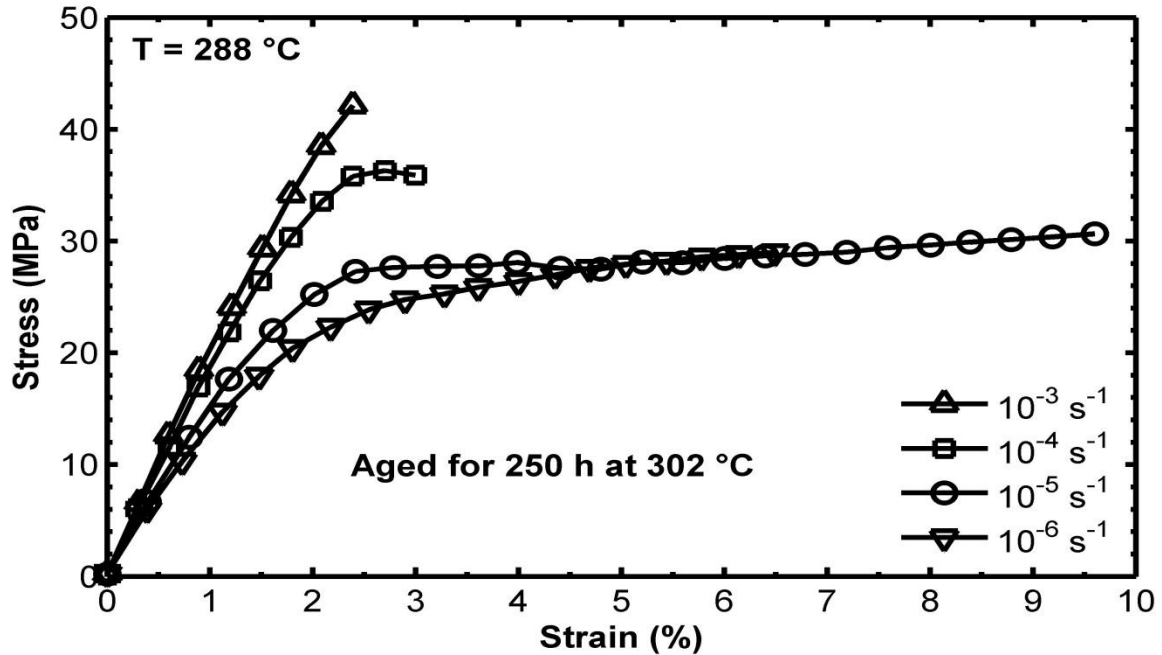


Figure 9.4 Stress-Strain curves for PMR-15 specimens aged for 250 h at 302 °C in argon obtained in tensile tests to failure conducted at constant strain rates of  $10^{-6}$ ,  $10^{-5}$ ,  $10^{-4}$  and  $10^{-3} \text{ s}^{-1}$  at 288 °C. The dependence of the stress-strain behavior on the strain rate is evident.

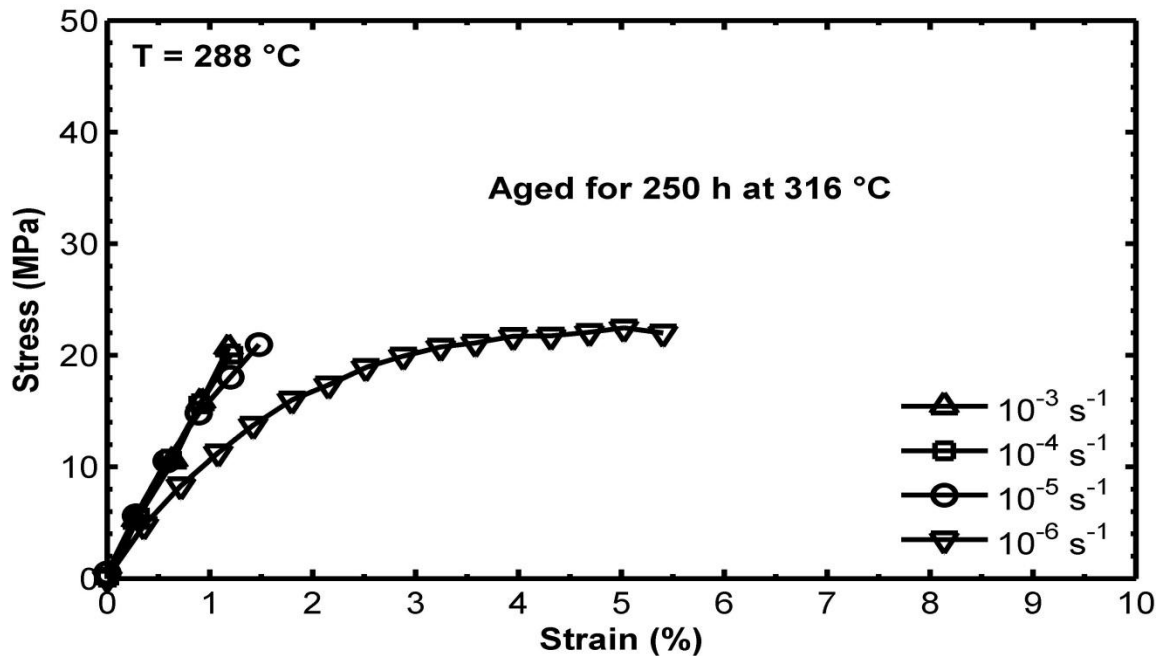
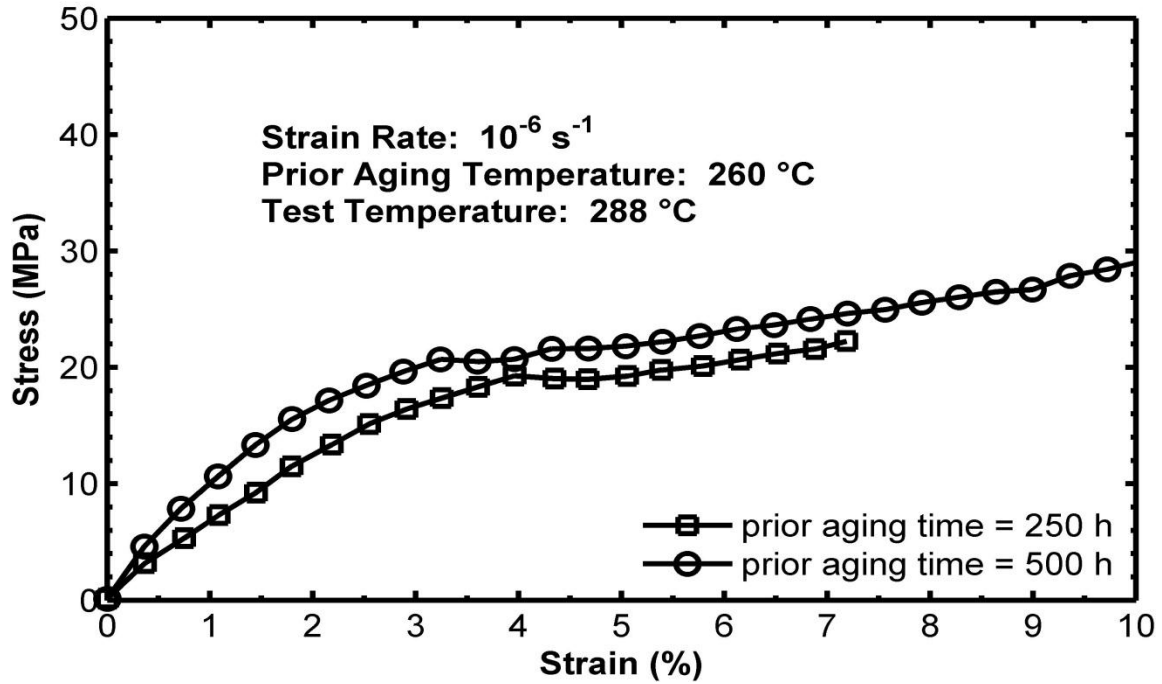


Figure 9.5 Stress-Strain curves for PMR-15 specimens aged for 250 h at 316 °C in argon obtained in tensile tests to failure conducted at constant strain rates of  $10^{-6}$ ,  $10^{-5}$ ,  $10^{-4}$  and  $10^{-3} \text{ s}^{-1}$  at 288 °C. The dependence of the stress-strain behavior on the strain rate is evident.

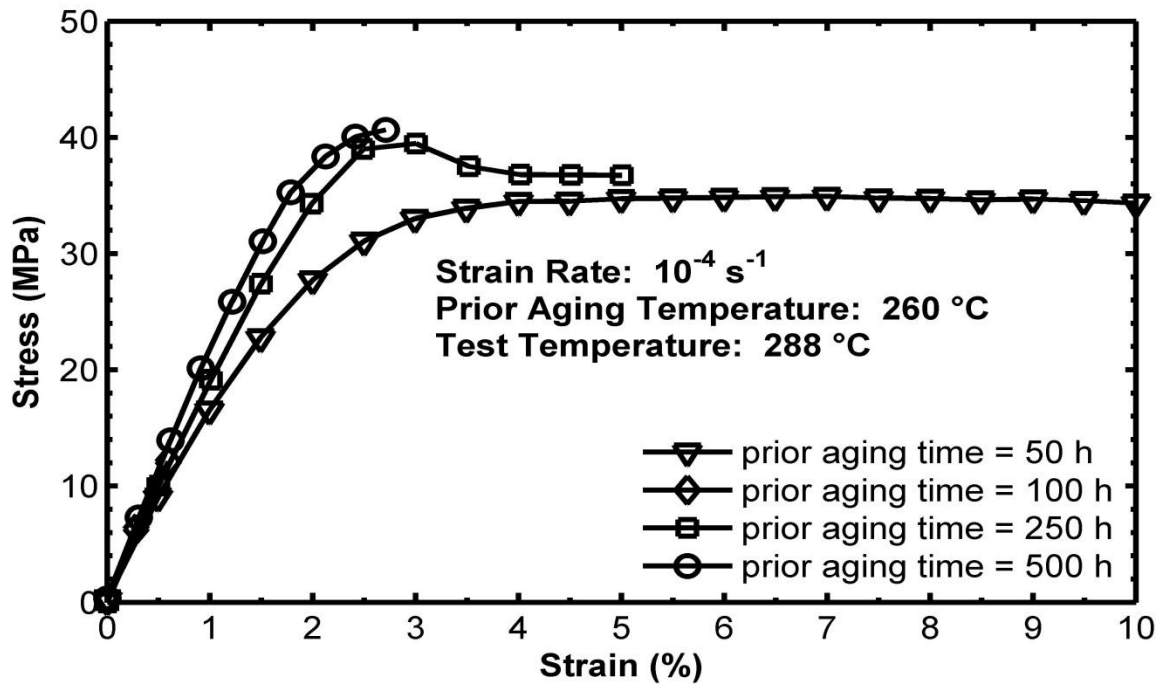


The stress-strain responses of specimens aged in argon at 260 and 302 °C for various durations obtained during strain-controlled tension to failure tests at 288 °C are shown in Figure 9.6 and Figure 9.7, respectively. Monotonic tensile stress-strain curves for specimens aged at 274 and 288 °C and tested at 288 °C are reported in Figures 6.10 - 6.13 of Wahlquist [21] and Figure 8.2 of McClung [19], respectively. It is noteworthy that prior aging in argon at temperatures in the 260-302 °C range does affect the stress-strain behavior of the material. For each prior aging temperature, the elastic modulus increases with prior aging time. Additionally, the shape of the knee of the stress-strain curve becomes more pronounced with increasing prior aging time. Furthermore, the delay in the departure from the quasi-linear behavior increases with an increase in aging time. Finally, prior aging in argon leads to an increase in the flow stress at each strain rate.

The effect of prior aging duration for specimens aged at 316 °C and tested at 288 °C is less clear. The stress-strain response of specimens aged in argon for various durations obtained during strain-controlled tension to failure tests performed at the rates of  $10^{-6}$ ,  $10^{-5}$ ,  $10^{-4}$  and  $10^{-3} \text{ s}^{-1}$  is presented in Figure 9.8, Figure 9.9, Figure 9.10 and Figure 9.11, respectively. Specimens tested at  $10^{-3}$  and  $10^{-4} \text{ s}^{-1}$  (Figure 9.11 and Figure 9.10) exhibit only quasi-linear behavior until failure and show little or no effect of aging duration on the quasi-elastic modulus. Specimens tested at  $10^{-5}$  and  $10^{-6} \text{ s}^{-1}$  (Figure 9.9 and Figure 9.8) do proceed into the flow stress region but unexpectedly a decrease in flow stress is observed with increasing prior aging duration. This is in contrast to the

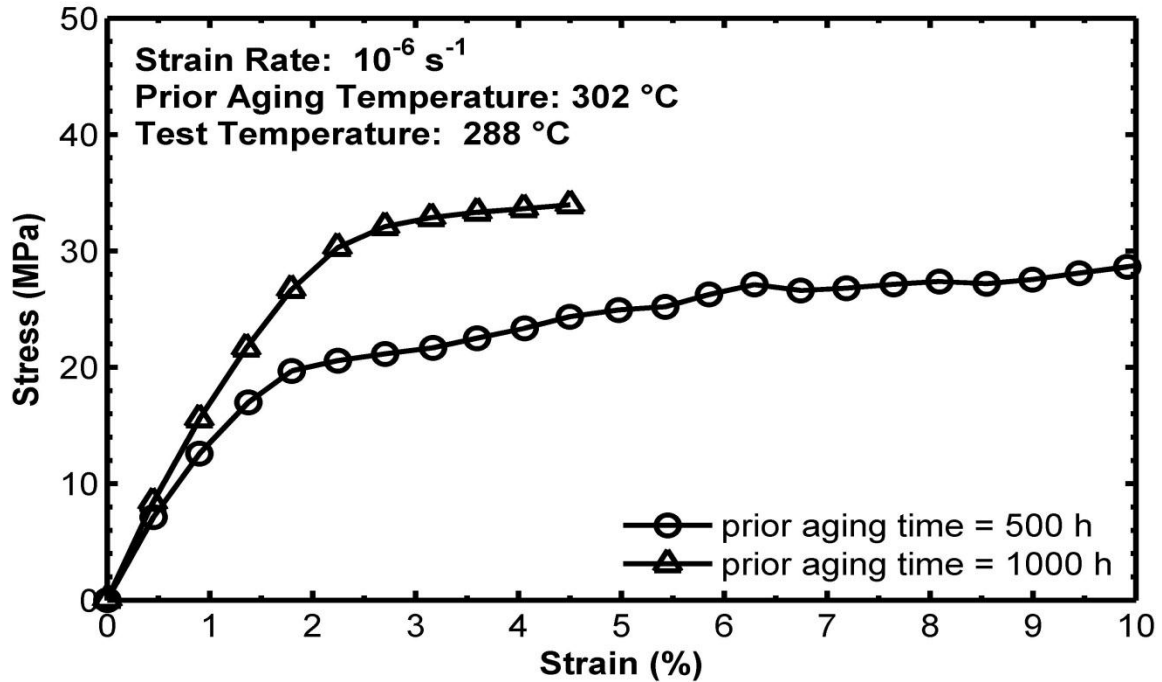


(a) Strain Rate =  $10^{-6} \text{ s}^{-1}$

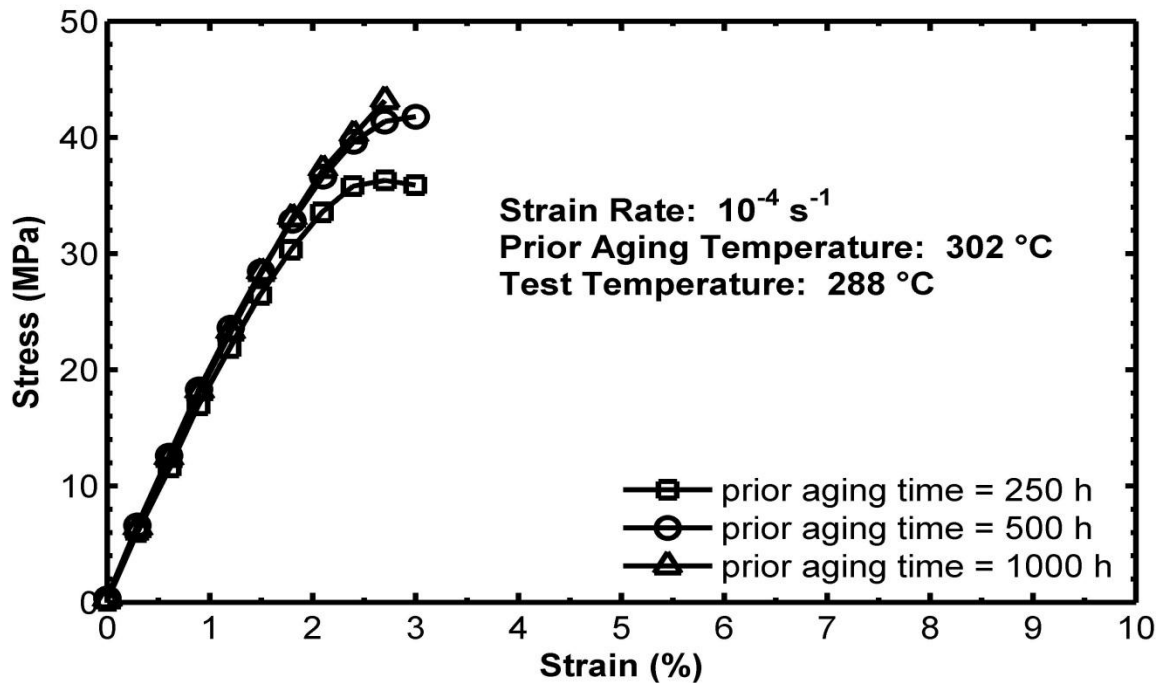


(b) Strain Rate =  $10^{-4} \text{ s}^{-1}$

Figure 9.6 Stress-strain curves for PMR-15 aged at  $260 \text{ }^\circ\text{C}$  in argon obtained in tensile tests to failure conducted at  $288 \text{ }^\circ\text{C}$  at constant strain rates of (a)  $10^{-6} \text{ s}^{-1}$  and (b)  $10^{-4} \text{ s}^{-1}$ .



(a) Strain Rate =  $10^{-6} \text{ s}^{-1}$



(b) Strain Rate =  $10^{-4} \text{ s}^{-1}$

Figure 9.7 Stress-strain curves for PMR-15 aged at  $302 \text{ }^\circ\text{C}$  in argon obtained in tensile tests to failure conducted at  $288 \text{ }^\circ\text{C}$  at constant strain rates of (a)  $10^{-6} \text{ s}^{-1}$  and (b)  $10^{-4} \text{ s}^{-1}$ .

increase in flow stress with prior aging duration observed with prior aging temperatures in the 260-302 °C range. Similar testing conducted by Ozmen [27] on specimens aged and tested at 316 °C yielded no clear relationship between aging duration and deformation behavior. Ozmen did report a reduced capacity for inelastic straining and a reduction in ultimate tensile strength with increased prior aging duration. Comparison of Ozmen's results for the material aged at 316 °C and tested at 316 °C with the results of the current research obtained for the specimens aged at 316 °C and tested at 288 °C suggests an important finding. Prior aging of PMR-15 polymer at 316 °C appears to degrade the overall strength and stiffness of the material and this degradation increases with aging duration.

In Chapter 6 the effect of test temperature on the deformation behavior of unaged PMR-15 polymer was explored. For a given strain rate, test temperature had a significant quantitative effect on the stress-strain behavior of the unaged PMR-15. This begs the question; does test temperature similarly affect the stress-strain behavior of previously aged PMR-15 polymer? While not a primary focus of this research effort, data was obtained that provides some insight into this matter. Stress-strain curves for PMR-15 aged for 250 h at 260 °C obtained in tensile tests to failure conducted at 260 and 288 °C and strain rates of  $10^{-4}$  and  $10^{-6} \text{ s}^{-1}$  are shown in Figure 9.12. Similar to the unaged PMR-15 polymer, material aged at 260 °C does not show a distinct linear range. However, the stress-strain curves obtained at different strain rates at each given test temperature do exhibit the same quasi-elastic slope upon leaving the origin. It is seen

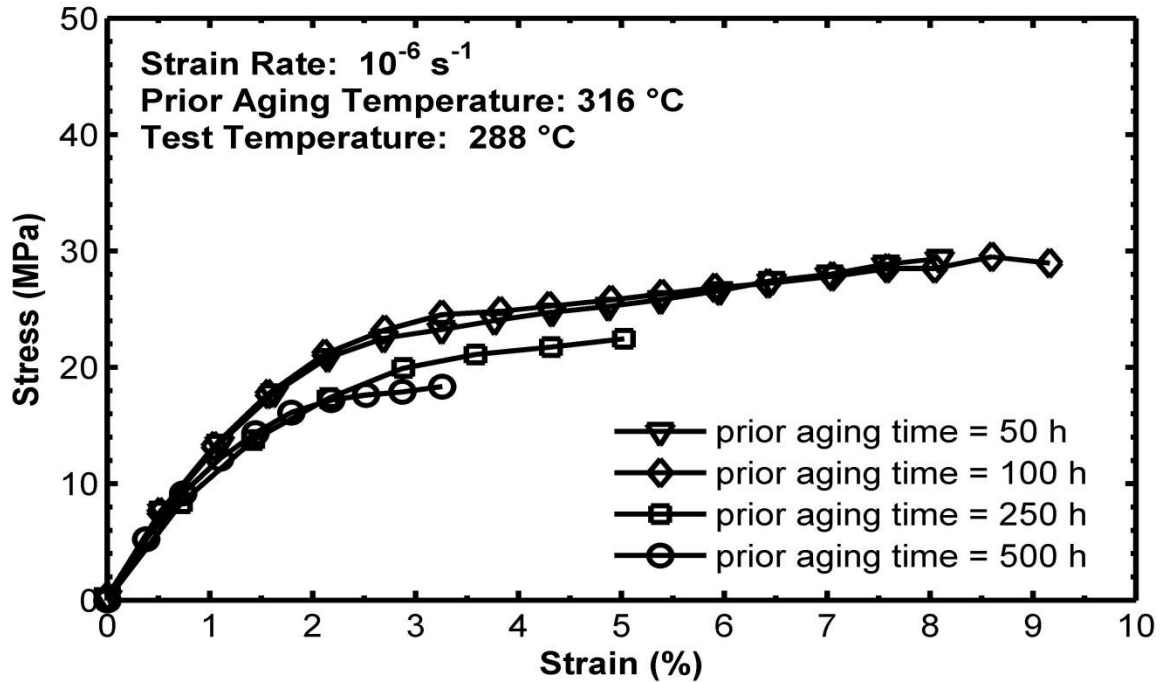


Figure 9.8 Stress-strain curves for PMR-15 specimens aged for various durations in argon at  $316 \text{ }^\circ\text{C}$  obtained in tensile tests to failure conducted at  $288 \text{ }^\circ\text{C}$  and constant strain rate of  $10^{-6} \text{ s}^{-1}$ .

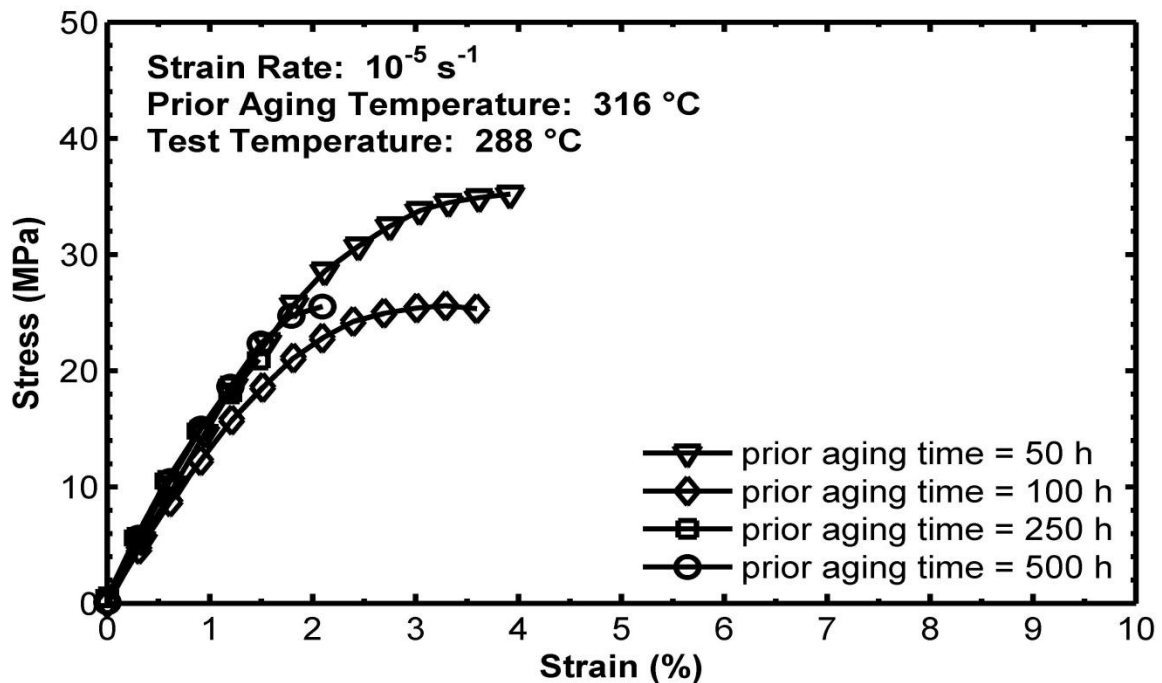


Figure 9.9 Stress-strain curves for PMR-15 specimens aged for various durations in argon at  $316 \text{ }^\circ\text{C}$  obtained in tensile tests to failure conducted at  $288 \text{ }^\circ\text{C}$  and constant strain rate of  $10^{-5} \text{ s}^{-1}$ .

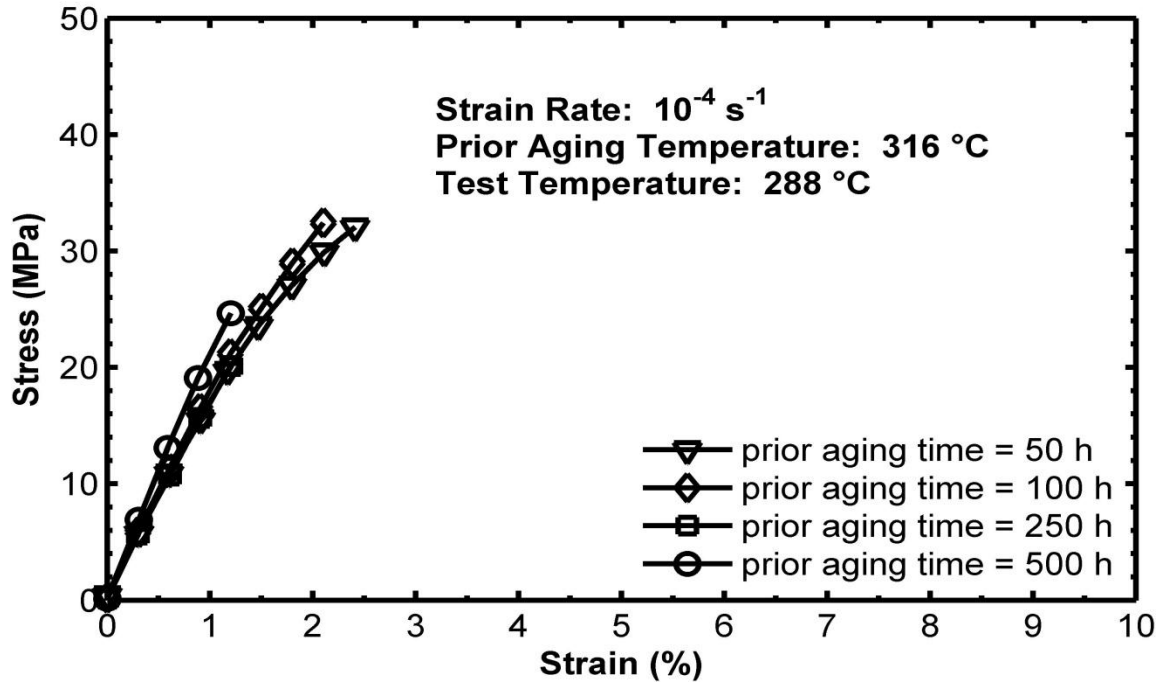


Figure 9.10 Stress-strain curves for PMR-15 specimens aged for various durations in argon at  $316 \text{ }^\circ\text{C}$  obtained in tensile tests to failure conducted at  $288 \text{ }^\circ\text{C}$  and constant strain rate of  $10^{-4} \text{ s}^{-1}$ .

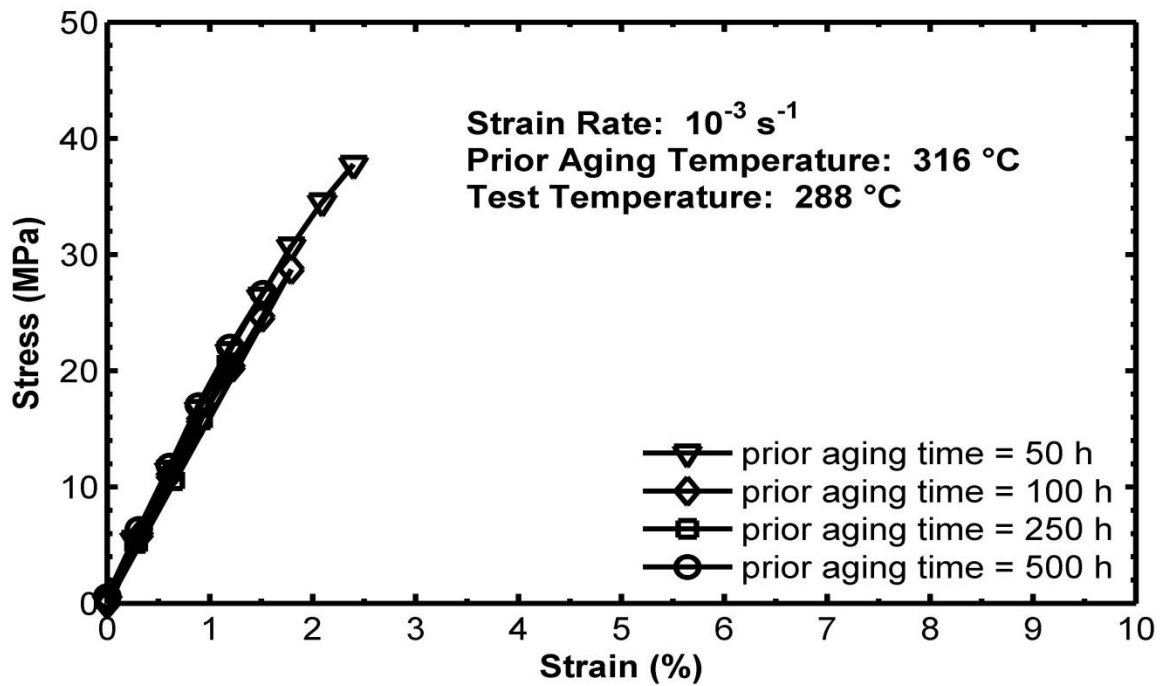


Figure 9.11 Stress-strain curves for PMR-15 specimens aged for various durations in argon at  $316 \text{ }^\circ\text{C}$  obtained in tensile tests to failure conducted at  $288 \text{ }^\circ\text{C}$  and constant strain rate of  $10^{-3} \text{ s}^{-1}$ .

that this quasi-elastic slope decreases with increasing test temperature. After the transition from the initial quasi-elastic to the inelastic regime, the material exhibits positive, nonlinear strain rate sensitivity. At 260 and 288 °C, the flow stress level increases with increasing strain rate. At a given strain rate, the flow stress level decreases with increasing temperature. Additionally, the shape of the stress-strain curve gradually changes as the strain rate increases. Transition from quasi-elastic behavior to inelastic flow becomes more pronounced with increasing strain rate. Moreover, at a given strain rate this transition becomes more prominent with decreasing temperature. The stress-strain curves obtained at slower strain rates depart from near linear behavior at much lower stress levels than those obtained at higher strain rates. As the test temperature increases, this effect is magnified. In a similar manner, stress-strain curves for PMR-15 aged for 250 h at 316 °C obtained in tensile tests to failure conducted at 288 and 316 °C and strain rates of  $10^{-4}$  and  $10^{-6} \text{ s}^{-1}$  are shown in Figure 9.13. The key manifestations of the influence of test temperature on the deformation behavior of the unaged PMR-15 and on the PMR-15 aged for 250 h at 260 °C are also observed for PMR-15 polymer aged for 250 h at 316 °C. A thorough examination of several prior aging temperatures and varying test temperatures would be required to quantitatively identify the specific relationships between prior aging temperature and test temperature and their synergistic effects on deformation behavior of the PMR-15 polymer.

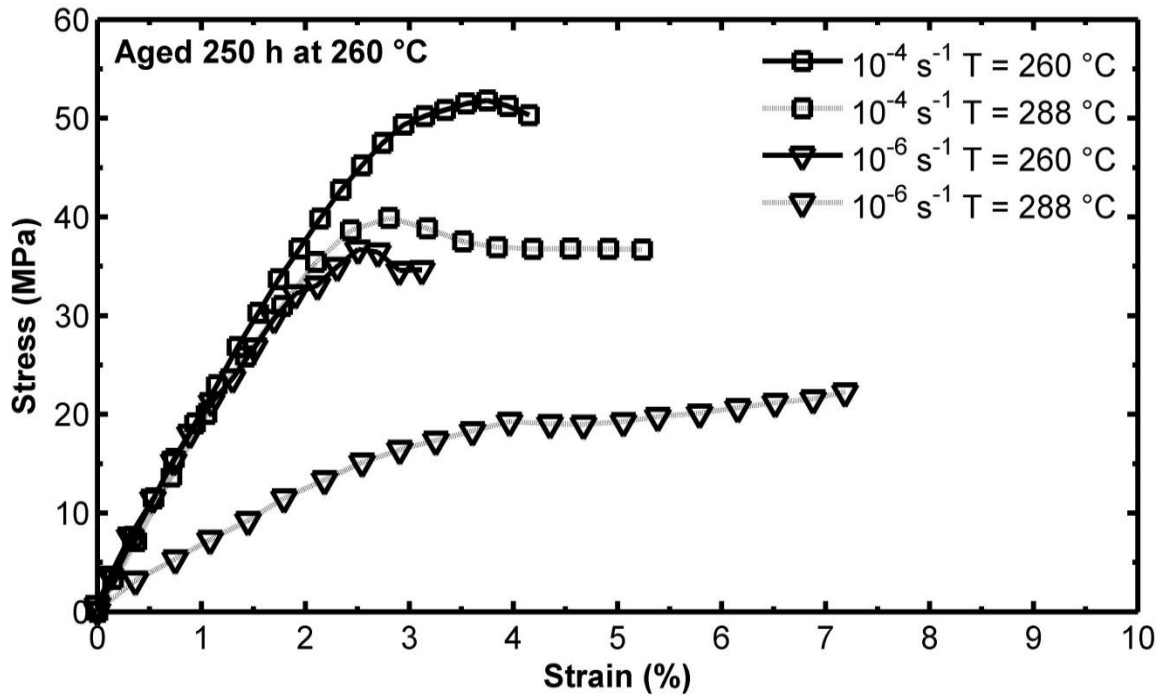
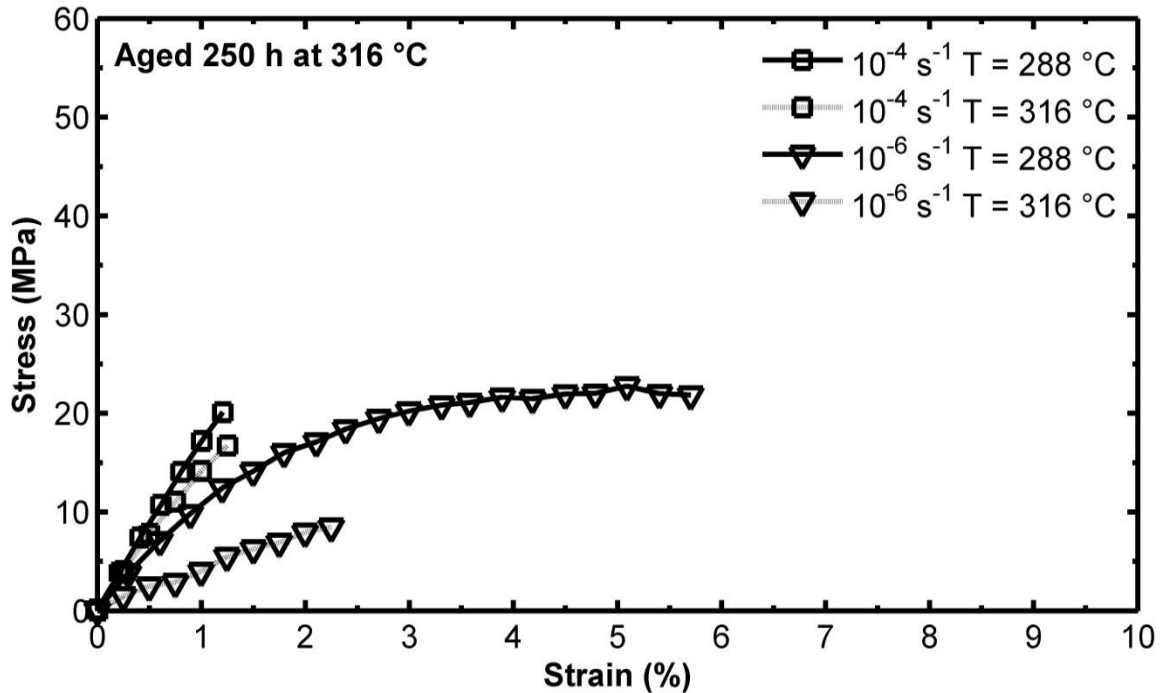


Figure 9.12 Stress-strain curves for PMR-15 specimens aged for 250 h in argon at 260 °C obtained in tensile tests to failure conducted at 260 and 288 °C and constant strain rates of  $10^{-4}$  and  $10^{-6} \text{ s}^{-1}$ . The influence of test temperature on the deformation behavior is evident. Data at 260 °C from [20].





**Figure 9.13** Stress-strain curves for PMR-15 specimens aged for 250 h in argon at 316 °C obtained in tensile tests to failure conducted at 288 and 316 °C and constant strain rates of  $10^{-4}$  and  $10^{-6}$  s $^{-1}$ . The influence of test temperature on the deformation behavior is evident. Data at 316 °C from [27].

As seen from the results presented above, prior aging at temperatures in the 260-316 °C range clearly has an effect on the deformation behavior of PMR-15. The dependence of that deformation behavior on *prior aging temperature* is less clear though. The stress-strain responses of specimens aged in argon for 50 h at 260, 274, 288, 302 and 316 °C obtained during strain-controlled tension to failure tests at strain rates of  $10^{-6}$ ,  $10^{-5}$ ,  $10^{-4}$  and  $10^{-3}$  s $^{-1}$  at 288 °C are presented in Figure 9.14, Figure 9.15, Figure 9.16 and Figure 9.17 respectively. Similar data for specimens aged for 100, 250, 500 and 1000 hours are presented in Figure 9.18 through Figure 9.33. What is common throughout these results is that there are no measureable differences in the elastic moduli of specimens aged for a given duration at various temperatures in the 260-316 °C range.

In each instance, for a given prior aging duration and strain rate, the elastic modulus was the same for every prior aging temperature investigated. Additionally, the slope of the stress-strain curve in the flow stress region (tangent modulus) for a given strain rate and prior aging time appears to be independent of prior aging temperature. The shape of the knee of the stress-strain curve is also independent of the prior aging temperature. There appears to be no relationship between the prior aging temperature and the strain at which the departure from quasi-linear behavior occurs. There is some variation in flow stress levels for tests conducted at various prior aging temperatures but there is no specific correlation between prior aging temperature and the flow stress level. A number of tests were duplicated resulting in scatter bands for flow stress levels for specific combinations of prior aging temperature, aging duration and strain rate, that were similar to variations in flow stress obtained for specimens subjected to identical prior aging and testing histories.

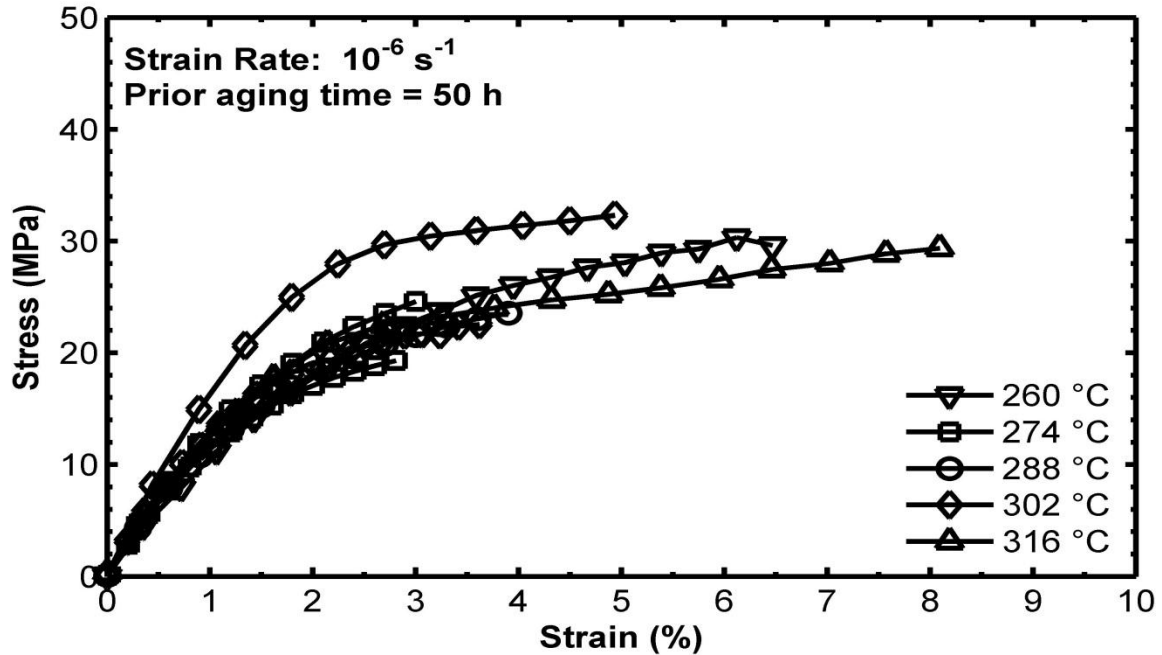


Figure 9.14 Stress-strain curves for PMR-15 specimens aged for 50 h at 260, 274, 288, 302 and 316 °C Obtained in tensile tests to failure at constant strain rate  $10^{-6} \text{ s}^{-1}$ . Data from [21] and [19] included.

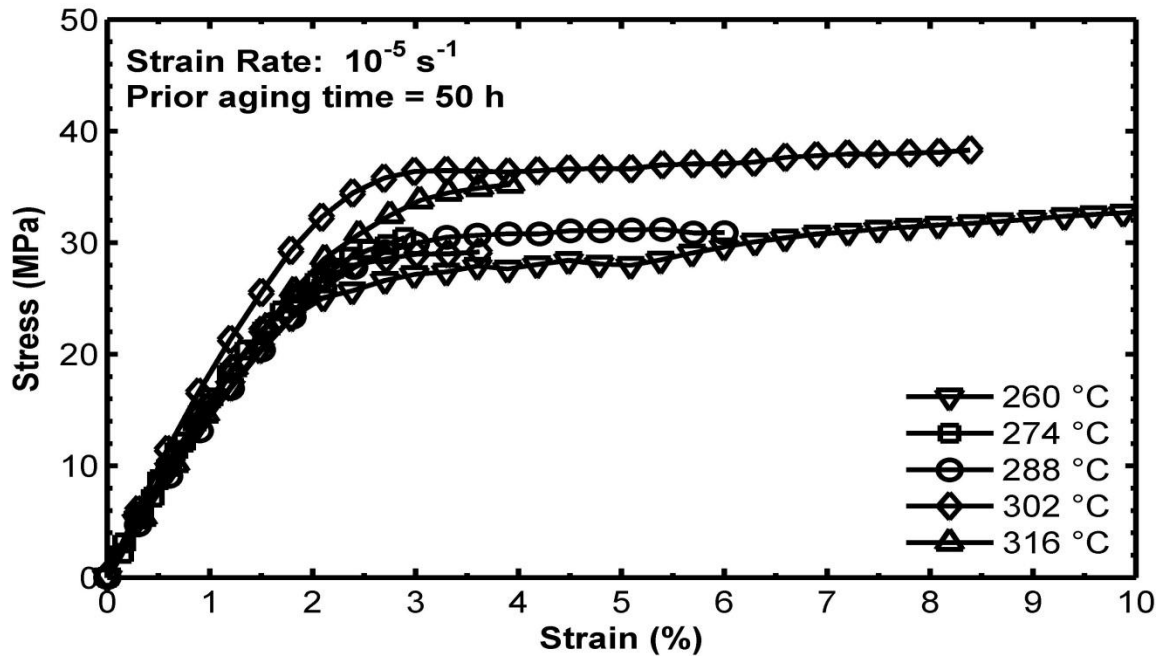


Figure 9.15 Stress-strain curves for PMR-15 specimens aged for 50 h at 260, 274, 288, 302 and 316 °C Obtained in tensile tests to failure at constant strain rate  $10^{-5} \text{ s}^{-1}$ . Data from [21] and [19] included.

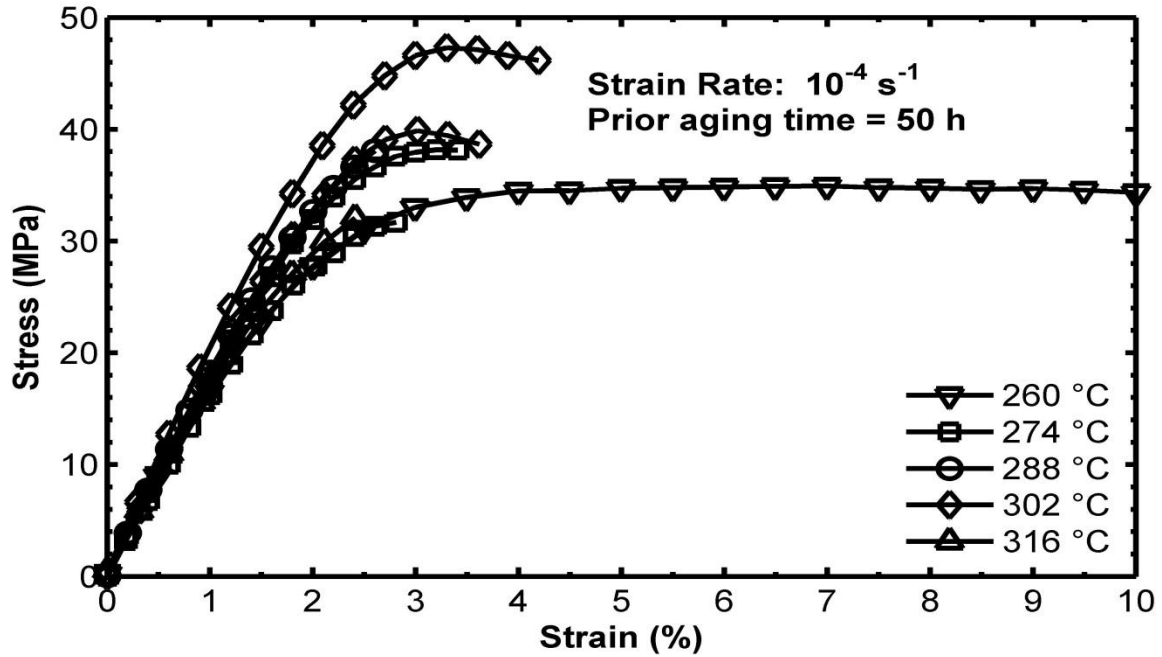


Figure 9.16 Stress-strain curves for PMR-15 specimens aged for 50 h at 260, 274, 288, 302 and 316 °C Obtained in tensile tests to failure at constant strain rate  $10^{-4} \text{ s}^{-1}$ . Data from [21] and [19] included.

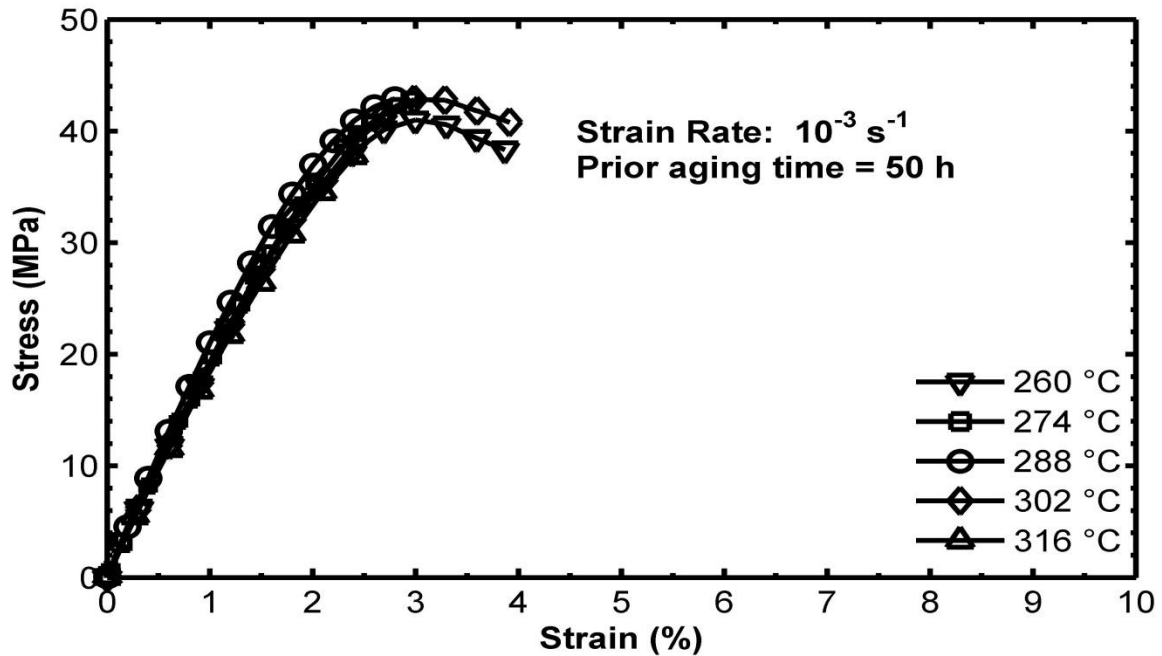


Figure 9.17 Stress-strain curves for PMR-15 specimens aged for 50 h at 260, 274, 288, 302 and 316 °C Obtained in tensile tests to failure at constant strain rate  $10^{-3} \text{ s}^{-1}$ . Data from [21] and [19] included.

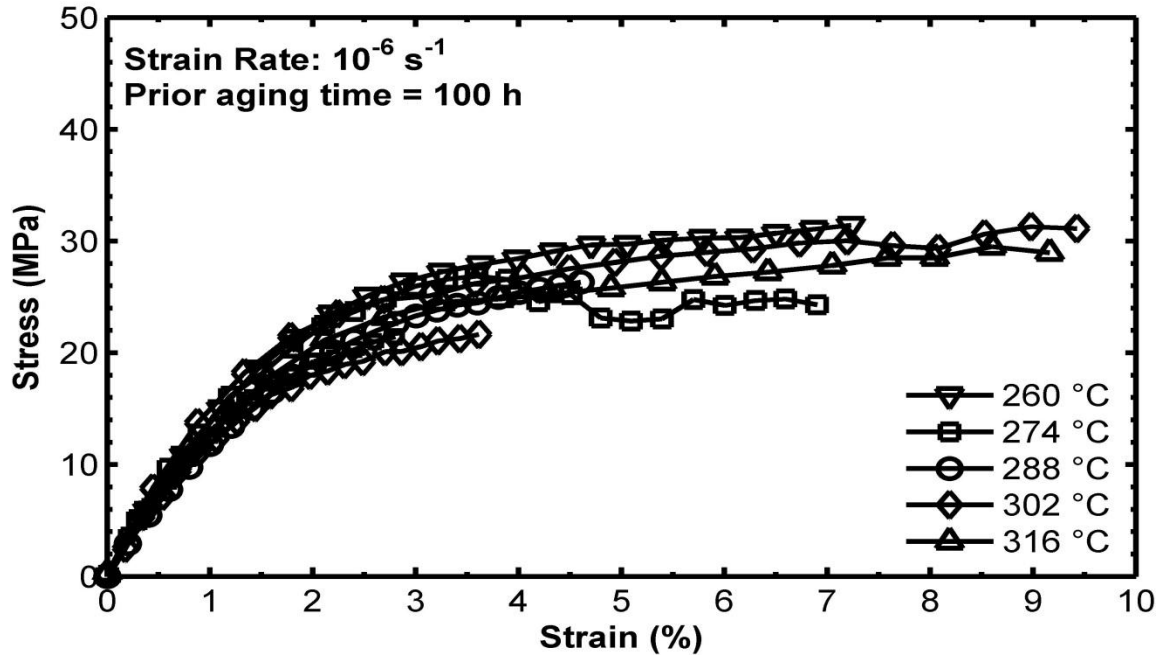


Figure 9.18 Stress-strain curves for PMR-15 specimens aged for 100 h at 260, 274, 288, 302 and 316 °C Obtained in tensile tests to failure at constant strain rate  $10^{-6} \text{ s}^{-1}$ . Data from [21] and [19] included.

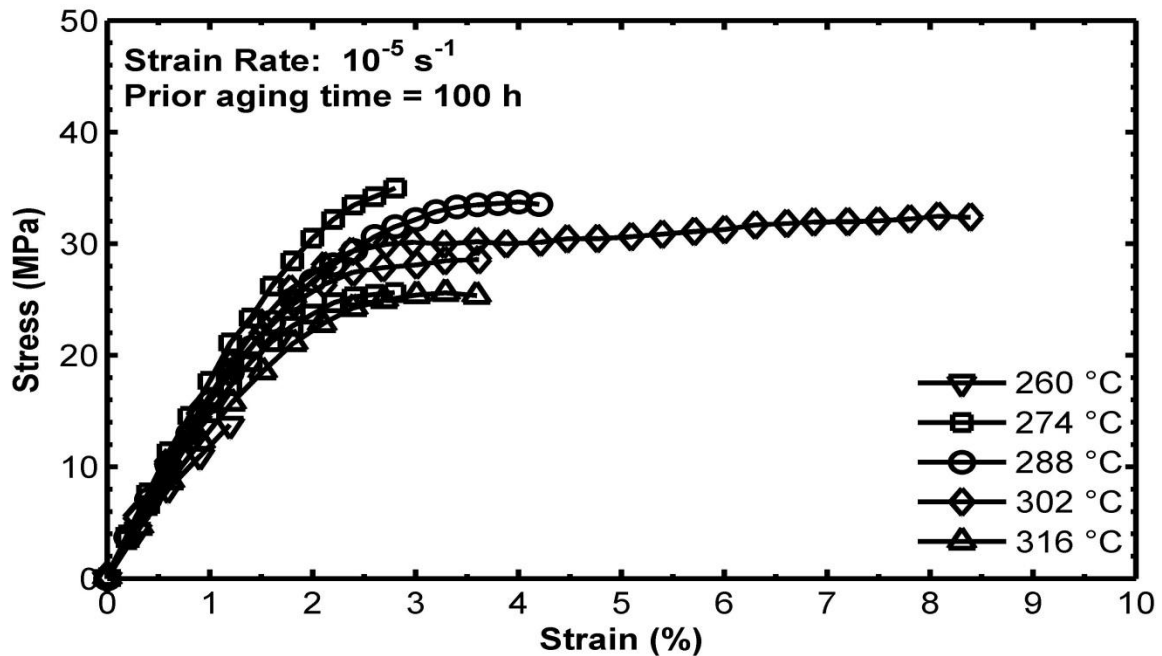


Figure 9.19 Stress-strain curves for PMR-15 specimens aged for 100 h at 260, 274, 288, 302 and 316 °C Obtained in tensile tests to failure at constant strain rate  $10^{-5} \text{ s}^{-1}$ . Data from [21] and [19] included.

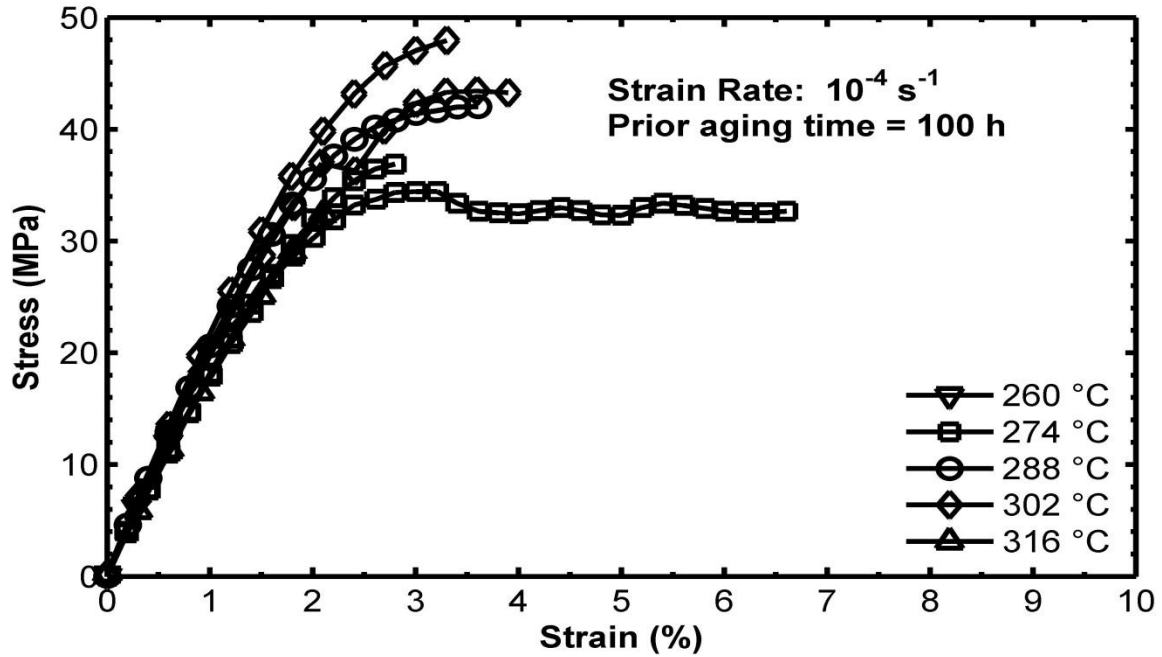


Figure 9.20 Stress-strain curves for PMR-15 specimens aged for 100 h at 260, 274, 288, 302 and 316 °C Obtained in tensile tests to failure at constant strain rate  $10^{-4} \text{ s}^{-1}$ . Data from [21] and [19] included.

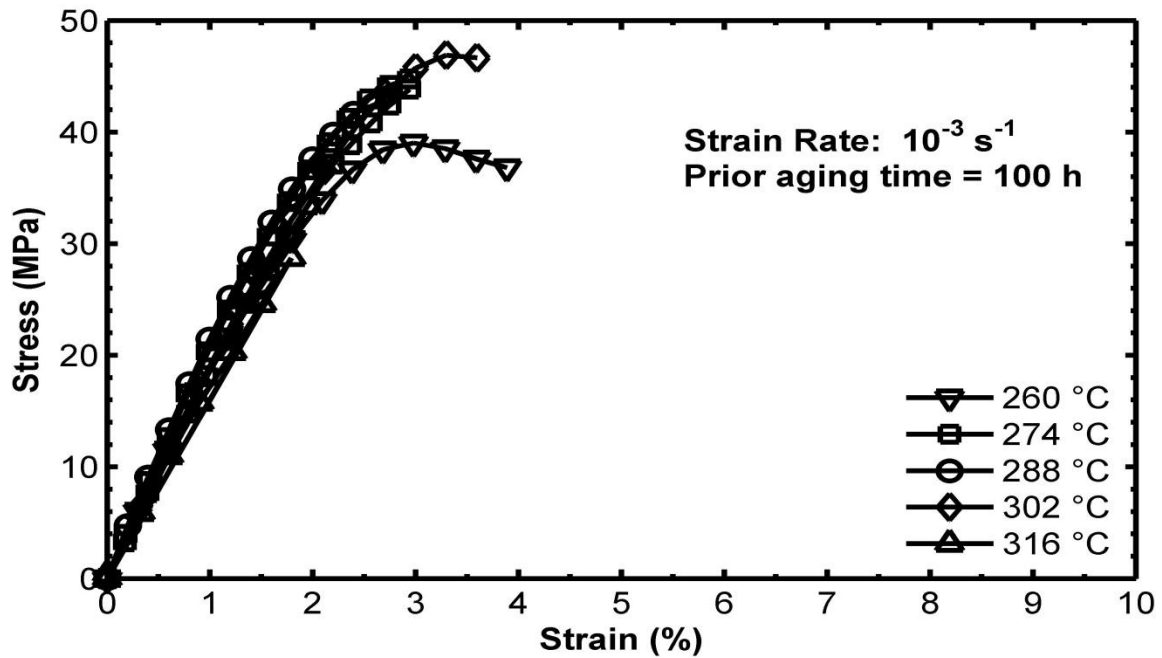


Figure 9.21 Stress-strain curves for PMR-15 specimens aged for 100 h at 260, 274, 288, 302 and 316 °C Obtained in tensile tests to failure at constant strain rate  $10^{-3} \text{ s}^{-1}$ . Data from [21] and [19] included.

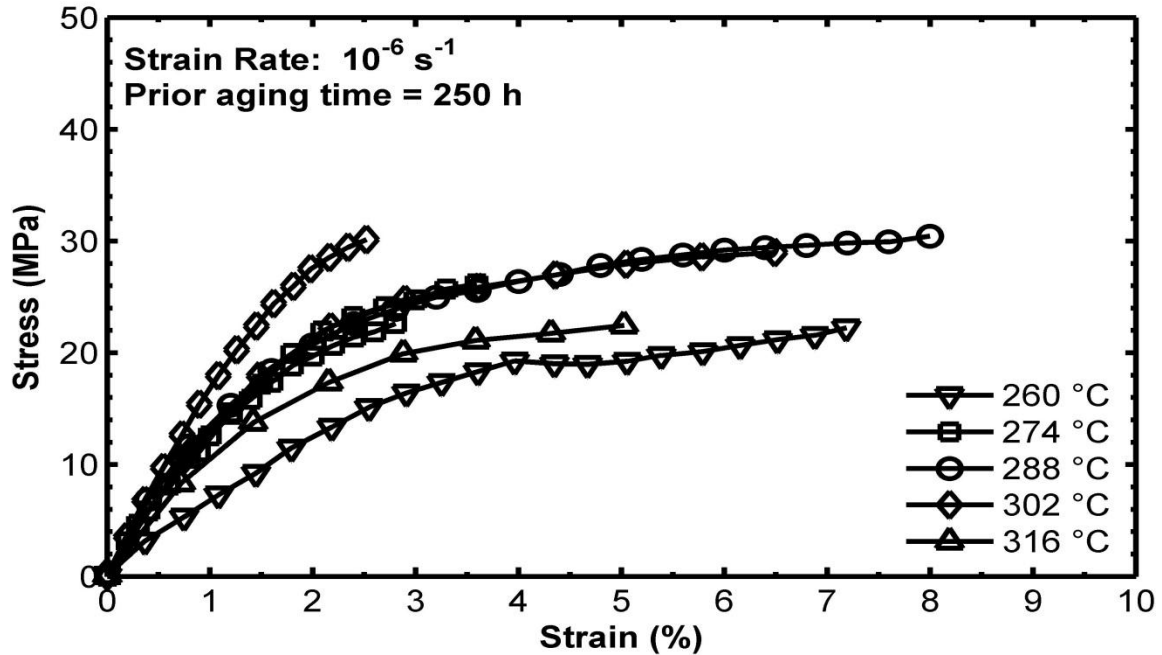


Figure 9.22 Stress-strain curves for PMR-15 specimens aged for 250 h at 260, 274, 288, 302 and 316 °C Obtained in tensile tests to failure at constant strain rate  $10^{-6} \text{ s}^{-1}$ . Data from [21] and [19] included.

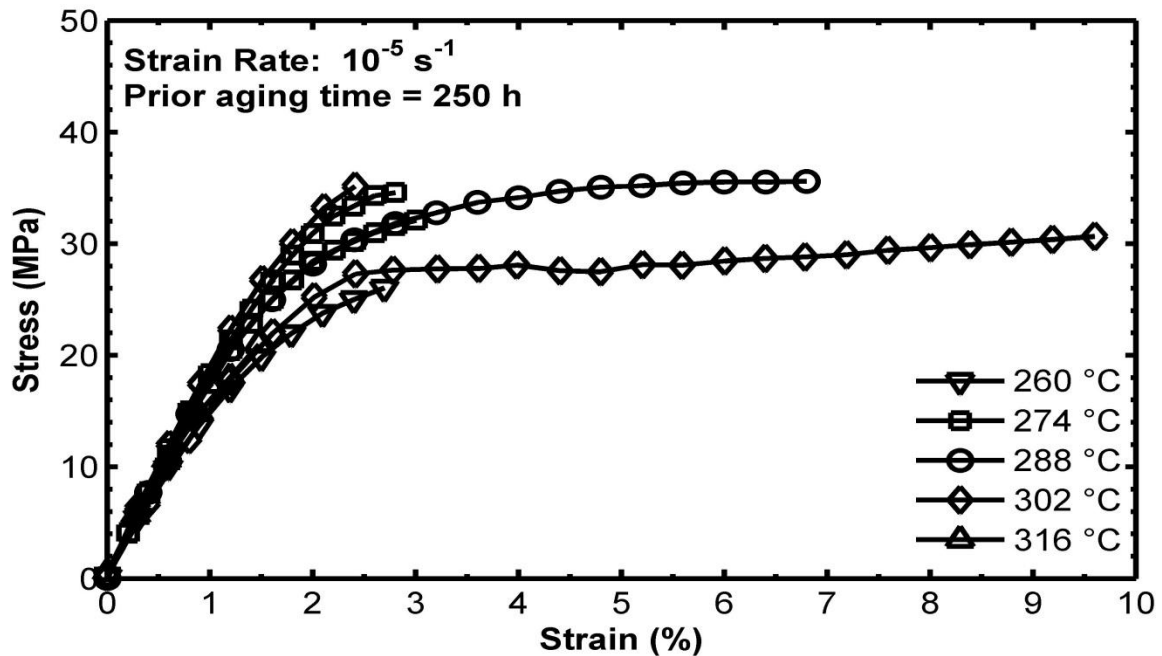


Figure 9.23 Stress-strain curves for PMR-15 specimens aged for 250 h at 260, 274, 288, 302 and 316 °C Obtained in tensile tests to failure at constant strain rate  $10^{-5} \text{ s}^{-1}$ . Data from [21] and [19] included.

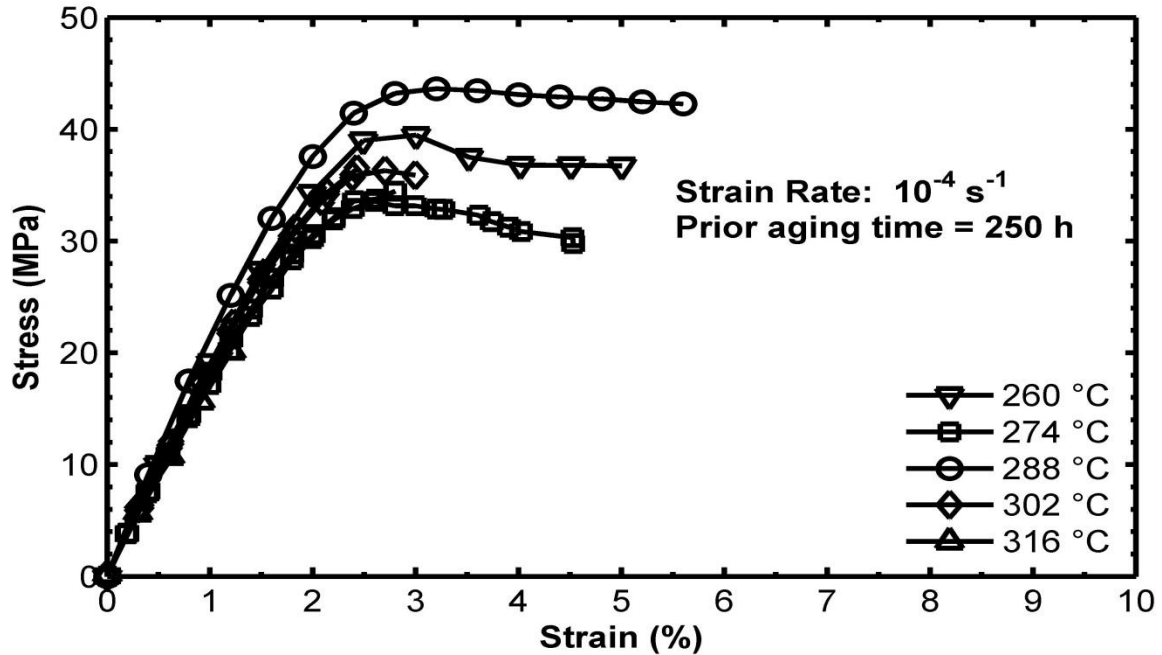


Figure 9.24 Stress-strain curves for PMR-15 specimens aged for 250 h at 260, 274, 288, 302 and 316 °C Obtained in tensile tests to failure at constant strain rate  $10^{-4} \text{ s}^{-1}$ . Data from [21] and [19] included.

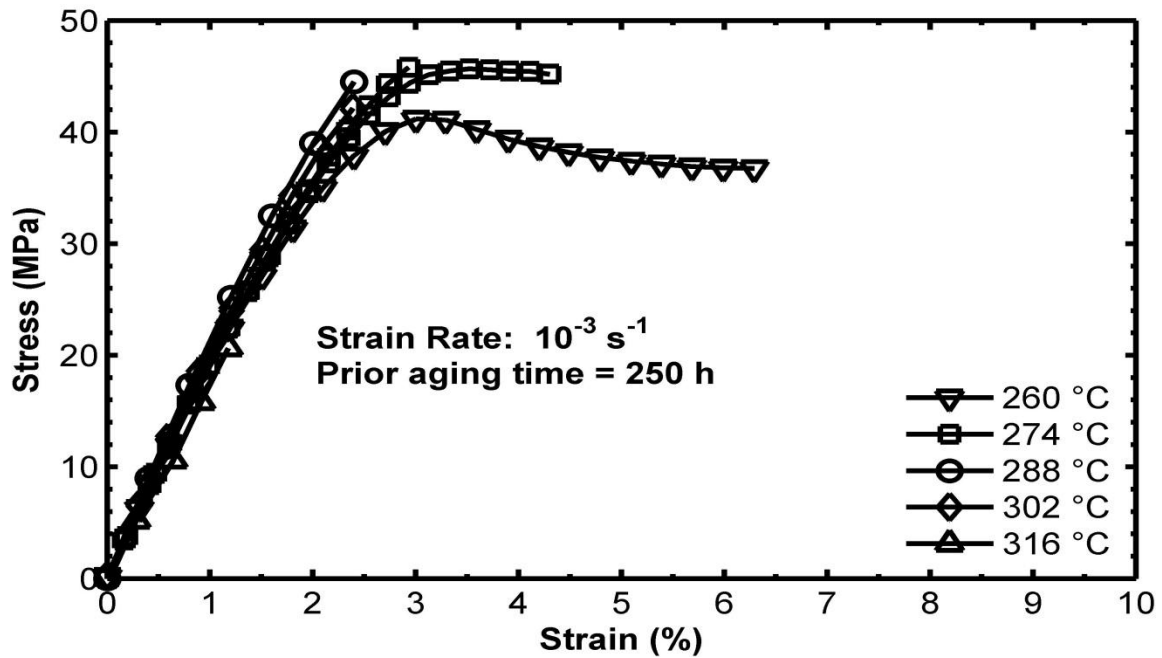


Figure 9.25 Stress-strain curves for PMR-15 specimens aged for 250 h at 260, 274, 288, 302 and 316 °C Obtained in tensile tests to failure at constant strain rate  $10^{-3} \text{ s}^{-1}$ . Data from [21] and [19] included.



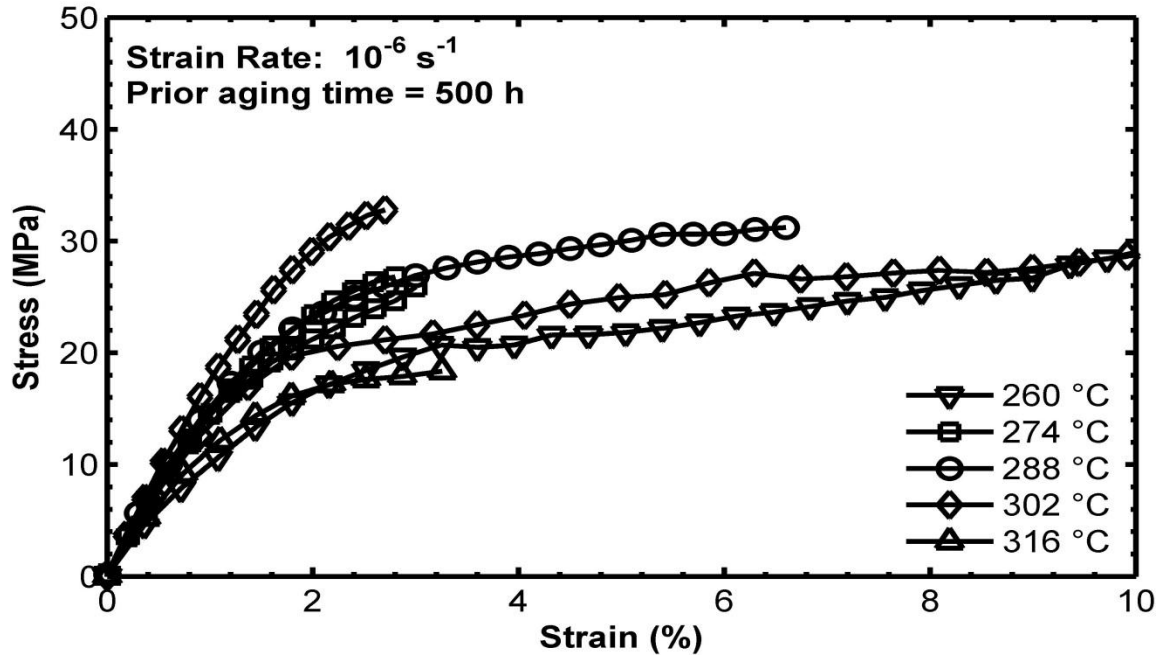


Figure 9.26 Stress-strain curves for PMR-15 specimens aged for 500 h at 260, 274, 288, 302 and 316 °C Obtained in tensile tests to failure at constant strain rate  $10^{-6} \text{ s}^{-1}$ . Data from [21] and [19] included.

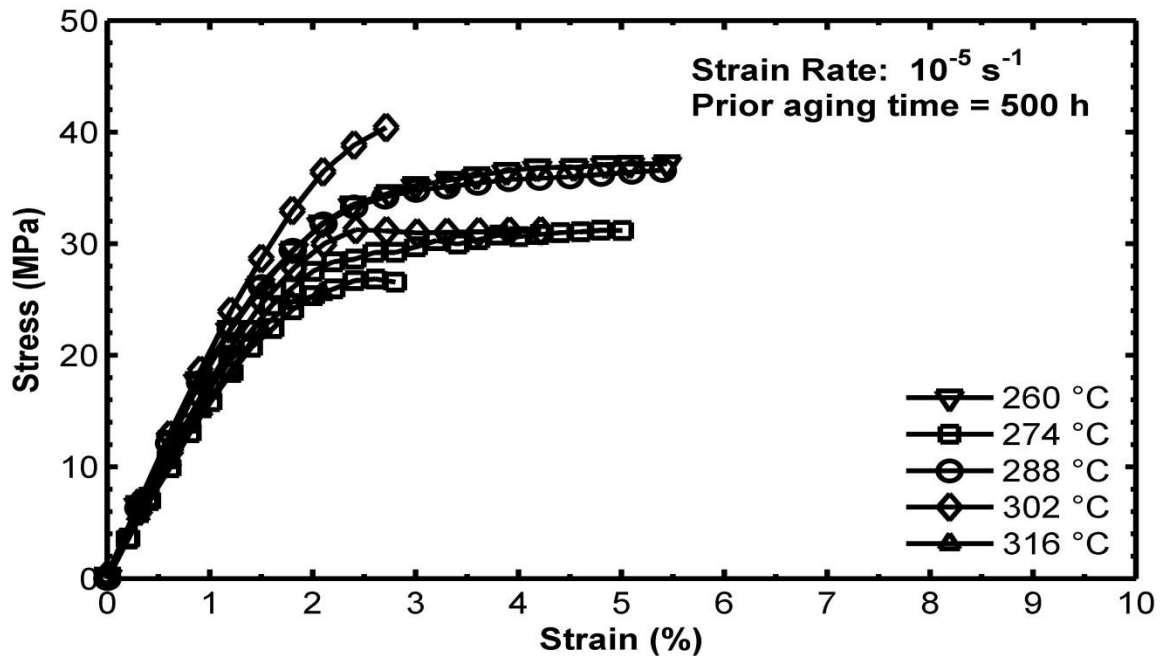


Figure 9.27 Stress-strain curves for PMR-15 specimens aged for 500 h at 260, 274, 288, 302 and 316 °C Obtained in tensile tests to failure at constant strain rate  $10^{-5} \text{ s}^{-1}$ . Data from [21] and [19] included.

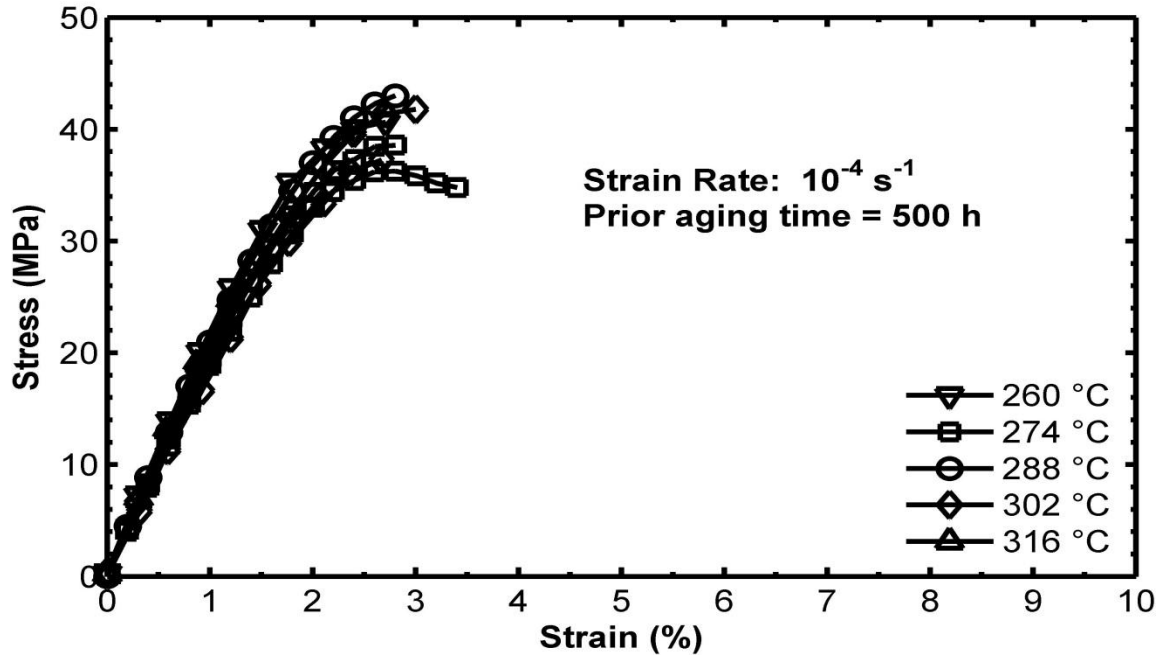


Figure 9.28 Stress-strain curves for PMR-15 specimens aged for 500 h at 260, 274, 288, 302 and 316 °C Obtained in tensile tests to failure at constant strain rate  $10^{-4} \text{ s}^{-1}$ . Data from [21] and [19] included.

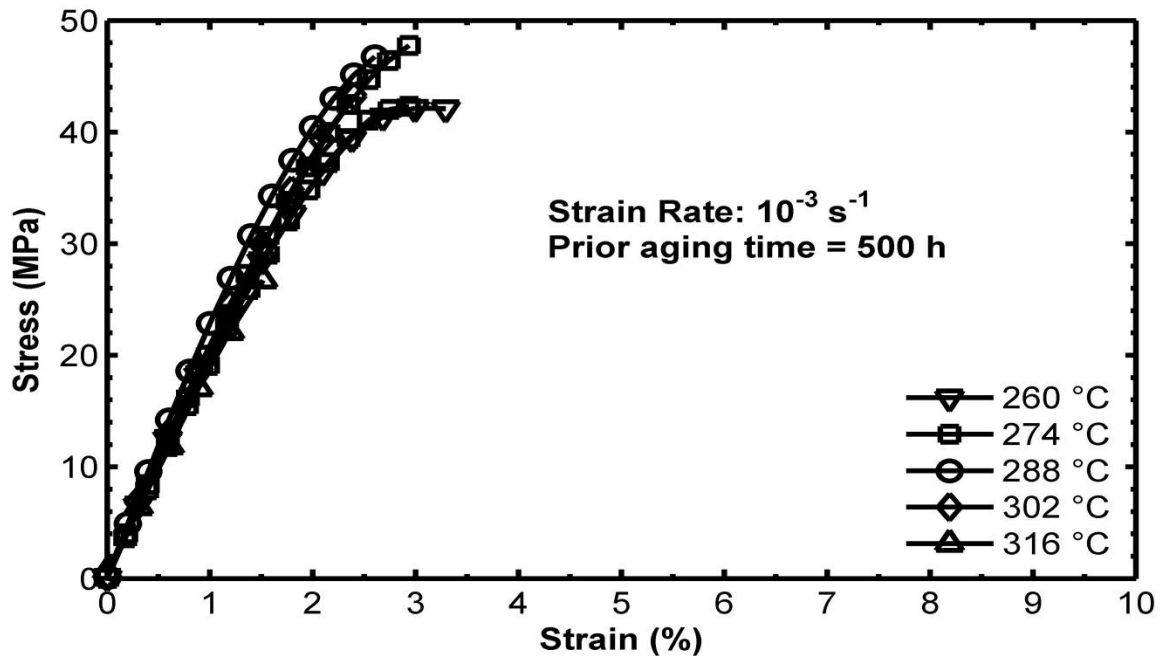


Figure 9.29 Stress-strain curves for PMR-15 specimens aged for 500 h at 260, 274, 288, 302 and 316 °C Obtained in tensile tests to failure at constant strain rate  $10^{-3} \text{ s}^{-1}$ . Data from [21] and [19] included.

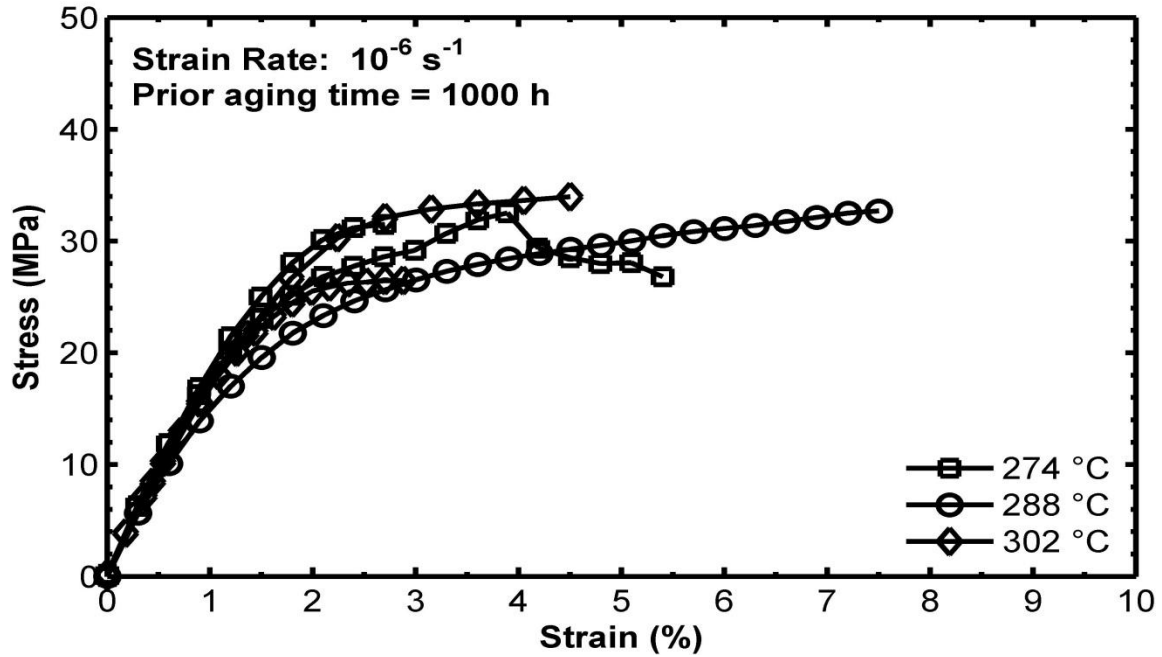


Figure 9.30 Stress-strain curves for PMR-15 specimens aged for 1000 h at 274, 288, and 302 °C Obtained in tensile tests to failure at constant strain rate  $10^{-6} \text{ s}^{-1}$ . Data from [21] and [19] included.

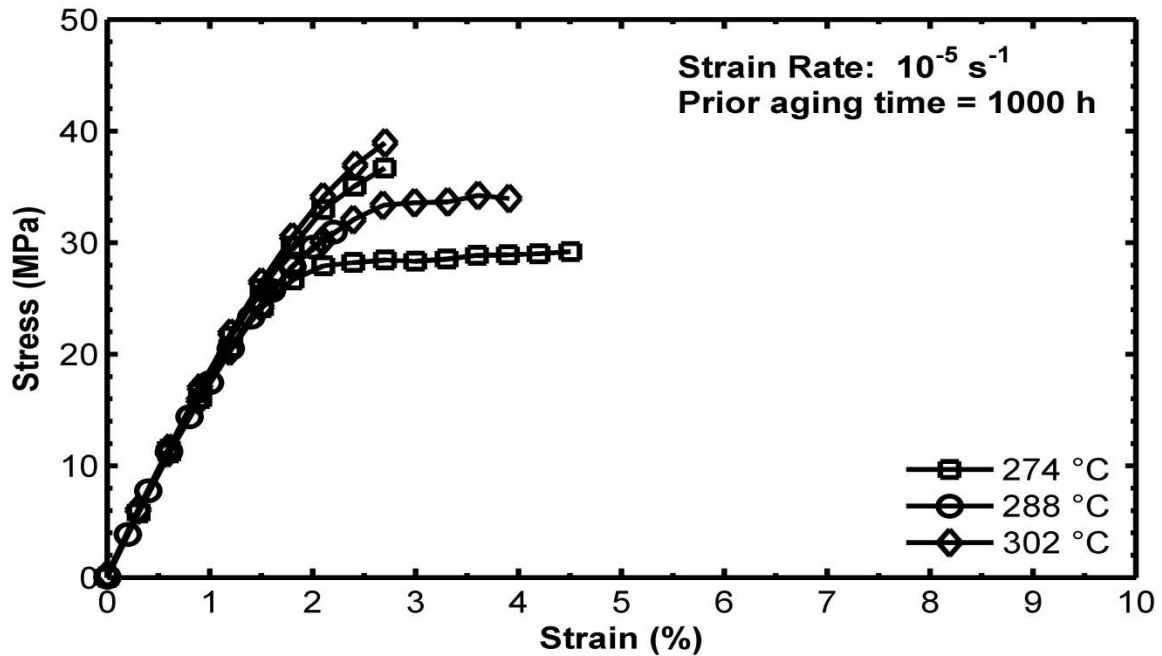


Figure 9.31 Stress-strain curves for PMR-15 specimens aged for 1000 h at 274, 288, and 302 °C Obtained in tensile tests to failure at constant strain rate  $10^{-5} \text{ s}^{-1}$ . Data from [21] and [19] included.

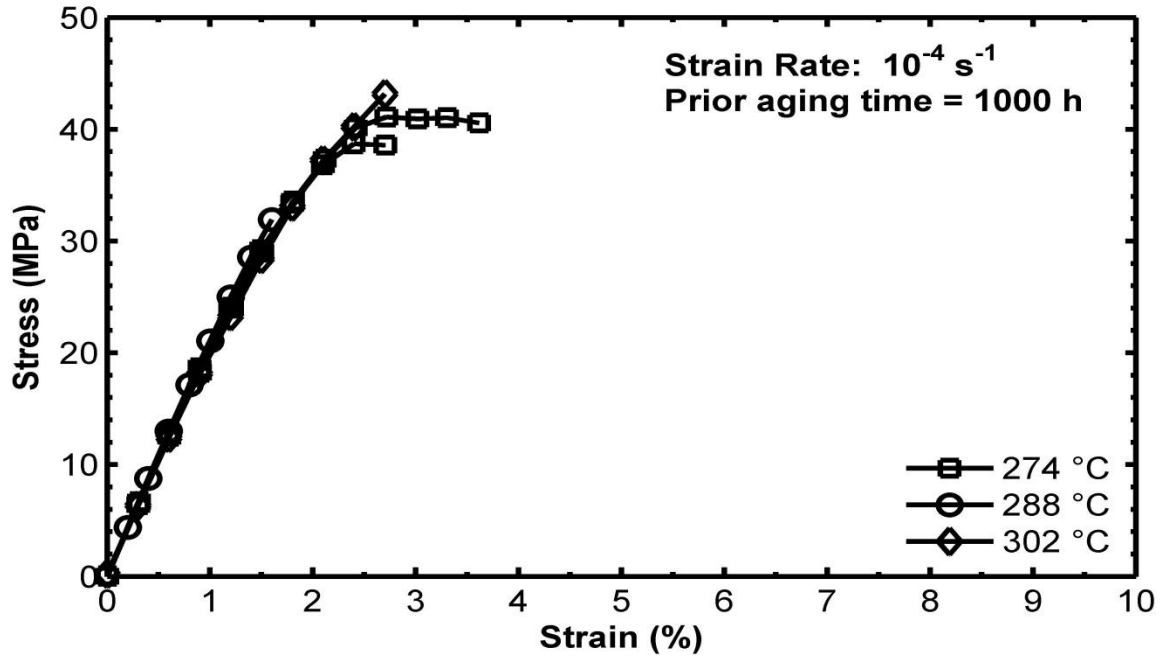


Figure 9.32 Stress-strain curves for PMR-15 specimens aged for 1000 h at 274, 288, and 302 °C Obtained in tensile tests to failure at constant strain rate  $10^{-4} \text{ s}^{-1}$ . Data from [21] and [19] included.

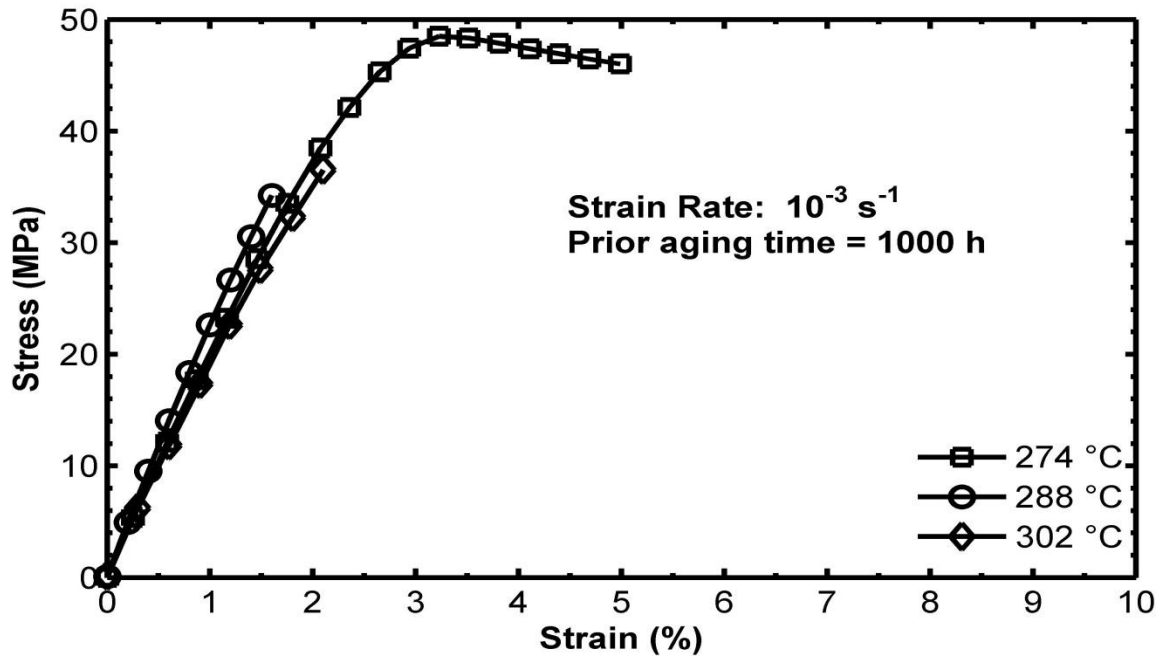


Figure 9.33 Stress-strain curves for PMR-15 specimens aged for 1000 h at 274, 288, and 302 °C Obtained in tensile tests to failure at constant strain rate  $10^{-3} \text{ s}^{-1}$ . Data from [21] and [19] included.

#### 9.4 Relaxation Behavior – Influence of Prior Aging Temperature

To evaluate the effects of prior aging on relaxation behavior, monotonic tests with a period of relaxation of fixed duration were conducted at 288 °C on specimens subjected to prior aging for 50-1000 hours at 260, 274, 288, 302 and 316 °C. In these strain-controlled tests, a specimen was loaded at a constant strain rate to a specific strain in the region of fully established inelastic flow, at which point a 12-h relaxation period was performed. After completion of the relaxation period, straining was resumed at a given strain rate and continued to specimen failure. The tests were carried out in strain control using the strain rates of  $10^{-6}$ ,  $10^{-5}$ ,  $10^{-4}$  and  $10^{-3}$  s<sup>-1</sup> during loading. A complete summary of the circumstances of these relaxation tests can be found in Table 12.6. Results of the relaxation tests are shown in Figure 9.34, Figure 9.35, Figure 9.36, Figure 9.37 and Figure 9.38. The stress drop vs. relaxation time curves in Figure 9.34 through Figure 9.38 reveal that prior aging temperature has little or no influence on the stress drop during relaxation. For a given prior aging duration and strain rate, the stress drop versus time curves for all prior aging temperatures are concomitant. Furthermore, in Figure 9.39 we observe that stress drop during relaxation of a fixed duration is independent of prior aging time for specimens aged at 260 °C. Similar results are observed for specimens aged at 274 °C in Figure 9.40 and at 302 °C in Figure 9.41. Severe embrittlement prevented extensive relaxation testing of specimens aged at 316 °C. Based on these results and on results reported by McClung [36] for PMR-15 aged at 288 °C, it is suggested that prior aging duration does not influence relaxation behavior of PMR-15 subjected to prior aging at temperatures in the 260-302 °C range.

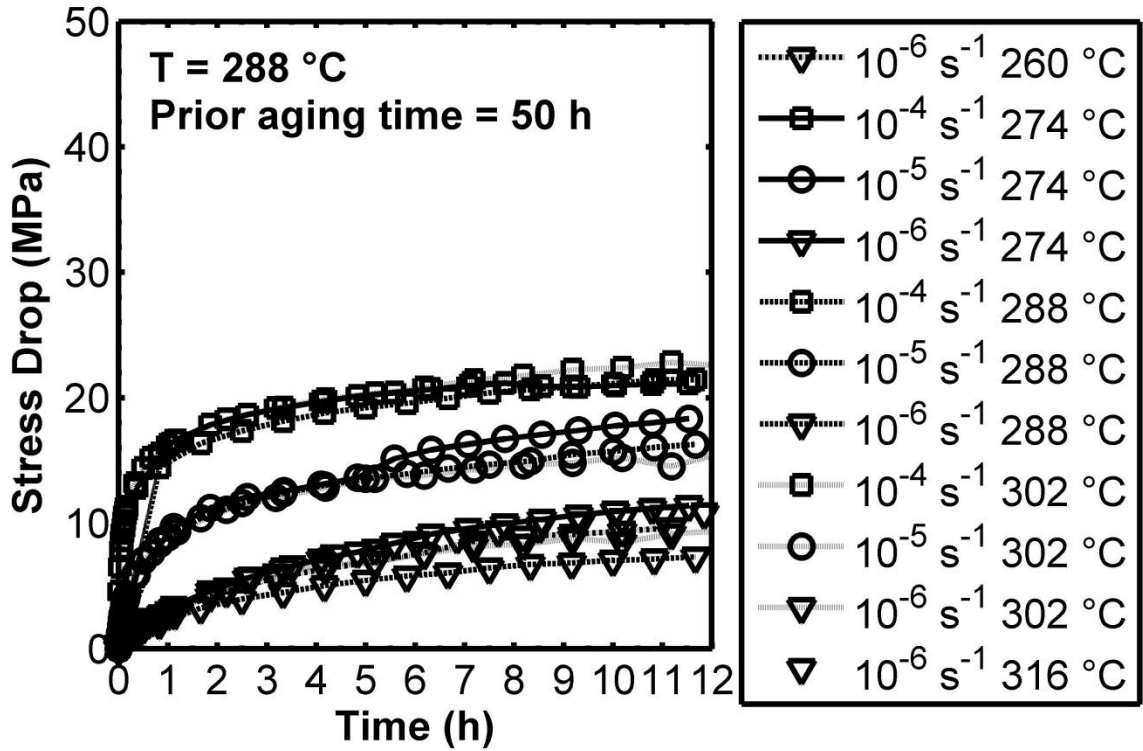


Figure 9.34 Stress decrease vs. relaxation time for PMR-15 specimens aged for 50 h at various temperatures in the 260-316 °C range. Stress drop during relaxation of a fixed duration is independent of prior aging temperature. Data from [21] and [19] are included.

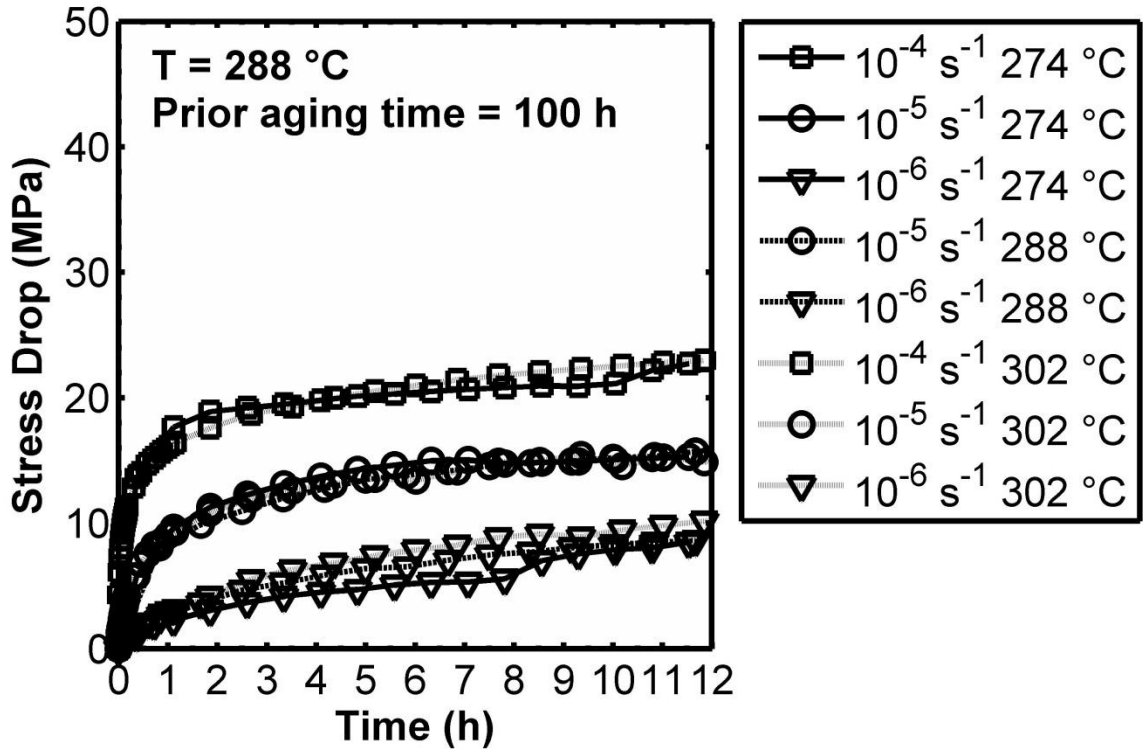


Figure 9.35 Stress decrease vs. relaxation time for PMR-15 specimens aged for 100 h at various temperatures in the 274-302 °C range. Stress drop during relaxation of a fixed duration is independent of prior aging temperature. Data from [21] and [19] are included.

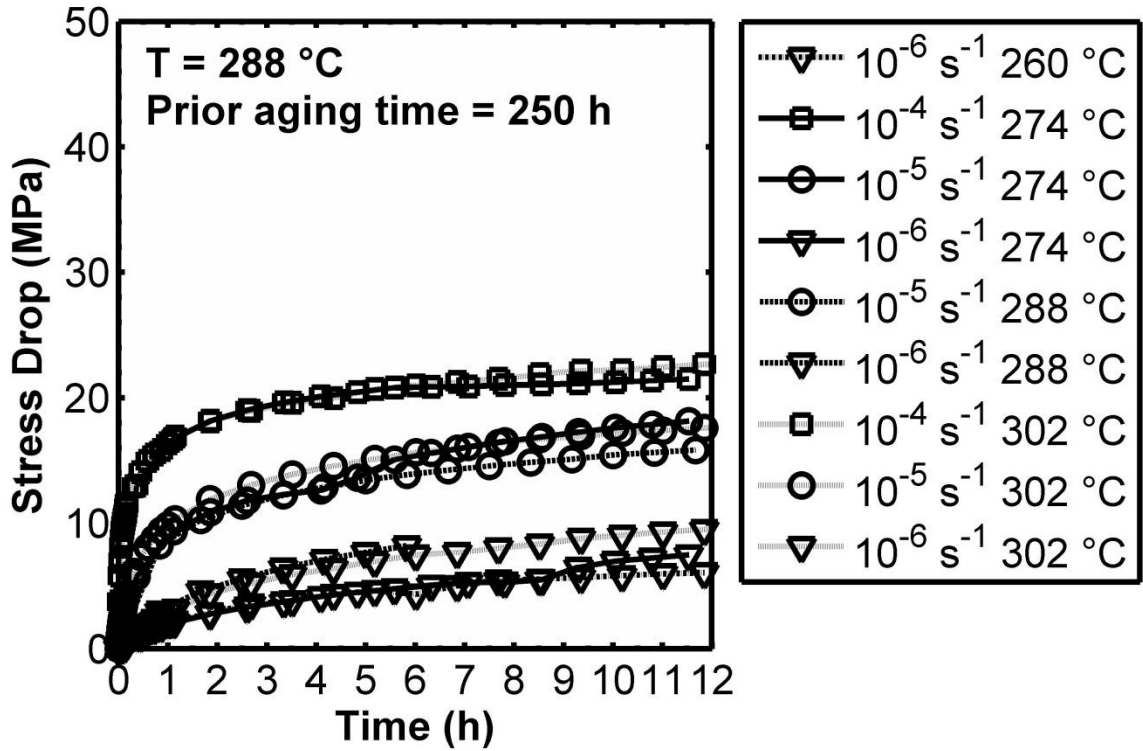


Figure 9.36 Stress decrease vs. relaxation time for PMR-15 specimens aged for 250 h at various temperatures in the 260-302 °C range. Stress drop during relaxation of a fixed duration is independent of prior aging temperature. Data from [21] and [19] are included.



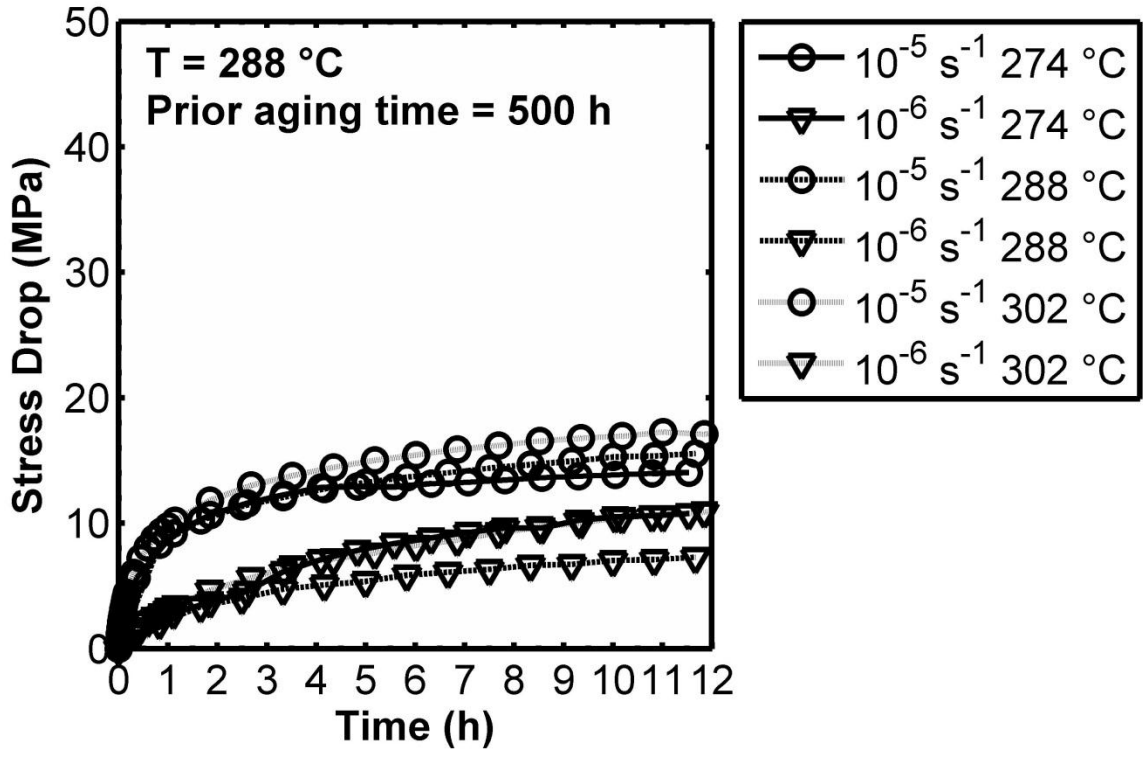


Figure 9.37 Stress decrease vs. relaxation time for PMR-15 specimens aged for 500 h at various temperatures in the 274-302 °C range. Stress drop during relaxation of a fixed duration is independent of prior aging temperature. Data from [21] and [19] are included.

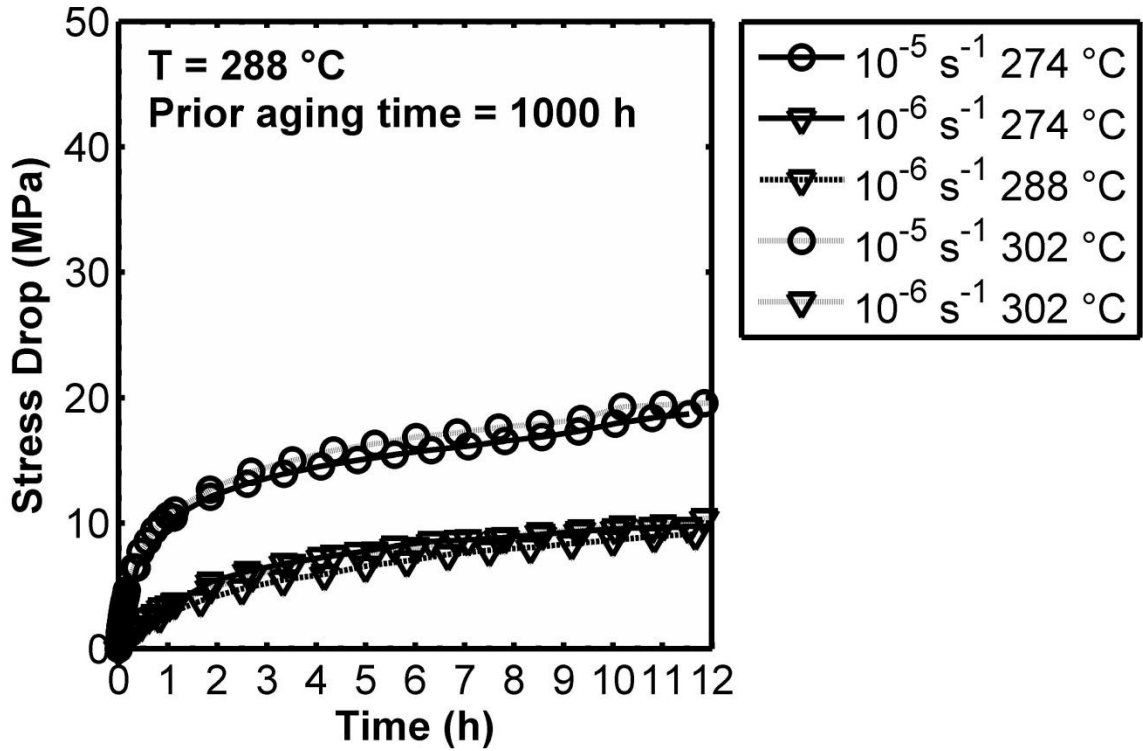


Figure 9.38 Stress decrease vs. relaxation time for PMR-15 specimens aged for 1000 h at various temperatures in the 274-302 °C range. Stress drop during relaxation of a fixed duration is independent of prior aging temperature. Data from [21] and [19] are included.

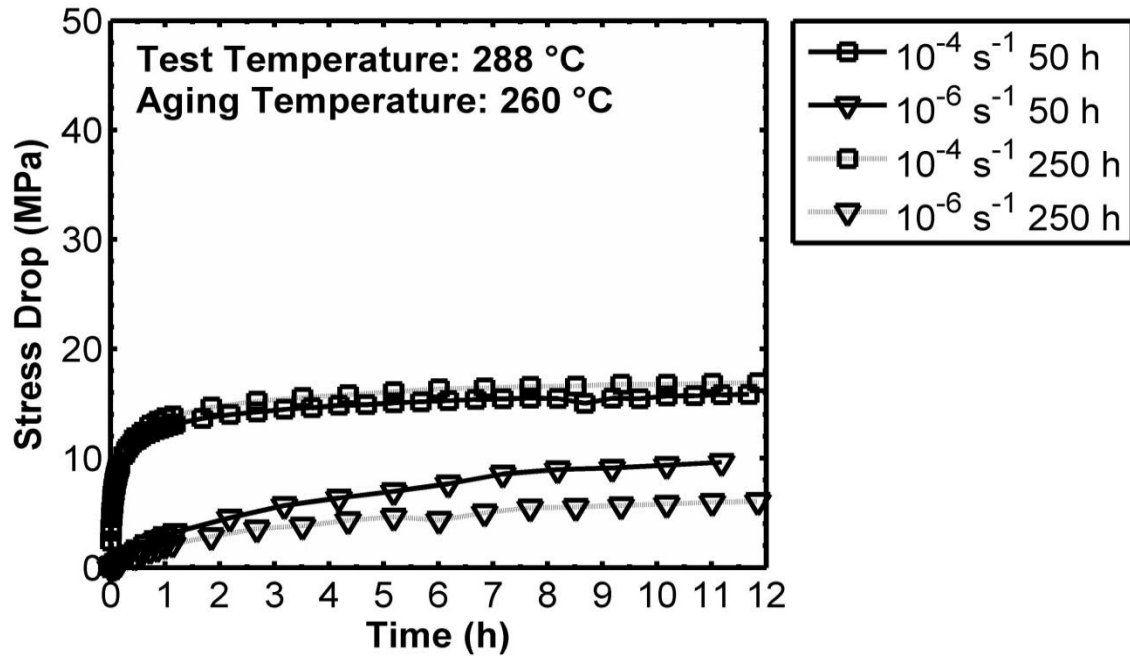
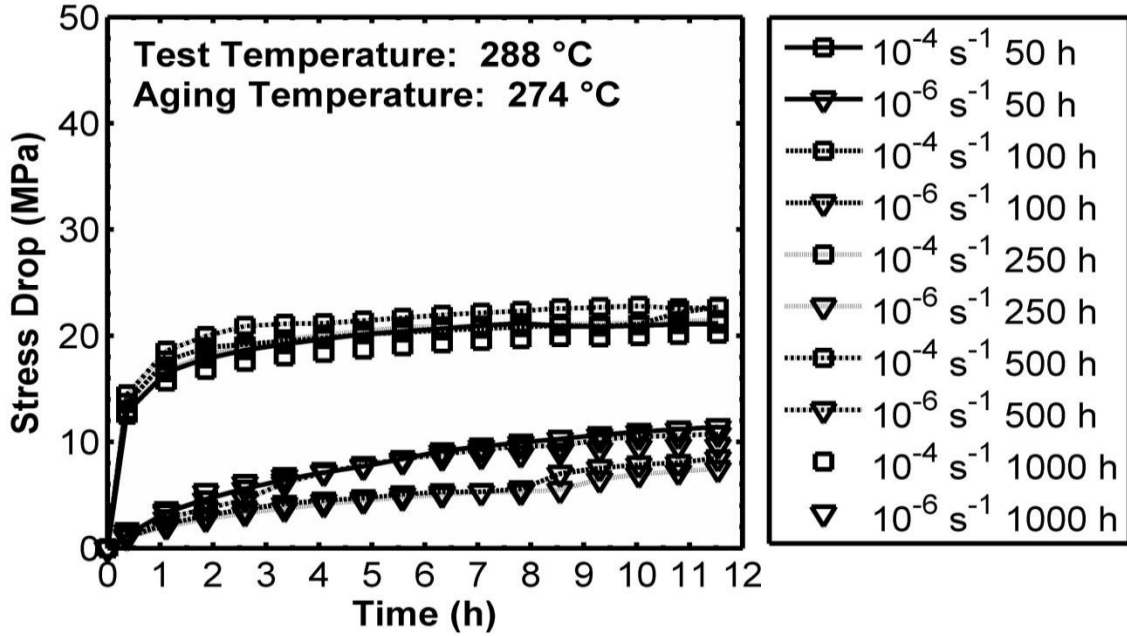
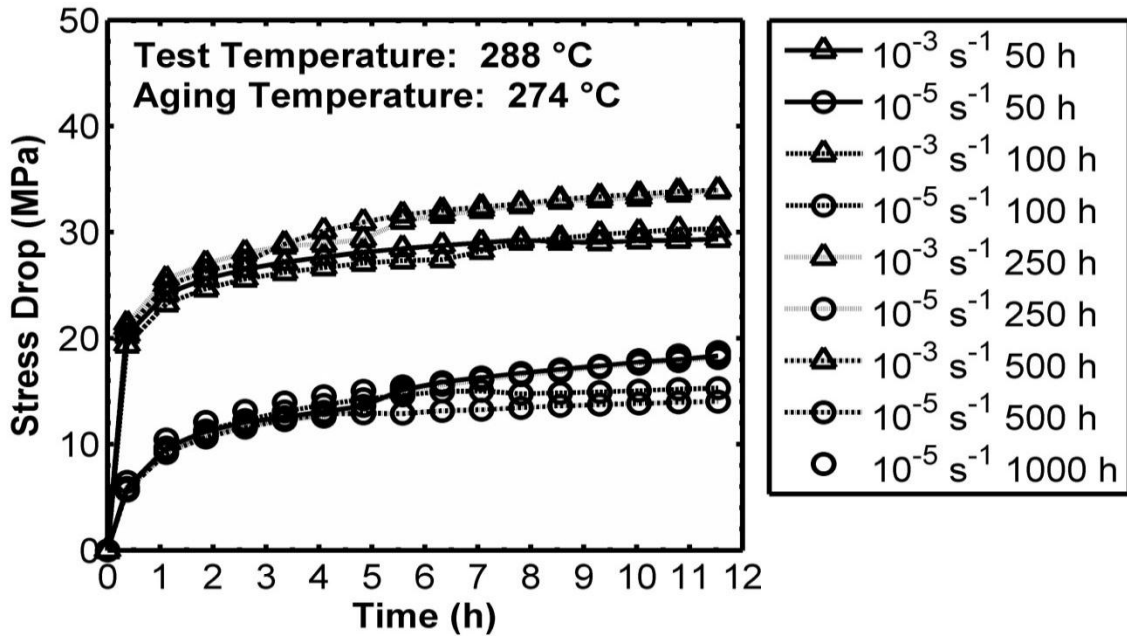


Figure 9.39 Stress decrease vs. relaxation time for PMR-15 specimens aged for various durations at 260 °C. Stress drop during relaxation of a fixed duration is independent of prior aging time.



(a) Prior strain rates =  $10^{-4}$  and  $10^{-6} \text{ s}^{-1}$



(b) Prior strain rates =  $10^{-3}$  and  $10^{-5} \text{ s}^{-1}$

Figure 9.40 Stress decrease vs. relaxation time for PMR-15 specimens aged for various durations at 274 °C. Stress drop during relaxation of a fixed duration is independent of prior aging time. Data from [21] are included.

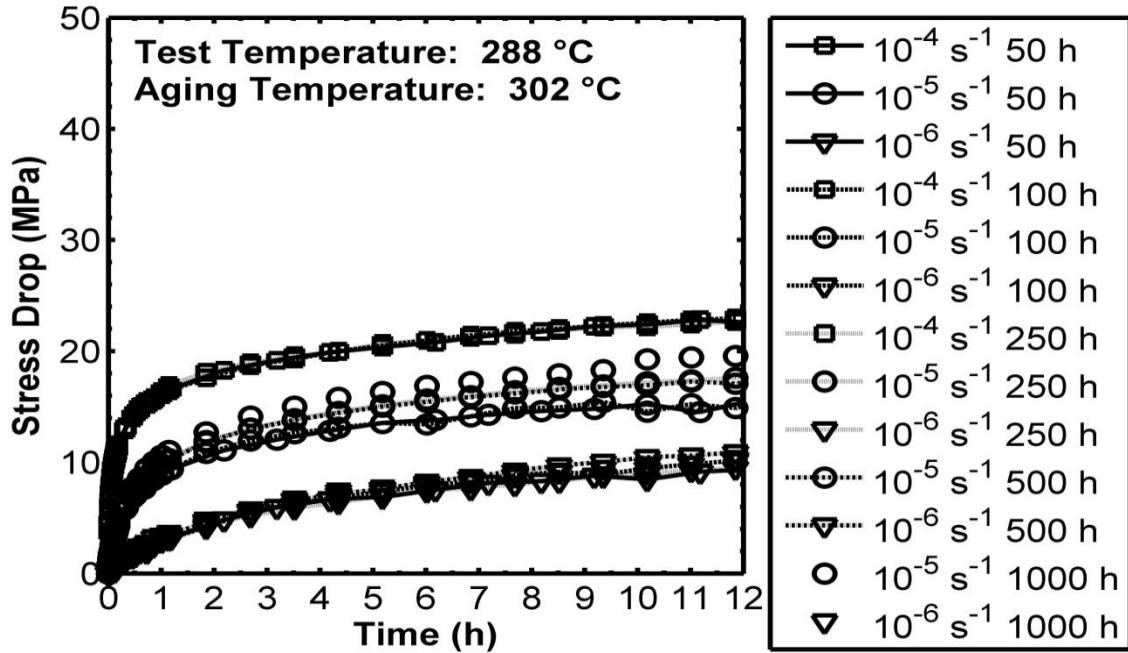


**Figure 9.41 Stress decrease vs. relaxation time for PMR-15 specimens aged for various durations at 302 °C. Stress drop during relaxation of a fixed duration is independent of prior aging time.**

### 9.5 Thermal Degradation of PMR-15

In Section 9.3 the deformation behavior of PMR-15 aged at 316 °C was discussed. In contrast to the behavior observed for material aged at 260, 274, 288 and 302 °C, PMR-15 aged at 316 °C exhibited a decrease, rather than an increase in flow stress level with increasing prior aging duration. This decrease in flow stress level may indicate a physical change in the microstructure of the material that does not occur at lower temperatures. This discontinuity in behavior suggests that 316 °C is above a threshold temperature at which a thermally activated degradation of the polymer takes place. In Figure 9.42 a comparison of the percent weight loss of PMR-15 aged in argon at various temperatures demonstrates a considerably greater weight loss for PMR-15 aged at 316 °C than for PMR-15 aged at lower temperatures. This increased weight loss during aging at 316 °C could be indicative of a degradation of the PMR-15 polymer that

is not occurring at lower temperatures. As reported by Chuang [83], the main chain imide ring of the PMR-15 polyimide undergoes thermal degradation to release ammonia ( $\text{NH}_3$ ), phenyl isocyanate ( $\text{ArN}=\text{C}=\text{O}$ ), carbon monoxide ( $\text{CO}$ ) and carbon dioxide ( $\text{CO}_2$ ) when subjected to elevated temperatures in an inert gas environment. The identification of the evolved gas species was accomplished by thermogravimetric analysis utilizing a Fourier transform infrared spectrometer (TGA-FTIR). The gas evolution profile shown in Figure 9 of Chuang [83] shows that thermal degradation is insignificant below approximately 305 °C but increases substantially as the temperature increases above 305 °C. While physical aging, chemical aging or continued cure during high temperature aging may result in increased yield stress and stiffness, the high temperature degradation of the polymer through chain scission will produce the opposite effect, causing a reduction in modulus [25] as is observed for PMR-15 aged at 316 °C.

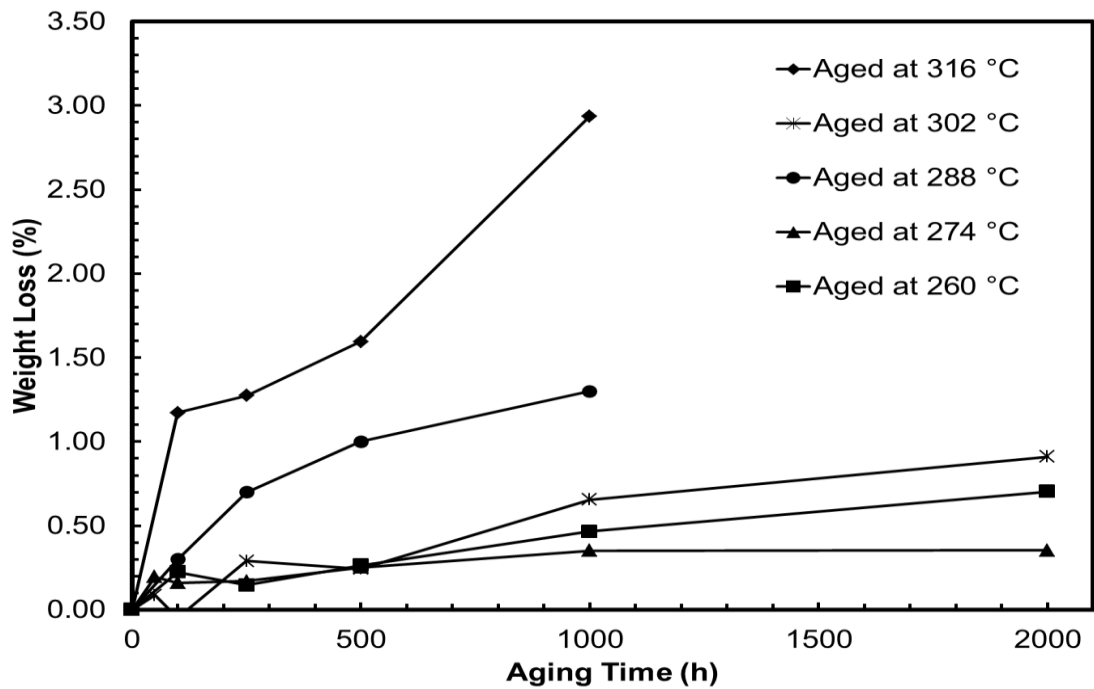


Figure 9.42 Comparison of percent weight loss for PMR-15 neat resin aged in argon at 260, 274, 288, 302 and 316 °C. Data at 260 °C from [20]. Data at 274 °C from [21]. Data at 288 °C from [22]. Data at 316 °C from [27].

## **9.6 Summary of the Key Effects of Prior Aging at Various Elevated Temperatures on the Deformation Behavior of PMR-15**

It has been demonstrated that prior isothermal aging at temperatures in the 260-316 °C range in argon does influence the mechanical behavior of PMR-15. In order to decouple the effects of prior aging temperature from those of the test temperature, experiments were conducted at 288 °C on specimens aged at various temperatures. The key features of the mechanical behavior of PMR-15 aged at 260-302 °C include:

- The initial slope of the stress-strain curve (elastic modulus) increases with prior aging duration
- The shape of the knee of the stress-strain curve becomes more pronounced with prior aging duration
- The departure from quasi-linear behavior is delayed with increased aging time
- The flow stress increases with prior aging duration
- Most importantly, prior aging temperature in the 260-302 °C range has little or no influence on deformation behavior of PMR-15

Testing of PMR-15 aged at 316 °C revealed an unexpected result, though. For that prior aging temperature, a decrease in flow stress was observed with increasing prior aging duration. This suggests that a degradation mechanism, not present at lower aging temperatures, is in effect during aging at 316 °C. Comparing the mechanical behavior of specimens aged for given durations up to 1000 h at various temperatures in the 260-302 °C range and tested at 288 °C reveals that there is no relationship between prior aging temperature and elastic modulus, tangent modulus, the shape of the knee of the



stress-strain curve or departure from quasi-linear behavior. While there is significant variation in flow stress levels for tests conducted on specimens aged at various temperatures, any possible relationship between prior aging temperature and flow stress level is clouded by data scatter. While beyond the scope of this research effort, a limited amount of data collected for PMR-15 polymer aged at 260 and 316 °C suggests that the relationship between test temperature and mechanical behavior observed for unaged material is also valid for aged PMR-15. Additionally, experimental data suggest that prior aging duration does not influence the relaxation behavior of PMR-15 for material aged in the 260-302 °C range.

The implications of these results are important; at temperatures in the 260-302 °C range the rate at which aging occurs is relatively constant. This greatly simplifies modeling as mechanical behavior depends only on prior aging duration and not on prior aging temperature. Additionally, preliminary data shows that it is likely that the effect of test temperature on the mechanical behavior of aged PMR-15 can be modeled in a manner similar to that for the unaged material. This is recommended as an area of future research. Modeling the mechanical behavior of material aged at 316 °C and higher would require additional experimental data to better determine the key features of the material behavior in that regime. The limited load carrying capacity resulting from the thermal degradation that occurs at 316 °C and above makes modeling mechanical behavior in that regime less relevant and is not recommended as an area of future research.

## 10 Enhanced Procedure for the Characterization of the VBOP Model

This chapter discusses an enhanced procedure for characterization of the VBOP model. The VBOP formulation and current characterization procedure are reviewed. The under-prediction of stress during relaxation and the behavior of the VBOP following a jump in rate are examined. Finally, a method of determining the equilibrium stress from data obtained during a McLean Type Dip Test (MTDT) is proposed and pertinent experimental data are reviewed.

### 10.1 Brief Review of the VBOP Formulation and Existing Characterization Procedure

#### 10.1.1 VBOP Formulation

The VBOP is a constitutive, state variable model where the inelastic strain rate depends on the overstress. It is comprised of a flow law (constitutive equation), three state variables (equilibrium stress  $g$ , isotropic stress  $A$ , and kinematic stress  $f$ ) with the dimensions of stress, and their growth laws.

The full three-dimensional formulation of the VBOP is provided by Ho [9]. For brevity, only the uniaxial form is presented here. The flow law is given by

$$\dot{\epsilon} = \frac{\dot{\sigma}}{E} + \frac{\sigma - g}{Ek} \quad (10.1)$$

where  $E$  is the elastic modulus and  $k$  is the viscosity function with dimension of time.

The evolution of the equilibrium stress is given by

$$\dot{g} = \Psi \frac{\dot{\sigma}}{E} + \Psi \left[ \frac{(\sigma - g)}{Ek} - \frac{(g - f)}{A} \left| \frac{(\sigma - g)}{Ek} \right| + n \frac{(\dot{\sigma} - \dot{g})}{E} \right] + \left[ 1 - \frac{\Psi}{E} \right] \dot{f} \quad (10.2)$$

In this equation,  $\Psi$  is the positive shape function, which governs the shape of the “knee” in the stress strain diagram and  $n$  is a material constant where  $0 < n < 1$ .

The kinematic stress sets the tangent modulus at the maximum strain of interest.

The evolution of the kinematic stress is given by

$$\dot{f} = \left[ \frac{|\sigma|}{\Gamma + |g|} \right] E_t \frac{(\sigma - g)}{Ek} \quad (10.3)$$

where  $E_t$  is the tangent modulus and  $\Gamma$  is the overstress invariant for the uniaxial case.

$$\Gamma = |\sigma - g| \quad (10.4)$$

The tangent modulus  $E_t$  is the slope of the stress-strain curve in the region where the inelastic flow is fully established.

The evolution of the isotropic stress is given by

$$\dot{A} = A_c [A_f - A] \left| \frac{\sigma - g}{Ek} \right| \quad (10.5)$$

In the case of many solid polymers, this can be simplified by setting  $A_c = 0$  and making  $A$  a constant if the material is cyclically neutral [7, 8, 10-14]. This has been shown to be an acceptable assumption for PMR-15 [19].

The shape function governs the transition from quasi-elastic to inelastic behavior.

The recommended form is given by Khan and Krempl [13, 14] as

$$\Psi = C_1 + (C_2 - C_1) e^{-C_3 |\varepsilon^{in}|} \quad (10.6)$$

where  $C_1$ ,  $C_2$ , and  $C_3$  are material constants. This function is positive, where  $E_t < \Psi < E$ .

The nonlinear viscosity function is given by Bordonaro [5] as

$$k = k_1 \left[ 1 + \frac{\Gamma}{k_2} \right]^{-k_3} \quad (10.7)$$

where  $k_1$ ,  $k_2$ , and  $k_3$  are material constants. This function acts as a repository for nonlinear viscous behavior [59].

### 10.1.2 Characterization Procedure

Up to this point, the model characterization procedure developed by McClung and Ruggles-Wrenn [28] was used to determine the VBOP model parameters from experimental data with only minor modifications. The elastic and tangent moduli were measured directly from experimental results. Then the isotropic stress was calculated by estimating the equilibrium stress from data obtained during relaxation tests conducted after loading at the slowest prior loading rate and utilizing the relationship

$$A = \{g - E_t \varepsilon\} \quad (10.8)$$

where the brackets  $\{n\}$  designate the asymptotic limit of  $n$ . Within the context of the VBOP, the equilibrium stress is assumed to be the measured stress when the Cauchy (applied) stress becomes stationary at the end of a sufficiently long period of relaxation. Since the isotropic stress is constant for a cyclically neutral material, the results of a single relaxation test can be utilized to calculate the overall value of  $A$ . The viscosity function was determined by a fit to the experimental stress drop during relaxation for prior strain rates of  $10^{-3}$ ,  $10^{-4}$ ,  $10^{-5}$  and  $10^{-6} \text{ s}^{-1}$  as previously shown in Figure 8.2 and Figure 8.6. In a departure from the procedure utilized by previous researchers, the viscosity function parameters were selected to fit the VBOP simulations to the

experimental stress values throughout the entire 12-h relaxation period instead of just the final two hours of relaxation. Then the shape function was determined by a fit to the knee of the stress-strain curve as shown in Figure 8.1. If shape function parameters could not be found that accurately predict the knee of the stress-strain curve, then the viscosity function parameters were re-evaluated. Repeated iterations between viscosity and shape function parameters were utilized to determine parameters for both functions that produced acceptable results. The model characterization procedure described in this paragraph is presented in Figure 10.1. The upper portion of the schematic represents the actual model characterization process or in other words, determination of VBOP model parameters that produce acceptable simulations of the data utilized to determine those same parameters. The lower portion of Figure 10.1 represents the model validation process. Model validation serves to determine if the VBOP model, utilizing the attendant model parameters, produces accurate predictions of mechanical behavior under conditions not utilized for model characterization. An example of model validation can be found in Section 8.3. Since model validation remains unchanged, the remainder of this chapter will focus on model characterization only.

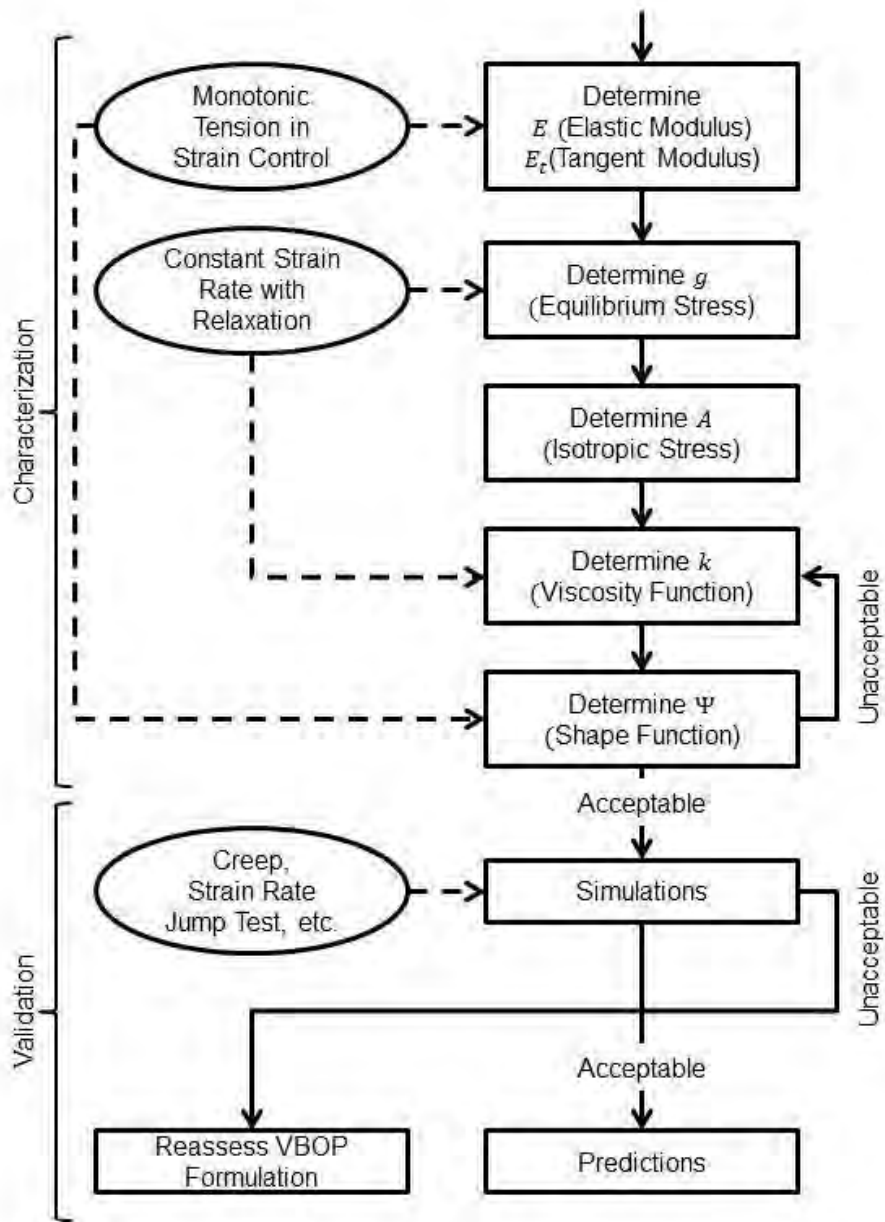


**Figure 10.1** Flowchart showing the systematic characterization procedure for VBOP model parameters.

## **10.2 Under-Prediction of the Flow Stress and the Equilibrium Stress in the Region of Fully Developed Plastic Flow**

When selecting model parameters for the VBOP using the procedure described in the previous section, model simulations tend to under-predict the stress and the equilibrium stress in the region of fully developed plastic flow. McClung [19] postulated that the equilibrium stress evolves during relaxation and this causes an unacceptably low value of equilibrium stress (and thus isotropic stress) to be established at the end of the period of relaxation. McClung suggested that iteratively increasing the value of isotropic stress  $A$  could improve the results. This effectively adds a second iteration loop to the characterization procedure as shown in Figure 10.2. While adding to the complexity of the procedure, this step is necessary since the equilibrium stress determined at the end of a period of relaxation is not the equilibrium stress utilized in Equation (10.8). In the remainder of this section, we will explore why this is true and investigate the behavior of the equilibrium stress during both relaxation and creep. Later, an enhancement to this additional iteration loop will be proposed to provide some tangible bounds on the value of the equilibrium stress and limit the scope of the iteration to make it more manageable.

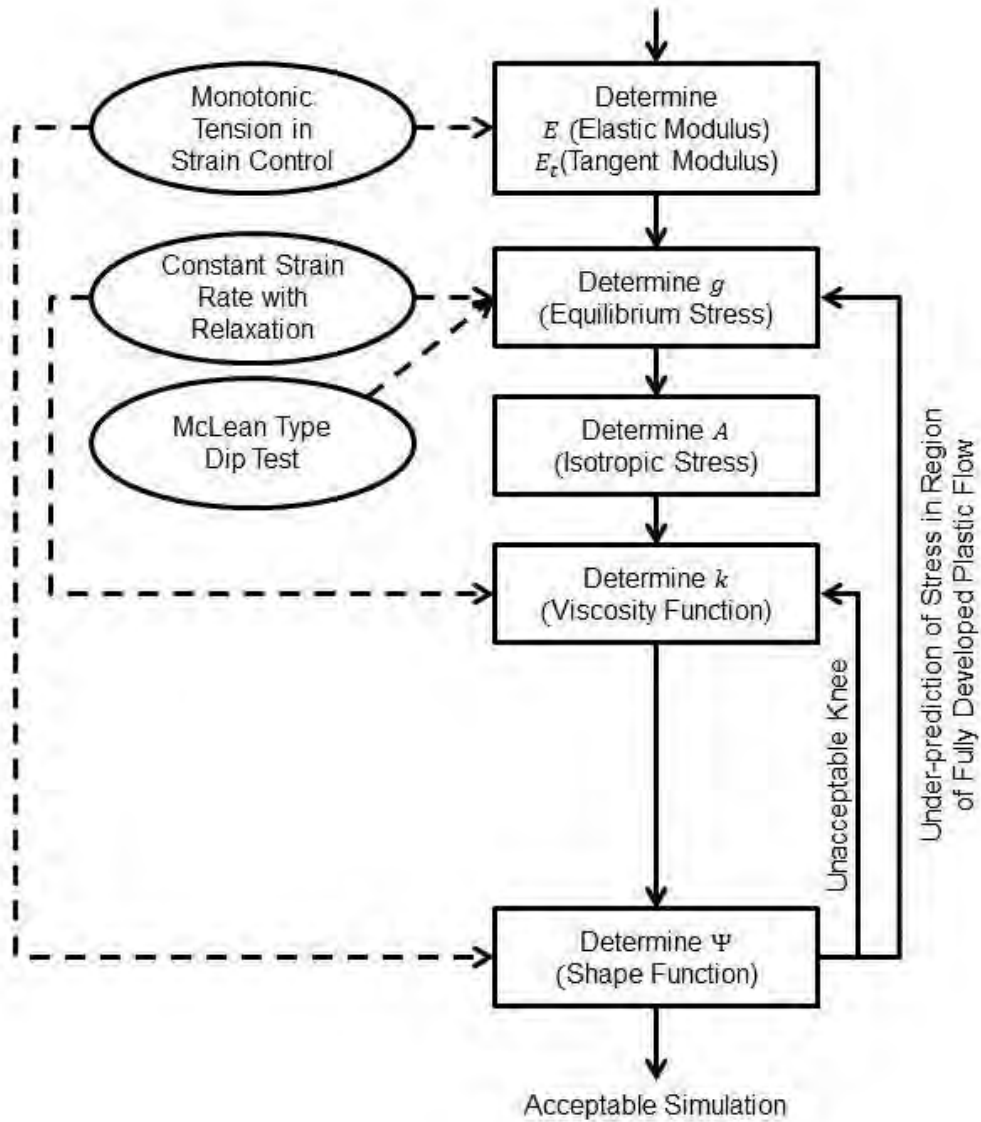


**Figure 10.2** Flowchart showing detail of the enhanced systematic characterization procedure for VBOP model parameters. Validation steps omitted for clarity.



### *10.2.1 VBOP Model Behavior during Change of Rate*

As previously noted, McClung [19] postulated that the equilibrium stress evolves during relaxation. In order to fully understand the implications of this, we must first examine the concept of the equilibrium stress. In the context of the VBOP, the equilibrium stress can be viewed as the stress that the material can sustain as all rates approach zero. Alternatively, the equilibrium stress can be thought of as a measure of the material's current equilibrium state in terms of the stress level that could be maintained without inducing a change to that equilibrium state. Deviation from the current equilibrium state will necessarily drive deformation behavior or a change in the equilibrium state of the material itself. If the applied stress is different from the equilibrium stress, deformation behavior such as creep may occur in order to reduce the difference between the applied and equilibrium stresses. Conversely, if deformation is restricted (such as in the case of relaxation) the equilibrium stress may evolve until a new equilibrium state is reached. More complicated loading paths, such as stress-or-strain controlled monotonic loading, involve continuous changes to the applied load or deformation but the concept of the equilibrium stress, as a measure of the current equilibrium state remains unchanged. While factors such as test temperature, prior aging duration or prior aging temperature may appear to affect the mechanical behavior of the material, it is suggested that in reality, those factors affect the rate at which the equilibrium state of the material evolves. The equilibrium stress is then simply a mathematical concept allowing one to keep track of this state and how much the currently applied stress or strain deviates from the equilibrium condition.

### 10.2.1.1 Relaxation

With a general understanding of the equilibrium stress concept, we now examine the behavior of equilibrium stress as it is modeled in the VBOP. Returning to the issue of the under-prediction of stress described above, the evolution of the equilibrium stress during relaxation complicates the notion that the stress value at the end of a sufficiently long period of relaxation can be used as an approximation of the value of the equilibrium stress just prior to beginning of relaxation. Following Krempl and Nakamura's [84] investigation of relaxation behavior for VBO, we analyze the behavior of the VBOP during relaxation following monotonic loading in strain control.

Let a superposed  $-$  and  $+$  denote a quantity immediately before and after a jump in rate such as that which occurs when constant strain rate abruptly "jumps" to zero at the beginning of the relaxation period. Writing equations (10.1) and (10.2) before and after the change in rate and subtracting the results yields

$$\dot{\sigma}^+ - \dot{\sigma}^- = E(\dot{\epsilon}^+ - \dot{\epsilon}^-) \quad (10.9)$$

and

$$\dot{g}^+ - \dot{g}^- = \frac{(1+n)\Psi}{\left[1 + \frac{n\Psi}{E}\right]E} (\dot{\sigma}^+ - \dot{\sigma}^-) \quad (10.10)$$

where  $\sigma$ ,  $g$ , and  $f$  are assumed to be continuous throughout.

Combining (10.9) and (10.10) results in an expression of the change in equilibrium stress in terms of strain rate.

$$\dot{g}^+ - \dot{g}^- = \frac{(1+n)\Psi}{\left[1 + \frac{n\Psi}{E}\right]} \Psi(\dot{\epsilon}^+ - \dot{\epsilon}^-) \quad (10.11)$$

Now the above equations are specialized for the case of relaxation ( $\dot{\epsilon}^+ = 0$ ) initiated when fully established flow has been reached. In this region, the stress rate  $\dot{\sigma}$  and the equilibrium stress rate  $\dot{g}$  are related to the strain rate by  $\{\dot{\sigma}\} = \{\dot{g}\} = E_t \dot{\epsilon}^-$  where  $\{ \}$  denotes the long-time asymptotic condition. From equation (10.9) and  $\dot{\epsilon}^+ = 0$

$$\dot{\sigma}^+ = (E_t - E)\dot{\epsilon}^- = -E\dot{\epsilon}^- \left[ 1 - \frac{E_t}{E} \right] \quad (10.12)$$

and combining equation (10.11) and  $\dot{\epsilon}^+ = 0$

$$\dot{g}^+ = \left[ E_t - \frac{(1+n)\Psi}{\left[ 1 + \frac{n\Psi}{E} \right]} \right] \dot{\epsilon}^- = -\Psi\dot{\epsilon}^- \left[ \frac{(1+n)}{\left[ 1 + \frac{n\Psi}{E} \right]} - \frac{E_t}{\Psi} \right] \quad (10.13)$$

Noting in Equation (10.12),  $E$  and  $\dot{\epsilon}^-$  are positive and recalling that  $\frac{E_t}{E} < 1$ , it is clear that the stress rate  $\dot{\sigma}^+$  during relaxation is negative. Additionally we observe that the equilibrium stress rate  $\dot{g}^+$  is also negative when  $E_t < \frac{(1+n)\Psi}{\left[ 1 + \frac{n\Psi}{E} \right]}$ . Assuming

$E_t < \Psi < E$  and  $0 < n < 1$  this is demonstrated

$$\begin{aligned} E_t &< \frac{(1+n)\Psi}{\left[ 1 + \frac{n\Psi}{E} \right]} \\ E_t \left[ 1 + \frac{n\Psi}{E} \right] &< (1+n)\Psi \\ \frac{E_t}{\Psi} + \frac{nE_t}{E} &< 1+n \\ \frac{E_t}{\Psi} < 1 \text{ and } \frac{nE_t}{E} &< n \end{aligned} \quad (10.14)$$

It follows that the equilibrium stress  $g^+$  decreases during relaxation.

The stress rate ratio  $\dot{\sigma}^+/\dot{g}^+$  is calculated by combining Equations (10.12) and (10.13)

$$\frac{\dot{\sigma}^+}{\dot{g}^+} = \frac{E - E_t}{\left[ \frac{(1+n)\Psi}{\left[1 + \frac{n\Psi}{E}\right]} - E_t \right]} \quad (10.15)$$

We observe that  $\dot{\sigma}^+/\dot{g}^+ > 1$  if  $E > \frac{(1+n)\Psi}{\left[1 + \frac{n\Psi}{E}\right]}$ . Knowing  $\Psi < E$  we demonstrate this is true

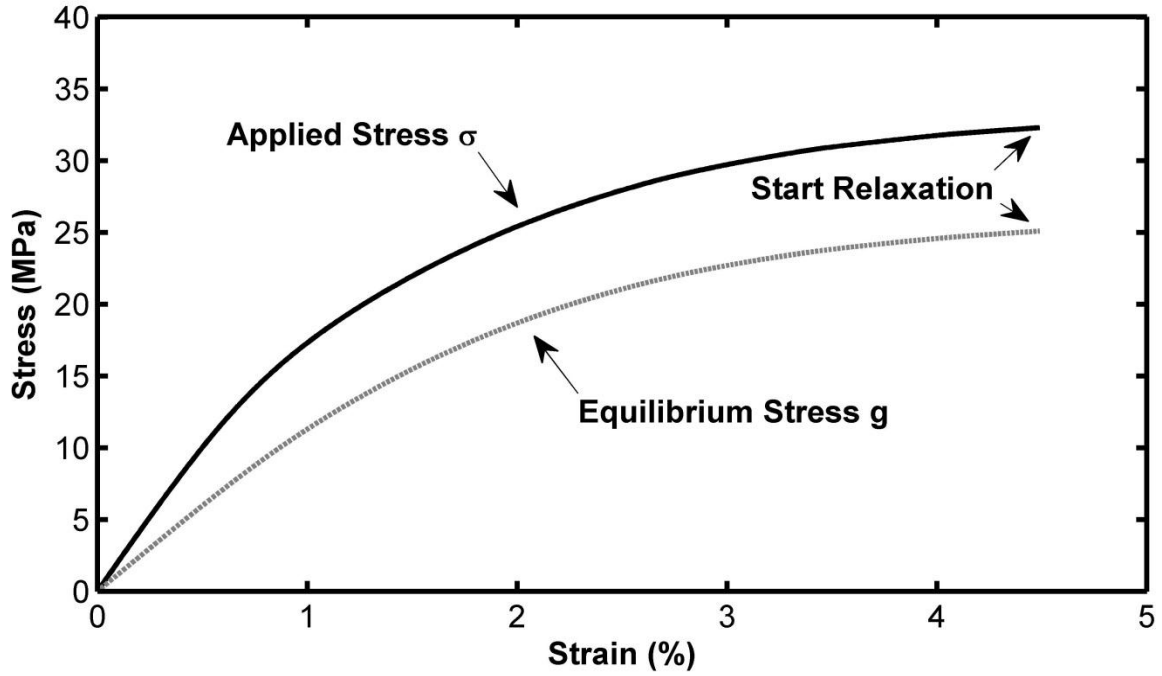
$$E > \frac{(1+n)\Psi}{\left[1 + \frac{n\Psi}{E}\right]}$$

$$E \left[1 + \frac{n\Psi}{E}\right] > (1+n)\Psi \quad (10.16)$$

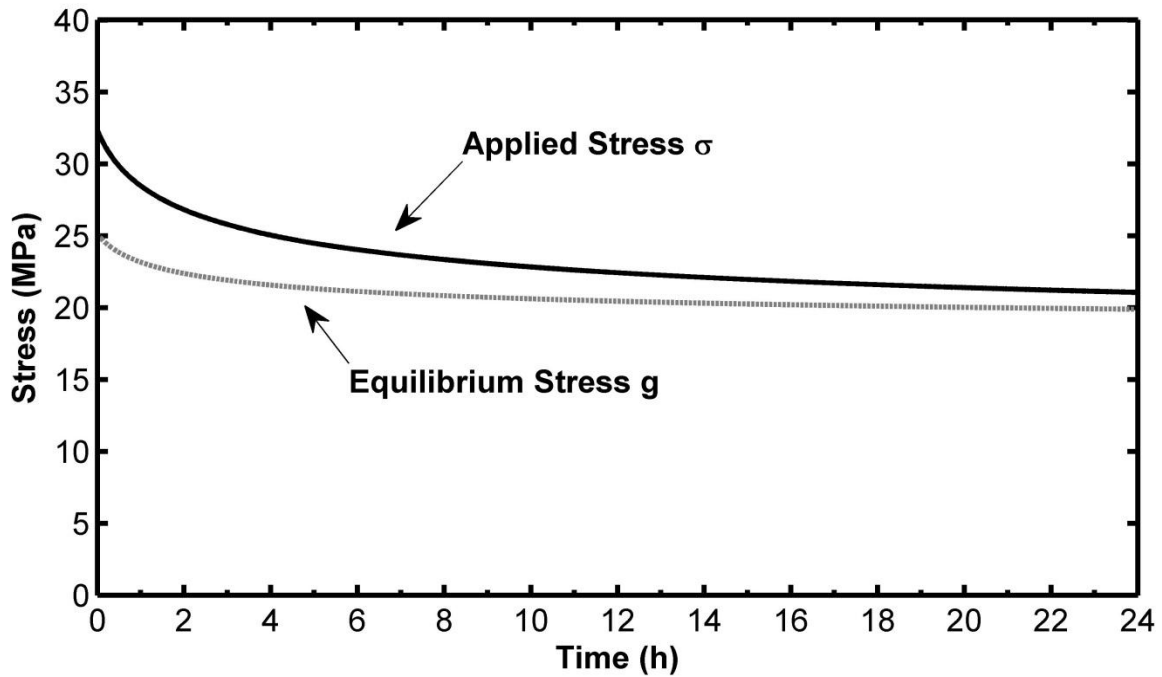
$$E + n\Psi > \Psi + n\Psi$$

$$E > \Psi$$

This is noteworthy since the fact that  $\dot{\sigma}^+/\dot{g}^+ > 1$  implies that the applied stress will eventually catch up with the equilibrium stress and relaxation will terminate. Figure 10.3 reveals the behavior of the applied and equilibrium stresses during relaxation as they are modeled by VBOP. In Figure 10.3(a), the difference between the applied stress and equilibrium stress is observed prior to the start of relaxation. In Figure 10.3(b), both stresses are seen to decrease during relaxation but as described above, the applied stress decreases faster than the equilibrium stress. In the long-time asymptotic condition, the applied stress catches the equilibrium stress and relaxation terminates. As a practical matter,  $\dot{\sigma}^+$  and  $\dot{g}^+$  quickly decrease to such a level that continued relaxation behavior is no longer experimentally detectable.



(a) Prior loading at  $10^{-6} \text{ s}^{-1}$



(b) Relaxation

**Figure 10.3** Evolution of applied and equilibrium stresses during (a) prior loading and (b) relaxation. VBOP predicts the applied stress will eventually catch up with the equilibrium stress and the relaxation will terminate.

### 10.2.1.2 Creep

Next we specialize equations (10.9) and (10.10) for the case of creep ( $\dot{\sigma}^+ = 0$ ). Again, we limit our analysis to the inelastic region and make use of the long-time asymptotic behavior of the VBOP model. From equation (10.9) and  $\dot{\sigma}^+ = 0$

$$\dot{\epsilon}^+ = \left[ 1 - \frac{E_t}{E} \right] \dot{\epsilon}^- \quad (10.17)$$

and combining equation (10.10) and  $\dot{\sigma}^+ = 0$

$$\dot{g}^+ = \left[ E_t - \frac{(1+n)\Psi E_t}{\left[ 1 + \frac{n\Psi}{E} \right] E} \right] \dot{\epsilon}^- \quad (10.18)$$

Note that the strain rate  $\dot{\epsilon}^+$  and equilibrium stress rate  $\dot{g}^+$  have the same sign. After loading to a given creep stress we note that the strain rate  $\dot{\epsilon}^+$  is positive since  $\dot{\epsilon}^-$  is positive and, because  $\frac{E_t}{E} < 1$ , the bracketed term of Equation (10.17) is also positive. Additionally, we observe that the equilibrium stress rate  $\dot{g}^+$  is also positive when  $\dot{\epsilon}^-$  is positive and the bracketed term of Equation (10.18) is positive. The bracketed term is positive when  $E > \frac{(1+n)\Psi}{\left[ 1 + \frac{n\Psi}{E} \right]}$ , as was previously demonstrated in (10.16)

The observation that the strain rate  $\dot{\epsilon}^+$  and equilibrium stress rate  $\dot{g}^+$  have the same sign implies that during positive creep strain, the equilibrium stress will increase until the equilibrium stress equals the flow stress and the overstress becomes zero at which time creep will cease. In Figure 10.4 the behavior of the applied and equilibrium stresses as modeled by the VBOP during creep is presented. While the applied (creep) stress is held constant the equilibrium stress increases as creep strain develops.

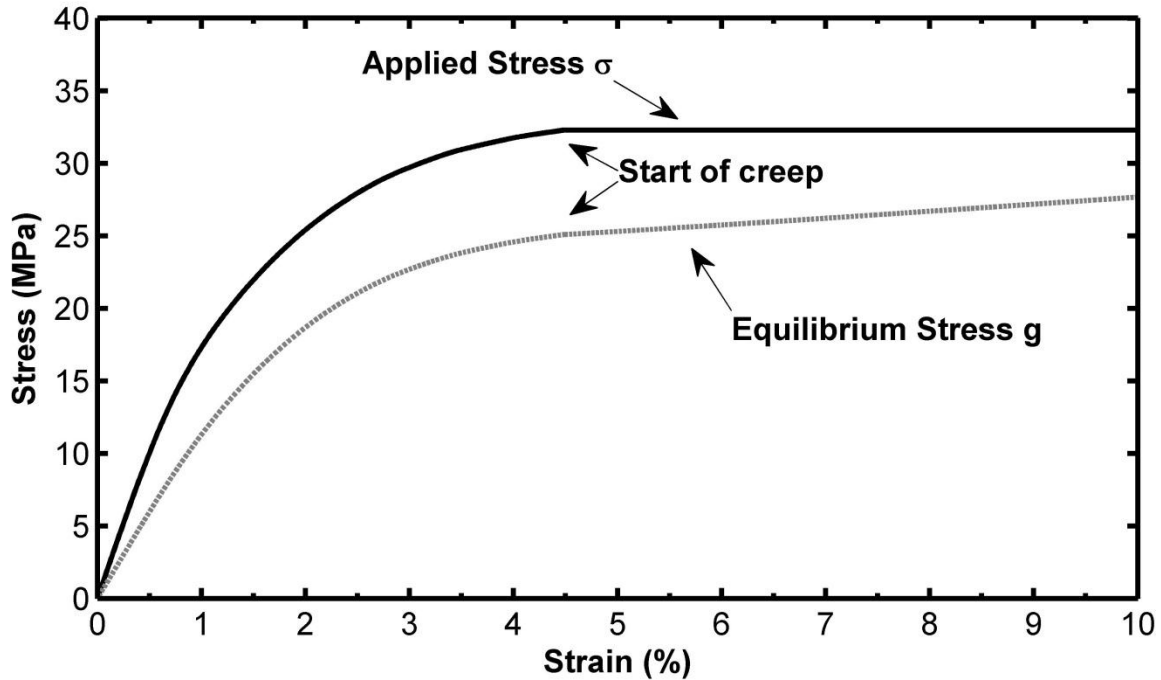


**Figure 10.4 Evolution of applied and equilibrium stresses during creep. VBOP predicts that during positive creep, the equilibrium stress will increase until the equilibrium stress equals the flow stress and the overstress becomes zero at which time creep will cease.**

### 10.3 Alternate Method to Assess the Equilibrium Stress

The characterization procedure for the VBOP requires a measurement of the equilibrium stress during monotonic loading at a given point in the region of fully developed plastic flow. This is so the isotropic stress may be calculated at that same point. Unfortunately, the equilibrium stress cannot be measured directly except when the applied stress becomes stationary. While this does occur after a sufficiently long period of relaxation, the equilibrium stress at the end of relaxation is not the same as the equilibrium stress prior to the start of relaxation, which is the sought value. In the example shown in Figure 10.3, the equilibrium stress decreases from 25 to 20 MPa during the period of relaxation. This is a substantial source of error when calculating the isotropic stress  $A$ . Since the numerical value of the equilibrium stress at the start of

relaxation is unknown unless one first assumes a value of the isotropic stress  $A$ , an iterative approach is required to choose a value of  $A$  that produces acceptable results. Since iteration of the viscosity and shape function parameters must be accomplished for each iterate of the isotropic stress, a substantial effort is required to select a set of parameters that produces good results.

Since it has been shown that the equilibrium stress decreases during a period of relaxation we may assume that the previous method of measuring the equilibrium stress, while somewhat inaccurate, does represent a lower bound of the equilibrium stress. If an upper bound to the value of the equilibrium stress could be found that would provide a range over which to iterate, and would greatly simplify the characterization procedure. The following discussion describes how a McLean type dip test can be utilized to assess the value of the equilibrium stress for a given prior strain rate and stress-strain of interest.

### *10.3.1 Utilization of the McLean Type Dip Test to Measure the Equilibrium Stress*

A McLean type dip test can be utilized as an alternate means of directly measuring the equilibrium stress. The McLean type dip test developed by Mitra and McLean [85] consists of monotonic loading in strain control, an instantaneous reduction in stress (or stress dip), followed by a period of creep. The stress dip-creep period combination is repeated if desired. Only a single stress dip-creep period combination was utilized per specimen during this effort.

In order to understand how a MTDT can be utilized to deduce equilibrium stress, it is instructive to reflect on our problem. We desire to measure the equilibrium stress during monotonic loading at a given point in the region of fully developed plastic flow.



The equilibrium stress can only be assessed when the applied stress becomes stationary. Unfortunately, during monotonic loading, this is not the case. This scenario though, can be imposed by utilizing a MTDT. At the conclusion of monotonic loading, it is possible to switch to load control mode and rapidly dip to a known stress level before the equilibrium stress has sufficient time to undergo significant evolution. Then, that known stress level can be maintained by the digital controller and the resulting creep behavior can be observed. If negative creep is observed, it is assumed that the stress dip reduced the applied stress to something less than the equilibrium stress. Conversely, if positive creep is observed, then the stress dip must have been to a level above the equilibrium stress. The initial magnitude of the creep strain rate is an indicator of the magnitude of the difference between the creep stress level and the current value of the equilibrium stress. Careful selection of the stress dip levels of two or more MTDTs can quickly bracket a range of possible equilibrium stress levels. Selection of the stress dip level that is precisely the same as the equilibrium stress should result in no creep. As will be shown in the following paragraph, this is unfortunately not the case.

### *10.3.2 Creep Rate Reversal*

During observation of PMR-15 creep tests conducted on the unloading path, Falcone and Ruggles-Wrenn [1] reported a reversal in the strain rate. When conducted on the unload path, creep strain initially decreased and then increased. Khan and Krempl [13] reported similar results during creep tests of polycarbonate. They found that when a creep test is conducted during unloading, creep might be positive (increase in creep strain relative to start value), negative (decrease in creep strain relative to start value) or

initially negative, but becoming positive after some time. When utilizing the MTDT to assess the equilibrium stress, this same strain rate reversal behavior is observed. This should be expected since the “stress dip” is nothing more than very rapid unloading. The current formulation of the VBOP cannot accommodate this behavior. While VBOP does predict negative creep if the applied stress is below the equilibrium stress, the VBOP formulation has no mechanism to cause positive creep once the equilibrium stress becomes equal to the applied stress. A two-element modification of the VBOP has been proposed by Khan [12] that does represent this behavior but at the cost of a systematic characterization procedure and as such, is not suitable for this research effort.

Although, the VBOP does not accommodate the strain rate reversal behavior, this does not prevent utilization of the MTDT as part of the enhanced systematic model characterization procedure. A small number (2-3) of MTDTs are typically sufficient to identify a creep stress level that is essentially the same as the equilibrium stress just prior to the dip. A final MTDT, dipping to the identified creep stress level, will result in a very small amount of negative creep followed by a strain rate reversal and then positive creep. Identification of this behavior is analogous to the identification of the previously discussed stationary applied stress. The use of the MTDT to identify a creep stress level that is essentially the same as the equilibrium stress just prior to the stress dip, depends on the assumption that the time required to accomplish the dip and subsequent observations of initial creep behavior, is far smaller than the time required for the continued evolution of the equilibrium stress. Theoretically, the MTDT calls for an instantaneous reduction in stress. In reality load was reduced at a controlled rate  $\dot{\sigma} = -150$  MPa/s. This short, yet finite, time required to reduce the load had a negligible

effect on the strain response, yet avoided dynamic effects associated with sudden load applications and/or reversals. Additionally, a small amount of time is required to observe the initial creep behavior. State-of-the-art servo hydraulic testing equipment can achieve an accurate dip in less than 0.1 s and the resulting creep strain rate reversal is observed in the first 200-300 s. During this short period, the equilibrium state (stress) of PMR-15 is assumed not to change substantially. The schematic creep strain versus time curve presented in Figure 10.5 shows a very small negative creep rate transitioning to a small positive creep rate. Assuming the negative and then positive creep rates are very small, over a period of a few minutes this behavior can be approximated with a creep rate  $\dot{\epsilon}$  of zero. When this occurs, the applied stress and the equilibrium stress can be considered equal. The positive creep strain that continues to develop is postulated to occur due to a change in the equilibrium state (stress) with time rather than a change driven by the overstress alone. Since such behavior is not represented by the existing VBOP formulation, it has no effect on the characterization of VBOP model parameters and can be left as an area of future research. In the next section, experimental data are reviewed and numerical tolerances for approximating creep strain rates as  $\dot{\epsilon} = 0$  are suggested.

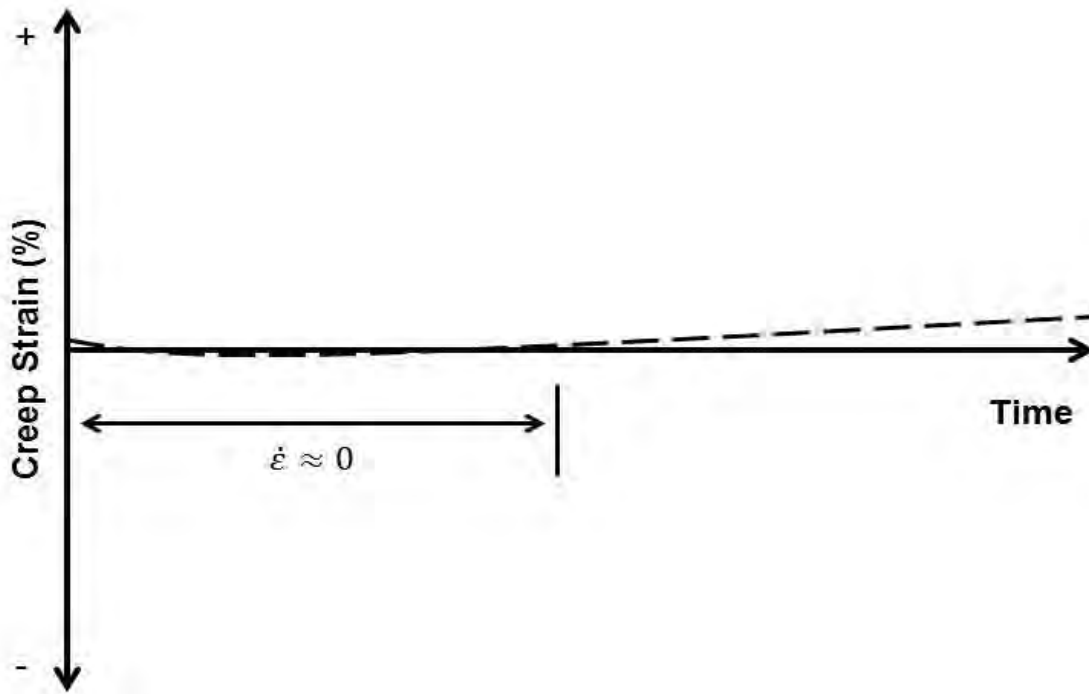


**Figure 10.5 Schematic showing typical creep strain versus time curve obtained during McLean type dip tests conducted during this effort. Creep strain rate reversal is apparent. Note the initial negative and then positive creep strain rates are very small and can be approximated with  $\dot{\epsilon} = 0$ .**

#### **10.4 Experimental Observations**

Several MTDTs were conducted at 274 and 302 °C, which incorporated constant strain rate loading at  $10^{-6} \text{ s}^{-1}$  in an effort to assess the equilibrium stress. Stress dips were initiated at 4.5 and 5 % strain for tests conducted at 274 and 302 °C, respectively. Stress dips were accomplished by switching to load control mode and commanding a decrease in stress at the rate of 150 MPa/s until the desired creep stress level was achieved and then maintained for 15-h. Creep strain was recorded during the ensuing period of creep. Note that only unaged PMR-15 neat resin specimens were tested.

#### *10.4.1 MTDT Results at 274 °C*

The results of three MTDTs conducted at 274 °C are presented in Figure 10.6. In each case, the stress dip portion of the stress-strain curve was nearly linear and was similar to the quasi-elastic portion of the monotonic loading stress-strain curve in both degree of linearity and slope. Stress dips were accomplished in less than 0.1 s and occasionally concluded with a small (~0.5 MPa) overshoot of the commanded creep stress level that was corrected by the digital controller in less than 10 s. It is assumed that this transient overshoot of the desired creep stress level did not affect the results of the test.

In the case of the first MTDT, immediately after dipping to 23.6 MPa a substantial negative creep strain was observed. This is indicative of the stress level at the end of the dip being below the equilibrium stress and that a smaller dip (higher creep stress level) is warranted during the next MTDT. On the second MTDT, a creep stress level of 28.1 MPa was reached. Again, significant negative creep strain was initially observed but creep strain rate reversal occurred and the specimen exhibited positive creep until failure. Ultimately a third, still smaller dip to 32.1 MPa was selected in order to obtain the creep stress level that resulted in a creep strain rate of approximately zero. As the stress reached 32.1 MPa, a very small amount of negative creep developed prior to a very gradual creep strain rate reversal followed by positive creep. The creep strain vs. time curve is shown in Figure 10.7. It is seen that virtually no creep strain was accumulated during the first 200 s of the creep period. Additionally, the very gradual creep strain rate reversal indicates that while the creep stress was initially slightly below the equilibrium stress, the equilibrium stress continued to evolve until the equilibrium

stress was equal to, and then below the applied creep stress level. While the micromechanical mechanism driving the continued evolution of the equilibrium stress is unclear, it is unlikely that a negative or positive overstress alone is responsible for this behavior since, at some point during the rate reversal the overstress was necessarily equal to zero. Since the reason for performing the MTDT was to identify the value of the equilibrium stress at a given stress and strain *prior* to the stress dip, the subsequent evolution of the equilibrium stress is not entirely relevant. It is sufficient to establish that the evolution of the equilibrium stress occurs at such a slow rate that for the purposes of calculating the isotropic stress it effectively remains unchanged during a short period immediately after the stress dip. It is suggested that objective numerical standards be established to identify what constitutes a creep strain rate of approximately zero. For this research effort, the creep strain rate was assumed to be zero when the measured creep strain remained within +/- 0.02 % for 200 seconds or longer.

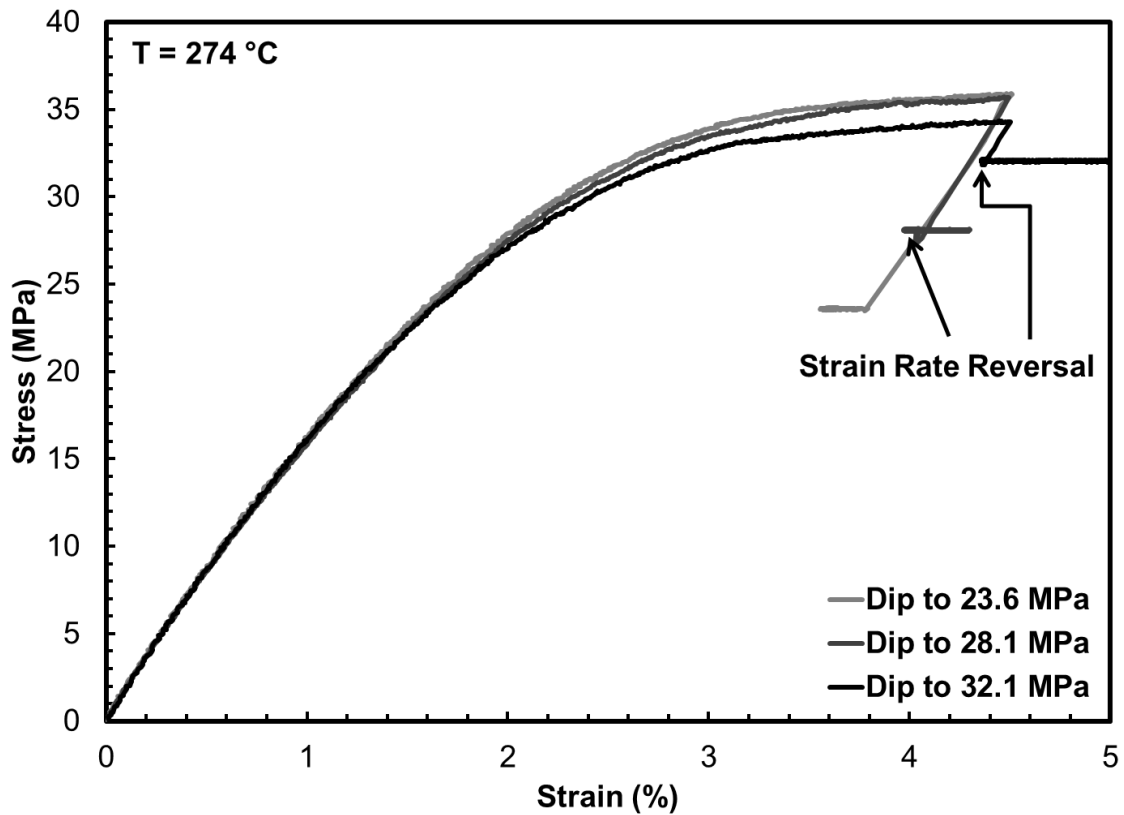
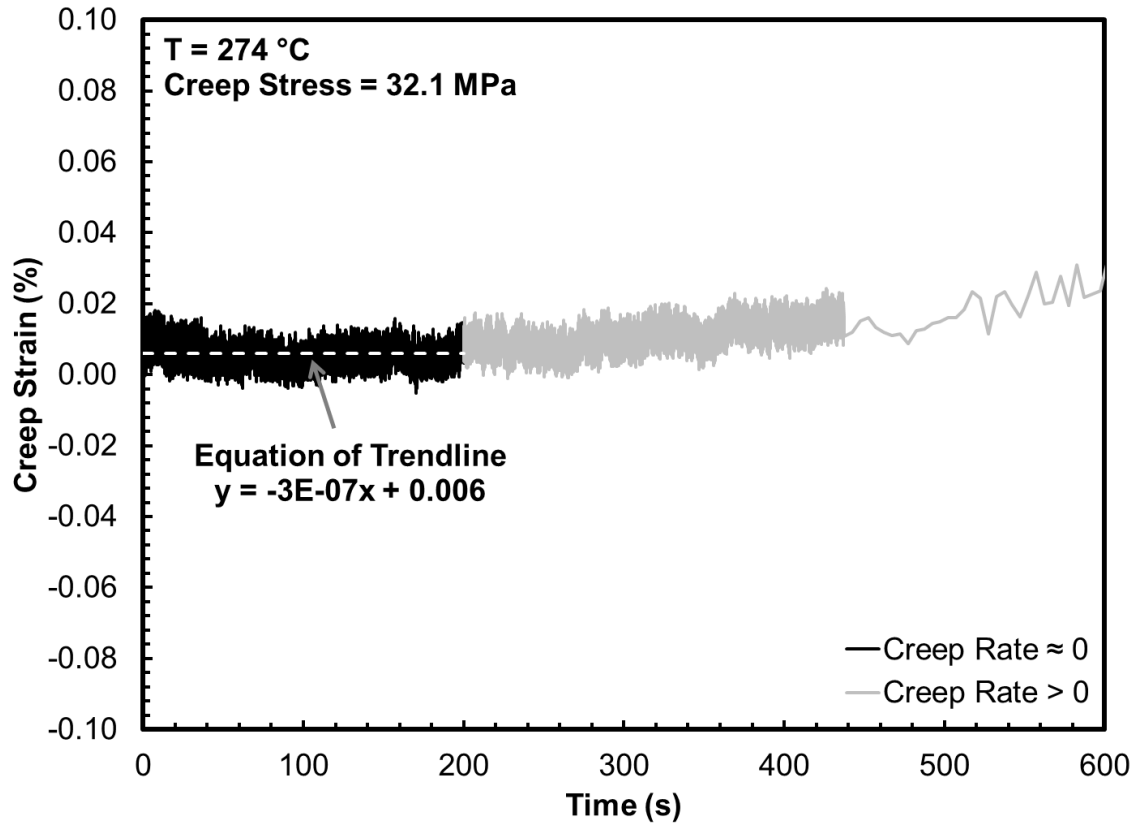


Figure 10.6 Experimental results obtained for PMR-15 polymer during three McLean type dip tests consisting of monotonic loading at  $10^{-6}\text{ s}^{-1}$  to 4.5 % strain followed by stress dip at 150 MPa/s and creep at 23.6, 28.1 and 32.1 MPa at 274 °C. Creep strain rate reversal was observed at 28.1 MPa and at 32.1 MPa. The creep test at 32.1 MPa produced only a small amount of negative creep prior to creep strain rate reversal suggesting that the applied stress and the equilibrium stress were equal.



**Figure 10.7** Creep curve pertaining to the MTDT with the creep stress of 32.1 MPa shown in Figure 10.6. Very slight negative creep is followed by creep strain rate reversal. Creep strain rate during first 200 seconds can be approximated with  $\dot{\epsilon} = 0$  indicating the applied stress and the equilibrium stress are equal.

#### 10.4.2 MTDT Results at 302 °C

The results of two MTDTs conducted at 302 °C are presented in Figure 10.8. Again, the stress dip portion of the stress-strain curve was nearly linear and was similar to the quasi-elastic portion of the monotonic loading stress-strain curve in both degree of linearity and slope. No significant transient overshoots of the desired creep stress level were apparent. During the first MTDT, substantial negative creep strain was observed after the stress dip to 9.1 MPa followed by creep strain rate reversal. A second MTDT was conducted utilizing a new specimen and a relatively small dip to 11.7 MPa. During



the period of creep at 11.7 MPa, a very small amount of negative creep was observed followed by a gradual strain rate reversal and positive creep. The creep strain vs. time curve for this test is shown in Figure 10.9. Again, it is seen that essentially no creep strain was accumulated during the first 200 s of the creep period and thus the equilibrium stress prior to the dip is assumed to be the same as the creep stress level immediately following the dip. As with specimens tested at 274 °C, the creep strain rate was assumed to be zero when the measured creep strain remained within +/- 0.02 % for 200 seconds or longer.

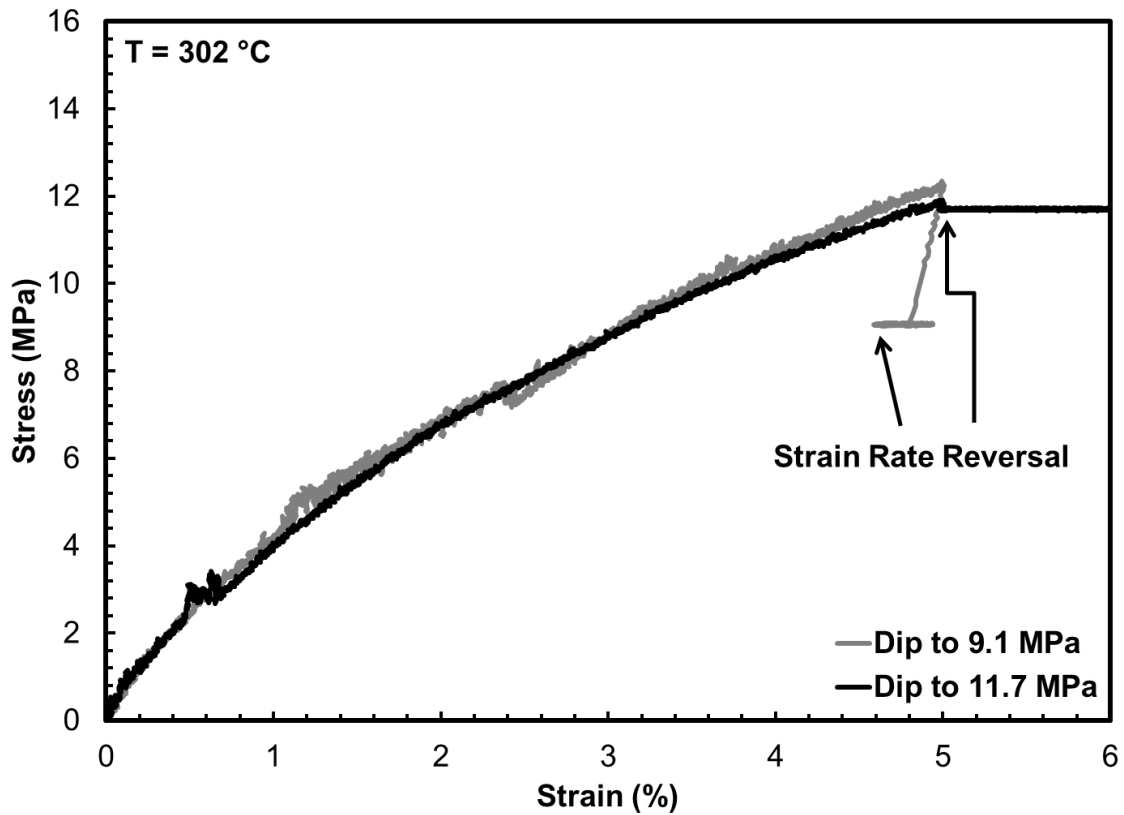


**Figure 10.8** Experimental results obtained for PMR-15 polymer during two McLean type dip tests consisting of monotonic loading at  $10^{-6} \text{ s}^{-1}$  to 5 % strain followed by stress dip at 150 MPa/s and creep at 9.1 and 11.7 MPa at 302 °C. Creep strain rate reversal was observed at 9.1 MPa and at 11.7 MPa. The creep test at 11.7 MPa produced only a small amount of negative creep prior to creep strain rate reversal suggesting that the applied stress and the equilibrium stress were equal.

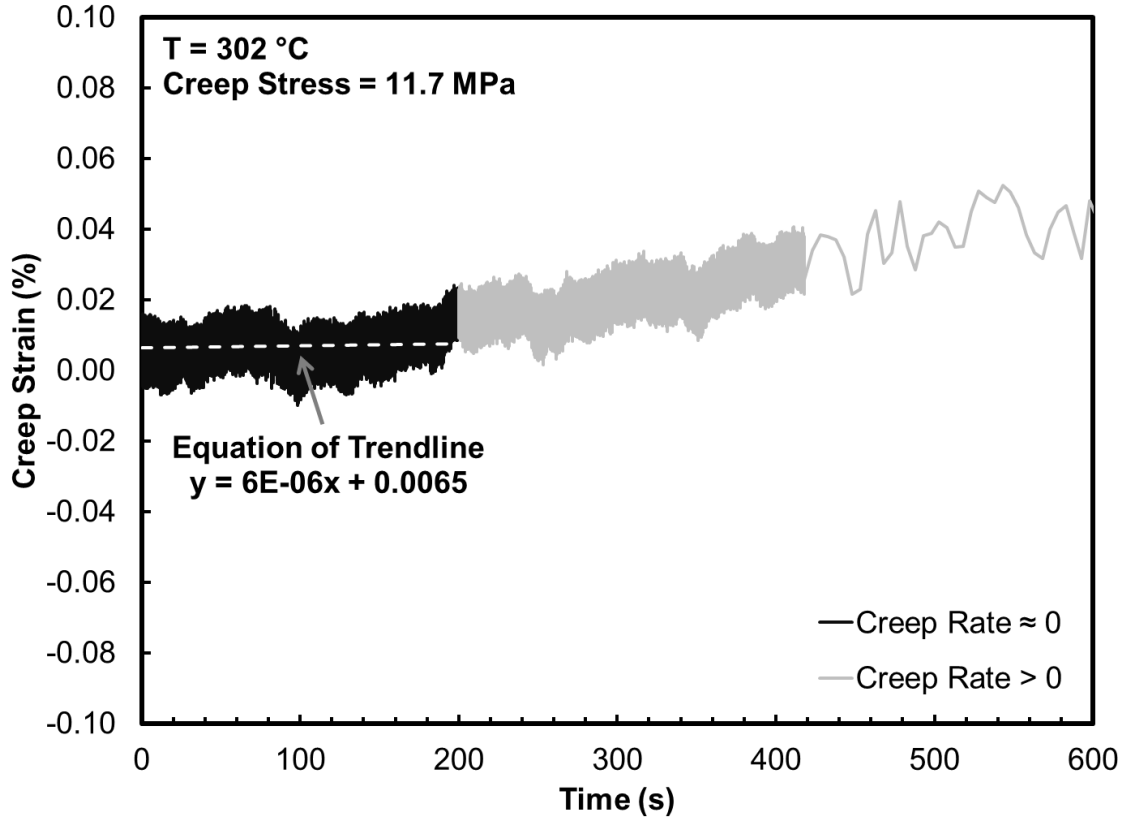


**Figure 10.9** Creep curve pertaining to the MTDT with the creep stress of 11.7 MPa shown in Figure 10.8. Very slight negative creep is followed by creep strain rate reversal. Creep strain rate during first 200 seconds can be approximated with  $\dot{\epsilon} = 0$  indicating the applied stress and the equilibrium stress are equal.

### 10.5 Comparison of Different Techniques to Determine Equilibrium Stress

As demonstrated in the previous section, the value for the equilibrium stress at a given stress-strain can be determined utilizing two or three MTDTs. Unlike the use of relaxation data method, this technique does not suffer from the under-prediction of stress and equilibrium stress as previously described in Section 10.2. Assuming that the applied stress at the end of a sufficiently long period of relaxation yields a value that is somewhat below the desired equilibrium stress we iteratively increase the isotropic stress until the VBOP simulation produces acceptable results. Since this is a rather complicated and

labor intensive process we desire to limit the range over which we iterate. The value of the equilibrium stress determined by using the MTDT data can serve as an upper bound on this iteration process.

Experimental data demonstrate that the value of the isotropic stress that yields the best modeling results is obtained from an equilibrium stress value that lies between the values determined by using the relaxation data and the MTDT data. In Figure 10.10 and Figure 10.11, we observe the applied stress at the end of periods of relaxation conducted at 274 and 302 °C respectively. Utilizing those values of applied stress and the previously determined tangent moduli  $E_t$  listed in Table 10.1, Equation (10.8) yields the isotropic stress value based on relaxation data,  $A_{relax}$ . In a similar manner, the isotropic stress values based on the MTDT data,  $A_{MTDT}$ , are calculated using the appropriate stress dip levels. The results are summarized in Table 10.1 along with the actual isotropic stress values utilized for the simulations of unaged PMR-15 polymer in Chapter 8. As shown in Table 10.1,  $A_{relax}$  and  $A_{MTDT}$  do indeed bound the isotropic stress utilized for modeling,  $A_{model}$ .

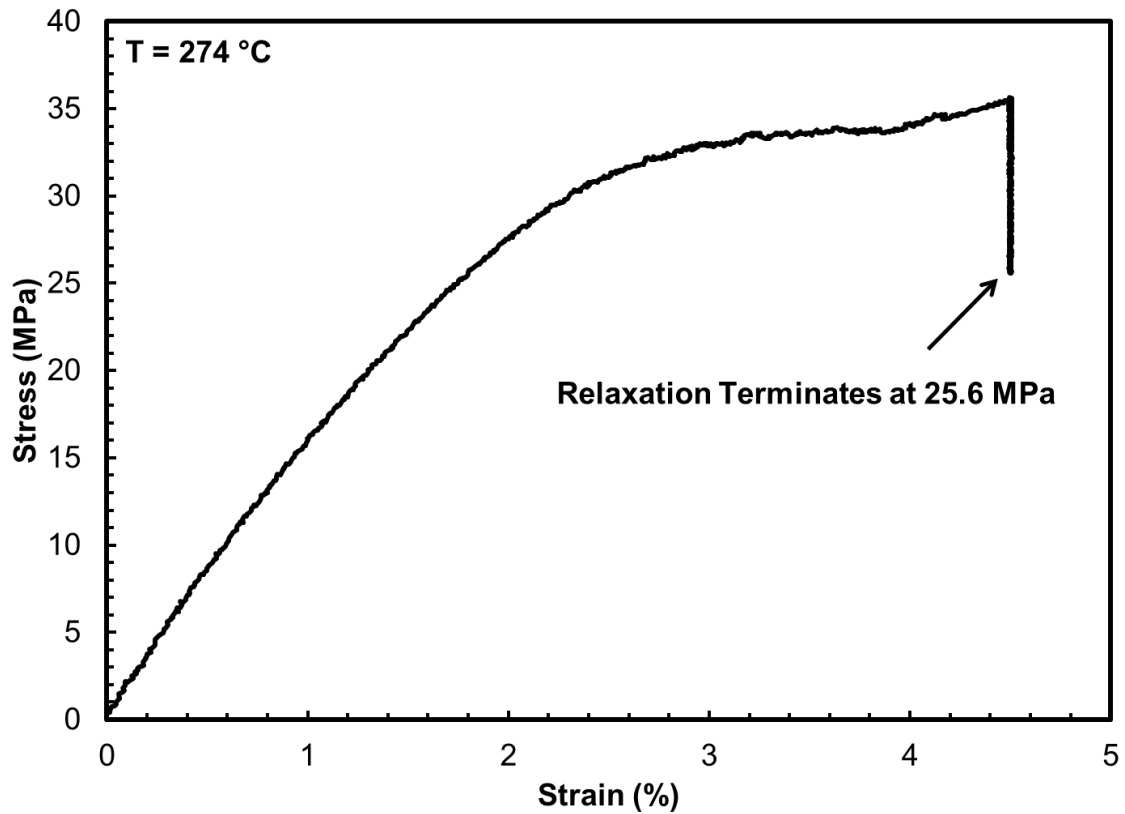


**Figure 10.10** Experimental results obtained for PMR-15 polymer during monotonic loading at  $10^{-6} \text{ s}^{-1}$  to 4.5 % strain followed by relaxation for 15 h at 274 °C. Relaxation terminated at the stress of 25.6 MPa.

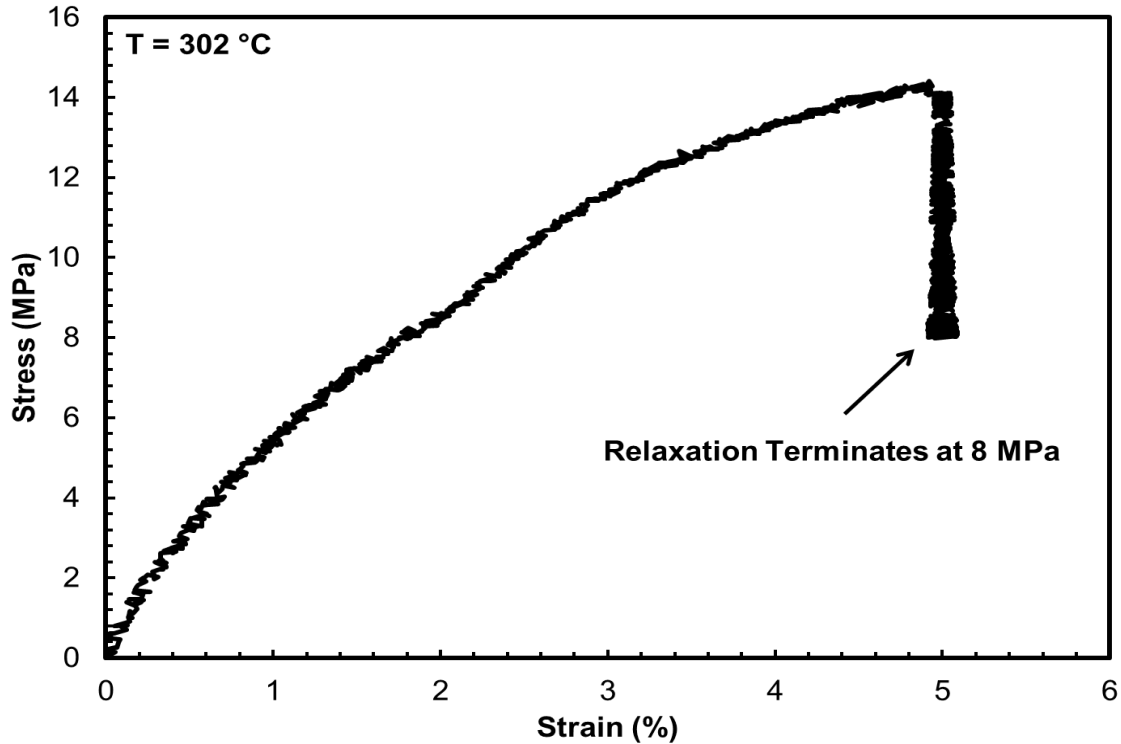


Figure 10.11 Experimental results obtained for PMR-15 polymer during monotonic loading at  $10^{-6} \text{ s}^{-1}$  to 5 % strain followed by relaxation for 15 h at 302 °C. Relaxation terminated at the stress of 8 MPa.

Table 10.1 Comparison of the Isotropic Stress Calculated from the Equilibrium Stress Obtained during Relaxation and McLean Type Dip Tests at 274 and 302 °C

274 °C					
$A_{relax}$ (MPa)	23.4	$A_{MTDT}$ (MPa)	29.9	$A_{model}$ (MPa)	24.0
$g_{relax}$ (MPa)	25.6	$g_{MTDT}$ (MPa)	32.1	$E_t$ (MPa)	49.9
302 °C					
$A_{relax}$ (MPa)	4.4	$A_{MTDT}$ (MPa)	8.1	$A_{model}$ (MPa)	8.0
$g_{relax}$ (MPa)	8.0	$g_{MTDT}$ (MPa)	11.7	$E_t$ (MPa)	71.6

## 11 Conclusions and Recommendations

### 11.1 Conclusions

A primary objective of this research was to develop an analytical capability to represent the effects of test temperature on the inelastic behavior of PMR-15 within the framework of the Viscoplasticity Based on Overstress for Polymers (VBOP) theory. To that end, experiments were conducted to identify the temperature range where PMR-15 exhibits viscoplastic deformation behavior and to identify the effects of test temperature on that deformation behavior. The existing VBOP constitutive model was augmented to account for the effects of temperature. A rigorous verification of the augmented VBOP was accomplished by comparing model predictions with experimental results.

The impact of this research is clear. It is now established that PMR-15 exhibits viscoplastic behavior at temperatures in the 274-316 °C range. A designer wishing to make use of the full load bearing capacity of this high-temperature polymer in applications designed to operate at elevated temperature must consider the effect of temperature on the design. The augmented VBOP has been demonstrated to accurately represent the inelastic behavior of PMR-15 at these elevated temperatures and thus could serve as the basis for a design and analysis tool as well as for a life prediction methodology.

A second objective of this research was to develop an analytical capability to represent the effects of prior aging temperature on the inelastic deformation behavior of PMR-15. The key features of the deformation behavior of PMR-15 subjected to prior aging at various operationally relevant temperatures were elucidated and the

phenomenological indicators of aging were identified. At temperatures in the 260-302 °C range, aging of the PMR-15 polymer occurs at a relatively constant rate and is independent of aging temperature. Additionally, experimental results demonstrated that prior aging temperature in the 260-302 °C range has no influence on the inelastic deformation behavior of PMR-15. Experimental results revealed that the effects of prior aging were consistent at each temperature in this range and depended only on aging time. The implication of this statement is critical. While the designer must account for the effect of aging over the useful life of the structural component, a detailed tracking or modeling of the variation of the temperature profile with time may not be necessary. This greatly simplifies the development and implementation of analytical design and service life prediction tools.

In addition to the original research objectives, an enhanced procedure for determining VBOP model parameters that utilizes a McLean Type Dip Test (MTDT) was developed. The use of MTDT data was proposed as an additional method to assess the equilibrium stress during monotonic loading. Comparison with experimental data demonstrates that the value of the isotropic stress that yields the best modeling results is obtained from an equilibrium stress value, which lies between the values determined by using relaxation data and MTDT data. The inclusion of the MTDT in the VBOP characterization procedure provides an upper bound on the possible value of the isotropic stress. Using the results of the MTDT to assess the equilibrium stress significantly improved the characterization of the isotropic stress and the overall characterization of the constitutive model. The successful application of the augmented VBOP constitutive model (or any constitutive model for that matter) depends on a well-defined



characterization procedure that provides a systematic and objective means of determining model parameters.

## **11.2 Recommendation for Future Research**

The current formulation of the VBOP does not have the capability to represent the strain rate reversal phenomenon observed during creep on the unloading path. In the current formulation, the evolution of the equilibrium stress is governed by the overstress and necessarily ceases when the overstress becomes zero. Within the existing model, the equilibrium stress cannot change once the overstress reaches zero. Examining the behavior of polymers, it is possible to imagine various micromechanical mechanisms operating in unison to resist tensile loading. During unloading, it might be possible that certain mechanisms continue to resist the tensile load while others may tend to return the specimen to the original state. Assuming these mechanisms operate on different time scales this may serve to explain the strain rate reversal behavior observed during creep after unloading.

Modeling of this behavior might be accomplished by modifying the current rheological model and associated constitutive equations to include two time-dependent modules that could work in unison during loading and in opposition during unloading. Such a model could potentially improve the representation of unloading behavior, creep and relaxation during unloading as well as recovery at zero stress.

## 12 Appendix

The purpose of this appendix is to allow the reader to quickly cross-reference which figure contains data from any particular test condition described throughout the manuscript. The test matrices are divided by test type and aged versus unaged PMR-15.

**Table 12.1 Cross-Reference of Experimental Data Obtained During Monotonic Tensile Tests to Failure of Unaged PMR-15 at Various Elevated Temperatures and Strain Rates**

Strain Rate	Test Temperature			
	274 °C	288 °C	302 °C	316 °C
$10^{-3} \text{ s}^{-1}$	Figure 6.1 Figure 8.1 Figure 8.12	Figure 6.2 Figure 8.3 Figure 8.14	Figure 6.3 Figure 8.5 Figure 8.16	Figure 8.23
$10^{-4} \text{ s}^{-1}$	Figure 6.1 Figure 8.1 Figure 8.12	Figure 6.2 Figure 8.3 Figure 8.13	Figure 6.3 Figure 8.5 Figure 8.16	Figure 8.23
$10^{-5} \text{ s}^{-1}$	Figure 6.1 Figure 8.1 Figure 8.12			
$10^{-6} \text{ s}^{-1}$	Figure 6.1 Figure 8.1 Figure 8.12	Figure 6.2 Figure 8.3 Figure 8.13	Figure 6.3 Figure 8.5 Figure 8.16	Figure 8.23

**Table 12.2 Cross-Reference of Experimental Data Obtained During Relaxation Following Monotonic Loading of Unaged PMR-15 at Various Elevated Temperatures and Strain Rates**

Strain Rate	Test Temperature			
	274 °C	288 °C	302 °C	316 °C
$10^{-3} \text{ s}^{-1}$	Figure 6.5 Figure 8.2 Figure 8.13		Figure 6.7 Figure 8.6 Figure 8.17	Figure 8.24
$10^{-4} \text{ s}^{-1}$	Figure 6.5 Figure 8.2 Figure 8.13	Figure 6.6 Figure 8.4 Figure 8.15	Figure 6.7 Figure 8.6 Figure 8.17	Figure 8.24
$10^{-5} \text{ s}^{-1}$	Figure 6.5 Figure 8.2 Figure 8.13	Figure 6.6 Figure 8.4 Figure 8.15	Figure 6.7 Figure 8.6 Figure 8.17	Figure 8.24
$10^{-6} \text{ s}^{-1}$	Figure 6.5 Figure 8.2 Figure 8.13	Figure 6.6 Figure 8.4 Figure 8.15	Figure 6.7 Figure 8.6 Figure 8.17	Figure 8.24

**Table 12.3 Cross-Reference of Experimental Data Obtained During Creep Following Monotonic Loading of Unaged PMR-15 at Various Elevated Temperatures and Strain Rates**

Strain Rate	Test Temperature and Creep Stress Level				
	274 °C 21 MPa	288 °C 21 MPa	302 °C 21 MPa	316 °C 21 MPa	316 °C 12 MPa
$10^{-3} \text{ s}^{-1}$			Figure 6.10 Figure 8.22	Figure 8.25	
$10^{-4} \text{ s}^{-1}$	Figure 6.8 Figure 8.20	Figure 6.9 Figure 8.21	Figure 6.10 Figure 8.22		Figure 8.26
$10^{-5} \text{ s}^{-1}$			Figure 6.10 Figure 8.22	Figure 8.25	Figure 8.26
$10^{-6} \text{ s}^{-1}$	Figure 6.8 Figure 8.20	Figure 6.9 Figure 8.21	Figure 6.10 Figure 8.22		Figure 8.26

**Table 12.4 Cross-Reference of Experimental Data Obtained During Monotonic Tensile Tests to Failure of PMR-15 Aged for 50-250 h at Elevated Temperature**

Aging Duration	Strain Rate	Prior Aging Temperature				
		260 °C	274 °C	288 °C	302 °C	316 °C
50 h	$10^{-3} \text{ s}^{-1}$	Figure 9.17	Figure 9.17	Figure 9.17	Figure 9.17	Figure 9.11 Figure 9.17
	$10^{-4} \text{ s}^{-1}$	Figure 9.6 Figure 9.16	Figure 9.16	Figure 9.16	Figure 9.16	Figure 9.10 Figure 9.16
	$10^{-5} \text{ s}^{-1}$	Figure 9.15	Figure 9.15	Figure 9.15	Figure 9.15	Figure 9.9 Figure 9.15 Figure 9.8
	$10^{-6} \text{ s}^{-1}$	Figure 9.14	Figure 9.14	Figure 9.14	Figure 9.14	Figure 9.8 Figure 9.14
100 h	$10^{-3} \text{ s}^{-1}$	Figure 9.21	Figure 9.21	Figure 9.21	Figure 9.21	Figure 9.11 Figure 9.21
	$10^{-4} \text{ s}^{-1}$	Figure 9.6 Figure 9.20	Figure 9.20	Figure 9.20	Figure 9.20	Figure 9.10 Figure 9.20
	$10^{-5} \text{ s}^{-1}$	Figure 9.19	Figure 9.19	Figure 9.19	Figure 9.19	Figure 9.9 Figure 9.19
	$10^{-6} \text{ s}^{-1}$	Figure 9.18	Figure 9.18	Figure 9.18	Figure 9.18	Figure 9.8 Figure 9.18
250 h	$10^{-3} \text{ s}^{-1}$	Figure 9.1 Figure 9.25	Figure 9.2 Figure 9.25	Figure 9.3 Figure 9.25	Figure 9.4 Figure 9.25	Figure 9.5 Figure 9.11 Figure 9.25
	$10^{-4} \text{ s}^{-1}$	Figure 9.1 Figure 9.6 Figure 9.12 Figure 9.24	Figure 9.2 Figure 9.24	Figure 9.3 Figure 9.24	Figure 9.4 Figure 9.7 Figure 9.24	Figure 9.5 Figure 9.10 Figure 9.13 Figure 9.24
	$10^{-5} \text{ s}^{-1}$	Figure 9.1 Figure 9.23	Figure 9.2 Figure 9.23	Figure 9.3 Figure 9.23	Figure 9.4 Figure 9.23	Figure 9.5 Figure 9.9 Figure 9.23
	$10^{-6} \text{ s}^{-1}$	Figure 9.1 Figure 9.6 Figure 9.12 Figure 9.22	Figure 9.2 Figure 9.22	Figure 9.3 Figure 9.22	Figure 9.4 Figure 9.22	Figure 9.5 Figure 9.8 Figure 9.13 Figure 9.22

**Table 12.5 Cross-Reference of Experimental Data Obtained During Monotonic Tensile Tests to Failure of PMR-15 Aged for 500-1000 h at Elevated Temperature**

Aging Duration	Strain Rate	Prior Aging Temperature				
		260 °C	274 °C	288 °C	302 °C	316 °C
500 h	$10^{-3} \text{ s}^{-1}$	Figure 9.29	Figure 9.29	Figure 9.29	Figure 9.29	Figure 9.11 Figure 9.29
	$10^{-4} \text{ s}^{-1}$	Figure 9.6 Figure 9.28	Figure 9.28	Figure 9.28	Figure 9.7 Figure 9.28	Figure 9.10 Figure 9.28
	$10^{-5} \text{ s}^{-1}$	Figure 9.27	Figure 9.27	Figure 9.27	Figure 9.27	Figure 9.9 Figure 9.27
	$10^{-6} \text{ s}^{-1}$	Figure 9.6 Figure 9.26	Figure 9.26	Figure 9.26	Figure 9.7 Figure 9.26	Figure 9.8 Figure 9.26
1000 h	$10^{-3} \text{ s}^{-1}$		Figure 9.33	Figure 9.33	Figure 9.33	
	$10^{-4} \text{ s}^{-1}$		Figure 9.32	Figure 9.32	Figure 9.7 Figure 9.32	
	$10^{-5} \text{ s}^{-1}$		Figure 9.31	Figure 9.31	Figure 9.31	
	$10^{-6} \text{ s}^{-1}$		Figure 9.30	Figure 9.30	Figure 9.7 Figure 9.30	

**Table 12.6 Cross-Reference of Experimental Data Obtained During Relaxation Following Monotonic Loading of PMR-15 Aged for Various Durations at Elevated Temperature**

Aging Duration	Strain Rate	Prior Aging Temperature				
		260 °C	274 °C	288 °C	302 °C	316 °C
50 h	$10^{-3} \text{ s}^{-1}$		Figure 9.40			
	$10^{-4} \text{ s}^{-1}$	Figure 9.39	Figure 9.34 Figure 9.40	Figure 9.34	Figure 9.34 Figure 9.41	
	$10^{-5} \text{ s}^{-1}$		Figure 9.34 Figure 9.40	Figure 9.34	Figure 9.34 Figure 9.41	
	$10^{-6} \text{ s}^{-1}$	Figure 9.34 Figure 9.39	Figure 9.34 Figure 9.40	Figure 9.34	Figure 9.34 Figure 9.41	Figure 9.34
100 h	$10^{-3} \text{ s}^{-1}$		Figure 9.40			
	$10^{-4} \text{ s}^{-1}$		Figure 9.35 Figure 9.40		Figure 9.35 Figure 9.41	
	$10^{-5} \text{ s}^{-1}$		Figure 9.35 Figure 9.40	Figure 9.35	Figure 9.35 Figure 9.41	
	$10^{-6} \text{ s}^{-1}$		Figure 9.35 Figure 9.40	Figure 9.35	Figure 9.35 Figure 9.41	
250 h	$10^{-3} \text{ s}^{-1}$		Figure 9.40			
	$10^{-4} \text{ s}^{-1}$	Figure 9.39	Figure 9.36 Figure 9.40		Figure 9.36 Figure 9.41	
	$10^{-5} \text{ s}^{-1}$		Figure 9.36 Figure 9.40	Figure 9.36	Figure 9.36 Figure 9.41	
	$10^{-6} \text{ s}^{-1}$	Figure 9.36 Figure 9.39	Figure 9.36 Figure 9.40	Figure 9.36	Figure 9.36 Figure 9.41	
500 h	$10^{-3} \text{ s}^{-1}$		Figure 9.40			
	$10^{-4} \text{ s}^{-1}$		Figure 9.40			
	$10^{-5} \text{ s}^{-1}$		Figure 9.37 Figure 9.40	Figure 9.37	Figure 9.37 Figure 9.41	
	$10^{-6} \text{ s}^{-1}$		Figure 9.37 Figure 9.40	Figure 9.37	Figure 9.37 Figure 9.41	
1000 h	$10^{-3} \text{ s}^{-1}$					
	$10^{-4} \text{ s}^{-1}$		Figure 9.40			
	$10^{-5} \text{ s}^{-1}$		Figure 9.38 Figure 9.40		Figure 9.38 Figure 9.41	
	$10^{-6} \text{ s}^{-1}$		Figure 9.38 Figure 9.40	Figure 9.38	Figure 9.38 Figure 9.41	

### 13 Bibliography

- [1] Falcone, C. M., and Ruggles-Wrenn, M. B., 2009, "Rate Dependence and Short-Term Creep Behavior of a Thermoset Polymer at Elevated Temperature," *Journal of Pressure Vessel Technology*, **131**, pp. 011403-1-011403-8.
- [2] Falcone, C. M., 2006, "Some Aspects of the Mechanical Response of PMR-15 Neat Resin at 288 Deg. C: Experiment and Modeling," Air Force Institute of Technology, Wright-Patterson Air Force Base, Ohio.
- [3] Balaconis, J. G., 2006, "Some Aspects of the Mechanical Response of BMI 5250-4 Neat Resin at 191 Degrees C: Experiment and Modeling," Air Force Institute of Technology, Wright-Patterson Air Force Base, Ohio.
- [4] Westberry, C. M., 2005, "Rate Dependence and Short-Term Creep Behavior of PMR-15 Neat Resin at 23 and 288 °C," Air Force Institute of Technology, Wright-Patterson Air Force Base, Ohio.
- [5] Bordonaro, C. M., 1995, "Rate Dependent Mechanical Behavior of High Strength Plastics: Experiment and Modeling," Rensselaer Polytechnic Institute, Troy, New York.
- [6] Bordonaro, C. M., and Krempl, E., 1992, "The Effect of Strain Rate on the Deformation and Relaxation Behavior of 6/6 Nylon at Room Temperature," *Polymer Engineering and Science*, **32**, (16), pp. 1066-1072.

[7] Colak, O. U., 2005, "Modeling Deformation Behavior of Polymers with Viscoplasticity Theory Based on Overstress," *International Journal of Plasticity*, **21**, (1), pp. 145-160.

[8] Colak, O. U., and Dusunceli, N., 2006, "Modeling Viscoelastic and Viscoplastic Behavior of High Density Polyethylene (HDPE)," *Journal of Engineering Materials and Technology*, **128**, (4), pp. 572-578.

[9] Ho, K., 1998, "Application of the Viscoplasticity Theory Based on Overstress to the Modeling of Dynamic Strain Aging of Metals and to the Modeling of the Solid Polymers, Specifically to Nylon 66," Rensselaer Polytechnic Institute, Troy, New York.

[10] Ho, K., and Krempl, E., 2002, "Extension of the Viscoplasticity Theory Based on Overstress (VBO) to Capture Non-Standard Rate Dependence in Solids," *International Journal of Plasticity*, **18**, (7), pp. 851-872.

[11] Khan, F., 2002, "The Deformation Behavior of Solid Polymers and Modeling with the Viscoplasticity Theory Based on Overstress," Department of Mechanical Engineering, Aeronautical Engineering and Mechanics, Rensselaer Polytechnic Institute, Troy, NY.

[12] Khan, F., 2006, "Loading History Effects on the Creep and Relaxation Behavior of Thermoplastics," *Journal of Engineering Materials and Technology*, **128**, pp. 564-571.



[13] Khan, F., and Krempl, E., 2004, "Pre-Necking and Post-Necking Relaxation and Creep Behavior of Polycarbonate: A Phenomenological Study," *Polymer Engineering and Science*, **44**, (9), pp. 1783-1791.

[14] Khan, F., and Krempl, E., 2006, "Amorphous and Semicrystalline Solid Polymers: Experimental and Modeling Studies of their Inelastic Deformation Behaviors," *Journal of Engineering Materials and Technology*, **128**, pp. 64-72.

[15] Krempl, E., and Bordonaro, C. M., 1995, "A State Variable Model for High Strength Polymers," *Polymer Engineering and Science*, **35**, (4), pp. 310-316.

[16] Krempl, E., and Ho, K., 2000, "An Overstress Model for Solid Polymer Deformation Behavior Applied to Nylon 66," *Proceedings of the ASTM Symposium*, R. A. Schapery and C. T. Sun, eds., **1357**, pp. 118-137.

[17] Krempl, E., and Khan, F., 2003, "Rate (Time)-Dependent Deformation Behavior: An Overview of some Properties of Metals and Solid Polymers," *International Journal of Plasticity*, **19**, (7), pp. 1069-1095.

[18] Krempl, E., 2000, "Viscoplastic Models for High Temperature Applications," *International Journal of Solids and Structures*, **37**, (1-2), pp. 279-291.

[19] McClung, A. J. W., 2008, "Extension of Viscoplasticity Based on Overstress to Capture the Effects of Prior Aging on the Time Dependent Deformation Behavior of a High-Temperature Polymer: Experiments and Modeling," Air Force Institute of Technology, Wright-Patterson Air Force Base, Ohio.

[20] Diedrick, B. K., 2010, "Effects of Prior Aging at 260 °C in Argon on Inelastic Deformation Behavior of PMR-15 Polymer at 260 °C: Experiment and Modeling," Air Force Institute of Technology, Wright-Patterson Air Force Base, Ohio.

[21] Wahlquist, J. A., 2010, "Effects of Prior Aging at 274 Deg C in Argon on Inelastic Deformation Behavior of PMR-15 Polymer at 288 Deg C: Experiment and Modeling," Air Force Institute of Technology, Wright-Patterson Air Force Base, Ohio.

[22] Broeckert, J. L., 2007, "Effects of Prior Aging at Elevated Temperature in Air and in Argon Environments on Creep Response of PMR-15 Neat Resin at 288 Deg C," Air Force Institute of Technology, Wright-Patterson Air Force Base, Ohio.

[23] NASA, 2003, "DMBZ Polyimides Provide an Alternative to PMR-15 for High-Temperature Applications," Online, 21 March 2010.  
<http://www.grc.nasa.gov/WWW/RT/RT1995/5000/5150c.htm>.

[24] Bowles, K.J., Papadopoulos, D.S., Scheiman, D.A., 2003, "A Limited Comparison of the Thermal Durability of Polyimide Candidate Matrix Polymers With PMR-15," TM-2003-211878, .

[25] Sperling, L.H., 2006, *Introduction to Physical Polymer Science*, John Wiley & Sons, Inc., Hoboken, New Jersey, pp. 845.

[26] Bowles, K.J., Papadopoulos, D.S., Inghram, L.L., 2001, "Longtime durability of PMR-15 matrix polymer at 204, 260, 288 and 316 C," NASA Glenn Research Center, NASA TM-2001-210602.

- [27] Ozmen, O., 2009, "Effects of Prior Aging at 316 Deg C in Argon on Inelastic Deformation Behavior of PMR-15 Polymer at 316 Deg C: Experiment and Modeling," Air Force Institute of Technology, Wright-Patterson Air Force Base, Ohio.
- [28] McClung, A. J. W., and Ruggles-Wrenn, M. B., 2009, "Strain Rate Dependence and Short-Term Relaxation Behavior of a Thermoset Polymer at Elevated Temperature: Experiment and Modeling," *Journal of Pressure Vessel Technology*, **131**, pp. 031405-1-031405-8.
- [29] Krempl, E., 1974, "Cyclic Creep- an Interpretive Literature Survey," *WRC Bulletin*, pp. 63-123.
- [30] Kitagawa, M., and Matsutani, T., 1988, "Effect of Time and Temperature on Nonlinear Constitutive Equation in Polypropylene," *J. Mater. Sci.*, **23**, (11), pp. 4085-4090.
- [31] Kitagawa, M., Zhou, D., and Qiu, J., 1995, "Stress-Strain Curves for Solid Polymers," *Polymer Engineering and Science*, **35**, (22), pp. 1725-1732.
- [32] Lemaitre, J., and Chaboche, J.L., 1994, *Mechanics of Solid Materials*, Cambridge University Press.
- [33] Krempl, E., 1979, "Viscoplasticity Based on Total Strain. the Modeling of Creep with Special Considerations of Initial Strain and Aging," *Journal of Engineering Materials and Technology (Transactions of the ASME)*, **101**, (4), pp. 380-386.

- [34] Ruggles, M. B., and Krempl, E., 1991, "Rate Sensitivity and Short-Term Relaxation Behavior of AISI Type 304 Stainless Steel at Room Temperature and at 650° C; Influence of Prior Aging," *Journal of Pressure Vessel Technology*, **113**, (3), pp. 385-391.
- [35] Ruggles-Wrenn, M. B., and Broeckert, J. L., 2008, "Effects of Prior Aging at 288 °C in Air and in Argon Environments on Creep Response of PMR-15 Neat Resin," *Journal of Applied Polymer Science*, **111**, pp. 228-236.
- [36] McClung, A. J. W., and Ruggles-Wrenn, M. B., 2009, "Effects of Prior Aging at 288° C in Argon Environment on Time-Dependent Deformation Behavior of a Thermoset Polymer at Elevated Temperature, Part 1: Experiments," *Journal of Applied Polymer Science*, **114**, (5), pp. 2956-2962.
- [37] Krempl, E., 1995, "From the Standard Linear Solid to the Viscoplasticity Theory Based on Overstress," *Proceedings of the International Conference on Computational Engineering Science*, S. N. Atluri, G. Yagawa and T. A. Cruse, eds. , **2**, pp. 1679–1684.
- [38] Cozzarelli, F.A., and Shames, I.H., 1997, *Elastic and Inelastic Stress Analysis*, Taylor & Francis, pp. 722.
- [39] Schapery, R. A., 1969, "On the Characterization of Nonlinear Viscoelastic Materials," *Polymer Engineering and Science*, **9**, (4), pp. 295-310.
- [40] Schapery, R. A., 1997, "Nonlinear Viscoelastic and Viscoplastic Constitutive Equations Based on Thermodynamics," *Mechanics of Time-Dependent Materials*, **1**, (2), pp. 209-240.

- [41] Zaoutsos, S. P., Papanicolaou, G. C., and Cardon, A. H., 1998, "On the Non-Linear Viscoelastic Behaviour of Polymer-Matrix Composites," *Composites Science and Technology*, **58**, (6), pp. 883-889.
- [42] Papanicolaou, G. C., Zaoutsos, S. P., and Cardon, A. H., 1999, "Prediction of the Non-Linear Viscoelastic Response of Unidirectional Fiber Composites," *Composites Science and Technology*, **59**, (9), pp. 1311-1319.
- [43] Cardon, A. H., Qin, Y., and Van Vossle, C., 2000, "Durability Analysis of Polymer Matrix Composites for Structural Applications," *Computers & Structures*, **76**, (1-3), pp. 35-41.
- [44] Xia, Z., and Ellyin, F., 1998, "Time-Dependent Behaviour and Viscoelastic Constitutive Modelling of an Epoxy Polymer," *Polymers & Polymer Composites*, **6**, (2), pp. 75-83.
- [45] Ward, I.M., 1983, *Mechanical Properties of Solid Polymers*, Wiley-Interscience, New York.
- [46] Xia, Z., Hu, Y., and Ellyin, F., 2003, "Deformation Behavior of an Epoxy Resin Subject to Multiaxial Loadings. Part II: Constitutive Modeling and Predictions," *Polymer Engineering and Science*, **43**, (3), pp. 734-748.
- [47] Xia, Z., Shen, X., and Ellyin, F., 2005, "Cyclic Deformation Behavior of an Epoxy Polymer. Part II: Predictions of Viscoelastic Constitutive Models," *Polymer Engineering and Science*, **45**, (1), pp. 103-113.

- [48] Zhang, Y., Xia, Z., and Ellyin, F., 2005, "Nonlinear Viscoelastic Micromechanical Analysis of Fibre-Reinforced Polymer Laminates with Damage Evolution," *International Journal of Solids and Structures*, **42**, (2), pp. 591-604.
- [49] McClung, A. J. W., and Ruggles-Wrenn, M. B., 2009, "Effects of Prior Aging at 288° C in Argon Environment on Time-Dependent Deformation Behavior of a Thermoset Polymer at Elevated Temperature, Part 2: Modeling with Viscoplasticity Theory Based on Overstress," *Journal of Applied Polymer Science*, **114**, (6), pp. 3389-3395.
- [50] Perzyna, P., 1963, "The Constitutive Equations for Rate Sensitive Plastic Materials," *Quarterly of Applied Mathematics*, **20**, (4), pp. 321-332.
- [51] Phillips, A., and Wu, H. C., 1973, "A Theory of Viscoplasticity," *International Journal of Solids and Structures*, **9**, (1), pp. 15-30.
- [52] Chaboche, J., and Rousselier, G., 1983, "On the Plastic and Viscoplastic Constitutive equations—Part I: Rules Developed with Internal Variable Concept," *Journal of Pressure Vessel Technology*, **105**, pp. 153.
- [53] Chaboche, J. L., and Rousselier, G., 1983, "On the Plastic and Viscoplastic Constitutive equations—Part II: Application of Internal Variable Concepts to the 316 Stainless Steel," *Journal of Pressure Vessel Technology*, **105**, pp. 159.
- [54] Chaboche, J. L., 1986, "Time-Independent Constitutive Theories for Cyclic Plasticity," *International Journal of Plasticity*, **2**, (2), pp. 149-188.

- [55] Bodner, S., and Partom, Y., 1975, "Constitutive Equations for Elastic-Viscoplastic Strain-Hardening Materials," *Journal of Applied Mechanics*, **42**, pp. 385.
- [56] Yao, D., and Krempl, E., 1985, "Viscoplasticity Theory Based on Overstress. the Prediction of Monotonic and Cyclic Proportional and Nonproportional Loading Paths of an Aluminum Alloy," *International Journal of Plasticity*, **1**, (3), pp. 259-274.
- [57] Krempl, E., 1987, "Models of Viscoplasticity some Comments on Equilibrium (Back) Stress and Drag Stress," *Acta Mechanica*, **69**, (1), pp. 25-42.
- [58] Cernocky, E. P., and Krempl, E., 1979, "A Non-Linear Uniaxial Integral Constitutive Equation Incorporating Rate Effects, Creep and Relaxation," *International Journal of Non-Linear Mechanics*, **14**, (3), pp. 183-203.
- [59] Cernocky, E. P., and Krempl, E., 1980, "A Theory of Thermoviscoplasticity Based on Infinitesimal Total Strain," *International Journal of Solids and Structures*, **16**, (8), pp. 723-741.
- [60] Liu, M. C. M., and Krempl, E., 1979, "A Uniaxial Viscoplastic Model Based on Total Strain and Overstress," *Journal of the Mechanics and Physics of Solids*, **27**, (5-6), pp. 377-391.
- [61] Yamada, H., and Li, C. Y., 1973, "Stress Relaxation and Mechanical Equation of State in Austenitic Stainless Steels," *Metallurgical and Materials Transactions B*, **4**, (9), pp. 2133-2136.

[62] Krempl, E., and Kallianpur, V. V., 1984, "Some Critical Uniaxial Experiments for Viscoplasticity at Room Temperature," *Journal of the Mechanics and Physics of Solids*, **32**, (4), pp. 301-314.

[63] Krempl, E., 1982, "The role of servocontrolled testing in the development of the theory of viscoplasticity based on total strain and overstress," *Anonymous ASTM International*, pp. 1.

[64] Krempl, E., McMahon, J. J., and Yao, D., 1986, "Viscoplasticity Based on Overstress with a Differential Growth Law for the Equilibrium Stress," *Mechanics of Materials*, **5**, (1), pp. 35-48.

[65] Kujawski, D., Kallianpur, V., and Krempl, E., 1980, "An Experimental Study of Uniaxial Creep, Cyclic Creep and Relaxation of AISI Type 304 Stainless Steel at Room Temperature," *Journal of the Mechanics and Physics of Solids*, **28**, (2), pp. 129-148.

[66] Ruggles, M. B., and Krempl, E., 1989, "The Influence of Test Temperature on the Ratchetting Behavior of Type 304 Stainless Steel," *Journal of Engineering Materials and Technology*, **111**, pp. 378.

[67] Kujawski, D., and Krempl, E., 1981, "The Rate (Time)-Dependent Behavior of Ti-7Al-2Cb-1Ta Titanium Alloy at Room Temperature Under Quasi-Static Monotonic and Cyclic Loading," *Journal of Applied Mechanics*, **48**, pp. 55.



[68] Ruggles, M. B., Cheng, S., and Krempl, E., 1994, "The Rate-Dependent Mechanical Behavior of Modified 9wt.%Cr-1wt.%Mo Steel at 538 °C," *Materials Science and Engineering: A*, **186**, (1-2), pp. 15-21.

[69] Majors, P., and Krempl, E., 1994, "The Isotropic Viscoplasticity Theory Based on Overstress Applied to the Modeling of Modified 9wt.%Cr-1wt.%Mo Steel at 538 °C," *Materials Science and Engineering: A*, **186**, (1-2), pp. 23-34.

[70] Dusunceli, N., and Colak, O. U., 2006, "High Density Polyethylene (HDPE): Experiments and Modeling," *Mechanics of Time-Dependent Materials*, **10**, (4), pp. 331-345.

[71] Flügge, W., 1975, *Viscoelasticity*, Springer, New York, pp. 194.

[72] Cernocky, E. P., and Krempl, E., 1980, "A Theory of Viscoplasticity Based on Infinitesimal Total Strain," *Acta Mechanica*, **36**, (3), pp. 263-289.

[73] Krempl, E., 1996, "A Small-Strain Viscoplasticity Theory Based on Overstress," *Unified Constitutive Laws of Plastic Deformation*, A. S. Krausz and K. Krauszeds., Academic Press, San Diego, pp. 281-318, Chap. 6.

[74] Ho, K., 2001, "Modeling of Nonlinear Rate Sensitivity by using an Overstress Model," *CMES- Computer Modeling in Engineering and Sciences*, **2**, (3), pp. 351-364.

[75] Krempl, E., and Ho, K., 2001, "Inelastic Compressible and Incompressible, Isotropic, Small Strain Viscoplasticity Theory Based on Overstress VBO," *Handbook of Materials Behavior Models*, J. Lemaitre ed., Academic Press, San Diego, pp. 336-348.

[76] Krempl, E., 2001, "Relaxation Behavior and Modeling," *International Journal of Plasticity*, **17**, (10), pp. 1419-1436.

[77] Maciucescu, L., 2002, "A Simplified Viscoplasticity Theory Based on Overstress for Low to High Homologous Temperature and Quasi-Static to Dynamic Applications," Rensselaer Polytechnic Institute, Troy, New York.

[78] Tachibana, Y., and Krempl, E., 1998, "Modeling of High Homologous Temperature Deformation Behavior using the Viscoplasticity Theory Based on Overstress (VBO): Part III - A Simplified Model," *Journal of Engineering Materials and Technology Transactions of the ASME*, **120**, (3), pp. 193-196.

[79] Klepaczko, J., 1975, "Thermally Activated Flow and Strain Rate History Effects for some Polycrystalline f.c.c. Metals," *Materials Science and Engineering*, **18**, (1), pp. 121-135.

[80] Ward, I.M., and Sweeney, J., 2004, *An Introduction to the Mechanical Properties of Solid Polymers*, John Wiley & Sons Inc.

[81] McClung, A. J. W., and Ruggles-Wrenn, M. B., 2008, "The Rate (Time)-Dependent Mechanical Behavior of the PMR-15 Thermoset Polymer at Elevated Temperature," *Polymer Testing*, **27**, (7), pp. 908-914.

- [82] Ruggles-Wrenn, M. B., and Ozmen, O., 2010, "The Rate (Time)-Dependent Mechanical Behavior of the PMR-15 Thermoset Polymer at 316° C: Experiments and Modeling," *Journal of Pressure Vessel Technology*, **132**, pp. 041403-1-041403-6.
- [83] Chuang, K. C., Bowles, K. J., Scheiman, D. A., 2001, "Synthesis and Characterization of a High Tg Polyimide (DMBZ-15)," K. L. Mittal, ed. **1**, pp. 113.
- [84] Krempl, E., and Nakamura, T., 1998, "The Influence of the Equilibrium Stress Growth Law Formulation on the Modeling of Recently Observed Relaxation Behaviors," *JSME International Journal Series A, Solid Mechanics and Material Engineering*, **41**, (1), pp. 103-111.
- [85] MITRA, S. K., and McLean, D., 1966, "Work Hardening and Recovery in Creep," *Proceedings of the Royal Society of London Series A, Mathematical and Physical Sciences*, **295**, (1442), pp. 288-299.

<b>REPORT DOCUMENTATION PAGE</b>			<i>Form Approved</i> OMB No. 0704-0188		
The public reporting burden for this collection of information is estimated to average 1 hour per response, including the time for reviewing instructions, searching existing data sources, gathering and maintaining the data needed, and completing and reviewing the collection of information. Send comments regarding this burden estimate or any other aspect of this collection of information, including suggestions for reducing this burden to Department of Defense, Washington Headquarters Services, Directorate for Information Operations and Reports (0704-0188), 1215 Jefferson Davis Highway, Suite 1204, Arlington, VA 22202-4302. Respondents should be aware that notwithstanding any other provision of law, no person shall be subject to any penalty for failing to comply with a collection of information if it does not display a currently valid OMB control number. PLEASE DO NOT RETURN YOUR FORM TO THE ABOVE ADDRESS.					
1. REPORT DATE (DD-MM-YYYY) 17-01-2012		2. REPORT TYPE Dissertation		3. DATES COVERED (From — To) Aug 2008 – Jan 2012	
4. TITLE AND SUBTITLE  The Effect of Elevated Temperature on the Inelastic Deformation Behavior of PMR-15 Solid Polymer			5a. CONTRACT NUMBER		
			5b. GRANT NUMBER		
			5c. PROGRAM ELEMENT NUMBER		
6. AUTHOR(S)  Chad E. C. Ryther, Maj, USAF			5d. PROJECT NUMBER		
			5e. TASK NUMBER		
			5f. WORK UNIT NUMBER		
7. PERFORMING ORGANIZATION NAME(S) AND ADDRESS(ES) Air Force Institute of Technology Graduate School of Engineering and Management (AFIT/EN) 2950 Hobson Way WPAFB OH 45433-7765			8. PERFORMING ORGANIZATION REPORT NUMBER  AFIT/DS/ENY/12-12		
9. SPONSORING / MONITORING AGENCY NAME(S) AND ADDRESS(ES) Air Force Office of Scientific Research Joycelyn S. Harrison, Ph.D. 875 N. Randolph Street, Suite 325, Room 3112 Arlington, VA 22203 (703) 696-6225 joycelyn.harrison@afosr.af.mil			10. SPONSOR/MONITOR'S ACRONYM(S) AFOSR		
			11. SPONSOR/MONITOR'S REPORT NUMBER(S)		
12. DISTRIBUTION / AVAILABILITY STATEMENT APPROVED FOR PUBLIC RELEASE; DISTRIBUTION UNLIMITED					
13. SUPPLEMENTARY NOTES This material is declared a work of the U.S. Government and is not subject to copyright protection in the United States.					
14. ABSTRACT The inelastic deformation behavior of PMR-15 neat resin, a high-temperature thermoset polymer, was investigated at temperatures in the 274-316 °C range. The experimental program was developed to explore the influence of temperature on tensile loading, relaxation and creep behaviors of PMR-15. The results demonstrate that the mechanical behavior of PMR-15 exhibits a strong dependence on temperature. During strain-controlled tensile loading, the slope of the stress-strain curve in the quasi-elastic region decreases and the flow stress level decreases with increasing temperature. During relaxation, the amount of the stress drop decreases with increasing temperature. Based on experimental results the Viscoplasticity Based on Overstress for Polymers theory was augmented to account for the effects of elevated temperature. Several model parameters were developed into functions of temperature. The augmented VBOP was then employed to predict the response of the PMR-15 polymer under various test histories at temperatures in the 274-316 °C range. Additionally, the effects of prior isothermal aging at various temperatures in the 260-316 °C range were evaluated. At each temperature investigated, the initial slope of the stress-strain curve and the flow stress increase with prior aging duration. Experimental results reveal for aging temperatures in the 260-302 °C range, mechanical behavior depends only on prior aging duration and not on prior aging temperature.					
15. SUBJECT TERMS Polymer, PMR-15, creep, relaxation, prior strain rate, prior loading history, nonlinear viscoplastic theory, aging, argon, VBO, VBOP					
16. SECURITY CLASSIFICATION OF:			17. LIMITATION OF ABSTRACT  UU	18. NUMBER OF PAGES  243	19a. NAME OF RESPONSIBLE PERSON Marina B. Ruggles-Wrenn, PhD
a. REPORT  U	b. ABSTRACT  U	c. THIS PAGE  U			19b. TELEPHONE NUMBER (Include Area Code) (937) 255-3636 x4641 marina.ruggles-wrenn@afit.edu